PP81-124985
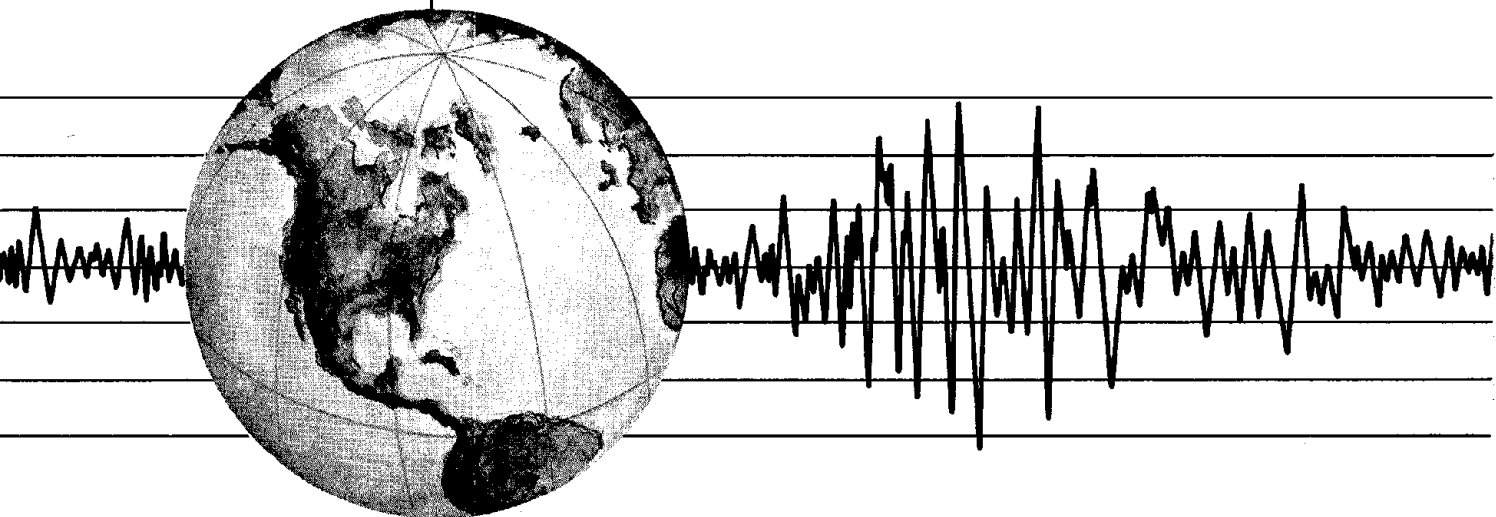
EARTHQUAKE ENGINEERING RESEARCH CENTER

CYCLIC INELASTIC BUCKLING OF TUBULAR STEEL BRACES

by
VICTOR A. ZAYAS
EGOR P. POPOV
STEPHEN A. MAHIN

COLLEGE OF ENGINEERING

UNIVERSITY OF CALIFORNIA · Berkeley, California

ABSTRACT

Experimental results are presented from tests on six individual brace members subjected to severe inelastic cyclic loading. The tubular brace specimens considered are one-sixth scale models of braces of the type used for offshore platforms. Each brace specimen is alternatively subjected to cycles of compressive inelastic buckling followed by tensile stretching. Examined are the effects resulting from different end fixity conditions (pinned vs. fixed), and from different diameter-to-wall thickness ratios (33 vs. 48). Also, the behaviors of heat treated braces are compared to the behavior of braces made from tubing as received from the manufacturer. The inelastic responses of the braces are presented and interpreted, including axial load-axial displacement hysteretic loops; axial load-midspan lateral deflection hysteretic loops; brace deflected shapes; brace energy dissipation; and inelastic axial strains, curvatures and rotations in plastic regions.

Special attention is directed to the deterioration of buckling load with inelastic cycling. Design code buckling formulas are for columns or braces that have not been previously yielded and have initial cambers within the code allowances. Cyclic inelastic loadings cause changes in the mechanical material properties of the braces which subsequently reduces the buckling load. A method of predicting the reduction in buckling load is presented. The changes in material properties are identified for a "critical section" within the plastic hinge of a brace and the reduced buckling loads under repeated cyclic loadings are calculated. The results are examined with respect to design procedures prescribed by the American Institute of Steel Construction and the American Petroleum Institute.

ACKNOWLEDGEMENTS

TABLE OF CONTENTS

LIST OF SYMBOLS

A	Load Point - Zero Load Before Compression
B	Load Point - Maximum Compressive Load
C	Load Point -Maximum Compressive Displacement
CIS	Cumulative Inelastic Strain (Centroidal)
CY	Cycle
D	Load Point - Zero Load After Compression
E	Load Point - Maximum Tensile Load
E_t	Tangent Modulus of Elasticity
F	Load Point- Zero Load After Tension
G3	Strain Gage Number 3 (Typical)
kL/r	Effective Slenderness Ratio
LB	Local Buckling
LP	Designation of Load Point
LVDT	Linear Variable Differential Transformer
M_p	Plastic Moment
P	Axial Load
P_y	Yield Load
ST	Designation for Strut
δ	Axial Displacement
δ_y	Axial Yield Displacement
Δ	Midspan Lateral Displacement
ϵ	Strain
σ	Stress
σ_y	Yield Stress
ϕ	Tube Section

CHAPTER 1

INTRODUCTION

The level of seismic forces that buildings located in regions of high seismic risk would be required to resist, if designed on an elastic basis alone, would generally raise the cost of construction to nearly prohibitive levels. Fortunately, it is not necessary to design for these large elastic forces, if ductile inelastic deformations can be permitted. Stresses beyond the elastic limit will cause permanent deformations and localized damage, but a properly designed structure will not collapse.

The concept of using braced frames in seismic-resistant design has received little attention until very recently due to the belief that such framing is not sufficiently ductile to withstand severe seismic disturbances. Consequently, the majority of large structural steel buildings in seismically active regions are designed as moment-resisting frames. For buildings having wide facades, such a structural system is economical and has been shown to be very satisfactory for resisting lateral forces caused by earthquakes. However, in some instances moment-resisting frames tend to be somewhat flexible, and although safe from collapse, during a severe earthquake, can develop costly non-structural damage. Moreover, by using moment-resisting frames alone, along a narrow width of a building, it may be very difficult, and economically impractical, to develop the required stiffness and strength to resist the lateral forces. Recent experience has shown that stiff buildings can behave well during major earthquakes [1]. For these reasons increasing attention is being given to the possibility of employing a variety of bracing schemes [2-8]. In these designs the braces can become subjected to severe cyclic axial loadings causing the braces to sequentially buckle and stretch inelastically.

To supplement the scant data available on the behavior of braces subjected to cyclic inelastic loadings, an extensive experimental program is being carried out at the University of California, Berkeley. Some twenty-four hot rolled steel sections commonly used in the building industry have already been tested [9]. All of these members conformed to the American Institute of Steel Construction (AISC) requirements for compact sections [10]. In order to

1

broaden the scope of these studies, tubular steel models representative of those employed in offshore construction were also included in the investigation. This report presents the findings from experimental tests on six tubular steel braces subjected to severe cyclic axial loadings.

Because of the stiffness and strength required to resist lateral forces due to the actions of wind, waves and currents, offshore construction has traditionally employed braced frames as standard design practice. Recent emphasis on seismic considerations in offshore construction has brought attention to the inelastic cyclic behavior of these types of braced frames. Applicable offshore design criteria specify a strength design requirement based on an elastic approach, and the levels of seismic design forces considered are comparable to those used for onshore structures. In addition, the 1977 and 1979 editions of the American Petroleum Institute (API) Recommended Practice for Planning, Designing, and Constructing Fixed Offshore Platforms each have stipulated ductility design requirements. The 1977 recommendations require offshore braced frames to remain stable under rare and intense earthquake motions capable of imposing displacements twice those of the strength design requirement. The 1979 recommendations require offshore platforms to be capable of absorbing at least four times the amount of energy absorbed at the strength design requirement with the structure remaining stable. Very little information is presently available regarding the inelastic cyclic behavior of tubular steel braced frames, their ductility capabilities, and their ability to absorb energy.

The main element required to maintain the overall structural integrity of a braced frame subjected to lateral forces is the brace. A typical load-deformation relationship of a brace subjected to a cycle of inelastic loading is schematically shown in Fig. 1.1. In stage A-B a plastic hinge is formed in the brace while loading in compression. In stages C-F, the brace is completely straightened by tensile stretching. Several simple macroscopic computer models have been developed to account for this type of hysteretic behavior [2,3,5,12,13]. One such model, implemented by Roeder and Popov [3], is illustrated in Fig. 1.2. The model approximates the behavior of a brace by defining a sequence of linear segments. The stiffness of the model in each segment must be selected on the basis of experimental results, or mathematical

formulations. At this time, accurate mathematical or numerical procedures for determining the form of the hysteretic loops are not fully developed. Consequently, experimental data are necessary, not only to assess current design procedures, but to obtain data with which analytical models can be developed and verified.

Unfortunately, only little experimental information is currently available regarding the hysteretic behavior of tubular brace members. An experimental investigation of brace members was carried out by Jain, Goel and Hanson at the University of Michigan in 1978 [8]. Small square tube (and angle) specimens were subjected to large cyclic static and dynamic displacements. Experimental investigations of tubular beam-column and brace members made from small diameter pipe are in progress at the University of Wisconsin-Milwaukee under the direction of D. R. Sherman. Preliminary results of this investigation are reported in Ref 14.

Objectives and Scope

In this report, experimental results from tests on six tubular braces subjected to cyclic inelastic loading are presented and evaluated. The objectives are to present the experimental data in a form which can later be utilized in analytical studies, and to interpret the experimental observations.

The brace specimens are one-sixth scale models of bracing members used in offshore structures. The dimensions of the test specimens were based on a representative X-braced offshore platform designed according to wave and earthquake criteria applicable to Southern California [15]. The response of specimens designed as semi-compact tubular braces, with a diameter-to-thickness (D/t) ratio of 48, are compared to the response of specimens considered fully compact with a diameter-to-thickness ratio of 33 [11]. The effects resulting from different end fixity conditions are examined. Also, the behavior of heat treated braces is compared to the behavior of braces made from tubing as received from the manufacturer. Experimental data presented and interpreted for the brace specimens include: axial force vs. axial displacement hysteretic loops; axial force vs. midspan lateral deflection hysteretic loops; brace deflected

shapes; brace energy dissipation; inelastic axial strains; and inelastic curvatures and rotations within plastic hinges. The deterioration of buckling load capacity with cycles of loading is accorded special attention and a method of predicting such deterioration is developed. The results of the research reported herein are examined with respect to design procedures prescribed by the AISC and API for axially loaded members.

CHAPTER 2

EXPERIMENTAL PROGRAM

The bracing member specimens were one-sixth scale models of braces found in a representative Southern California offshore platform (Fig. 2.1a). At this scale the cross braces were represented by 4-inch (102 mm) diameter steel tubing. Specimens of two dimensions were fabricated: a first group with a diameter-to-thickness ratio of 33 and a second group with a ratio of 48. The first group simulated fully compact A36 steel members able to maintain their capacity through large inelastic deformations [11], whereas the second group modeled A36 steel members capable of developing their full plastic load capacity without being able to withstand large inelastic deformations.

To assess the effect of end restraint on brace behavior, two bounds on the possible end conditions were considered: both ends pinned and both ends fixed. The ends of the first four specimens were pinned and those of the remaining two specimens were fixed. The actual end restraint of braces in a braced frame would depend on a variety of factors -- such as frame configuration and loading, connection detailing, member slenderness and initial camber, joint flexibility, and inelastic behavior of adjacent members -- and would ordinarily fall in the range of restraint between the two bounds.

The pinned-end struts (Struts 1-4) were 74-3/8 in. (1.89 m) long, the distance between the center of the intersection of the cross braces and the face of the jacket leg (Fig. 2.1b) The specimen length, from pin to pin, included heavy end support clevises that contained roller bearings and attachment plates (Fig. 2.2). The effect of the heavy end sections on the buckling load of the struts was calculated to be less than 3%. The fixed-end specimens (Struts 5 and 6) were 70-1/4 in. (1.78 m) long between points of fixity, the distance between the face of the jacket leg and a point within the thick-walled insert of the cross joint (Fig. 2.1b). The effective slenderness ratios, kL/r, were 54 and 25 for the pinned-end and fixed-end specimens, respectively.

The test specimens were made of AISI 1020 mild steel tubing. (AISI 1020 is a mild steel similar in carbon content and properties to A36.) Because of the drawing process used in its manufacture, the material properties of this tubing in the as-received condition are considerably different from the A36 steel welded pipe used in full scale construction. To achieve properties in the test specimens closer to those encountered in full scale braces and to assess the effect of material properties on test specimen behavior, four of the tubes used in the test specimens were annealed by heating to 1600 ^{O} F (870 ^{O} C) and oven-cooling to 1000 ^{O} F (538 ^{O} C). Full scale construction pipe will have initial residual stresses that differ from the annealed test tubing; however, the effect of these initial residual stresses on cyclic inelastic buckling should not be significant after the first inelastic cycle. Two specimens were not annealed in order that the effect of the as received material properties on the structural response could be assessed.

The geometric properties, end restraint condition, heat treatment, and initial horizontal and vertical cambers of individual specimens are summarized in Table 2.1.

Experimental Setup

The experimental apparatus used for the tests on the strut specimens is illustrated in Figs. 2.3 through 2.6. One end of the strut was either pinned or rigidly connected to a stiff braced steel foot frame attached to a concrete reaction block. The other end of the strut was attached to a double-acting hydraulic jack that was pin-connected to another concrete reaction block. For the pinned-end specimens, the jack and specimen were connected by a head pin assembly which was restrained horizontally by a single side arm. For the fixed-end specimens, the strut was rigidly bolted to a head unit that was restrained against rotation and translation normal to the axis of the specimen by means of two parallel side arms. Bolts in slotted holes were used to restrain translation or rotation of the head unit in the vertical plane (Fig. 2.5a). Photogrammetric records verified to within .0016 rad. that in the fixed-end condition, the specimens achieved full fixity.

6

The initial cambers present in the tubular specimens were carefully measured, and the specimens were oriented so that initial buckling would be expected to occur in a horizontal plane. The small frictional forces present in the test setup were measured so that they could be accounted for when the data were reduced. The friction forces were found to be 0.4 kips (1.78 kN) and 0.8 kips (3.56 kN) for the pinned and fixed test setups, respectively.

Instrumentation

Linear variable differential transformers (LVDT's) were used to measure axial displacement and linear potentiometers were used to measure midspan horizontal lateral displacement of the strut specimens (Fig. 2.2 and 2.7). Linear potentiometers were also used to measure midspan vertical lateral displacement of the fixed-end specimens where a component of buckling could occur in the vertical plane. The axial load on the specimens was measured by a load cell attached to the loading ram.

Photogrammetric instrumentation was used to determine the deflected shape of the struts. Aluminum foil targets were evenly spaced longitudinally along the centerline of the members, and the camera was stationed on an overhead crane approximately twenty feet above the specimen. Glass plate film was used; pictures were taken at predetermined points in the loading cycles. The plates were read on an X-Y comparator and the actual and normalized deflected shapes were plotted by a CDC 6400 Cal Comp Plotter.

SR-4 strain gages were placed at strategic locations along each member. Strain gages were concentrated where plastic hinges were expected to form. Reduced strain gage data provided strain histories at specified points, cross-section curvature histories, and plastic hinge rotations.

Data from the load cell, LVDT's, linear potentiometers, and strain gages were recorded on a Data General Nova Computer high speed data acquisition system. During the tests load and displacement response parameters were also monitored on X-Y recorders and visual observation records of local buckling phenomena and tearing were kept. (Fig. 2.8).

Loading Procedure

All specimens were subjected to quasi-static cycles of reversing axial displacement. These cycles generally included compressive inelastic buckling followed by tensile stretching. The prescribed displacement sequence was designed to represent ductility levels expected in braces within the Southern California example structure subjected to severe seismic loading [12]. The same displacement history was designed for the early cycles of all six test struts. The history prescribed for the first seven loading cycles was as follows. Axial displacement was uniformly incremented 0.07 in. per cycle during cycles 1 through 5. On reaching ± 0.35 in. during the fifth cycle, the imposed displacement was held constant until cycle 7. The loading for subsequent cycles varied depending on the behavior of the individual struts.

The displacement pattern applied to each strut is illustrated in Figs. 2.9 through 2.14. Struts 3 and 4, fabricated from the unannealed tubing, were unable to follow the prescribed displacement history. Both fractured during the tensile phase of cycle 3. These struts were repaired and testing resumed with the tensile displacements limited to prevent fracture.

Load points within a cycle have been identified by a letter code system as illustrated for a typical hysteretic loop in Fig. 2.15a and from a loading schematic in Fig. 2.15b. This system of identification is used throughout the report.

Material Properties

The material properties influence the brace behavior through the fundamental characteristics of yield point stress level, stress-strain curve shape, and elongation capacity. Differences in yield points, if the yield points are in fact discernible, can, in part, be accounted for by normalizing brace response parameters. This normalization is accomplished by dividing load (or displacement) levels in each strut by its respective yield load (or yield displacement). Nevertheless, a similar yield point for the model and full scale brace is desirable in order to retain the correct relationship between brace displacement ductility and frame displacements of the example structure. Also, to model inelastic behavior correctly it is important to have similar stress-

8

strain curve shape and elongation capacities.

Two material types were used to fabricate the specimens: annealed and unannealed (as received) steel tubing. The effect of annealing is clearly indicated in the tensile stress-strain curves plotted in Figs. 2.16 through 2.18 for coupons taken from each type of material. The stress-strain curve for the annealed material is elastic-plastic, similar to that for A36 steel. The average yield strength of the annealed material as measured from the coupon tests was 35 ksi (242 MPa). Ultimate strengths of approximately 52 ksi (359 MPa) were typically obtained at strains of about 14% and fractures occurred at strains of about 28%.

The yield strength of the unannealed material, based on a 0.2% strain offset, was considerably higher; equal to 92 ksi (635 MPa) for the tubing with an 0.083 in. (2.1 mm) wall thickness, and 74 ksi (511 MPa) for the tubing with an 0.120 in. (3.0 mm) wall thickness. No discernible yield point and no plastic plateau appear in the unannealed material stress-strain curves. The unannealed material coupons fractured at strains of less than 8%.

Material tests were also performed on full cross-sections of pipe. The tests were of two types: compression stub test (Figs. 2.19 and 2.20) and cyclic tests (Figs. 2.21 and 2.22). Stress-strain curves from compression stub tests were generally used for predicting first buckling loads of struts. The cyclic tests were used to quantify the extent of the Bauschinger effect that results from inelastic yield and strain reversals. In all the material tests the unannealed material behaved differently for specimens with 0.083 in. (2.1 mm) wall thickness and 0.120 in. (3.0 mm) wall thickness, whereas there was no apparent wall thickness effect for the annealed material. The average yield stress of the annealed material from the full cross-section material tests was 31 ksi (214 MPa).

A summary of the initial yield stresses for the six test struts is presented in Table 2.2. The initial yield stress for the unannealed struts is based on a 0.2% strain offset from the coupon tests. The reported initial yield stress for the annealed struts is based on the first discernible yield plateau, as averaged from the cyclic and compression stub tests. In general, the coupon tests showed 4-5 ksi (31 MPa) higher yield stresses than the full section cyclic and

9

compression stub tests. The yield stresses observed in the test struts (reported in Chapter 3) agree with the stresses observed in the cyclic and compression stub tests. The higher stresses observed in the coupon tests could be a result of cutting out and machining the coupon specimens.

Based on the initial yield stress, initial axial yield loads (P_y) and yield displacements (δ_y) were computed and are also listed in Table 2.2. These computed yield loads and yield displacements are used to normalize the brace hysteretic plots and energy dissipation data presented in the following chapter.

CHAPTER 3

OVERALL BEHAVIOR OF STRUT SPECIMENS UNDER CYCLIC LOADING

The test struts were subjected to cyclic inelastic axial displacements. The principal param-
eters monitored during the tests have been plotted in the form of hysteretic loops. These plots
are not only a valuable means of viewing the overall response history of the tested struts, but
they also lay the ground work for additional data reduction and subsequent development of
information related to deterioration of buckling loads, energy dissipation, and plastic hinge for-
mation. Details of inelastic behavior within plastic hinge regions are discussed in Chapter 4.

Hysteretic Behavior

The axial load vs. axial displacement curves for the six strut specimens are shown in Figs.
3.1 through 3.14; the lateral deflections that correspond to the early loading cycles are shown in
Figs. 3.15 through 3.20. Maximum compressive and tensile loads attained in each cycle of
loading are reported in Table 3.1; maximum compressive and tensile displacements are reported
in Table 3.2.

Strut 1 was subjected to a preliminary compressive pulse when the load control system
was activated. Residual strains ranging from 0.006 in./in. in compression to 0.004 in./in. in
tension were recorded following the pulse. The initial camber of the strut, 0.12 in. (3.0 mm),
increased to 0.25 in. (6.4 mm) as a result of this preliminary loading. Thus, Strut 1 started
cycle 1 with previous inelastic straining and an initial camber larger than the other struts. As a
result, the cycle 1 buckling load attained was 25% lower than that predicted by AISC formulae
[10]. (The factor of safety has been removed from the AISI formulae for all AISC buckling
predictions made in this report.)

The buckling load of Strut 1 decreased significantly in each loading cycle subsequent to
cycle 1 (Fig. 3.1). The post-buckling compressive load of the strut decreased rapidly with
increasing displacement during each cycle. The axial stiffness for tension loading deteriorated
significantly with each cycle. Full tensile load is attained when all fibers within a cross-section

11

have yielded in tension. The greater the compressive displacement within a given cycle, the greater are the resulting strains within the plastic hinge due to inelastic rotation. After unloading in compression, a residual inelastic rotation remains in the strut. When the direction of loading is reversed and the strut is loaded in tension, the tensile displacement required to develop full tensile yielding depends on the prior compressive displacement and on the magnitude of the residual inelastic rotation. While the full tensile capacity of Strut 1 was developed during the first six cycles, the capacity was achieved at tensile displacements approximately equal to the preceding compressive displacement applied.

Local buckling was observed at the middle of Strut 1 during cycle 3. Local buckles tended to straighten out under tensile load, but reformed when compressive load was again applied. Tears developed in the steel during cycle 5 owing to the large local strain reversals associated with this behavior. Both strength and stiffness rapidly deteriorated during subsequent cycles (Fig. 3.2).

The hysteretic curves for Strut 2 during cycles 1 through 5 (Fig. 3.3) are generally similar to those for Strut 1. Since the diameter-to-thickness ratio of Strut 2 was smaller and the cross-sectional area 44% greater, the tensile and compressive load capacities of Strut 2 were greater. A slight ovaling of the cross-section at the midspan of Strut 2 occurred during the fourth cycle. Local buckling developed in this region during the fifth cycle and tearing of the steel initiated during the tension portion of cycle 8 (Fig. 3.4). As a consequence of the smaller diameter-to-thickness ratio of Strut 2, local buckling was delayed and the strength of Strut 2 deteriorated less than the strength of Strut 1 during later cycles.

The axial load vs. midspan lateral deflection curves for Struts 1 and 2 are given in Figs 3.15 and 3.16. These indicate that the initial camber in the two pinned-end specimens existing prior to cycle 1 was nearly eliminated by tension yielding during the first cycle of loading.

Strut 3 was identical to Strut 1, except that the former was not annealed. Because the yield strength of the material in the unannealed tube was very high, this specimen did not buckle in cycle 1 (Fig. 3.5). First buckling of Strut 3 occurred in cycle 2, and the maximum

compressive load then achieved was only 85% of the buckling load predicted by the AISC and API recommended formulas [10,11]. Failure to attain the compressive capacity predicted by the code is attributed to the rounded stress-strain curve of the unannealed material (Figs. 2.17 and 2.20). Strut 3 fractured during the tensile phase of cycle 3. The fracture occurred in the heat-affected zone in the tubing adjacent to the weld. The strut was repaired and tested again with tensile displacements limited to avoid re-fracture. Hysteretic loops for the post fracture testing (cycles 4-8) are shifted so that compression loading of cycle 4 corresponds with elastic tensile unloading of cycle 3. Compression displacements after cycle 4 differ from the prescribed displacement loading history by the amount of the shift. Local buckling occurred at the mid-length during cycle 4. Tearing occurred in the region of local buckling during the sixth loading cycle even though tensile forces were limited after the third cycle. The strength and stiffness of the specimen decreased substantially after local buckling was initiated (Fig. 3.6).

The geometric properties and end conditions of Strut 4 were identical to those of Strut 2, but the former differed from Strut 2 in that it was unannealed. Although this strut was fabricated from a heavier tube than was Strut 3, the compressive force attained was not as high. It can be observed from the compression stub tests (Fig. 2.20) that the 0.120 in. (3.0mm) wall thickness material has a notably rounded stress-strain curve and this would contribute to lowering the buckling load of Strut 4. In addition, the imposed displacement during cycle 2 did not suffice to develop the full buckling capacity of Strut 4; whereas the buckling load for cycle 3 was decreased due to the Bauschinger effect resulting from tension yielding during cycle 2 (Fig. 3.7). Similar to Strut 3, Strut 4 fractured during the tensile phase of cycle 3. Again, the strut was repaired and testing resumed with cycle 4 at limited tensile displacements. No local buckling was observed during testing of Strut 4. The hysteretic loops for cycle 5 through 10 were remarkably stable because no local buckling occurred (Fig. 3.8).

The ductility ratio, as defined here, is the ratio of the maximum applied axial displacement to the elastic displacement at initiation of tensile yielding of the gross section. The ductility ratios for the unannealed test specimens were only 38% and 45% of those for the annealed

13

specimens. Thus, the inelastic deformations of the unannealed specimens were less severe. Moreover, tensile forces in Struts 3 and 4 were limited to avoid fracture at the welds. Because of the reduced inelastic tensile stretching, the lateral displacement and inelastic rotation at the midspan were less severe for the unannealed specimens. Local buckling of these struts was delayed because of the lesser inelastic straining and therefore the deterioration of strength differed from that of the annealed specimens.

Strut 5 was similar to Strut 1 except that its ends were fixed. The maximum compressive load carried by this specimen, which occurred during load cycle 3, was within 2% of the value predicted using the AISC formulas (Fig. 3.9). The deterioration of the buckling load and the loss of energy dissipation capacities during subsequent loading cycles (Figs. 3.10 and 3.11) was not as severe as exhibited by Strut 1. Local buckling was observed during cycle 5, first at the foot and then at the midspan of the specimen. With additional cycling, the center hinge deteriorated more quickly than that at the foot and eventually tore open in tension.

A pictorial history of the local buckling phenomenon is presented in Figs. 3.21 through 3.25 for Strut 5 as an example of the general local buckling behavior exhibited by all of the struts. The overall buckled strut, depicted in Fig. 3.21, shows concentrations of rotations at the locally buckled regions. Figures 3.22 through 3.25 show the evolution of local buckling, straightening after tension, and eventual tearing in tension for the center and foot sections.

The maximum compressive load developed by the other fixed-end specimen, Strut 6, was within 1% of the value predicted using the AISC formulas. When this compressive load was reached during cycle 3, noticeable lateral buckling occurred, accompanied by a sudden loss of about 5 kips (22.4 kN) (Fig. 3.12). Thereafter, the strength of the specimen deteriorated little during cycles 4 through 10. During cycle 10, the specimen buckled locally at three locations: first at the midspan, then at the head end, and finally at the foot. Continued loading through cycle 16 resulted in deterioration of the compressive strength (Figs. 3.13 and 3.14).

The hysteretic curves for the fixed-end specimens differ considerably from those obtained for the pinned-end specimens. The difference can be primarily attributed to the lower

slenderness ratio [8]. Both fixed-end specimens show larger enclosed areas and better energy dissipation characteristics for the hysteretic curves as compared to those of the pinned-end specimens. Post-buckling strength of the fixed-end specimens deteriorated less and the initial stiffness for loading in tension were significantly higher.

The axial load vs. midspan lateral deflection curves for Struts 5 and 6 are given in Figs. 3.19 and 3.20. These midspan lateral deflections were about one-fifth of the values corresponding to pinned-end specimens (Figs. 3.15 and 3.16) with the same axial displacement. These smaller lateral deflections, and, hence, smaller plastic hinge rotations, helped delay local buckling and maintain the strength of the fixed-end specimens during inelastic cycling. The reported midspan lateral deflection for the fixed-end struts are displacement in the horizontal plane. A vertical component of midspan lateral deflection also existed which measured approximately 25% and 15% of the horizontal components for Struts 5 and 6, respectively. The magnitude of vectorial sum of both components is approximated 3% and 1% higher than the magnitude of the horizontal component alone for Struts 5 and 6, respectively.

Normalized Load vs. Axial Displacement

To clarify the differences in behavior of the six specimens the load vs. axial displacement plots for cycles 1 through 5 have been normalized by dividing the load and displacement, by P_y and δ_y, respectively. These plots, shown in Figs. 3.26-3.28 emphasize the lower displacement ductility levels of the loading histories for the unannealed struts. The unannealed struts exhibited brittle behavior and could not sustain cycling at large tensile ductility levels. The reduced compressive ductility levels for the unannealed struts are a consequence of the higher yield displacements (δ_y) The applied compressive displacements were approximately equal for all struts.

Deterioration of Buckling Loads

The difference in cyclic performance between struts is in part exemplified by the deterioration of buckling loads. The cyclic buckling loads have been listed in Table 3.1 and are graphically presented in normalized form in Fig. 3.29. This figure illustrates the superior performance of the fixed-end struts over the pinned-end struts. Moreover, for each of three strut pairs with D/t of 48 and 33, (pinned annealed, pinned unannealed, fixed annealed), the figure shows that the struts with D/t=33 clearly outperformed the struts with D/t=48 in percentage retainment of their original buckling load.

Deflected Shapes

The deflected shapes obtained from the photogrammetric data for the six struts are plotted in Figs. 3.30 through 3.37. The deflections are deviations from the initial position at the beginning of a test. The lateral deflections have been exaggerated to emphasize the shape.

The buckled shape of Strut 1 during cycles 1 and 2 (Fig. 3.30a and b) was sinusoidal. During the compression stage of cycle 3, curvature concentrated within the center plastic region (Fig. 3.30c). The deflected shape that remained after unloading in compression is shown in Fig. 3.30d. The residual curvature that remained in the center region and the reverse curvature adjacent thereto that developed while the specimen was loaded in tension is illustrated by Fig. 3.30e. During cycles 4, 5, and 6, the buckled shape of Strut 1 deteriorated due to local buckling and residual curvature (Figs. 3.30f, g, h).

It was stated earlier that initial cambers were essentially removed by yielding in tension. The small negative deflections seen in Fig. 3.31a for Strut 2, cycle 2, at load point A are due to the removal of initial camber eccentricities by yielding in tension during the first loading cycle.

Although the deflected shape of Strut 2 during cycle 2 at load point C (Fig. 3.31b) is asymmetric, it gradually became symmetrical during cycles 3 and 4 (Figs. 3.31d and e). Residual curvature and deflection were evident by cycle 5 at point A (Fig. 3.31f). The deflected shape of the specimen gradually became irregular during cycles 5 through 8 (Figs.3.31g and h).

16

The deflected shapes of the unannealed struts (Figs. 3.32 and 3.33) did not show a discernible central plastic region in the early cycles. The deflected shape of Strut 3 was sinusoidal until local buckling began (cycle 4), subsequently the curvature concentrated in the central region (Fig. 3.33). The sinusoidal deflected shape of Strut 4 (Fig. 3.32) was remarkably regular throughout the test since no local buckling occurred.

The deflected shapes for the fixed-end Struts 5 and 6 are presented in Fig. 3.34 and 3.35. Strut 5 had a asymmetric buckled shape (Fig. 3.34) with maximum deflections occurring off center, closer to the foot end. Consequently, less inelastic rotations resulted at the head plastic hinge and thus, this hinge did not develop local buckling. Strut 6 illustrates a classic fixed-fixed buckled shape (Fig. 3.35). There was little deterioration in the shape through the first nine cycles, since local buckling did not occur until cycle 10. For both fixed-end struts plastic rotations can be noted at the ends of the members. These are plastic rotations occurring within the member tubing. As mentioned previously, full fixity of the end plates was verified through photogrammetric techniques.

The deflected shapes of individual specimens are compared in Fig. 3.36. The comparison illustrates the following points:

a)   For the same cycle and axial displacement, the deflected shape of the pinned-end, thinner strut ($D/t = 48$) shows a more irregular shape and greater concentrations of plastic rotations than that of the thicker strut ($D/t = 33$) (Fig. 3.36a).

b)   The lateral deflection of the pinned-end specimen, Strut 2, was considerably greater than that of the corresponding fixed-end specimen, Strut 6, at the same axial displacement (Fig. 3.36b).

c)   For the same cycle and compressive axial displacement, the lateral displacements of the unannealed specimen, Strut 4, was 30% of that for the similar annealed specimen, Strut 2 (Fig. 3.36c).This is due to the lesser tensile stretching in the unannealed specimens.

d)   The difference between the tensile stretching of the annealed and unannealed struts can be accounted for by considering the total travel of compressive axial displacement from load point A to load point C. When plotted for equal amounts of total compressive travel, the lateral deflections are approximately the same for both specimens (Fig. 3.36d).

Further comparisons for deterioration in deflected shape are illustrated in Fig. 3.37. To facilitate comparisons of changes in shape, the lateral displacements have been normalized by the maximum lateral displacement in each cycle. The normalized deflected shapes for four of the struts, plotted for cycles 3 and 6, emphasize the change in shape that occurred during those three cycles of loading.

Energy Dissipation

Energy dissipation is an important response parameter for inelastic cyclic loading. The energy dissipated during all loading cycles was measured for each of the six test struts from their axial load vs. axial displacement plots; these values are listed in Table 3.3. The energy dissipated during each loading cycle E_i was normalized by dividing it by the energy dissipation of a nonbuckling, rigid-perfectly plastic element, RP_i, with the same yield load (P_y) and cycled through the same displacements (See Fig. 3.38 insert). For purposes of this discussion, E_i/RP_i, is defined to be the energy dissipation efficiency of a test strut. Displacements and yield loads as parameters are thus de-emphasized, which facilitates comparisons of energy dissipation between struts with different displacement histories or yield loads. Moreover, the energy dissipation of the rigid-perfectly plastic element represents the hypothetical maximum value for a strut subjected to the same axial displacements. Thus, energy dissipation efficiencies are a means of quantifying the deterioration of the capacity of a strut to dissipate energy with cycles. The energy dissipation efficiency in each cycle (E_i/RP_i) for the six test struts are listed in Table 3.3 as well as plotted in Fig. 3.38.

To facilitate comparisons of the energy dissipations, the cumulative sum of cycle dissipation efficiencies vs. cycle number are plotted in Fig. 3.39. Since the energy dissipation efficiency of a rigid-perfectly plastic strut is equal to unity in each cycle, the cumulative dissipation efficiency is equal to the cycle number. In this way, the ordinate divided by the abscissa of Fig. 3.39 represents the energy dissipation efficiency of the test struts cumulative over all preceding cycles. The energy dissipation of the rigid-perfectly plastic element represents 100% efficiency. The cumulative cycle dissipation efficiencies of an ideal elastic-perfectly plastic non-buckling element were also calculated and plotted in Fig. 3.39.

The elastic-perfectly plastic element is useful for comparison. However, observe that during early cycles of loading the test struts can dissipate more energy than the ideal elastic-perfectly plastic element. For instance, prior to reaching the axial yield load the ideal elastic-perfectly plastic nonbuckling element dissipates no energy. On the other hand, the test struts may dissipate energy because of some inelastic material response or buckling.

The responses of the test struts with respect to efficiency of energy dissipation can be grouped into three strut pairs with D/t of 48 and 33: pinned-unannealed, pinned-annealed, and fixed-annealed (Fig.3.39). The response of each pair of specimens is similar until the later loading cycles, at which time the specimens with a D/t=48 prove less efficient. The cumulative efficiency (ordinate divided by abscissa) of Struts 3 and 4 (pinned-unannealed specimens) were the poorest, less than 22%. The cumulative efficiency of Struts 1 and 2 (pinned annealed specimens) in cycle 3 was approximately 47% and 49%, respectively, and decreased to 31% and 36% by cycle 7. The cumulative efficiency of Struts 5 and 6 (fixed-end specimens) was 37% and 41% during cycle 3 and increased to 47% by cycle 7. The cumulative efficiency of the ideal elastic-plastic element was 53% in cycle 3 and 70% in cycle 7.

The best energy dissipation of all test specimens was shown by Strut 6. The superior performance of this strut is attributable to its fixed-ends and its lower D/t ratio. After nine cycles of loading, the dissipation efficiency of Strut 6 was 65% of the efficiency of the ideal elastic-plastic element.

The quantification of the efficiency of a brace element in dissipating energy allows comparisons on the effectiveness of a braced frame to dissipate energy. As illustrated in Fig.3.38, a properly detailed brace can absorb a significant amount of energy, although generally not as efficiently as an ideal elastic-perfectly plastic element. A properly detailed beam in a moment-resisting frame can at best be expected to behave as an elastic-perfectly plastic element. However, considering a braced frame and a moment resisting frame of similar geometry, and designed for similar lateral loads, the braced frame will have the advantage of dissipating energy at considerably lower values of frame lateral displacements.

CHAPTER 4

INELASTIC BEHAVIOR AT PLASTIC HINGES - ANNEALED STRUTS

For general structural design and analysis purposes, the overall behavior of the struts described in Chapter 3 is of primary importance. Many of the aspects of this overall behavior can be explained through study of the plastic hinge regions. In this chapter, data reduced from the SR-4 strain gage readings will be examined and interpreted in an effort to gain insight into variations in strain histories and local buckling phenomena.

Plots of several example strain gage readings are included in Appendix A (Figs. A.1 through A.22). Strain gage data have been reduced in a variety of ways in order to emphasize certain aspects of response. The strains at a cross-section, for example, are reduced to centroidal axial strains, cross sectional curvatures and subsequently to rotations over a length. All data reduced from strain gage readings are reported only up to the point where local buckling is detected. After local buckling has occurred, the strain gage readings near the section of local buckling can neither be related to the centroidal axial strains nor to the cross-sectional curvatures. A knowledge of the inelastic strain history is important, because the material properties of a strut and the development of local buckles are affected by the history of inelastic straining.

Local buckling is an extremely complex phenomenon. Data from tests on six strut specimens hardly suffices as the basis from which the local buckling problem can be conclusively resolved. In this report, parameters thought to be of importance in the evolution of local buckling are analyzed. The underlying purpose is to present empirical data by which local buckling can be estimated and, if possible, can later be incorporated into an analytical model of brace behavior.

Basic Considerations of Brace Inelastic Buckling

The inelastic buckling of a strut results in the development of plastic hinges; that is, regions where inelastic curvatures occur. The number of plastic hinges that will form in a given strut is determined by the number of hinges required to form the collapse mechanism for that strut. Thus, one plastic hinge forms in a pinned-end strut and three such hinges in a fixed-end strut (Fig. 4.1). For purposes of these discussions, the center plastic hinge will be assumed to consist of two equivalent plastic regions which extend from the section at which the inelastic curvature is greatest to the sections where inelastic curvatures vanish. Using this definition, a pinned-end strut may be said to have *two* equivalent plastic regions at the center (Fig. 4.1a). At the ends of a fixed-end strut, plastic regions are defined to extend from the specimen end plates to those sections where inelastic curvatures have reduced to zero, and as for a pinned-end strut, two more plastic regions can be identified at the center. On this basis a fixed-end strut may be said to have four equivalent plastic regions (Fig. 4.1b).

The static relationships between the axial force P, the fully plastic moment capacity M_p, and the midspan lateral deflection Δ for the ideal pinned-end and fixed-end struts are given in Fig. 4.1. The plastic moment capacity M_p varies with the axial force P as given by the interaction curves shown in Fig. 4.2.

The superior axial load vs. axial displacement performance of the fixed-end struts compared to the pinned-end struts, noted in Chapter 3, can be explained with the aid of Figs. 4.1 and 4.2. According to the static equilibrium relationships, the P/M_p ratio of a fixed-end strut is double the P/M_p ratio of a pinned-end strut, at equal midspan *lateral* deflections. For the same size members with equal lateral displacement, the axial load capacity for a fixed-end strut is larger than the axial load which can be carried by the pinned-end strut, but it is less than twice as large because of the axial load-moment interaction (Fig. 4.2). The larger axial loads in the fixed-end strut will cause an increase in the amount of compressive centroidal axial straining. Increased compressive axial straining will result in a shorter centroidal axis length. If equal compressive *axial* displacements are applied to both types of struts, the shorter centroidal axis

length of the fixed-end strut will result in lesser magnitudes of midspan lateral deflection for this strut. Also, the reverse direction of curvature from the points of inflection to the ends of the fixed-end strut, compared to the center portion of the strut (Fig. 4.1), will contribute to lesser magnitudes of midspan lateral deflection. Consequently, the lesser midspan lateral deflections that result when equal axial displacements are applied will further increase the axial load capacity of the fixed-end strut relative to the pinned-end struct according to the static relationship. In agreement with these considerations, the experimentally observed midspan lateral deflections of the fixed-end struts (reported in Chapter 3) were approximately one-fifth of the magnitudes corresponding to pinned-end struts with the same axial displacements. Moreover, the load carried by the fixed-end struts was larger as evidenced by the shape of the hysteretic loops.

Curvature in Plastic Hinge Regions

Curvatures at a cross-section were calculated from the strain gage readings, by dividing the difference of two strain gage readings by the distance between the gages. Plots of curvatures at a section are included in Appendix A, Figs. A.23 through A.59.

Strain readings were observed to differ up to 0.002 in/in. from an assumption of linear strains within a cross-section. The variations from linear straining were investigated and attributed to local bending within the wall of the tube. The variations due to local bending should not exist at the mid-thickness of the tube wall. For the gross behavior of a cross-section the assumption of plane sections remaining plane appears to be valid.

The strain gages were externally mounted on the tubes (Fig. 2.2). It was found that for curvatures computed from two diametrically opposed strain gages the variations due to local bending would cancel. Centroidal axial strains computed from two strain gages could include variations up to 0.002 in./in. due to local bending effects. For centroidal axial strains computed from four strain gages the variations due to local bending would cancel.

Once a strut buckled, lateral buckling in subsequent cycles always occurred in the same direction. Curvatures as reported in this discussion are established as positive for the directions that result when a strut is in the primary buckled deflected shape. The lengths of plastic regions for each cycle are measured as the regions where positive inelastic curvatures develop at maximum compressive displacement. Curvatures for Strut 1 within the center plastic regions are plotted in Figs. 4.3 and 4.4 at the load points that correspond to maximum compressive and maximum tensile displacements, respectively. (For definition of load points see Fig. 2.15a). Similar plots for Strut 2 are shown in Figs. 4.5 and 4.6. Note, that these two struts differed only in their wall thickness. The plastic hinge in Strut 1 extended beyond the strain-gaged region and permitted data reduction for only one of the center plastic regions. The center of the plastic hinge was chosen as the section with maximum curvature during cycle 1. The reported data for Strut 2 are based on an average of both center plastic regions.

The following points can be summarized from the curvature plots for Struts 1 and 2:

1) Local buckling occurred at or adjacent to sections of maximum curvature.

2) Plastic hinges in Strut 2 (D/t=33) were approximately 36% shorter than those for Strut 1 (D/t=48).

3) The magnitude of curvature within individual cycles was larger for Strut 2 than for Strut 1.

4) Maximum curvatures at the onset of local buckling were 61% smaller for Strut 1 than for Strut 2.

5) The residual curvatures at maximum tensile displacement were larger for Strut 2 than for Strut 1.

Curvatures for Strut 5 are plotted in Figs. 4.7 and 4.8 for the foot plastic hinge region. Similar plots for Strut 6 are shown in Figs. 4.9 and 4.10. Curvatures at load points for maximum compressive and tensile displacements are plotted for each cycle up to the load point of local buckling. Foot hinge curvature results for Struts 5 and 6 can be summarized as follows:

24

1) Increased inelastic rotations are realized through a growth of plastic hinge length rather than from greater curvature magnitudes.

2) Strut 6 (D/t=33) sustained maximum curvature excursions three times greater than did Strut 5 (D/t=48) prior to local buckling.

3) For the first three loading cycles, Strut 5 did not buckle laterally, but did yield axially. Curvatures recorded for these cycles were apparently caused by adjusting to a difference in angle between the strut and the end plate. No such curvatures were observed in Strut 6.

For ideal symmetrically buckled struts with constant plastic moment capacity M_p, the moment gradient of a fixed-end strut is double that of a pinned-end strut of the same length. The higher moment gradient should result in shorter plastic hinges for the idealized fixed-end strut. However, the length of the plastic hinges of the test fixed-end struts were as long as the plastic hinges of the pinned-end struts. (Tables 4.1 through 4.4). This can be attributed to axial load-moment interaction. The higher axial loads in the fixed-end struts cause a reduction in the plastic moment M_p capacity. A reduction in plastic moment will cause a reduction in the moment gradient. Thus, a fixed-end strut could have equal or even smaller moment gradients than a similar pinned-end strut. The length of the plastic hinge that will develop in either strut will depend both on the moment gradient and the moment difference between the fully plastic and first yield interaction curves (Fig. 4.2).

Detailed strain data were obtained only at the foot hinges for Struts 5 and 6. For ideal symmetrically buckled fixed-end struts, the head and both center plastic regions should have the same distribution of curvature as the foot plastic region. The test specimen were, of course, not perfectly uniform and symmetric; initial imperfections, asymmetric buckling, slight differences in end restraints, and welding effects contribute to differences in the distribution of curvature. Although the distribution of curvature at the head, foot, and both center regions are not precisely the same, the general characteristics of the different plastic regions should be similar.

Inelastic Rotations

Plastic hinge rotations were estimated from cross-section curvatures. The inelastic rotations were obtained by integrating the cross-section curvatures (Fig. 4.3 through 4.10) over the lengths of the plastic regions. Rotations for maximum displacement load points C and E are listed in Tables 4.1 through 4.4. Rotations calculated at load points C and E include small elastic rotations on the order of 0.003 rad./in. (0.118 rad/m.) as well as the inelastic rotations. The magnitude of the elastic rotations is less than the accuracy of calculations (±0.005 rad.), thus the inelastic rotations were taken equal to the total rotation.

The relation between inelastic rotation and maximum curvature is important in estimating curvature when only rotation is known. The magnitude of rotation for maximum displacement load points have been plotted against the maximum curvature within the plastic hinge (Fig. 4.11). Data from maximum tension and maximum compression load points have been included in the same figure. While an accurate empirical relation cannot be developed from these data, the plots serve to represent the rotation-curvature relation qualitatively.

The inelastic rotation excursion during a loading cycle is the difference between inelastic rotations at load points C and E. Cumulative inelastic rotation is the sum of the absolute value of the inelastic rotation excursions for both compressive and tensile loadings. The cumulative rotation is a measure of the total flexural deformations at the plastic hinge. Cumulative inelastic rotations are also listed in Tables 4.1 and 4.4. Significance of these calculations may be summarized as follows:

1) Larger cumulative inelastic rotations occurred prior to local buckling for the plastic regions of struts with a D/t=33 than for those of struts with a D/t=48.

2) Almost twice as much (190%) inelastic rotation was accumulated at the foot region of fixed-end Strut 6 (D/t=33) than at the center region of pinned-end Strut 2 (D/t=33) before local buckling occurred.

3) At the foot region of fixed-end Strut 5 (D/t=48) the accumulated inelastic rotation was 0.55 times that which occurred at the center hinge of pinned-end Strut 1 (D/t=48). This is an opposite trend to that in Struts 6 and 2, although in both fixed-end struts local buckling occurs at a later cycle.

In summary, the cumulative inelastic rotations alone do not show a direct relation to the occurrence of local buckling. One must conclude that other factors, such as curvatures and strains, could be important parameters affecting the development of local buckling. These parameters will be quantitatively examined in the following section.

Cumulative Curvature and Centroidal Axial Strain

Cumulative inelastic curvature is defined as the sum of the absolute value of inelastic curvature excursions for both compressive and tensile loading. Cumulative inelastic centroidal axial strain is defined in an analogous manner.

Centroidal axial strain and cross sectional curvature completely define the strain distribution at a cross-section if it is assumed that plane sections remain plane. Accordingly, cumulative inelastic centroidal axial strain and cumulative inelastic curvature are a measure of the inelastic history for the entire cross-section. The material properties of the strut are affected by inelastic straining and the inelastic strain history is important in the development of local buckles.

Inelastic curvature excursions and inelastic centroidal axial strain excursions have been summed from the initial load points up to the first occurrence of local buckling. Cumulative inelastic curvatures within plastic hinges are plotted in Figs. 4.12 to 4.15. The cumulative inelastic centroidal axial strains along the lengths of the struts are plotted in Figs. 4.16 to 4.19. The following observations can be made from these figures:

1)   The axial strain along the struts was highly nonuniform; almost all inelastic axial strain occurred in the plastic hinge regions.

2)   In Struts 1 and 2 the section of maximum cumulative curvature at the center hinges occurred near the centerline of the strut for all cycles, but varied slightly in its location for different cycles. In Struts 5 and 6 for all cycles the cumulative curvature at the foot hinges occurred at a section nearest to the end plate.

3)   The section of maximum cumulative axial strain occurred at the same section as the maximum cumulative curvature for 96% of the load points plotted.

4)   Local buckling occurred at the section where cumulative curvature was the maximum at some time during the loading history.

5)   Inelastic curvatures can occur in early cycles near the end plates to accommodate any slight initial difference in angle between the strut and the end plate. Such inelastic curvature may also induce axial straining of the strut centroidal axis near the end plates. During early loading cycles, such curvatures and axial strains were noted in Strut 5.

The similar pattern in the cumulative axial strain and curvature graphs can be explained from considerations of static equilibrium. The greater the inelastic curvature, the smaller is the available effective area for resisting applied axial load. Since the axial load is equal along the strut length, at the sections where the curvature is highest a greater axial strain must take place. Hence, the cumulative axial strain gives an indication of the extent of inelastic curvature that has occurred at a section. The relationship between axial load capacity and moment capacity at a cross-section was noted previously in the section on basic considerations.

Occurrence of Local Buckling

API Recommendations state that braces with a diameter-to-wall thickness ratio of less than $1300/F_y$ are fully compact sections capable of developing their full plastic capacity through large inelastic deformations [11]. Struts 2 and 6, with a D/t ratio of 33, are compact section

under this definition, but during severe cyclic loading developed local buckling and lost capacity. Criteria based on monotonic loading are not sufficient to preclude such local buckling of braces under severe cyclic loading. According to API Recommendations, Struts 1 and 5, with a D/t ratio of 48 should be capable of developing their full plastic load capacity, but only through limited plastic rotations. These struts with a D/t of 48 did buckle locally before the similar struts with D/t of 33. All of the annealed struts were able to develop their full plastic load capacity prior to local buckling.

A summary of several parameters measured at the first occurrence of local buckling is presented in Table 4.5. Cumulative inelastic curvature, axial strain, and compressive fiber strain are reported for the four annealed struts at the section of local buckling. The location of the compressive fiber is taken as the point where local buckling developed; the strain history for this fiber is more severe than for any other fiber in the cross-section. Cumulative inelastic strain and curvature are important parameters of strain history, but do not completely define it. The magnitude of inelastic curvature excursions is also important. The maximum curvature excursion is included in the table. The physical ramifications of this parameter imply that a strut will respond differently to a few large cycles than it will to many small cycles, even if the total cumulative inelastic deformation is the same. Also included in Table 4.5 are the strut loads at the onset of local buckling and the cumulative energy dissipation. Conclusions which can be reached from this table of strut parameters measured at the onset of local buckling are as follows:

1) The struts with D/t of 48 buckled locally at approximately half the cumulative inelastic axial strain and compressive fiber strain compared to the struts with a D/t of 33.

2) Larger maximum curvature excursions result in lesser cumulative inelastic strains at local buckling.

3) The fixed-end Struts 5 and 6 accumulated 112% and 170% more axial strain, respectively, than the corresponding pinned-end Struts 1 and 2.

4) The fixed-end Struts 5 and 6 dissipated 206% and 293% more energy, respectively, than the corresponding pinned-end Struts 1 and 2. That the fixed-end struts dissipate more energy than the pinned-end struts could be expected from the fact that they have 4 equivalent plastic regions versus 2 such plastic regions for the pinned-end struts. When only one-half of the total energy dissipation for the fixed-end struts is considered, Struts 5 and 6 still dissipated 53% and 96% more energy than the corresponding pinned-end Struts 1 and 2.

5) Struts 2 and 6 with D/t ratios of 33 dissipated 215% and 304% more energy, respectively, than the corresponding Struts 1 and 5 with D/t ratios of 48. Higher energy dissipations are to be expected because of the higher yield loads. If the energy dissipations are divided by the yield load, thus removing yield load as a parameter, Struts 2 and 6 (D/t=33) still dissipated 119% and 183% more energy than Struts 1 and 5 (D/t=48).

From the information in the table it can be concluded that cumulative strain, cumulative curvature, maximum curvature excursions, and energy dissipation are important in local buckling. These parameters could be used to estimate the onset of local buckling in braces of similar cross-sections. However, not enough cases have been tested to adequately develop an empirical relationship between local buckling and the parameters examined.

Once local buckling does occur, the deterioration of the brace capacity is controlled by the local buckled region. Inelastic rotations after local buckling cause further deterioration in the strength of the locally buckled section thereby reducing the strut capacity. Cumulative inelastic rotations after local buckling were calculated from photogrammetric data. An empirical relationship between compressive capacity and cumulative inelastic rotation for pinned-end struts is indicated in Fig. 4.20. Such empirical relations can be used to model the strut capacities after local buckling. The cumulative brace energy dissipations (Table 3.3) could also serve as a

similar empirical parameter for local buckling. An analytical method of predicting compressive cyclic capacity of struts before the onset of local buckling is presented in the next chapter.

CHAPTER 5

PREDICTION OF BUCKLING LOADS - ANNEALED STRUTS

It was observed in the experiments that the buckling load capacity of a column deteriorates with each successive inelastic load cycle. While design code formulas predict the first buckling loads of columns, an alternative formulation is required to predict the reduced buckling loads of columns or braces which have experienced previous inelastic straining.

The basic theory for predicting the first inelastic buckling loads of a column may be credited to Engesser who first proposed a solution to this problem in 1889 [17]. Current design code formulas employing similar methods have been verified by numerous experiments and can be used with confidence to compute the initial buckling load of a column or brace. It must be recognized, however, that the code formulas are for columns which have not been previously yielded and with initial camber within the code allowances. A structure subjected to severe earthquake, wind, or wave loadings, may develop yielding or buckling in the braces and columns. The capacities of such structures could significantly reduce during and following such loadings.

A large residual camber, resulting from a previous buckling excursion, is one reason to expect a reduced buckling capacity in a subsequent buckling cycle. Not as apparent, but equally important, is the fact that previous inelastic straining of a member will alter the mechanical properties of the material thereby causing a reduction in the compressive load carrying capacity. A column that has experienced only tensile yielding or a buckled column that has been re-straightened by tensile yielding will exhibit a reduced buckling load capacity as a result of these changes. The extent of the changes depends on the inelastic strain history to which the column has been subjected. The changes in the material stress-strain relationship due to previous inelastic strains and strain reversals, commonly referred to as the Bauschinger effect, must be accounted for in calculating the cyclic buckling capacity of columns. Development of cyclic constitutive material property models for predicting changes in the material properties is a subject of current active research [16].

32

The prediction of buckling loads specified by the AISC has its theoretical basis in the tangent modulus concept. According to this approach [17] a column of homogeneous material exhibiting nonlinear stress-strain properties will experience bifurcation of the equilibrium state when the average axial stress, P/A, is equal to:

$$\sigma_{cr} = \frac{P}{A} = \frac{\pi^2 E_t}{(kL/r)^2} \tag{5.1}$$

Where E_t, the tangent modulus, is the slope $d\sigma/d\epsilon$ of the stress-strain curve at the stress σ_{cr}. In the elastic range of material behavior this equation results in the Euler column load.

The AISC provisions for columns are given by two formulas [10].

$$F_a = \frac{12\,\pi^2 E}{23\,(kL/r)^2}; \quad \text{for } kL/r \geqslant C_c \tag{5.2a}$$

$$F_a = \frac{\left[1 - \dfrac{(kL/r)^2}{2C_c^2}\right] F_y}{\dfrac{5}{3} + \dfrac{3}{8}\dfrac{(kL/r)}{C_c} - \dfrac{1}{8}\dfrac{(kL/r)^3}{C_c^2}}; \quad \text{for } kL/r < C_c \tag{5.2b}$$

where

$$C_c = \sqrt{2\pi^2 \frac{E}{F_y}}$$

and $\left[\dfrac{5}{3} + \dfrac{3}{8}\dfrac{(kL/r)}{C_c} - \dfrac{1}{8}\dfrac{(kL/r)^3}{C_c^{\,3}}\right]$ is a variable safety factor.

The first formula (Eq. 5.2a) for columns with large slenderness ratios, is applicable in the elastic range of material behavior; the other (Eq. 5.2b), is a parabolic approximation for a solution based on a variable tangent modulus. This second formula is applicable to stockier columns and is suitable for residual stress distributions and material stress-strain relationships typical of steel column sections used in the building industry. When the residual stress distribution or the material stress-strain properties differ from those assumed in AISC formulas, it is more accurate to determine the true stress-strain properties and to use the tangent modulus

formula for predicting buckling loads. The stress-strain properties should realistically account for the residual stresses. For a previously buckled or yielded column both the material properties and the residual stress distribution differ from those assumed in the AISC formula. It will be shown in the following section that a generalized tangent modulus approach can be developed which will account for the degradation of compressive load capacity due to changes in material properties of inelastically cycled columns, if a proper representation of the material stress-strain relation is made.

A Generalized Tangent Modulus Procedure

The tangent modulus method assumes that the material of a column under consideration is homogeneous. This assumption is not strictly true for an inelastically cycled column because the inelastic strain history varies both within a cross-section and along the length of the member and thus the material properties also vary. However, a critical section within the plastic hinge of the column can be chosen that has material properties which may be assumed to control the buckling load. The deteriorating load capacity of a column can be reasonably well estimated if the changing material properties that correspond to the critical section are taken into account.

These changes in material properties are related to the Bauschinger effect. The Bauschinger effect is an indication of the fact that the stress-strain curve becomes more rounded after inelastic strain reversals (Fig. 2.21). Within the rounded region, the tangent modulus of the material at a given stress level is smaller when compared to that of the virgin material stress-strain curve. Since the critical buckling stress is, according to Eq. 5.1, directly proportional to the tangent modulus (holding all other parameters constant), it too will decrease. Typically, the more severe the inelastic straining to which a material has been subjected, the more rounded the stress-strain curve will become, and a column of this material will buckle at lower axial loads.

Once buckling occurs, the material properties of the plastic hinge would be expected to control the buckling load since these sections experience the most severe strain histories. Thus, the critical section would lie within the plastic hinge region. The critical section is chosen as the one with the most severe centroidal axial strain history. A close relationship between centroidal axial strain and cross-section curvature has been noted previously in Chapter 4.

Once the critical cross-section has been identified the most representative strain history within the cross-section must be chosen. To do this it will be assumed that the amount of Bauschinger effect that results in the material is related to the cumulative sum of the inelastic strains. Consider, for example, the critical cross-section of Strut 2 (strain gages 9, 10, 11, and 12 - Figs. A.6 and A.7). During the first four cycles gage 10 located at the extreme tensile fiber accumulates 0.026 in./in. inelastic strain, and the extreme compressive fiber at gage 12 accumulates 0.112 in./in. inelastic strain. This strain pattern is similar to that for the plastic hinge regions of the other struts tested -- that is, the compressive fibers experienced a more severe strain history than the tensile fibers. Therefore, within the same member cross-section the stress-strain curve for the compressive fiber would be more rounded than that for the tensile fiber, and the compressive fiber would exhibit smaller tangent moduli at equal stresses. The centroidal fibers underwent an intermediate level of inelastic straining, 0.041 in./in. (average of strain for gages 9 and 11).

Since the tangent modulus method considers only a single material relationship, the strain history of the centroidal fiber (centroidal axial strain) is chosen to represent the material behavior for the strut. The centroidal axial strain history represents an average of the material properties for the critical cross-section. Moreover, for the purpose of applying the tangent modulus theory of buckling, it is assumed in this treatment that the material properties at the centroid of the critical section apply for the entire column.

The material properties used to determine the tangent modulus E_t have been determined from experimentally obtained stress-strain curves. The stress-strain curves from compression

35

tests on pipe stubs were used to predict the first buckling load of virgin struts. Stress-strain curves from cyclic tests on short lengths of pipes were used to predict material properties and buckling loads once the struts have undergone inelastic straining. Alternatively, the material properties could be obtained by analytical means, if a comprehensive cyclic material constitutive law with sufficient accuracy in predicting the first derivative is available.

Prediction of First Buckling Load

In Table 5.1, the first buckling loads as calculated by the tangent modulus method and by AISC formulae are listed, along with the buckling loads observed during testing. The AISC-predicted loads do not include the customary safety factor, and $F_y = 31$ ksi was used as obtained from the material tests on pipe stubs.

The tangent modulus predictions of the first buckling loads for the struts with no previous inelastic straining are based on stress-strain curves from the compression tests of pipe stubs (Fig. 2.19). These curves exhibit classic elastic-perfectly plastic behavior. This was also true for the coupon tests (Fig. 2.16), and the first loading of the cyclic test (Fig. 2.21)

As noted in Chapter 3, strut 1 experienced inelastic straining prior to cycle 1. The buckling load predicted for Strut 1 using the tangent modulus method (Table 5.1) is based on the stress-strain relationships for material with previous inelastic straining. The AISC formula, which does not account for the effects of previous inelastic straining, predicted a higher load. The method employed to estimate the reduction in buckling capacity because of changes in material properties due to inelastic straining is discussed below.

Deterioration of Buckling Loads

As noted earlier, when inelastic strain reversals occur, a change in the stress-strain relationship of the material results. Therefore, the first step in predicting the deterioration of buckling loads under cyclic loading is to devise a means of determining the material properties as a function of inelastic strain history.

A cyclic test on a short pipe specimen of annealed material provides the characteristic stress-strain curves for inelasticity cycled material. However, since the strain history of each individual strut was different from that of the cyclic material test, strut strain histories must somehow be related to the cyclic material test. This was done by matching the amount of cumulative inelastic straining.

The basic cyclic material test (Figs. 2.21 and 5.1) can be best utilized when considered as three separate curves. The portion of the cyclic test identified in these figures as curve 1 is a stress-strain curve for previously unyielded (virgin) material. Note, that the compression test curve (Fig. 2.19) and the cyclic test curve 1 are essentially the same. Cyclic test curve 2 is a stress-strain curve for a material which had a previous inelastic tensile strain excursion of 0.0056 in./in.. Cyclic test curve 3 is a stress-strain curve for a material which had an inelastic tensile strain excursion of 0.0056 in./in. and an inelastic compressive strain excursion of 0.0104in./in. resulting in a previous cumulative inelastic strain of 0.0160 in./in.. Each successive curve corresponds to an increased cumulative inelastic strain (CIS) as well as to an increase in the magnitude of strain excursion. In the experiments the struts were loaded such that the maximum inelastic strain excursion in each successive cycle also increased. The increasing magnitudes of strain excursions tend to accentuate the Bauschinger effect in each successive cycle of either the strut loading, or material test.

The compression and cyclic test stress-strain relations for three different values of previous cumulative inelastic strain are used to develop data for predicting cyclic buckling loads of the struts. For this purpose, tangent moduli for the three available stress-strain curves are determined and plotted versus the corresponding stresses (Fig. 5.2), and Eq. 5.1 is rearranged to yield the critical slenderness ratio in terms of the corresponding stress and tangent modulus:

$$(kL/r)_{cr} = \pi\sqrt{E_t/\sigma} \qquad (5.3)$$

Using Eq. 5.3 and Fig.5.2 the column curves shown in Fig. 5.3 have been constructed. From these curves three different values of critical stress, each corresponding to a different value of

cumulative inelastic strain, can be obtained for a given slenderness ratio kL/r. In Figs. 5.4a and 5.4b the variation of the critical stress as predicted by the tangent modulus method is plotted versus the cumulative inelastic strain for column slenderness ratios of 25 and 54, respectively. The experimentally observed critical stresses for the struts with the same slenderness ratios are also plotted in these figures.

Critical stresses for the struts for any given cycle of loading prior to local buckling are estimated by entering Fig. 5.4 with the total inelastic strain accumulated during preceding cycles. The predicted buckling loads are given in Table 5.2. The curves in Fig. 5.4 clearly show that the critical stresses decrease with increasing cumulative inelastic strain. For the annealed struts (Struts 1,2,5, and 6), the experimentally observed critical stresses are in reasonably good agreement with the predicted values.

The experimental results clearly demonstrate that the compressive load capacity of struts deteriorates with inelastic cycling. The conventional AISC formulas by which column buckling loads are predicted do not account for this deterioration under inelastic cycling and therefore should not be used to predict column response for such conditions. The cyclic buckling load of struts determined using the generalized tangent modulus method were in good agreement with experimental values. (Table 5.2).

Observations on predicting the buckling loads of struts subjected to inelastic cycling as described in this report can be summarized as follows:

1) Accurate information on the material properties under inelastic cyclic loading is essential.

2) The procedure described does not apply after local buckling occurs.

3) The tangent modulus concept assumes the material properties of the column are homogeneous. The strain history used for determining the material properties is taken from the section within the plastic hinge region that has undergone the most severe straining.

4)   The inelastic strain history that best represents the average material properties of the critical cross-section is that of the centroidal fiber.

5)   Inelastic axial strain is related to inelastic curvature at a section.

6)   Inelastic axial strain varies considerably along the length of a column. The average axial strain (total deformation divided by a total column length) is not sufficient to define the material properties of the critical section.

The generalized tangent modulus procedure described above provides an estimate in the reduction of the buckling capacity of a column due to changes in the material properties. The buckling capacity of a column will also reduce due to a large residual camber. If there is a significant residual camber after load applications a reduction in the buckling capacity for camber must also be applied. The loading sequence of the experimental struts was such that the residual cambers were relatively small in the early cycles. In each cycle, compressive loads were followed by tension yielding excursions of sufficient magnitude to re-straighten the member. The axial load vs. midspan lateral deflection plots are given in Figs. 3.15, 3.16, 3.19 and 3.20 for the annealed struts.

For cycles in which buckling load predictions were made, Struts 1 and 6 actually had less residual camber in later cycles than they did prior to cycle 1. Struts 2 and 5 had maximum residual cambers of 0.20 in. (5 mm) and 0.05 in. (1 mm), respectively, for cycles in which buckling predictions were made. These residual cambers were considered small and a camber reduction factor to the estimated buckling load was not applied. A method for estimating the reduction factor for residual camber is given in Ref. 9.

The generalized tangent modulus procedure for estimating reductions in the buckling capacity of columns due to changes in material properties is applicable up to the point of local buckling. Since local buckling is a major concern in thin-walled pipes, the predictions of cyclic buckling loads for the test struts had this limitation.

CHAPTER 6

INELASTIC BEHAVIOR OF THE UNANNEALED STRUTS

The inelastic behavior of the unannealed struts is sufficiently different from that of the annealed ones to be treated separately. The mechanical properties of the unannealed material significantly differed from those for the annealed material as is evident from the coupon tests (Fig. 2.18). These material properties also differ significantly from those found in members used in the building and offshore industries. Therefore, the behavior of these unannealed struts is of limited interest and a detailed study of their inelastic behavior was not pursued.

Characteristics of the Material Properties

The Drawn-Over-Mandril process utilized in manufacturing the pipes used in the experiments imparts a high degree of work hardening into the steel. Some of the struts (1, 2, 5, and 6) were annealed to relieve this work hardening so that their material properties more closely represent those of full scale structural members used in construction. The as received struts (3 and 4) were tested to evaluate the necessity of annealing the test specimens to be representative of the behavior of large pipes. The structural inelastic responses of the unannealed struts were found to be significantly different from those of the annealed struts (Figs. 3.26 and 3.27).

Using a 0.2% offset strain, the coupon tests of the unannealed material indicate σ_y was 92 ksi (635 MPa) for the 0.083 in. (2.1 mm) wall thickness, and 74 ksi (511 MPa) for the 0.0120 in. (3.0 mm) wall thickness. These are 197% and 139% higher than the yield strengths of the annealed material.

Stress-strain curves for unannealed material coupons, cyclic stub specimens, and compression stub tests are shown in Figs. 6.1 and 6.2. Because of the high degree of work hardening already existing in the steel, the stress-strain curves differ with each pipe sample, type of test employed and the direction of loading. For example, at a strain of 0.006 in./in. on the thinner walled pipe (Fig. 6.1) stresses from different tests range from 71 ksi (490 MPa) to 94 ksi (649 MPa). Therefore, a large scatter exists in the material stress-strain curves, both in stress and in

tangent modulus E_t at any given strain level .

Prediction of Buckling Loads

As discussed in the previous chapter, estimations of the deterioration of buckling loads under cyclic loading depends on the ability to determine changes in material properties. For the unannealed struts the increase in inelastic strain due to the applied cyclic strains is a small percentage of the inelastic strain already induced by the manufacturing process. Nevertheless, the generalized tangent modulus procedure was applied to the unannealed struts, and the results are presented in Table 6.1.

Tangent modulus predictions of the first buckling loads are given in Table 6.1a along with the actual buckling loads and the buckling loads given by the AISC formulae. (Note, first buckling of Struts 3 and 4 occurs in cycle 2.) The AISC load predictions are based on the yield stresses determined by the 0.2% offset strain method for the coupon test results. The first buckling loads for Struts 3 and 4 were 15% and 35%, respectively, below those given by the AISC formulae.

As can be seen from Figs. 6.1 and 6.2, compression tests on the unannealed pipe show a more rounded stress-strain curve and lower stress levels for a greater strain compared to the coupon tensile tests. The tangent modulus method using the compression stub test stress-strain curves predicts the first cycle buckling loads for Struts 3 and 4 to within 4% and 3% respectively, of the actual values. The full cross-section compression tests include residual stress effects present in the unannealed material.

Estimates of buckling loads in later cycles are based on the material stress-strain curves obtained from the unannealed cyclic stub tests. Column curves for predicting the critical stresses, Figs. 6.3 and 6.4, were prepared in the same way as for the annealed struts. These curves were used to predict cyclic buckling loads for Struts 3 and 4. For example, the amount of cumulative inelastic strain for the cyclic stub test curve 3 was matched with a similar amount of cumulative inelastic strain for a cycle of the strut tests (Table 6.1b). The loads predicted

using the corresponding tangent modulus were not in agreement with the actual loads. For Strut 4 the buckling load for cycle 5 predicted using the cyclic material test results was higher than the predicted load for cycle 2 using the compression test. The reason is the higher yield stresses of the cyclic test. Note that all three curves of the cyclic stub test for the thick walled material show yielding at significantly higher stress levels than the compression stub test (Fig. 6.2). Also, cyclic curve 3 for tension loading shows yielding at higher stress levels than cyclic curve 2 for compression loading. Thus, the scatter in the material stress-strain curves due to different sample of pipe and directions of loading are greater than the changes in the material properties resulting from the cyclic loading.

To properly apply the generalized tangent modulus procedure as presented in Chapter 5, to the unannealed struts, a considerably more comprehensive cyclic material test program would be required. Since it appears that the unannealed struts do not realistically represent actual tubular members used in practice, such a further evaluation is not warranted.

CHAPTER 7

CONCLUSIONS

The struts discussed in this report are grouped into three different pairs: pinned-end annealed, pinned-end unannealed, and fixed-end annealed. Each pair consists of one strut with a D/t of 48 and one with a D/t of 33. Based on the reported experimental results and their evaluation, several important conclusions can be reached. These can be summarized as follows:

1) For all three pairs, the struts with D/t of 33 clearly out performed the ones with D/t of 48 in percentage retainment of their original buckling load.

2) Local buckling of thin walled pipes greatly contributes to their deterioration. The onset of local buckling is followed by a rapid deterioration in the overall structural response of a strut with continued cyclic loadings. For all three pairs, local buckling occurred later in the struts with D/t of 33 than in the struts with D/t of 48. Hence, in the design of tubular structures for seismically active regions, bracing members with the lower D/t ratio are preferable for avoiding local failures under repeated cyclic loadings.

3) Cyclic inelastic load applications can cause local buckling and loss of capacity of tubular members that, under API recommendations, are considered to be adequate for maintaining their capacity through substantial concentrated inelastic deformation $(D/t \leqslant 1300/F_y)$. Hence, API criteria, based on monotonic loading, do not necessarily preclude local buckling of tubular braces under severe cyclic loading.

4) Brace end conditions have a significant effect on the overall structural response of strut members subjected to cyclic loadings. The responses of fixed-end pair of braces showed less pinched hysteretic loops, slower deterioration of buckling capacity, delayed onset of local buckling and improved efficiency in energy dissipation compared to those of the pinned-end braces. The superior performance of the fixed-end struts is attributed to their lower kL/r ratio.

5) In simulating the behavior of real braces using reduced-scale models, the steel tubes must be annealed before testing. In small tubes the steel in the as-received condition may be highly work-hardened, and the stress-strain curves for such a material bear little resemblance to the A36 steel used in the field. By annealing the specimens, the typical mechanical behavior for mild steel is restored. Although residual stresses associated with manufacture of large diameter welded tubing are not present, the annealed tubing are more realistic than the as received material. The pair of braces tested in the as-received condition proved to be too brittle to sustain cyclic loading at large inelastic ductility levels, and failed in the welded regions. The difference in the mechanical material properties of the unannealed pair caused a significant difference in their overall structural response. Normalized axial loads and axial displacements obtained by dividing the loads and displacements by the yield loads and the yield displacements, respectively, are not sufficient to account for the observed difference in cyclic response caused by the difference in material properties.

6) Cyclic inelastic loading causes changes in the mechanical properties of the material in a strut which tend to reduce the strut's buckling load. If the changes in the material properties can be adequately assessed, the reduction in the buckling load can be estimated using the generalized tangent modulus procedure described in Chapter 5. If the cyclic load applications result in increased residual brace cambers, a camber reduction factor must also be applied [9].

Recommendations for Future Research

As previously stated, local buckling is a major concern for the thin-walled tubular braces typical of those employed in braced steel structures. Local buckling can be expected in members subjected to the large axial deformations which may be encountered during an exceptionally severe earthquake. The phenomenon of local buckling has not been isolated in this

investigation, nor studied in sufficient detail to accurately estimate its onset and effect on subsequent deterioration in brace capacity. Full size local buckling tests of tubular sections under cyclic load application accompanied by analytical studies are suggested for investigating this problem.

Realistic analytical models of brace elements are essential for accurate prediction of the response of braced steel structures subjected to severe earthquake ground motions. Several analytical models have previously been employed to represent the inelastic cyclic behavior of bracing members [3, 5, 13, 15]. In the light of new experimental data, these analytical models should be re-examined and, if necessary, improved to better represent cyclic brace behavior. Since the hysteretic response of a brace element is strongly dependent on the kL/r ratio, an analytical model should account for this fact in a realistic manner. The reduction in buckling load with cyclic load applications should be included in such a model.

REFERENCES

1. Sozen, M. A. and Roesset, J., "Structural Damage Caused by the 1976 Guatemala Earthquake," *Structural Research Series No. 426,* University of Illinois, Urbana, Champaign, March 1976.

2. Popov, E. P., Takanashi, K., and Roeder, C. W., "Structural Steel Bracing Systems: Behavior Under Cyclic Loading," *EERC Report No. 76-17,* Earthquake Engineering Research Center, University of California, Berkeley, June 1976.

3. Roeder, C. W., and Popov, E. P., "Inelastic Behavior of Eccentrically Braced Frames Under Cyclic Loading," *EERC Report No. 77-18,* Earthquake Engineering Research Center, University of California, Berkeley, CA, August 1977.

4. Popov, E. P., and Roeder, C. W., "A Structural Support System for Long Span Roofs in Seismic Regions," *Proceedings,* AISS Conference, Alma-Ata, USSR. Vol. 2, Mir Publishers, 1977, pp. 274-281.

5. Nilforoushan, R., "Seismic Behavior of Multi-Story K-Braced Frame Structures," *University of Michigan Research Report UMEE 73R9,* November, 1973.

6. Hanson, R. D., Goel, S. C., And Berg, G. V., "Seismic Behavior of Staggered Truss Framing Systems - Design Procedure for Earthquake Loading," *University of Michigan Research Report UMEEE No. 175,* January 1973.

7. Shign, P., "Seismic Behavior of Braces and Braced Steel Frames," *University of Michigan Research Report UMEE 77R1,* July 1977.

8. Jain, A. L., Goel, S. C., and Hanson, R. D., "Hysteresis Behavior of Bracing Members and Seismic Response of Braced Frames with Different Proportions," *University of Michigan Research Report UMEE 78R3,* July 1978.

9. Popov, E. P., "Inelastic Behavior of Steel Braces Under Cyclic Loading," *Proceedings,* 2nd U.S. National Conference on Earthquake Engineering, Stanford University, CA, Aug. 1979.

10. American Institute of Steel Construction, *Manual of Steel Construction,* Seventh Edition, New York, 1970.

11. American Petroleum Institute, "Recommended Practice for Planning, Designing, and Constructing Fixed Offshore Platforms," Dallas, Texas, Ninth Edition, November, 1977; Tenth Edition, March 1979.

12. Gates, W. E., Marshall, P. W., and Mahin, S. A., "Analytical Methods for Determining the Ultimate Earthquake Resistance of Fixed Offshore Structures," *Proceedings,* Offshore Technology Conference, Houston, Texas, 1977.

13. Jain, A. K. and Goel, S. C., "Hysteresis Models for Steel Members Subjected to Cyclic Buckling or Cyclic End Moments and Buckling," *University of Michigan Research Report UMEE 78R6*, December 1978.

14. Sherman, D. R., "Cyclic Inelastic Behavior of Beam Columns and Struts," *Preprint 3302*, ASCE Convention and Exposition, Chicago, October 1978.

15. Marshall, P. W., Gates, William E., and Anagnostopoulos, Stavros, "Inelastic Dynamic Analysis of Tubular Offshore Structures," *Proceedings*, Offshore Technology Conference, Houston, Texas, 1977.

16. Popov, Egor P. and Ortiz, Miguel, "Macroscopic and Microscopic Cyclic Metal Plasticity," *Proceedings*, Third Engineering Mechanics Specialty Conference, ASCE, Austin, Texas, September 1979.

17. Galambos, Theodore, V., *Structural Members and Frames*, Prentice-Hall, 1968.

Strut (1)	End Conditions (2)	Heat Treatment (3)	Wall Thickness in. (mm) (4)	D/t (5)	$\frac{kL}{r}$ (6)	Initial Camber in. (mm)	
						Horizontal (7)	Vertical (8)
1	Pinned	Annealed	0.083 (2.1)	48	54	0.25 (6.4)	0.00 (0.0)
2	Pinned	Annealed	0.120 (3.1)	33	54	0.06 (1.5)	0.03 (0.8)
3	Pinned	As Received	0.083 (2.1)	48	54	0.00 (0.0)	0.00 (0.0)
4	Pinned	As Received	0.120 (3.1)	33	54	0.03 (0.8)	0.00 (0.0)
5	Fixed	Annealed	0.083 (2.1)	48	25	0.13 (3.3)	0.00 (0.0)
6	Fixed	Annealed	0.120 (3.1)	33	25	0.18 (4.6)	0.03 (0.8)

Table 2.1 Characteristics of 4-in. (102-mm) Diameter Strut Specimens

Strut	σ_y Average From Material Test (ksi)	Nominal Cross-Section Area (in^2)	Length of Tubing (in)	P_y (kips)	δ_y (in)
1	31	1.02	55.38	31.6	0.058
2	31	1.46	55.38	45.3	0.058
3	92	1.02	55.38	93.8	0.173
4	74	1.46	55.38	108.0	0.139
5	31	1.02	70.25	31.6	0.074
6	31	1.46	70.25	45.3	0.074

Table 2.2   Strut Yield Loads Predicted
From Material Test

(1 kip = 4.45 kN; 1 in. = 25.4 mm;
1 ksi = 6.9 MPa)

		1	2	3	4	5	6	7	8	9	10	11	12	13	14	Tol. (kips)
Strut 1	$P_{Comp.\ Max.}$	23.0*	21.5	19.5†	16.2	13.8	10.8	4.1								±0.5
	$P_{Ten.\ Max.}$	28.0	30.3	30.0	30.1	29.8	17.0	2.8								
Strut 2	$P_{Comp.\ Max.}$	43.7	40.0*	31.3	27.5	23.5†	22.0	16.8	14.0	6.0						±0.5
	$P_{Ten.\ Max.}$	44.7	44.0	44.0	43.1	43.0	38.6	33.0	19.0	6.0						
Strut 3	$P_{Comp.\ Max.}$	51.0	60.4*	46.9	44.8†	24.0	19.2	13.7	6.6							±0.5
	$P_{Ten.\ Max.}$	49.5	82.9	86.5	59.7	60.1	24.5	4.5	0.0							
Strut 4	$P_{Comp.\ Max.}$	40.7	57.5*	54.5	55.7	41.9	38.9	37.6	38.4	38.4	39.0					±0.5
	$P_{Ten.\ Max.}$	56.1	97.2	99.7	84.6	89.4	89.0	98.5	101.6	102.5	102.8					
Strut 5	$P_{Comp.\ Max.}$	28.0	31.5	32.5	32.0*	28.0†	23.0	20.0	17.5	16.0	14.0	12.0	9.8	7.0		±1.0
	$P_{Ten.\ Max.}$	31.2	32.5	33.0	32.5	32.0	32.0	30.0	29.5	26.5	23.0	17.0	13.0	10.2		
Strut 6	$P_{Comp.\ Max.}$	28.0	42.0	44.5*	40.0	38.5	37.5	37.0	36.5	35.5	35.0†	34.5	30.5	28.0	27.0	±1.0
	$P_{Ten.\ Max.}$	35.0	44.0	44.5	44.0	44.0	44.0	42.5	42.5	43.5	43.0	43.0	42.0	41.0	41.8	

*Cycle in which noticeable lateral buckling first occurred

†Cycle in which local buckling first occurred

Table 3.1   Maximum Compressive and Tensile
Loads in Each Cycle

(1 kip = 4.45 kN)

50

CYCLE

		1	2	3	4	5	6	7	8	9	10	11	12	13	14	TOL. (in.)
Strut 1	$\delta_{Comp.\ Max}$	-.072	-.142	-.212	-.282	-.356	-.367	-.367	-.369							
	$\delta_{Ten.\ Max}$	.076	.141	.210	.279	.346	.358	.359	.348							
Strut 2	$\delta_{Comp.\ Max}$	-.073	-.140	-.216	-.282	-.357	-.358	-.363	-.360	-.350						
	$\delta_{Ten.\ Max}$	.074	.141	.209	.278	.345	.350	.344	.341	.343						
Strut 3	$\delta_{Comp.\ Max}$	-.075	-.138	-.194	-.225	-.303	-.307	-.310	-.309							
	$\delta_{Ten.\ Max}$	.072	.142	.170	.080	.082	.067	.061	-							
Strut 4	$\delta_{Comp.\ Max}$	-.070	-.145	-.200	-.285	-.354	-.351	-.351	-.351	-.351	-.351					
	$\delta_{Ten.\ Max}$	.070	.14-	.164	.052	.065	.061	.100	.112	.125	.138					
Strut 5	$\delta_{Comp.\ Max}$	-.068	-.144	-.218	-.284	-.358	-.354	-.356	-.403	-.454	-.500	-.553	-.668	-.703		
	$\delta_{Ten.\ Max}$	.062	.140	.210	.277	.347	.347	.343	.346	.344	.343	.345	.346	.346		
Strut 6	$\delta_{Comp.\ Max}$	-.065	-.143	-.213	-.286	-.358	-.362	-.367	-.416	-.473	-.527	-.578	-.627	-.674	-.680	
	$\delta_{Ten.\ Max}$	.069	.142	.214	.282	.342	.338	.330	.330	.338	.372	.394	.426	.472	.576	

Table 3.2   Maximum Compressive and Tensile
Displacements in Each Cycle

(1 in. = 2.54 cm)

CYCLES		1	2	3	4	5	6	7	8	9	10	11	12	13	14
	E_i	2.97	7.47	10.66	9.82	10.46	7.09	2.87							
Strut 1	RP_i	6.95	14.50	23.19	31.92	40.67	44.05	44.94							
	E_i/RP_i	0.43	0.52	0.46	0.31	0.26	0.16	0.06							
	E_i	4.00	11.95	15.36	17.89	17.32	14.00	11.67	9.06	4.84					
Strut 2	RP_i	9.97	20.74	33.66	45.75	58.52	62.02	62.38	61.97	61.38					
	E_i/RP_i	0.40	0.58	0.46	0.39	0.30	0.23	0.19	0.15	0.08					
	E_i	0.56	9.18	15.00	12.59	8.45	7.29	3.21							
Strut 3	RP_i	20.82	39.21	54.31	54.59	64.53	63.88	66.13							
	E_i/RP_i	0.03	0.23	0.28	0.23	0.13	0.11	0.05							
	E_i	0.98	7.15	13.19	18.15	19.10	18.41	21.28	23.98	25.16					
Strut 4	RP_i	22.68	46.44	60.05	67.72	79.27	77.87	82.30	83.59	88.02					
	E_i/RP_i	0.04	0.15	0.22	0.27	0.24	0.24	0.26	0.29	0.29					
	E_i	1.00	6.37	13.53	20.66	23.05	17.67	16.00	16.81	17.57	15.56	13.59	12.07	9.40	
Strut 5	RP_i	6.26	13.52	22.69	30.87	39.72	41.87	41.87	44.94	48.13	51.00	54.42	61.68	63.61	
	E_i/RP_i	0.16	0.47	0.60	0.67	0.58	0.42	0.38	0.37	0.37	0.31	0.25	0.20	0.15	
	E_i	0.82	9.30	15.24	24.22	32.33	33.59	32.87	34.92	38.59	39.36	44.18	43.07	43.51	46.47
Strut 6	RP_i	9.01	19.39	31.26	43.94	56.31	59.34	59.16	63.28	68.81	75.56	82.94	90.01	97.85	105.14
	E_i/RP_i	0.09	0.48	0.49	0.55	0.57	0.57	0.56	0.55	0.56	0.52	0.53	0.48	0.44	0.44

E_i = energy absorbed in cycle i (kip-inch)

RP_i = energy absorbed in ideal rigid-plastic element (kip-inch)

Table 3.3 Energy Absorption Per Cycle (1 kip-in = 0.113 kN-m)

Load Points	Length of Plastic Region ±0.5 in (±12.7 mm)	Inelastic Rotation in Plastic Region ±0.005 radian	Cum. Inelastic Rotation in Plastic Region radians	Max. Comp. Load kips (kN)
1C	10.25 (260.3)	0.017	0.017	23.0 (102.3)
1E		-0.006	0.040	
2C	12.50 (317.5)	0.045	0.091	21.5 (95.7)
2E		-0.005	0.141	
3LB	13.00 (330.2)	0.057	0.203	19.5 (86.8)

Table 4.1 Plastic Region Inelastic Rotations – Strut 1

Load Points	Length of Plastic Region* ±0.5 in (±12.7 mm)	Inelastic Rotation in Plastic Region ±0.005 radian	Cum. Inelastic Rotation in Plastic Region radians	Max. Comp. Load kips (kN)
3C	8.25 (209.5)	0.060	0.060	31.5 (140.2)
3E		0.007	0.113	
4C	8.75 (222.2)	0.093	0.199	27.5 (122.4)
4E		0.016	0.276	
5LB	8.12 (206.2)	0.061	0.321	23.5 (104.6)

* $\frac{1}{2}$ length of center plastic hinge.

Table 4.2 Plastic Region Inelastic Rotations – Strut 2

Load Points	Length of Plastic Region ±0.5 in. (±12.7 mm)	Inelastic Rotation in Plastic Region radians	Cum. Inelastic Rotation in Plastic Region radians	Max. Comp. Load kips (kN)
1C	4 (101.6)	−0.0029	0.0029	28.0 (124.6)
1E		−0.0087	0.0087	
2C	6 (152.4)	−0.0055	0.0119	31.5 (140.2)
2E		−0.0165	0.0229	
3C	10 (254.0)	−0.0046	0.0348	32.5 (144.6)
3E		−0.0145	0.0447	
4C	10 (254.0)	0.0131	0.0723	32.0 (142.4)
4E		−0.0135	0.0989	
5LB	10 (254.0)	−0.0014	0.1110	28.0 (124.6)

Table 4.3   Foot Plastic Region Inelastic Rotations – Strut 5

Load Points	Length of Plastic Region ±0.5 in. (±12.7 mm)	Inelastic Rotation in Plastic Region radians	Cum. Inelastic Rotation in Plastic Region radians	Max. Comp. Load kips (kN)
2E		0	0	
3C	4 (101.6)	0.0135	0.0135	49.5 (220.3)
3E		-0.0077	0.0347	
4C	6 (152.4)	0.0217	0.0642	40.0 (178.0)
4E		-0.0075	0.0935	
5C	10 (254.0)	0.0372	0.1382	38.5 (171.3)
5E		0.0005	0.1750	
6C	10 (254.0)	0.0427	0.2172	37.5 (166.9)
6E		-0.0042	0.2642	
7C	10 (254.0)	0.0432	0.3117	37.0 (164.6)
7E		-0.0037	0.3587	
8C	10 (254.0)	0.0467	0.4092	36.5 (162.4)
8E		0.0005	0.4555	
9C	10 (254.0)	0.0527	0.5077	35.5 (158.0)
9E		0.0012	0.5592	
10LB	10 (254.0)	0.0580	0.6160	35.0 (155.7)

Table 4.4 Foot Plastic Region Inelastic Rotations – Strut 6

	STRUT 1 (D/t = 48)	STRUT 2 (D/t = 33)	STRUT 5 (D/t = 48)	STRUT 6 (D/t = 33)
Cycle at Local Buckling	3	5	5	10
Load at Local Buckling (kips)	12.2	17.8	28.0	30.6
Cumulative Inelastic Curvature (radians/in.)	0.021	0.048	0.019	0.091
Cumulative Inelastic Axial Strain (in./in.)	0.034	0.057	0.072	0.154
Cumulative Inelastic Compressive Fiber Strain (in./in.)	0.069	0.148	0.116	0.347
Maximum Curvature Excursion (radians/in.)	0.007	0.014	0.004	0.009
Cumulative Inelaastic Rotation (radians)	0.203	0.321	0.111	0.616
Cumulative Energy Dissipated (kip-in.)	21.1	66.5	64.6 (32.3)*	261.2 (130.6)*
Magnitude of Curvature at L.B. (radians/in.)	0.007	0.015	0.000	0.010
Magnitude of Compressive Fiber Strain at L.B. (in./in.)	-0.021	-0.039	-0.003	-0.038

* $\frac{1}{2}$ total strut energy.

Table 4.5 Summary of Rotations, Curvatures Strains, and Energy Dissipation at First Occurrence of Local Buckling

(1 kip = 4.45 kN, 1 in. = 25.4 mm)

Strut No.	Buckling Load by Tangent Modulus Method (kips)	Buckling Load by AISC Formulas (Without Factor of Safety) (kips)	First Buckling Load from Test (kips)
1	24.3	29.2	23
2	45.3	41.7	43.7
5	31.6	31.1	31.5
6	45.3	44.5	44.5

Note: Tolerances of predicted loads are ±0.5 k due to curve plotting
accuracy limits.

Table 5.1   Predictions of First
Buckling Loads-Annealed Struts

(1 kip = 4.45 kN)

		Cumulative Inelastic Centroidal Strain* (in/in)	Predicted Buckling Load (kips)	Actual Buckling Load (kips)
Strut 1	CY 1	.00407	24.3	23.0
	CY 2	.01017	20.0	21.5
	CY 3	.01815	19.4	19.5
	CY 4	.03115	Beyond Local Buckling	16.2
	CY 5	.03979	Beyond Local Buckling	13.8
Strut 2	CY 1	0	45.3	43.7
	CY 2	.0002	43.8	40.0
	CY 3	.01470	28.2	31.3
	CY 4	.03070	26.0	27.5
	CY 5	.04885	Beyond Local Buckling	23.5
Strut 5	CY 1	0	31.6	Elastic Cycle; No Buckling
	CY 2	~ 0	31.6	31.5
	CY 3	~ 0	31.6	32.5
	CY 4	.00010	31.6	32.0
	CY 5	.01591	27.9	28.0
Strut 6	CY 1	0	45.3	Elastic Cycle; No Buckling
	CY 2	0	45.3	42.0
	CY 3	.00020	45.3	44.5
	CY 4	.00119	43.1	40.0
	CY 5	.01062	40.0	38.5

*Based on center hinge

Table 5.2   Predicted Buckling Loads for Annealed Struts (1 kip = 4.45 kN)

Strut No.	Tangent Modulus Method (kips)	AISC Formulae (Without Factor of Safety) (kips)	Actual First Buckling Load in Test (kips)
3	57.8	70.8	60.4
4	59.5	88.0	57.5

(A)   First Buckling Load

	Cumulative Inelastic Strain in Cyclic Material Test (in/in)	Cycle of Strut Test With Similar Cumulative Strain History	Cumulative Inelastic Centroidal Strain Preceding Strut Test Cycle Noted (in/in)	Predicted Buckling Load From Cyclic Material Test (kips)	Actual Buckling Load in Noted Cycle (kips)
Strut 3	.017	4th	.013	52.3	44.8
Strut 4	.020	5th	.017	65.1	55.7

(B)   Buckling Load in Later Cycle

Table 6.1 Predicted Buckling Loads for Unannealed Struts
(1 kip = 4.45 kN)

FIGURES
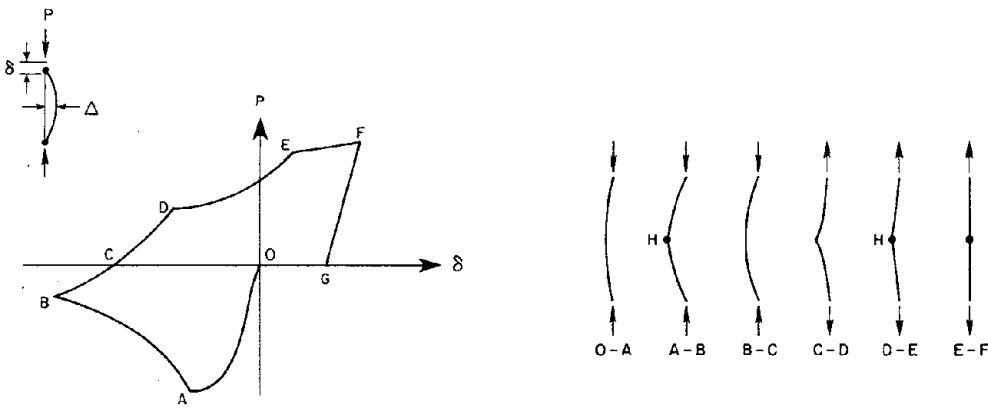
A) Hysteretic Behavior   B)   Zones of Behavior

Fig. 1.1   Typical load deformation Relationship of a Brace Member [2]
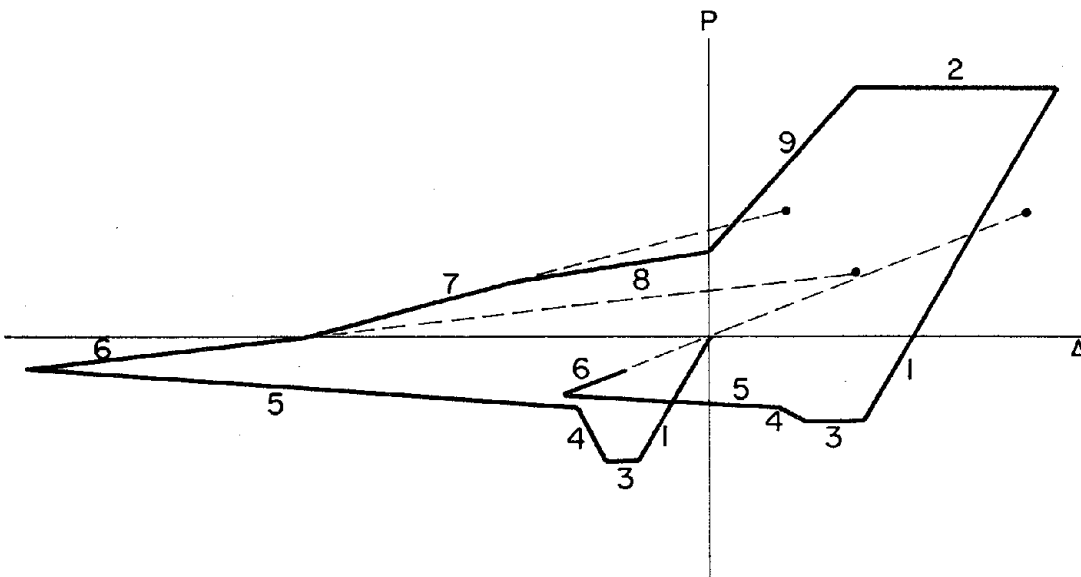
Fig. 1.2   Linearized Model of Post-Buckling Brace Behavior [3]
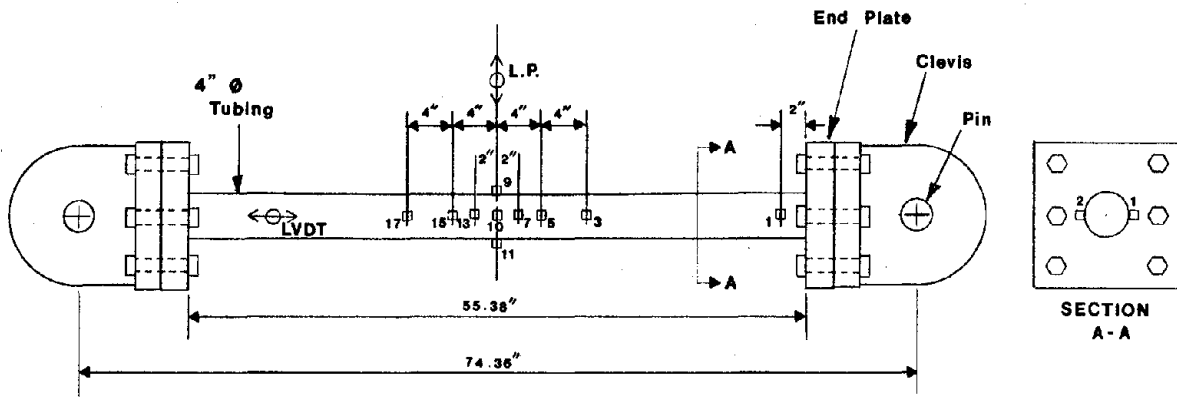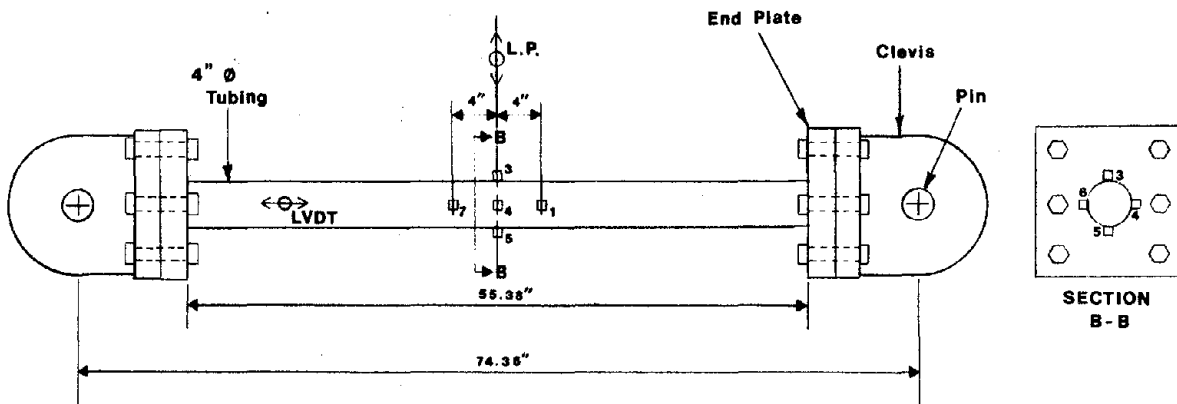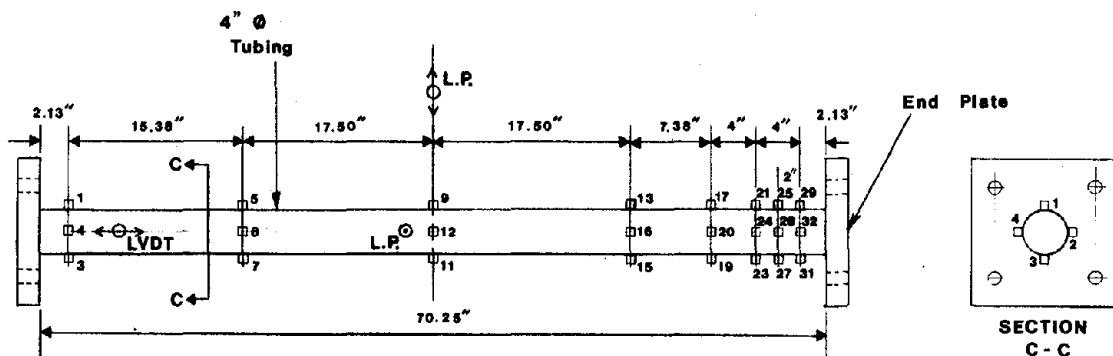
a) Frame Elevation

b) 1:6 Scale Model of a Braced Panel

Fig. 2.1 Southern California Example Structure (1 in. = 25.4 mm)

Fig. 2.2   Test Specimens (1 in. = 25.4 mm)
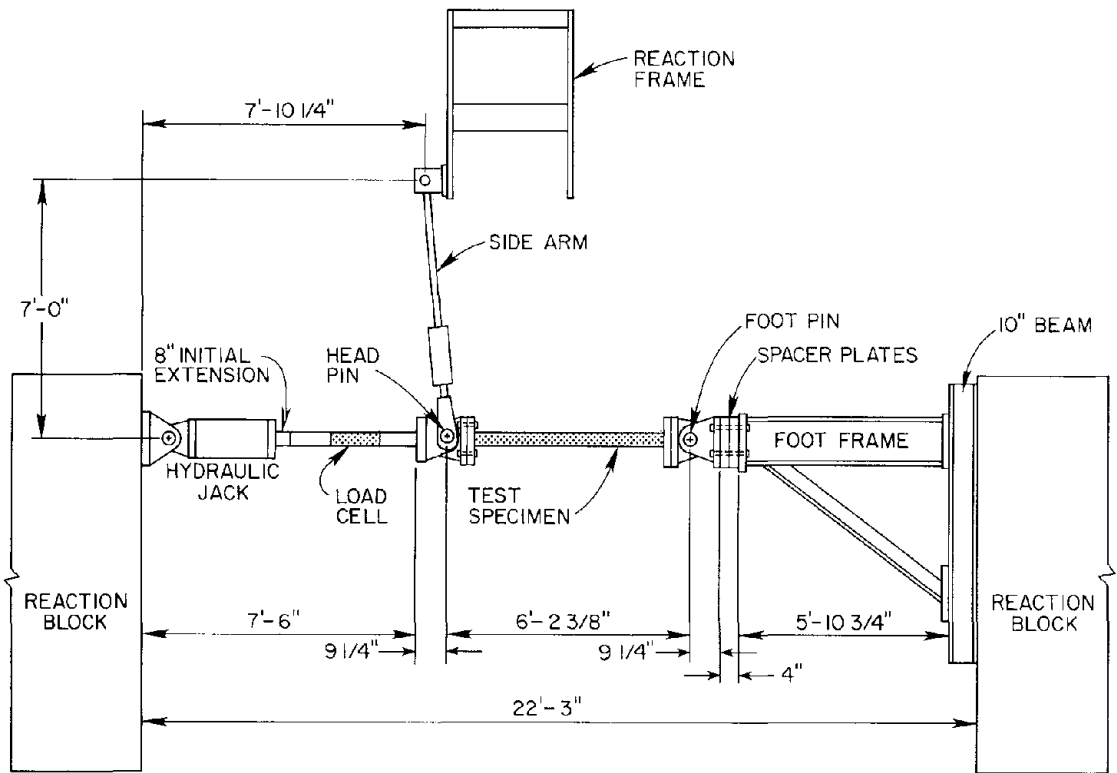
(a) PINNED-PINNED TEST LAYOUT
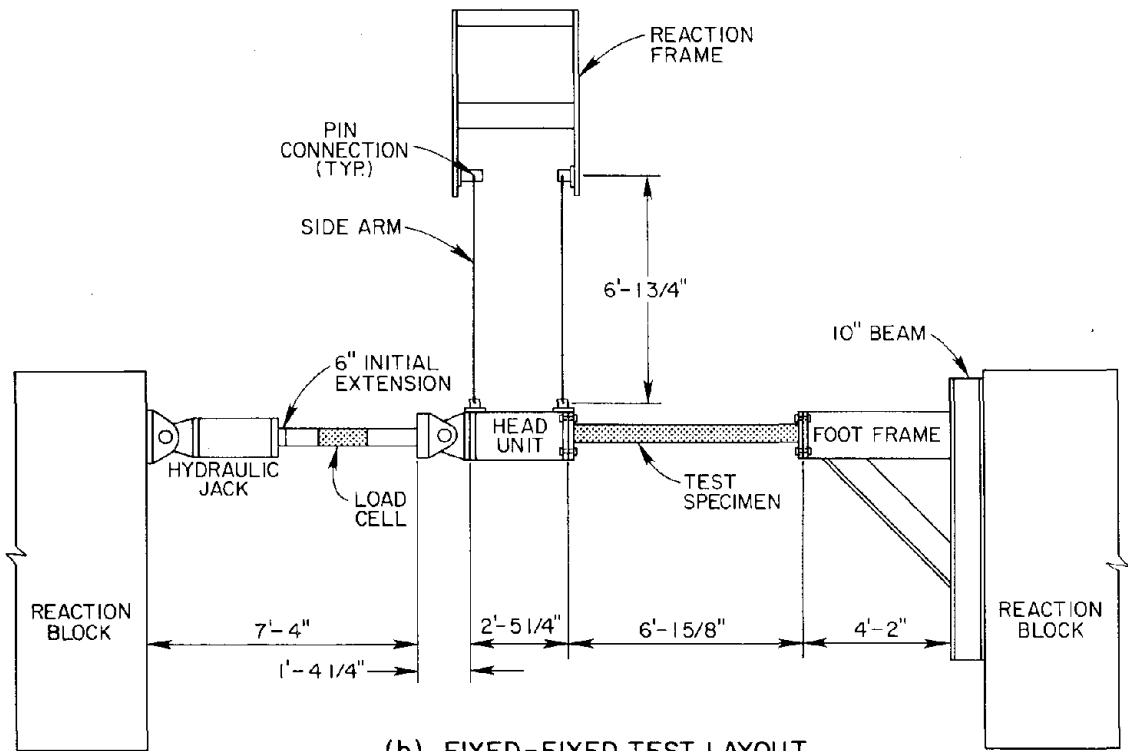
(b) FIXED-FIXED TEST LAYOUT

Fig. 2.3 Experimental Test Set-Up (1 in. = 25.4 mm)
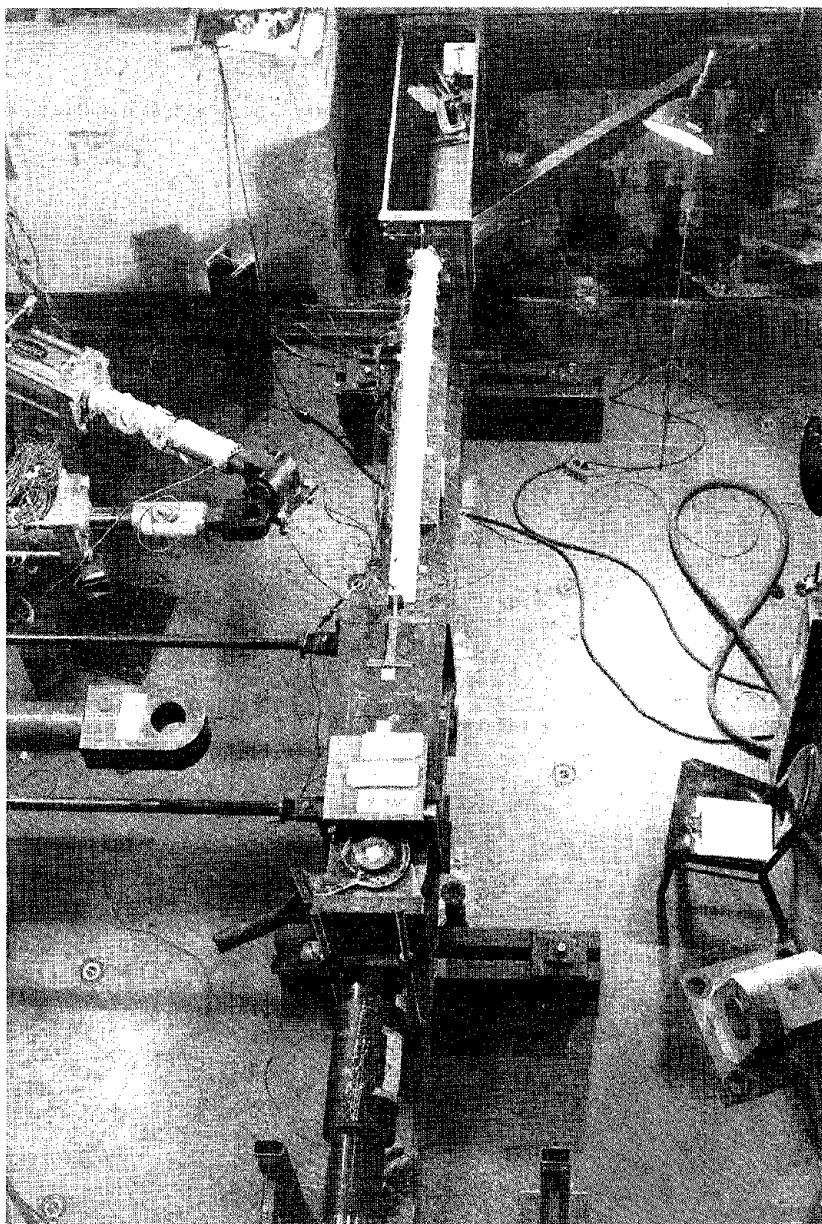
Fig. 2.4 Fixed-Fixed Experimental Setup
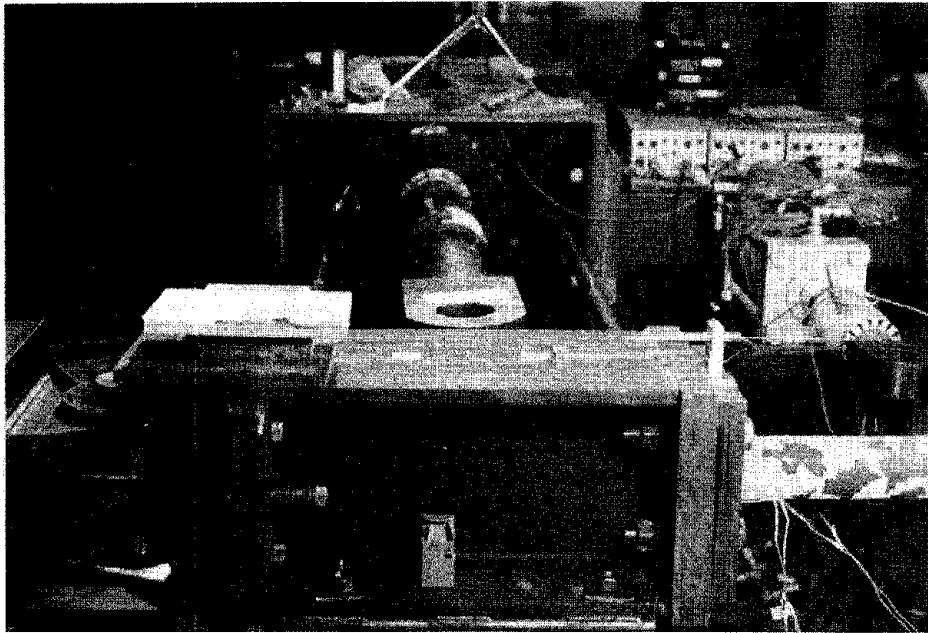
a) Head Unit
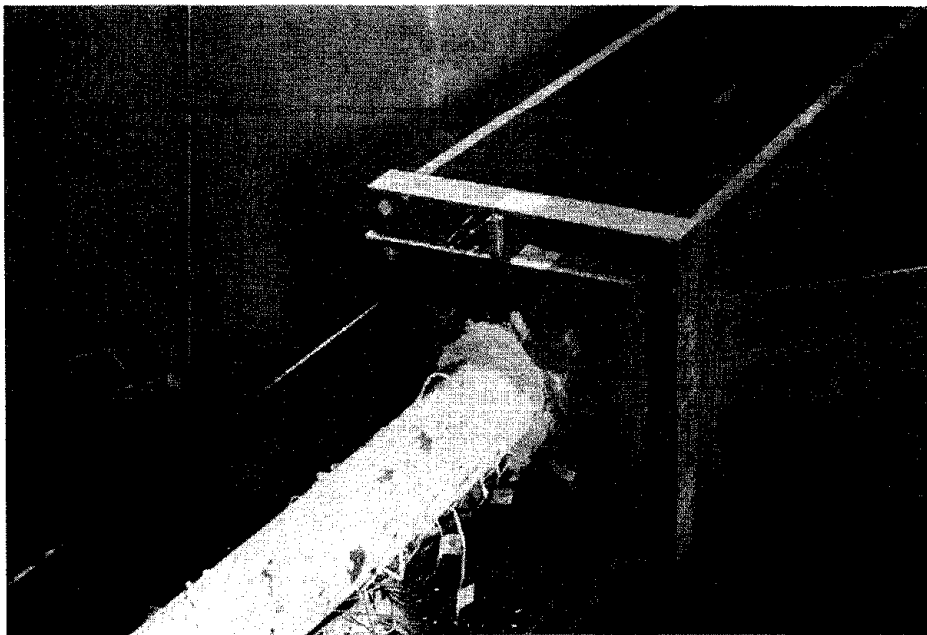
b) Specimen Connection to Foot Frame

Fig. 2.5 Fixed-Fixed Experimental Setup

a) Load Control Equipment

b) Clevis Used for Pin Connection

Fig. 2.6 Experimental Equipment

68
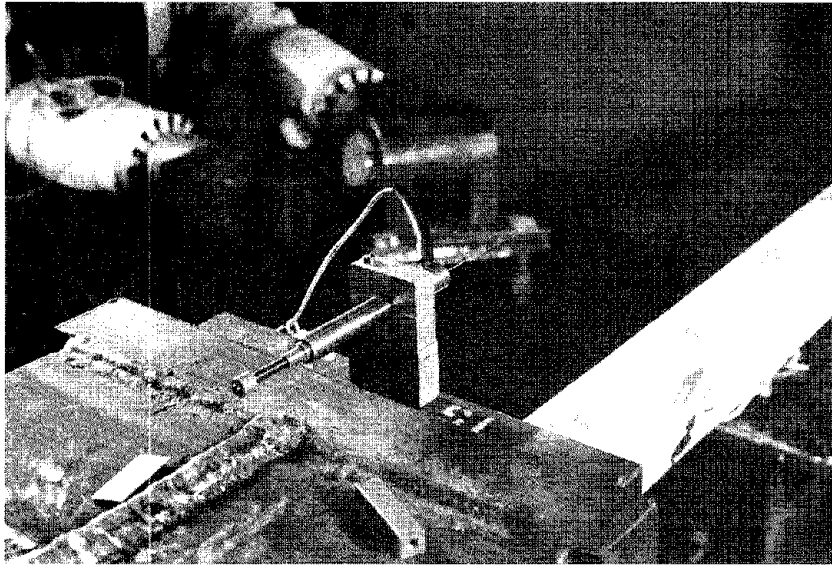
a) LVDT Used for Measuring Axial Displacement
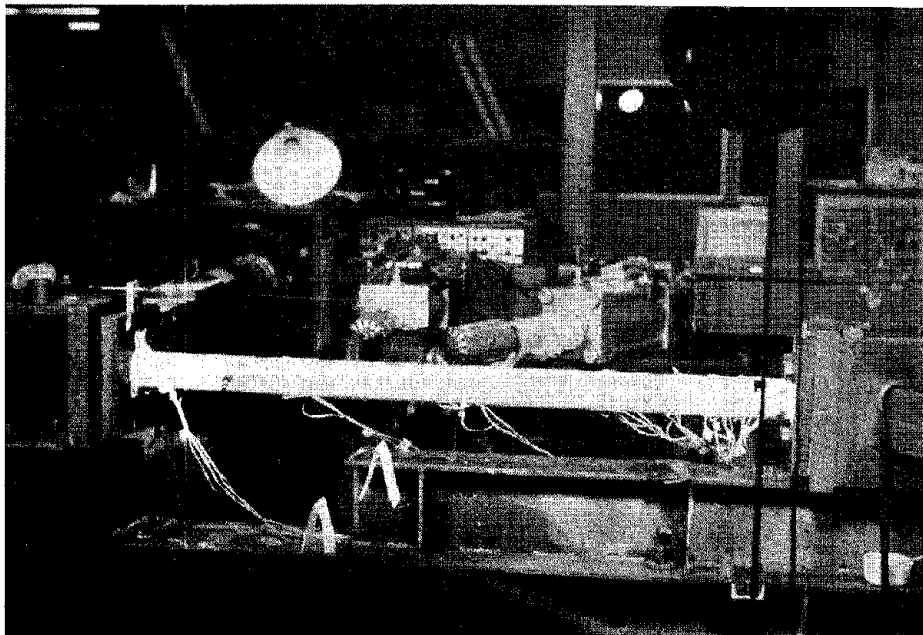
b) Specimen with Strain Gages and LVDT

Fig. 2.7   Instrumentation

a) Data Feedback -- Continuous Recording on X-Y Plotters
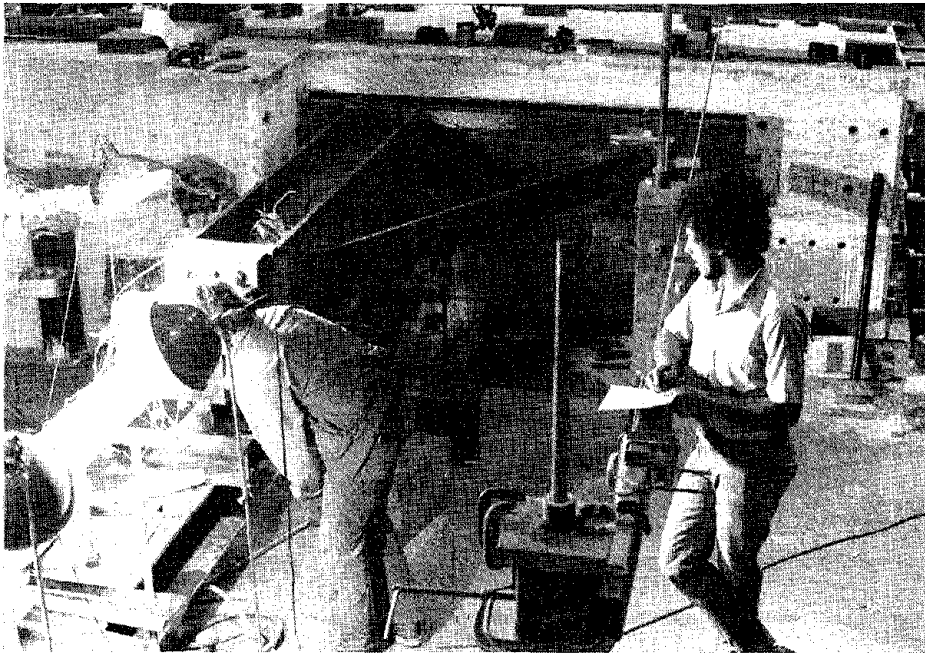
b) Recording Visual Observations

Fig. 2.8 Data Recording
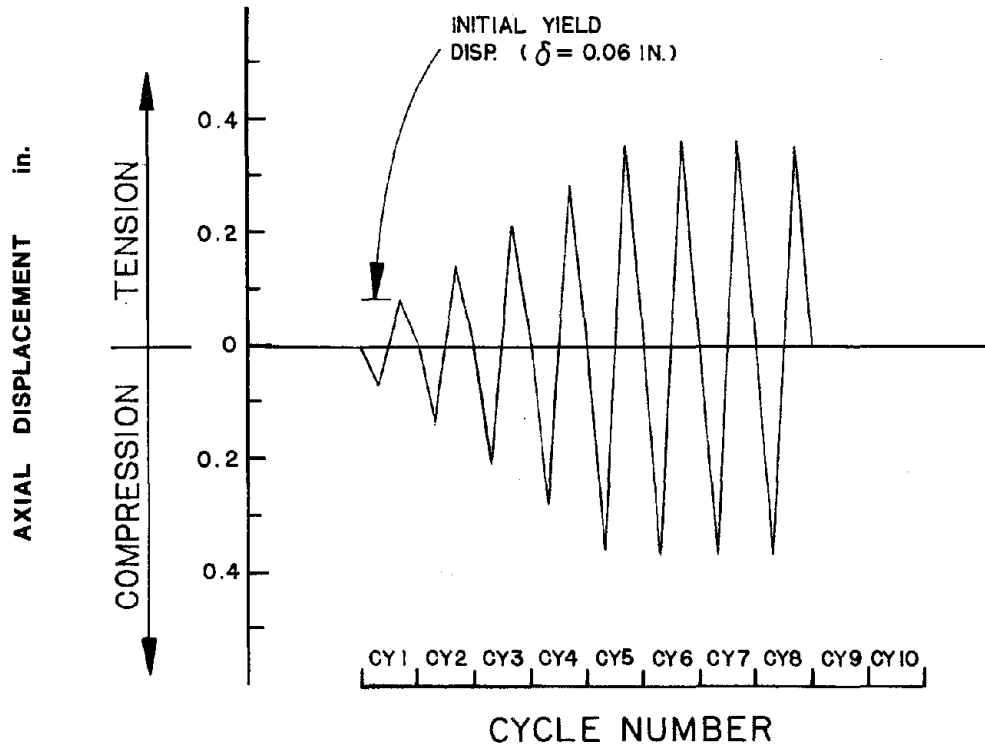
Fig. 2.9   Loading Sequence - Strut 1 (1 in. = 25.4 mm)
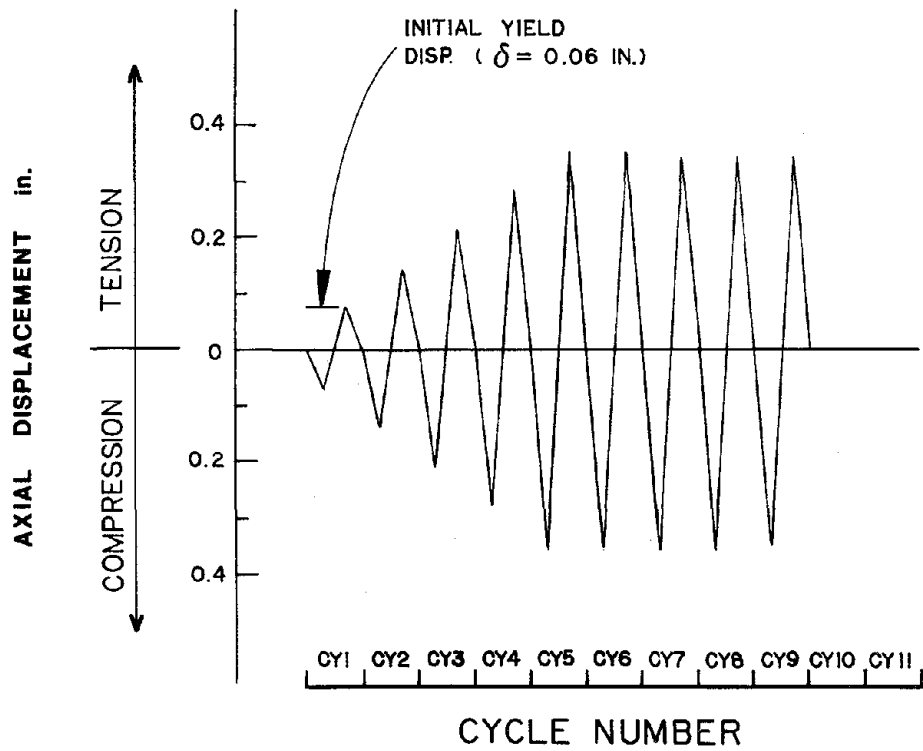
Fig. 2.10 Loading Sequence - Strut 2 (1 in. = 25.4 mm)
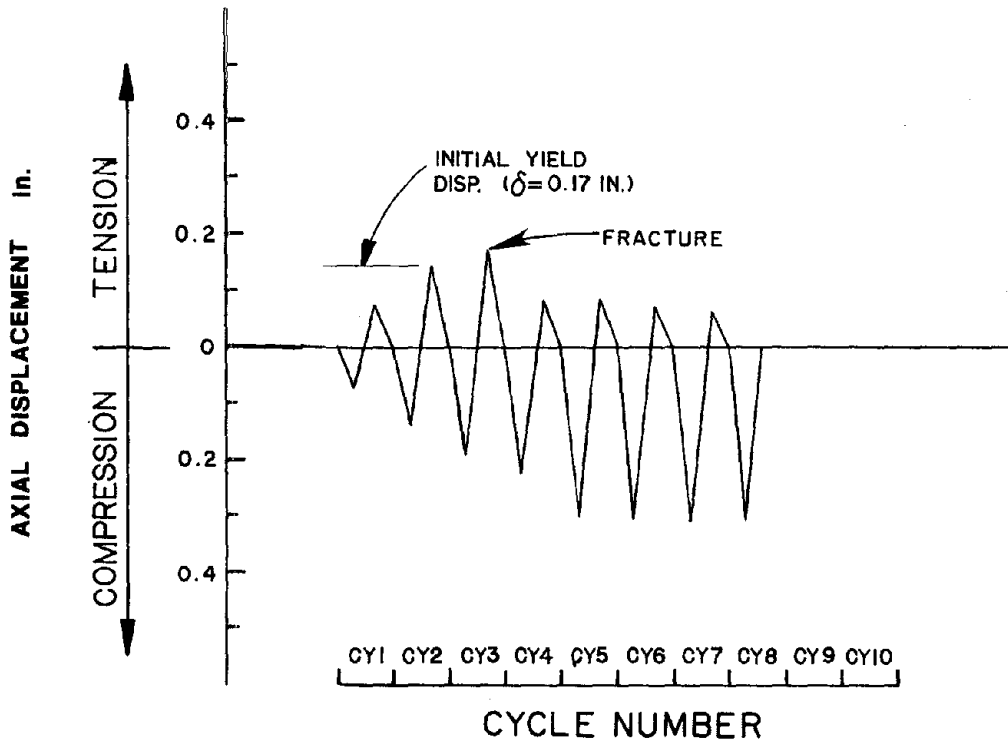
Fig. 2.11 Loading Sequence – Strut 3 (1 in. = 25.4 mm)
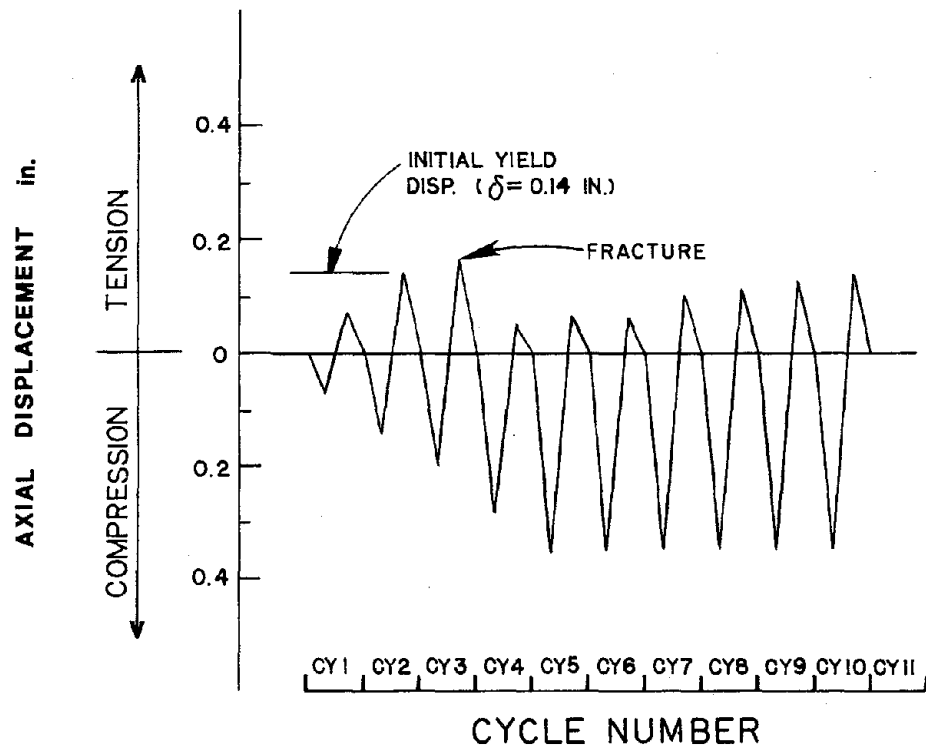
Fig. 2.12 Loading Sequence – Strut 4 (1 in. = 25.4 mm)
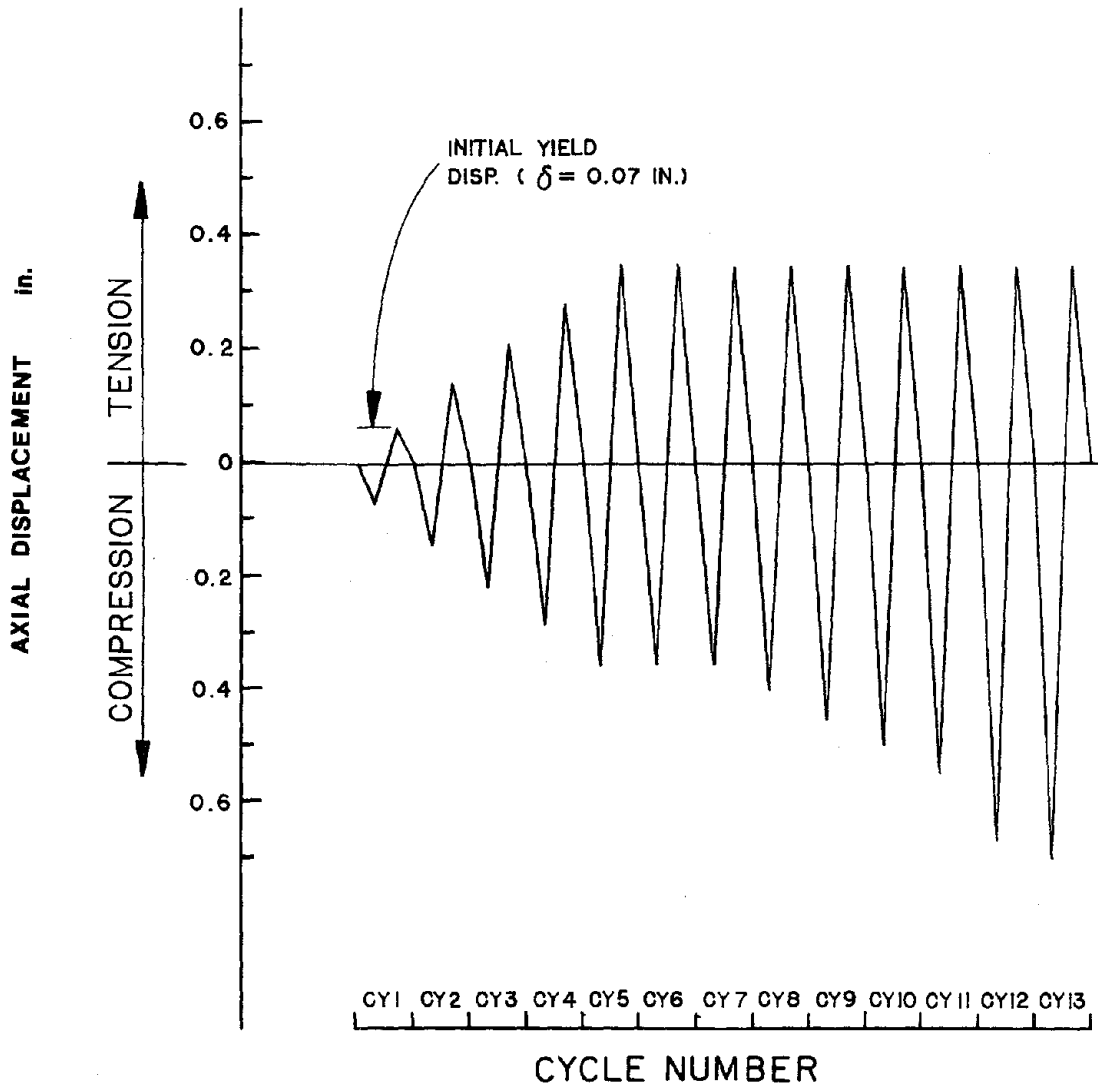
Fig. 2.13 Loading Sequence - Strut 5 (1 in. = 25.4 mm)
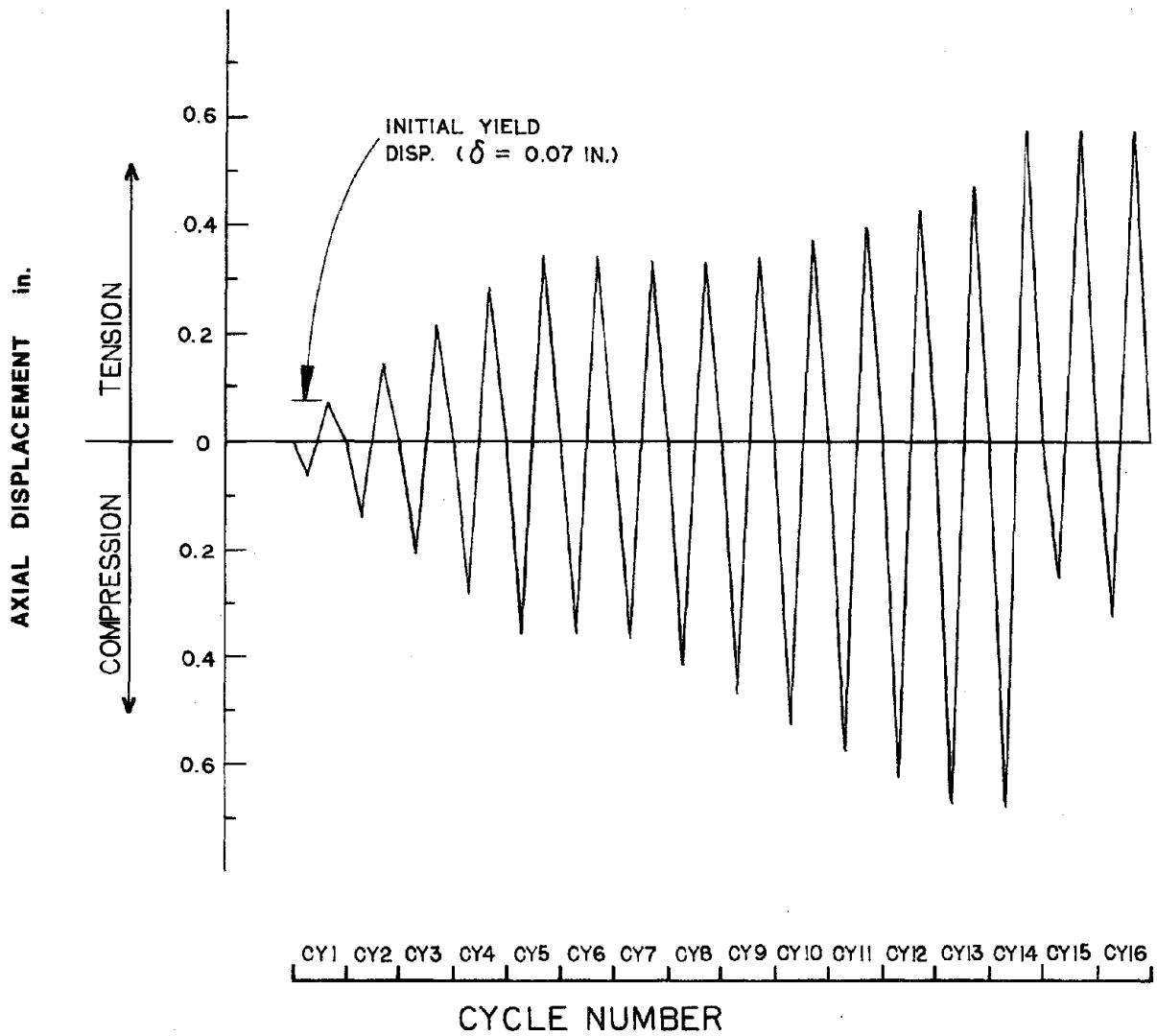
Fig. 2.14 Loading Sequence – Strut 6 (1 in. = 25.4 mm)
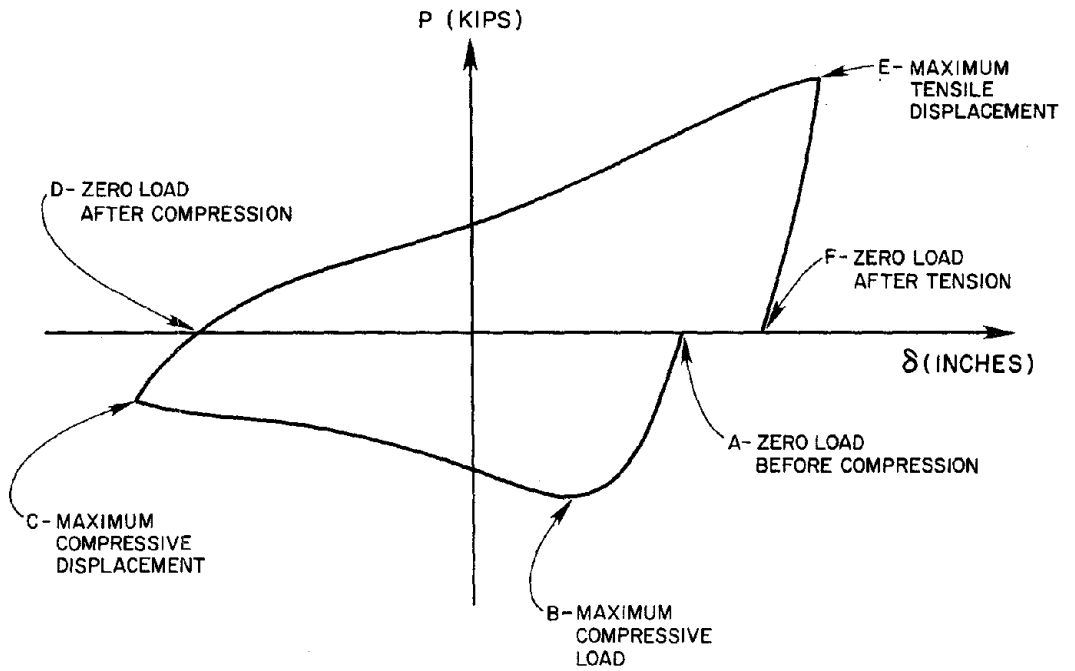
a) Typical Hysteretic Response
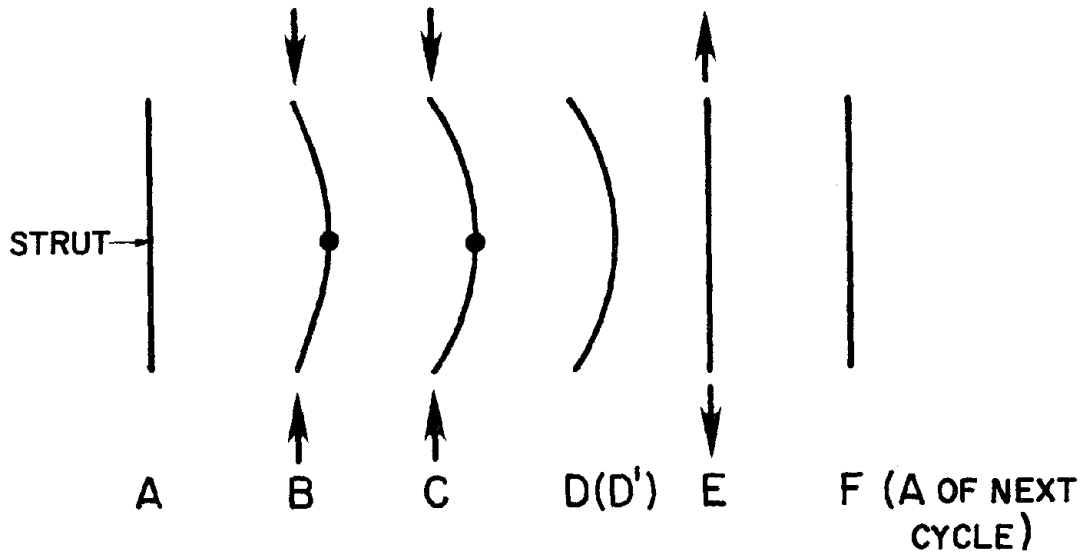
b) Loading Schematic

Fig. 2.15 Load Points on a Typical Cycle
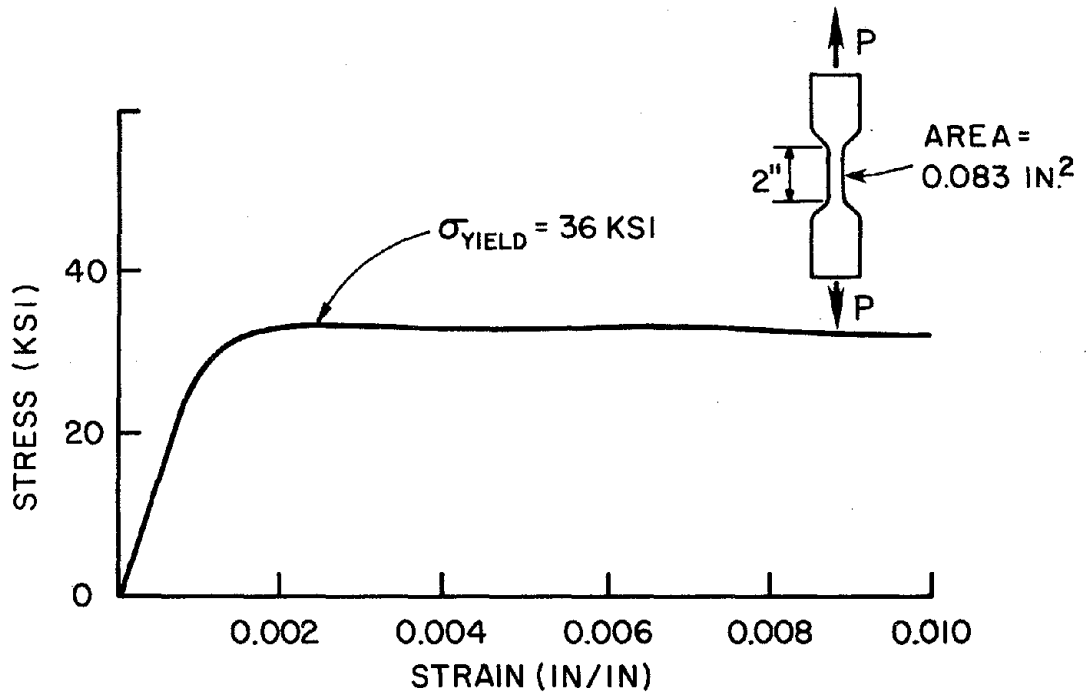
(a) 0.083" WALL THICKNESS
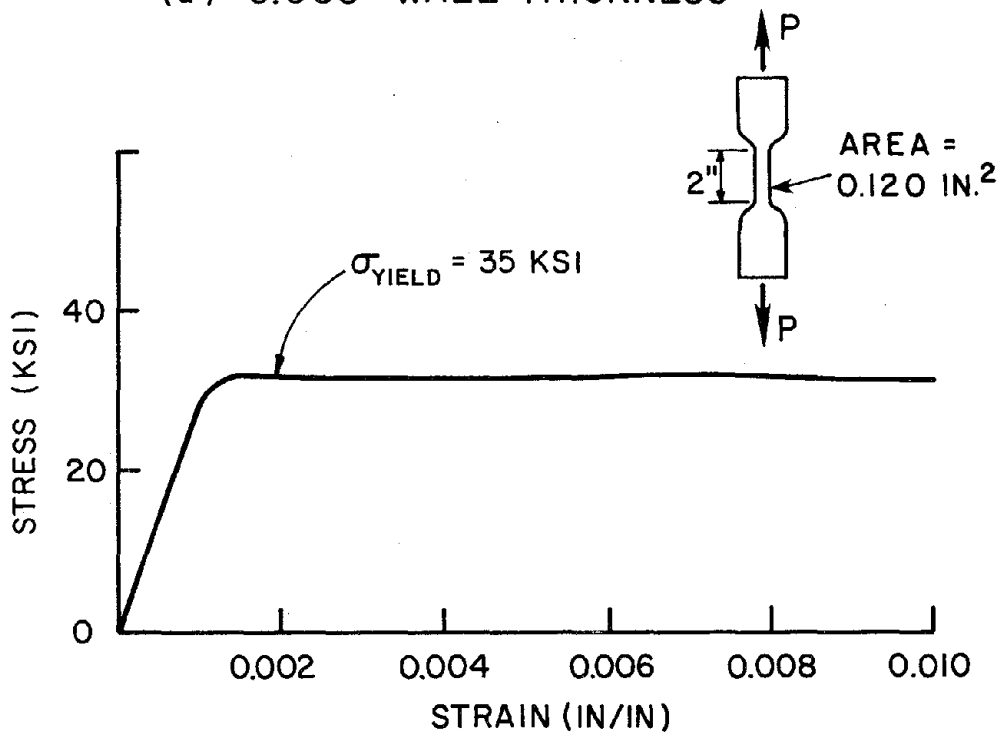
(b) 0.120" WALL THICKNESS

Fig. 2.16   Coupon Test Results – Annealed Material at Small Strains
(1 ksi = 6.9 MPa)

78
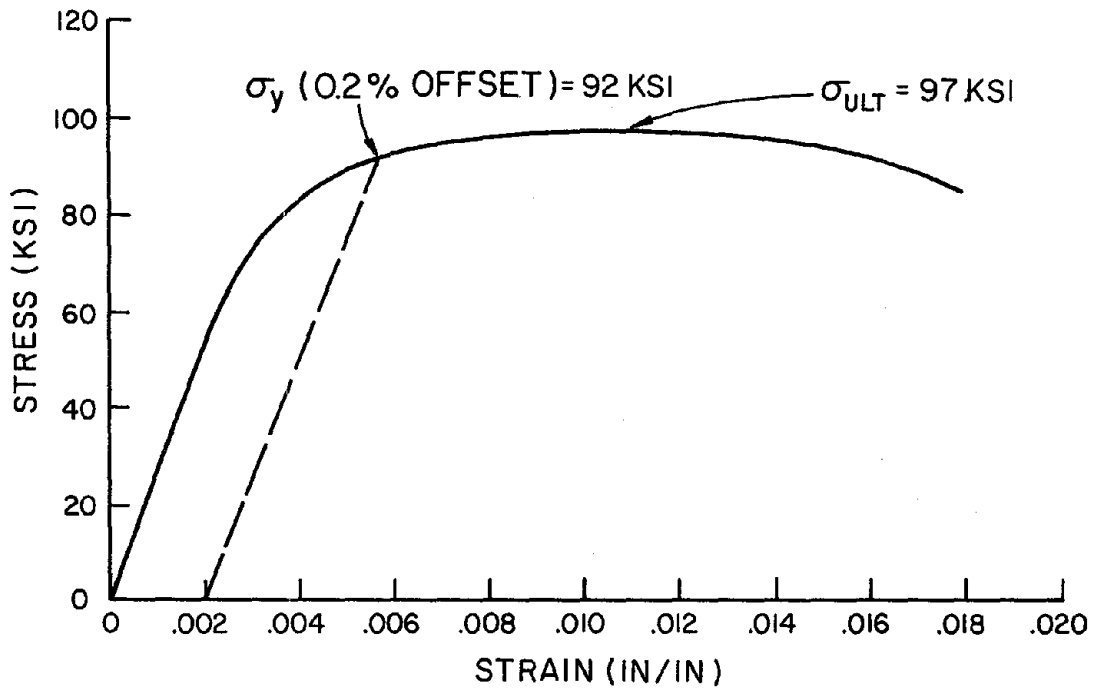
(a) 0.083" WALL THICKNESS

(b) 0.120" WALL THICKNESS

Fig. 2.17   Coupon Test Results – Unannealed Material at Small Strains
(1 ksi = 6.9 MPa)
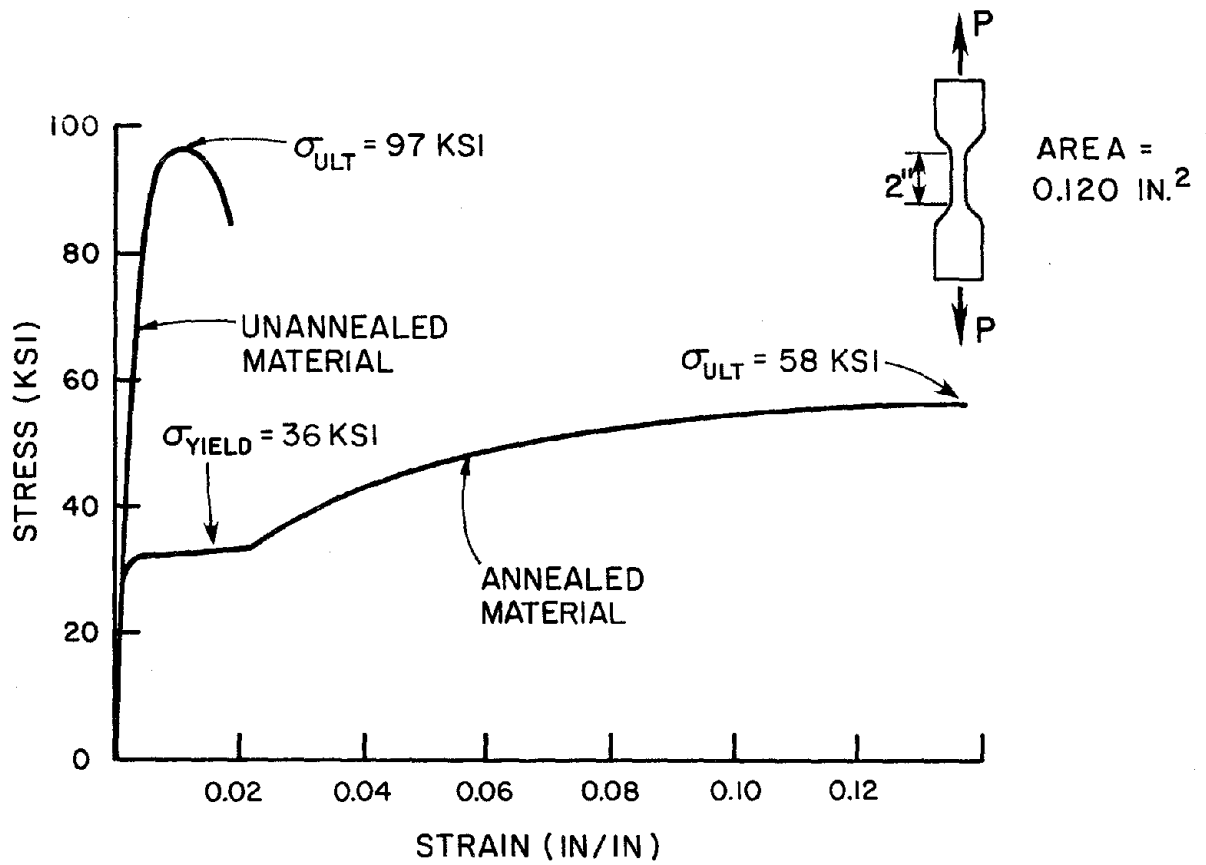
Fig. 2.18 Coupon Test Results – Annealed & Unannealed at Large Strains
(1 ksi = 6.9 MPa)
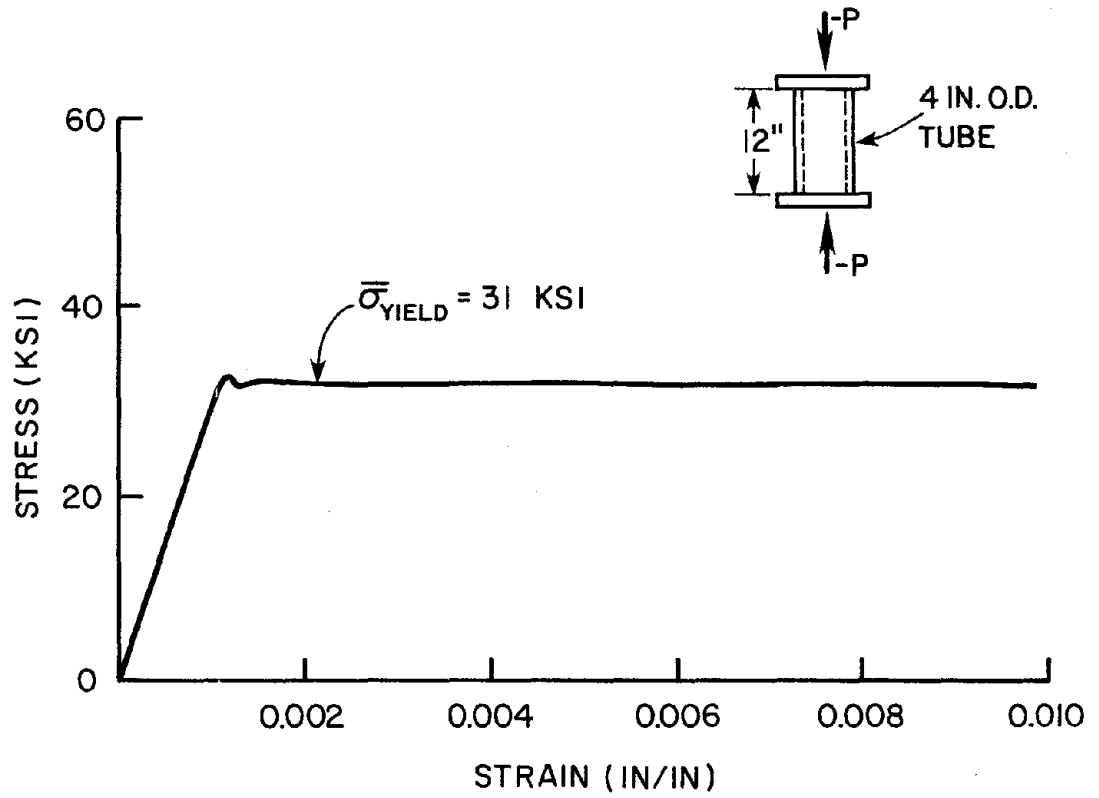
Fig. 2.19   Compression Test of Full Section – Annealed Material
(1 ksi = 6.9 MPa)
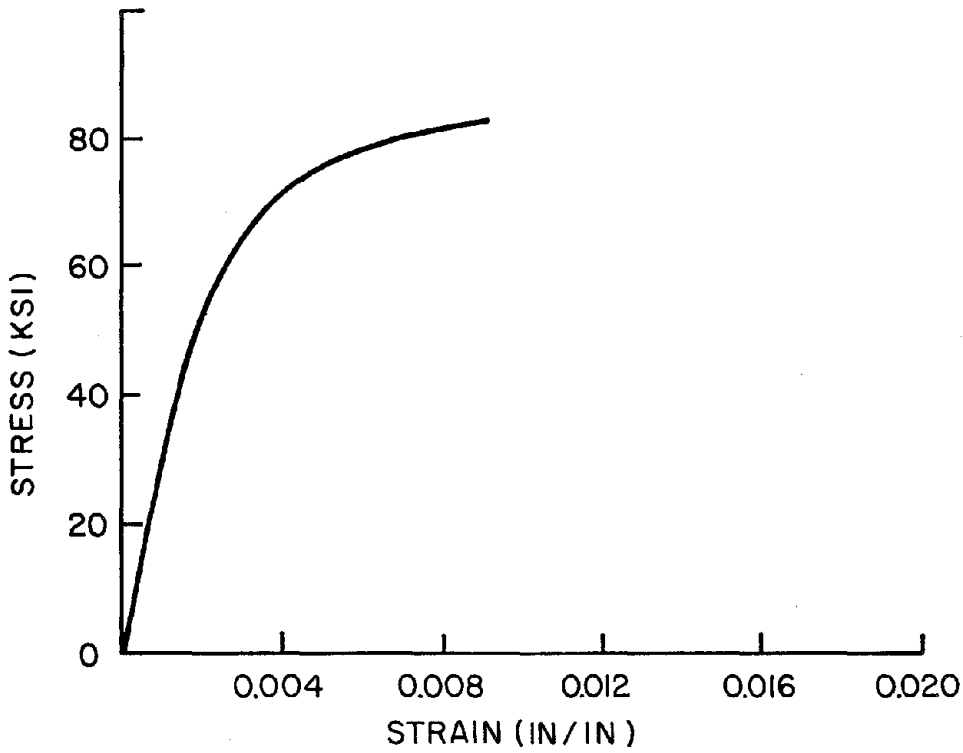
(a) 0.083" WALL THICKNESS
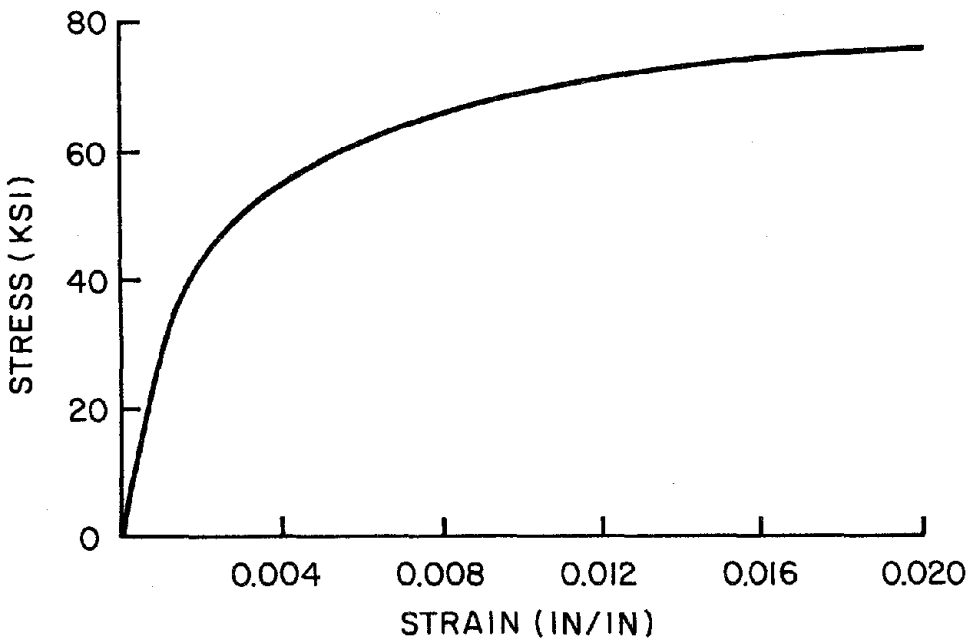
(b) 0.120" WALL THICKNESS

Fig. 2.20   Compression Test of Full Section - Unannealed Material
(1 ksi = 6.9 MPa)
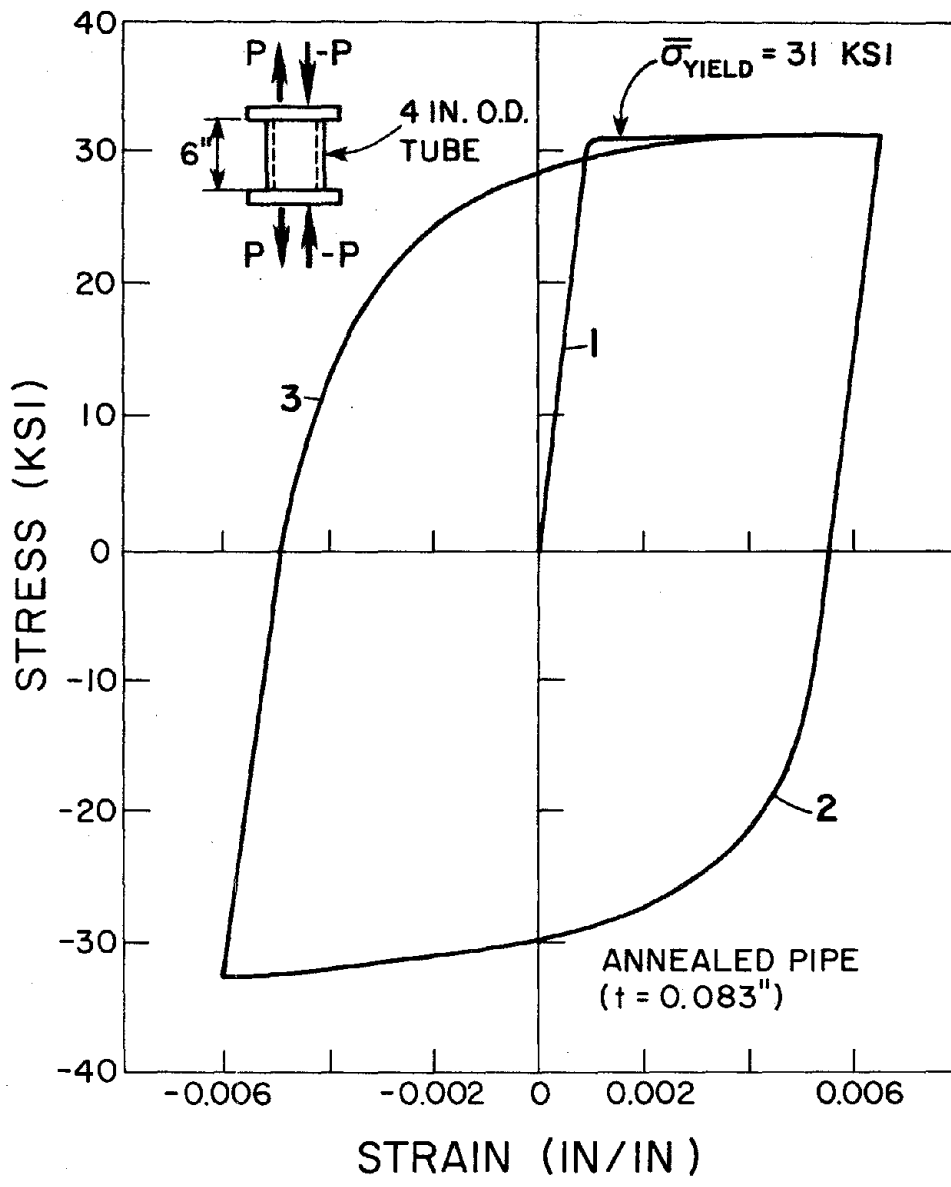
Fig. 2.21 Cyclic Test – Annealed Material
(1 ksi = 6.9 MPa)
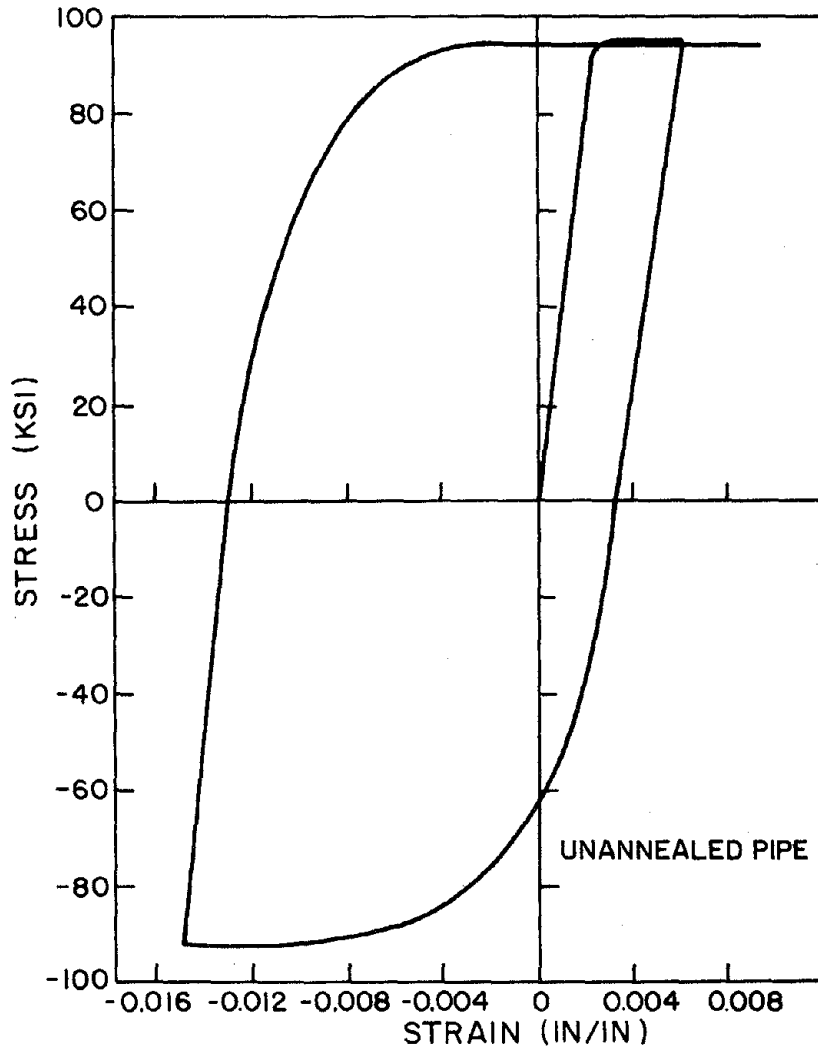
(a) 0.120" WALL THICKNESS
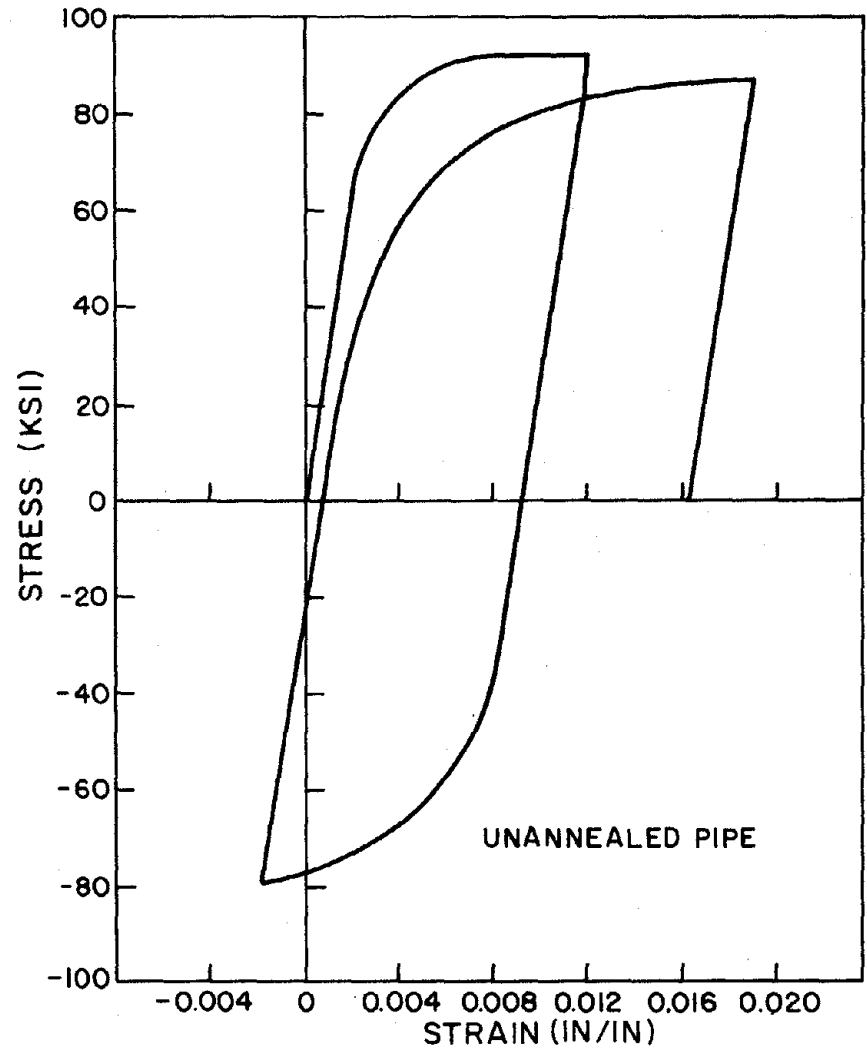
(b) 0.083" WALL THICKNESS

Fig. 2.22   Cyclic Test – Unannealed Material
(1 ksi = 6.9 MPa)
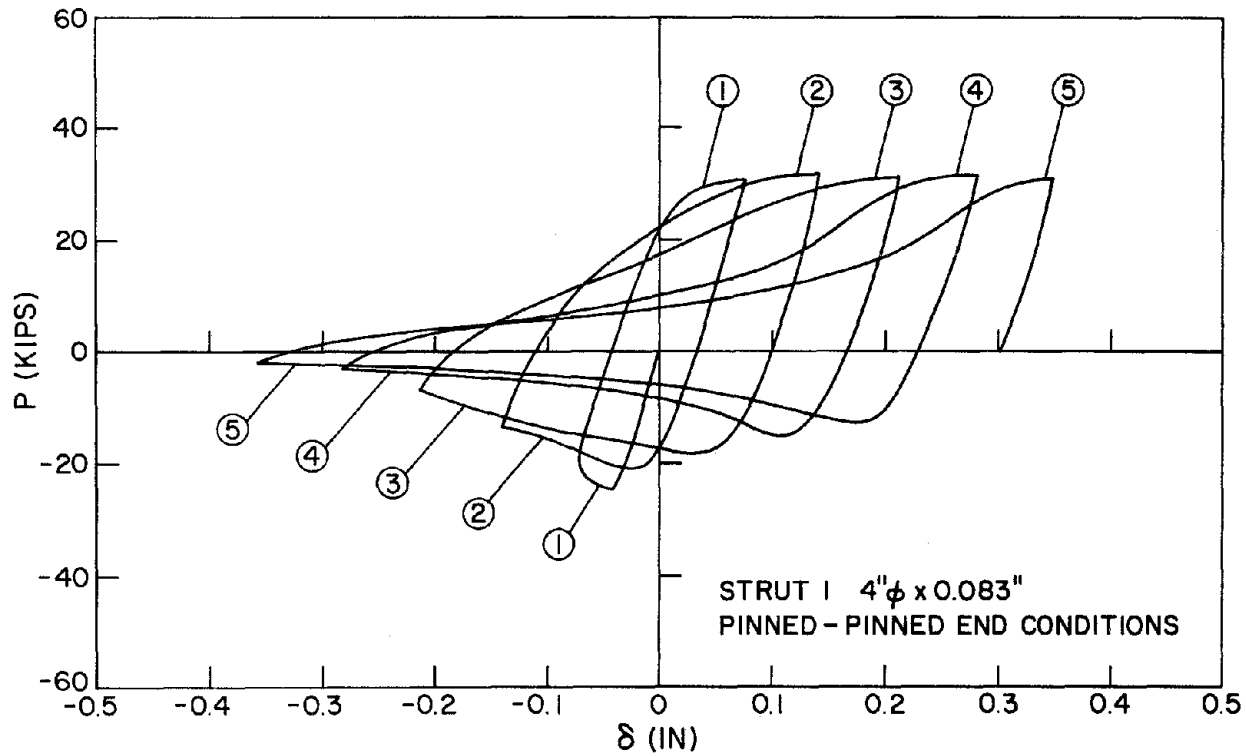
Fig. 3.1 Axial Load vs. Axial Displacement — Strut 1, Cycles 1-5
(1 kip = 4.45 kN; 1 in. = 25.4 mm)
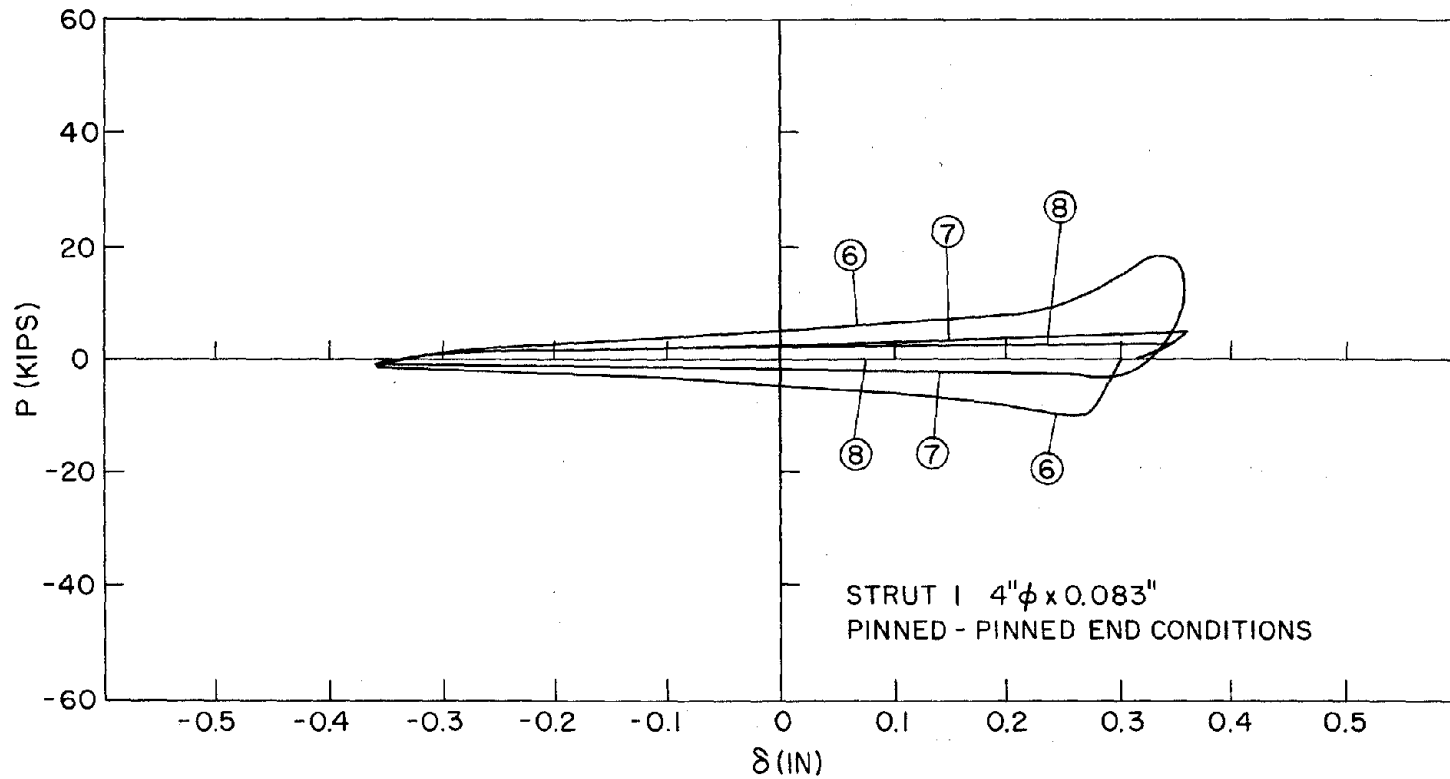
Fig. 3.2 Axial Load vs. Axial Displacement – Strut 1, Cycles 6-8
(1 kip = 4.45 kN; 1 in. = 25.4 mm)
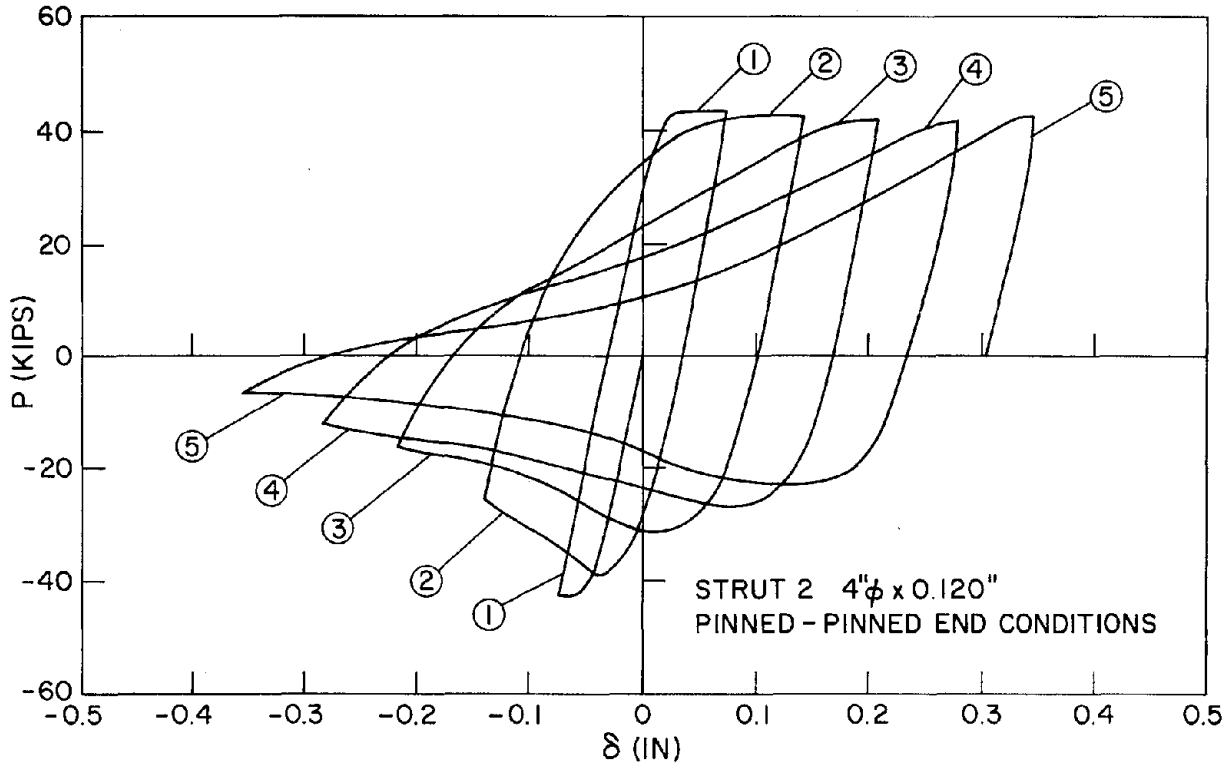
Fig. 3.3 Axial Load vs. Axial Displacement — Strut 2. Cycles 1-5
(1 kip = 4.45 kN; 1 in. = 25.4 mm)

Fig. 3.4 Axial Load vs. Axial Displacement - Strut 2, Cycles 6-9
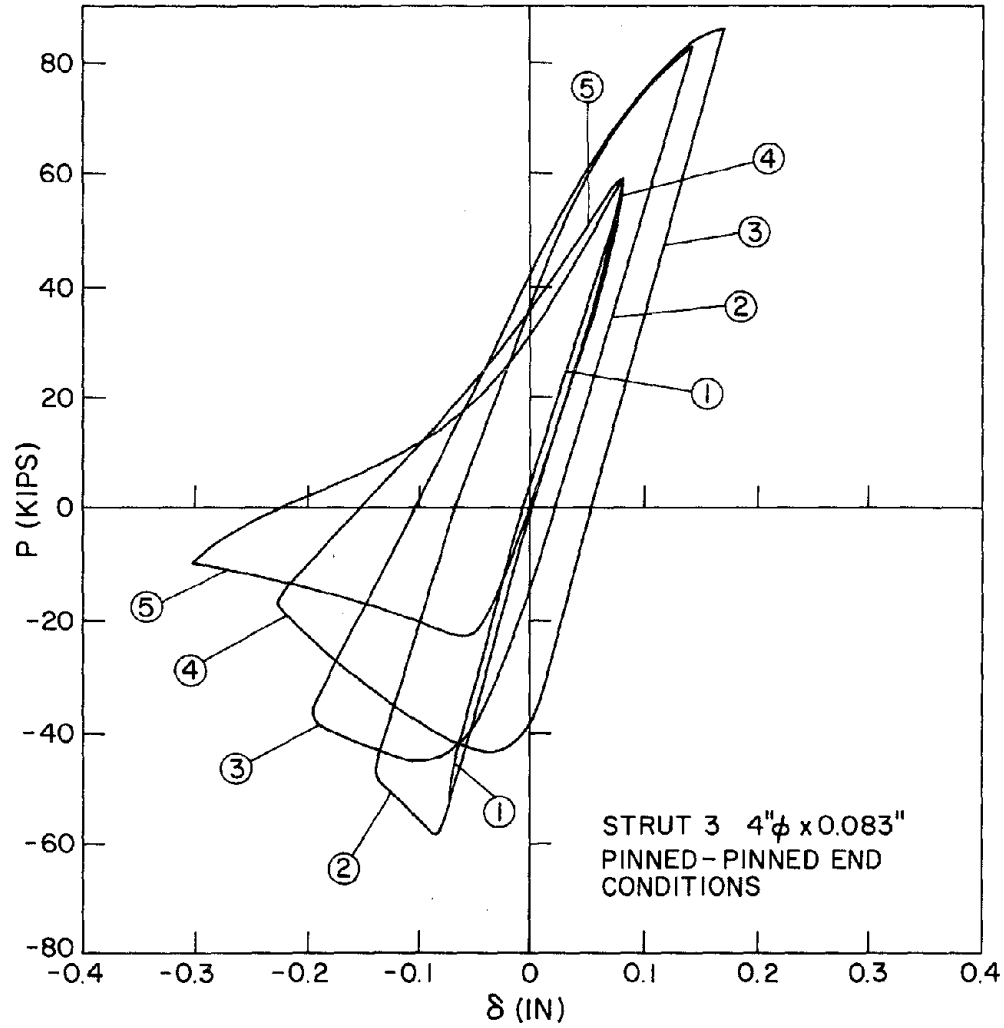
Fig. 3.5   Axial Load vs. Axial Displacement − Strut 3, Cycles 1-5
(1 kip = 4.45 kN; 1 in. = 25.4 mm)
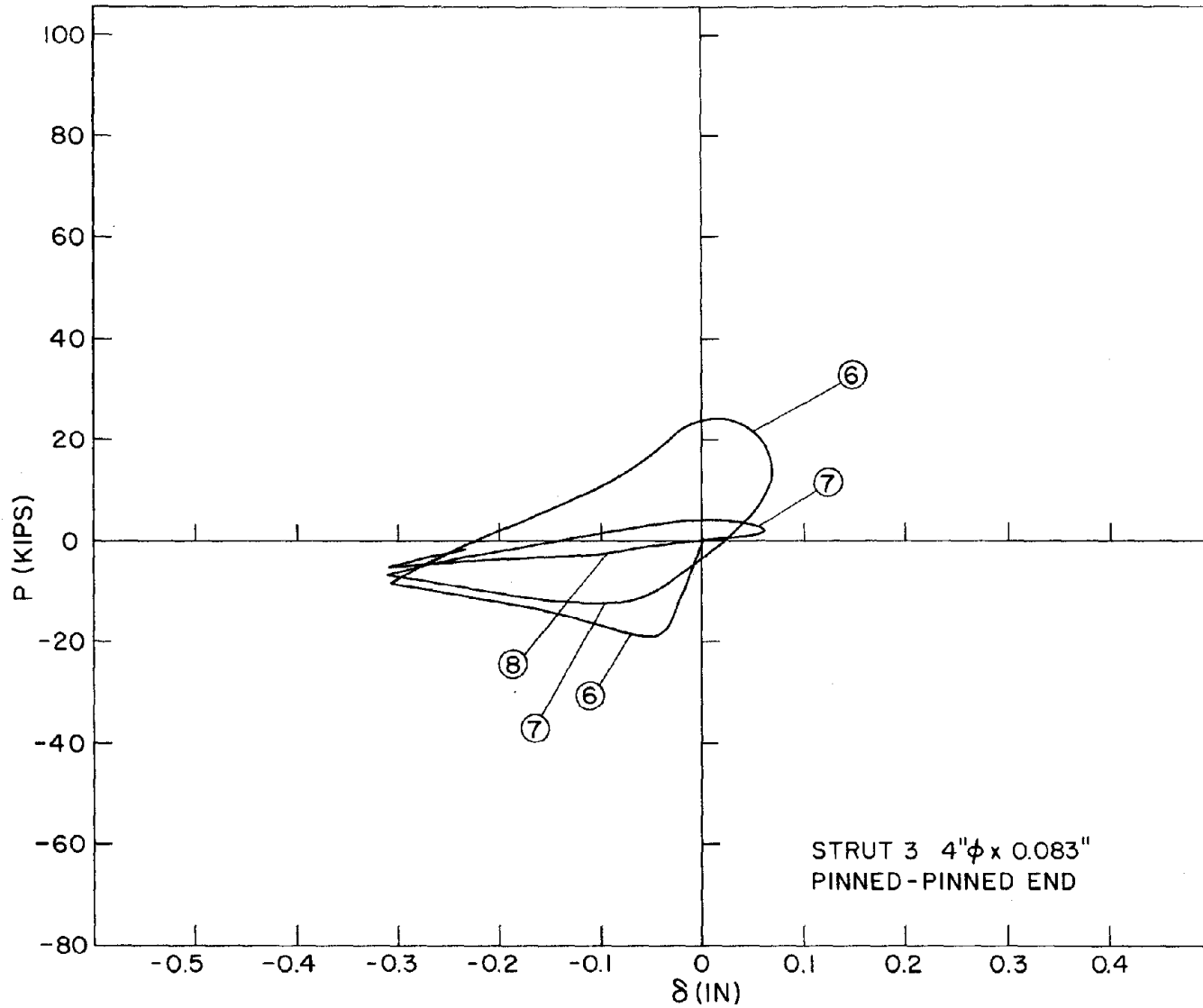
Fig. 3.6   Axial Load vs. Axial Displacement – Strut 3, Cycles 6-8
(1 kip = 4.45 kN; 1 in. = 25.4 mm)
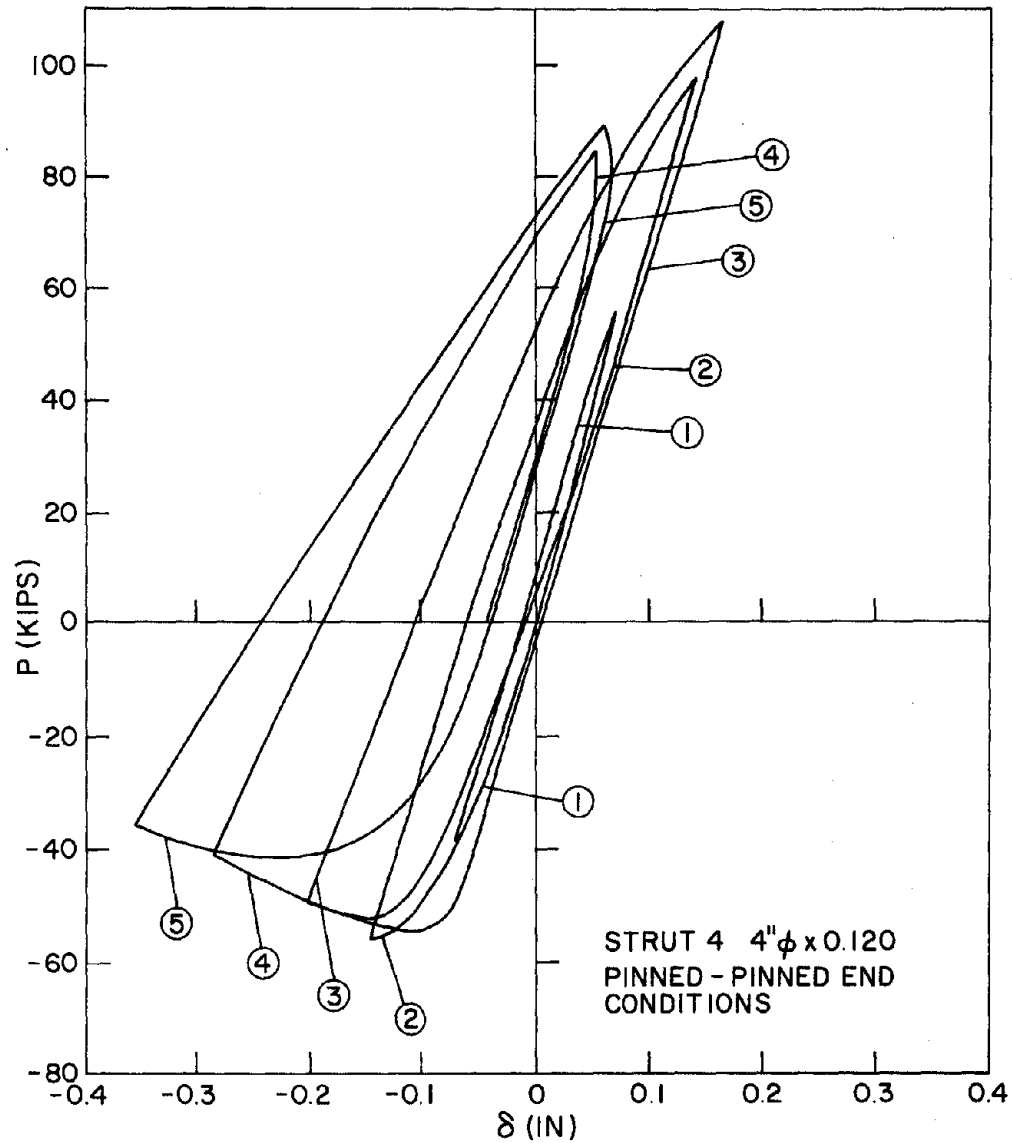
Fig. 3.7   Axial Load vs. Axial Displacement – Strut 4, Cycles 1-5
(1 kip = 4.45 kN; 1 in. = 25.4 mm)
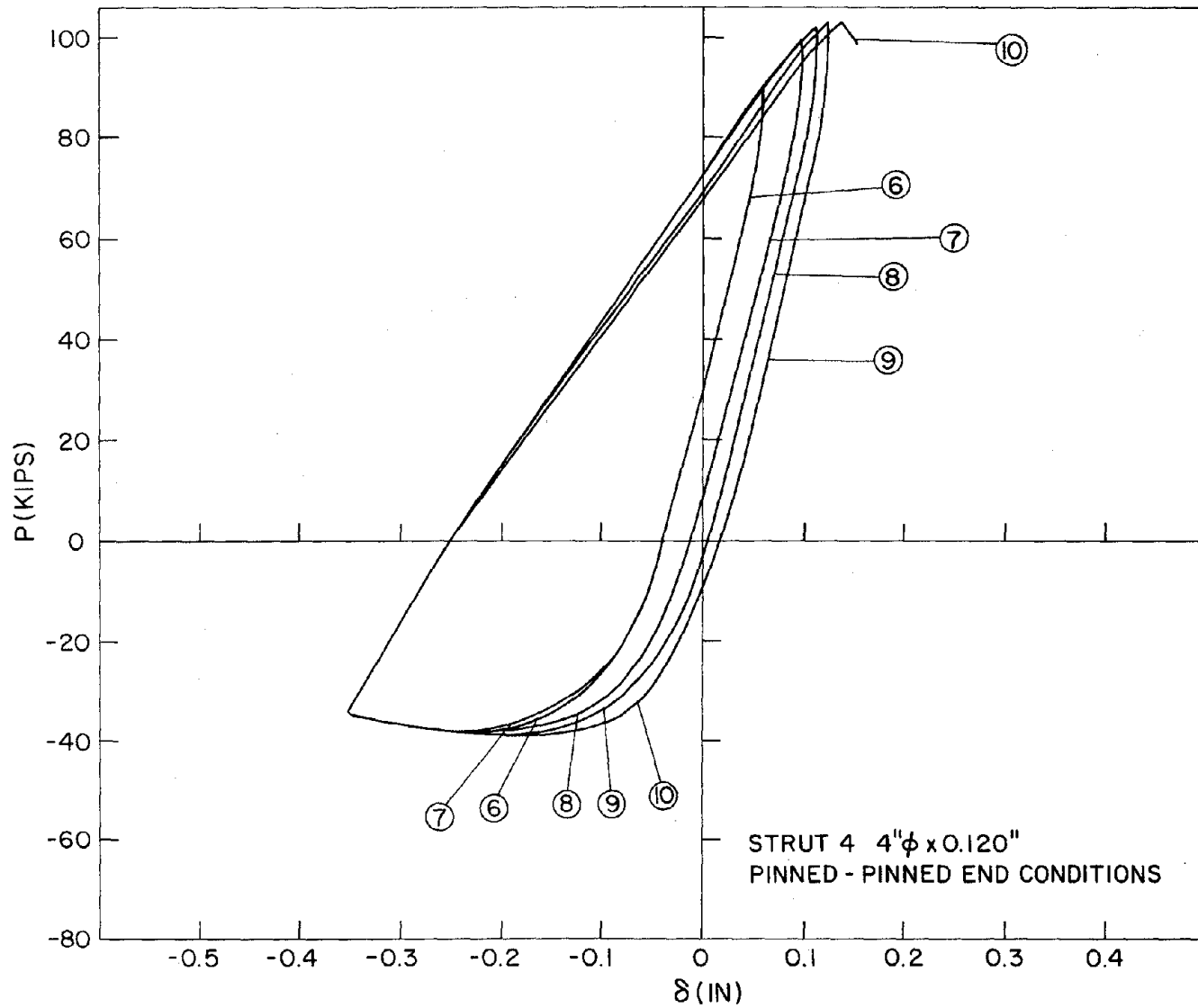
Fig. 3.8 Axial Load vs. Axial Displacement – Strut 4, Cycles 6–10
(1 kip = 4.45 kN; 1 in. = 25.4 mm)
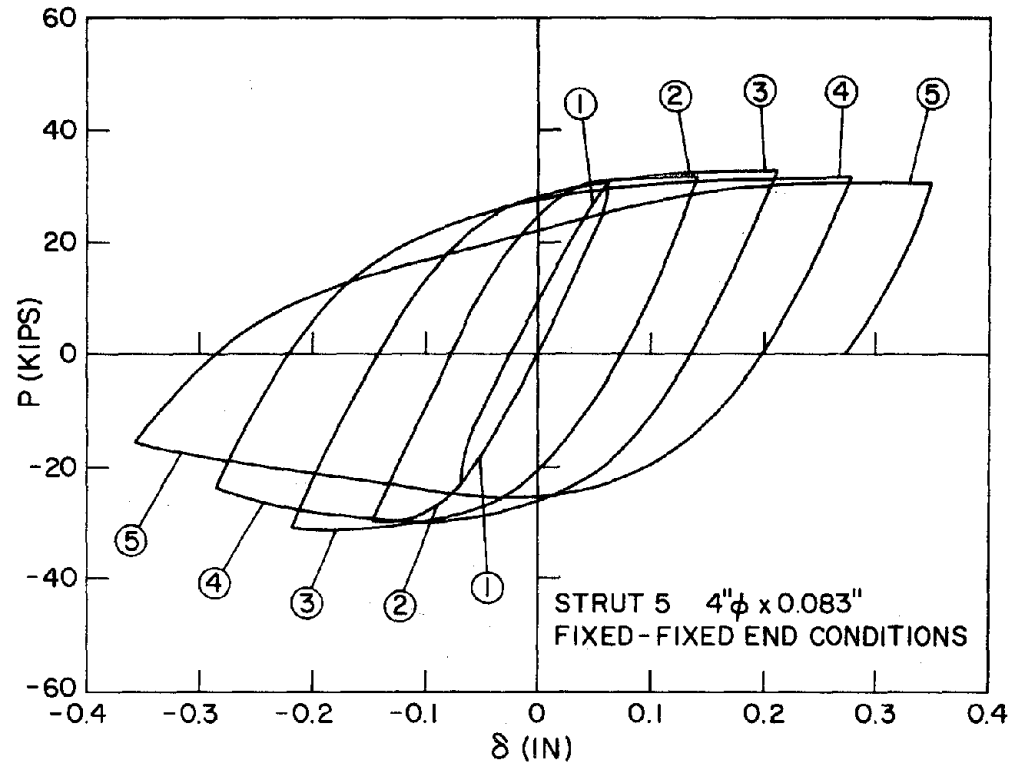
Fig. 3.9 Axial Load vs. Axial Displacement – Strut 5, Cycles 1-5
(1 kip = 4.45 kN; 1 in. = 25.4 mm)
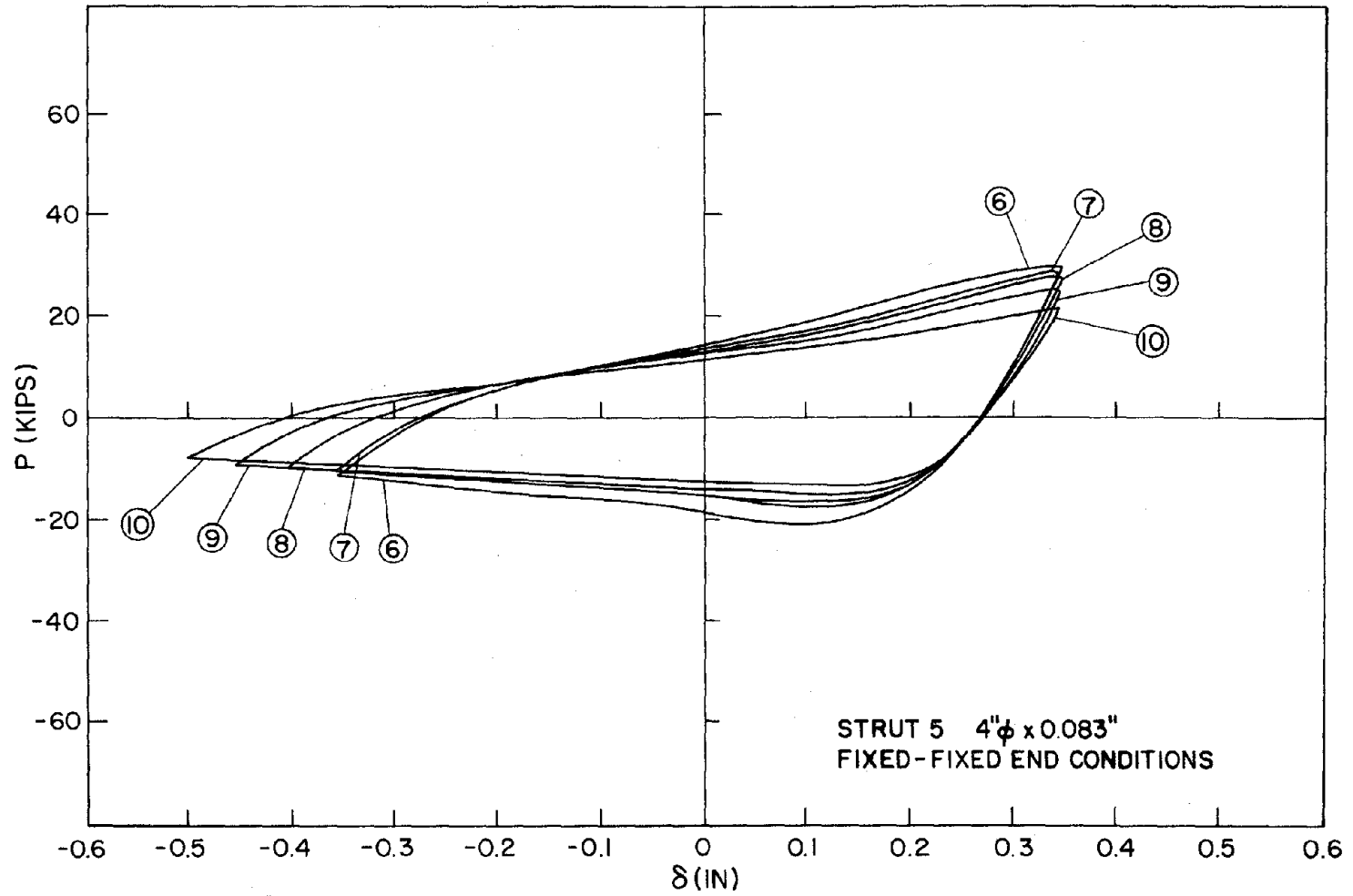
Fig. 3.10 Axial Load vs. Axial Displacement – Strut 5, Cycles 6-10
(1 kip = 4.45 kN; 1 in. = 25.4 mm)
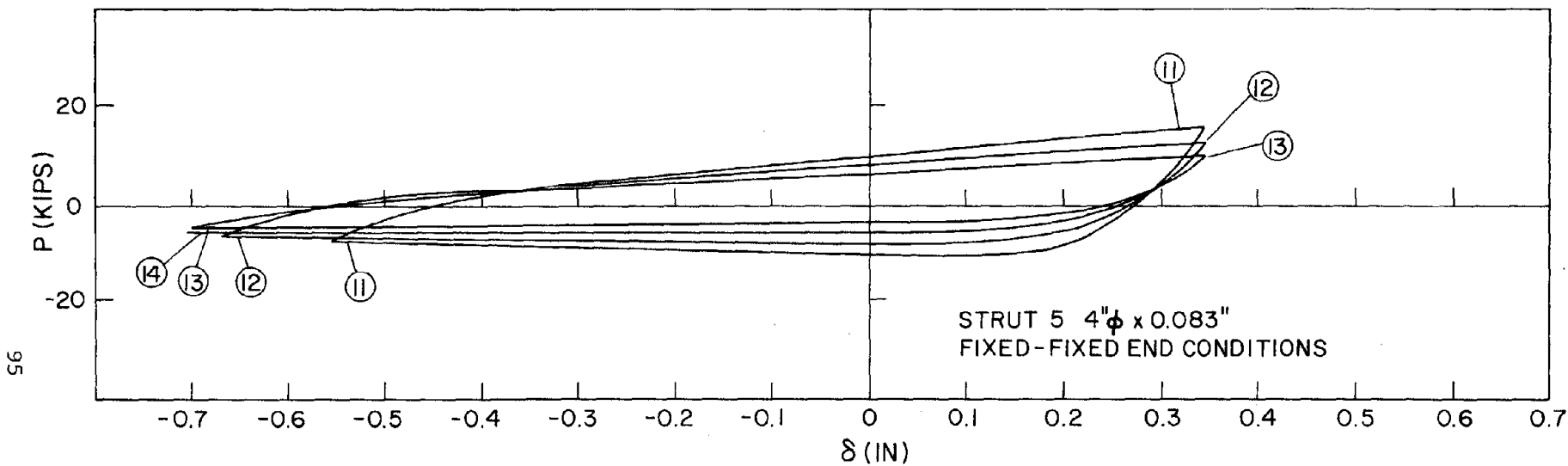
Fig. 3.11 Axial Load vs. Axial Displacement – Strut 5, Cycles 11-13
(1 kip = 4.45 kN; 1 in. = 25.4 mm)

95
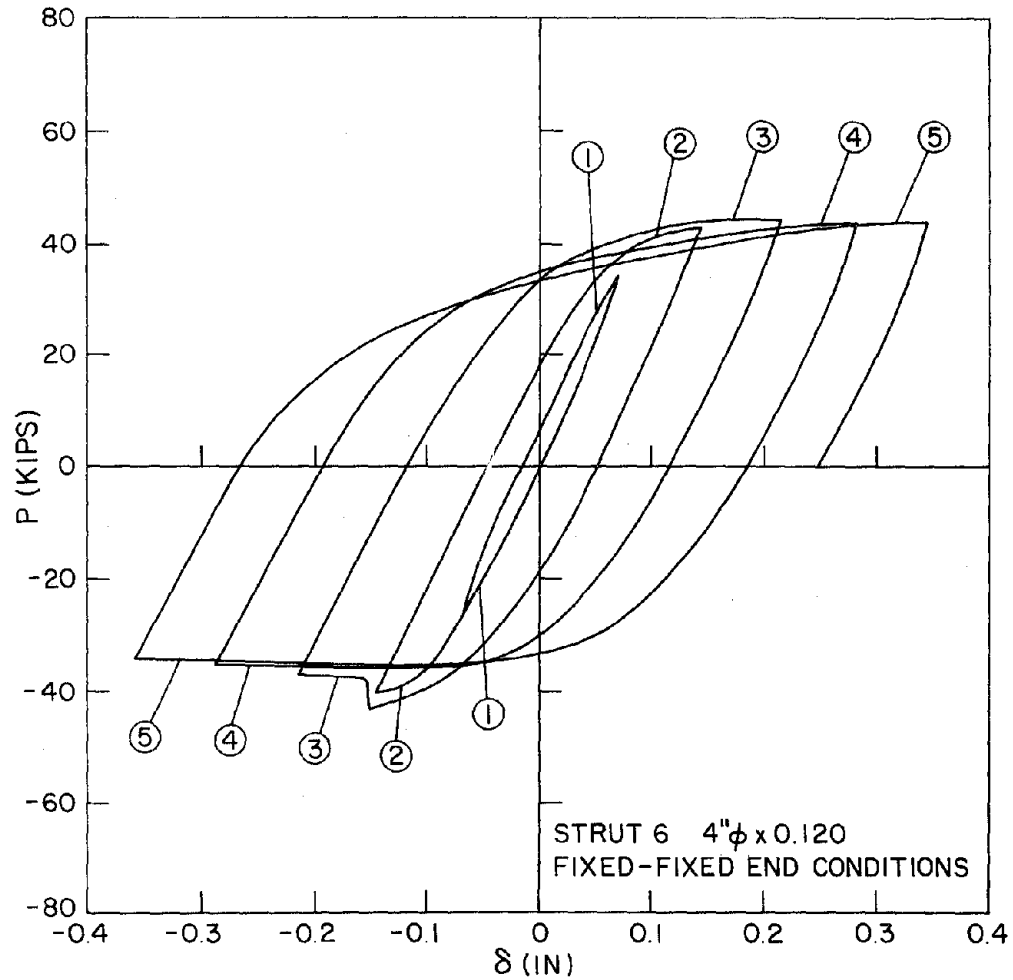
Fig 3.12   Axial Load vs. Axial Displacement - Strut 6, Cycles 1-5
(1 kip = 4.45 kN; 1 in. = 25.4 mm)
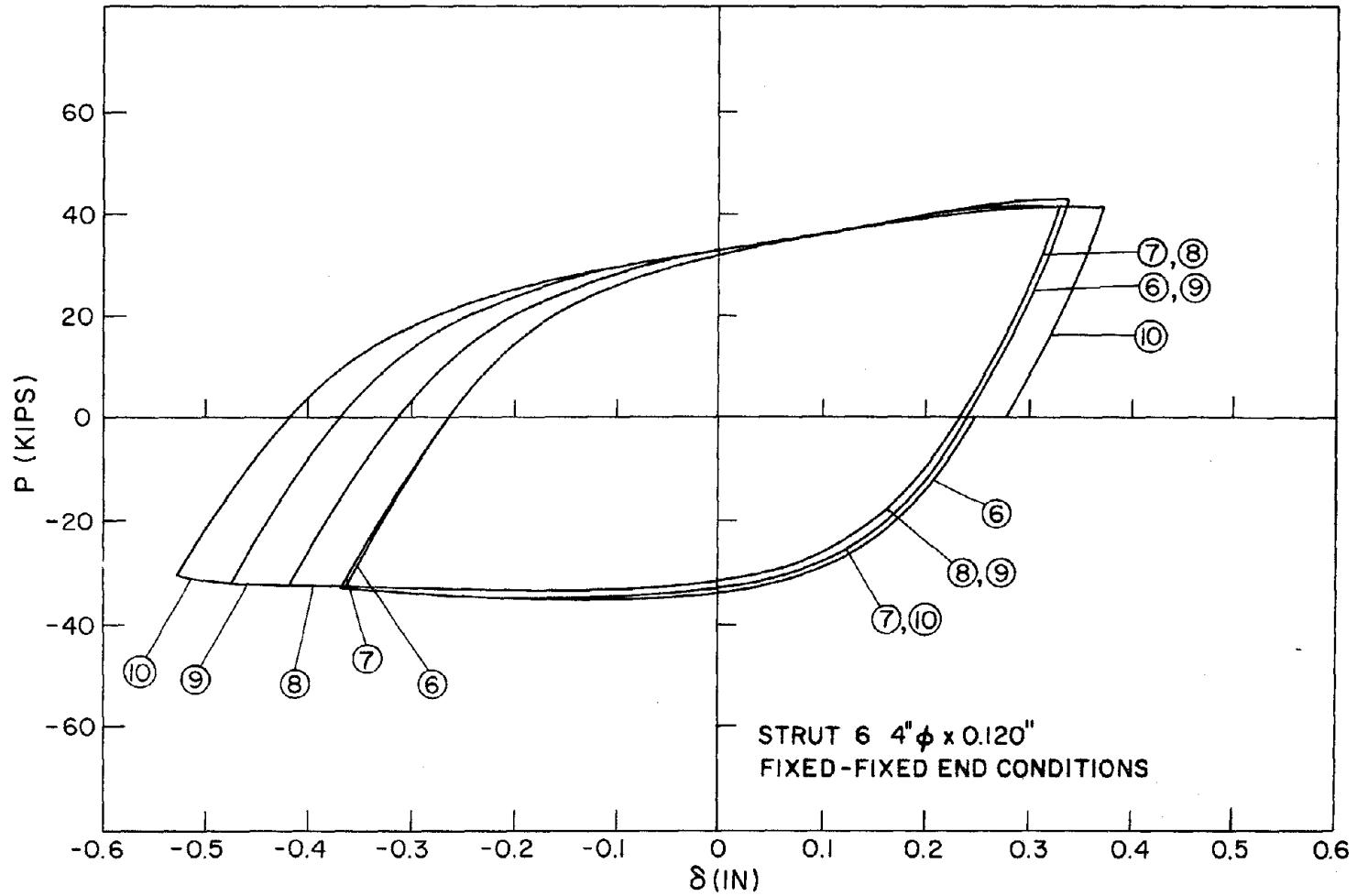
Fig. 3.13 Axial Load vs. Axial Displacement – Strut 6, Cycles 6-10
(1 kip = 4.45 kN; 1 in. = 25.4 mm)
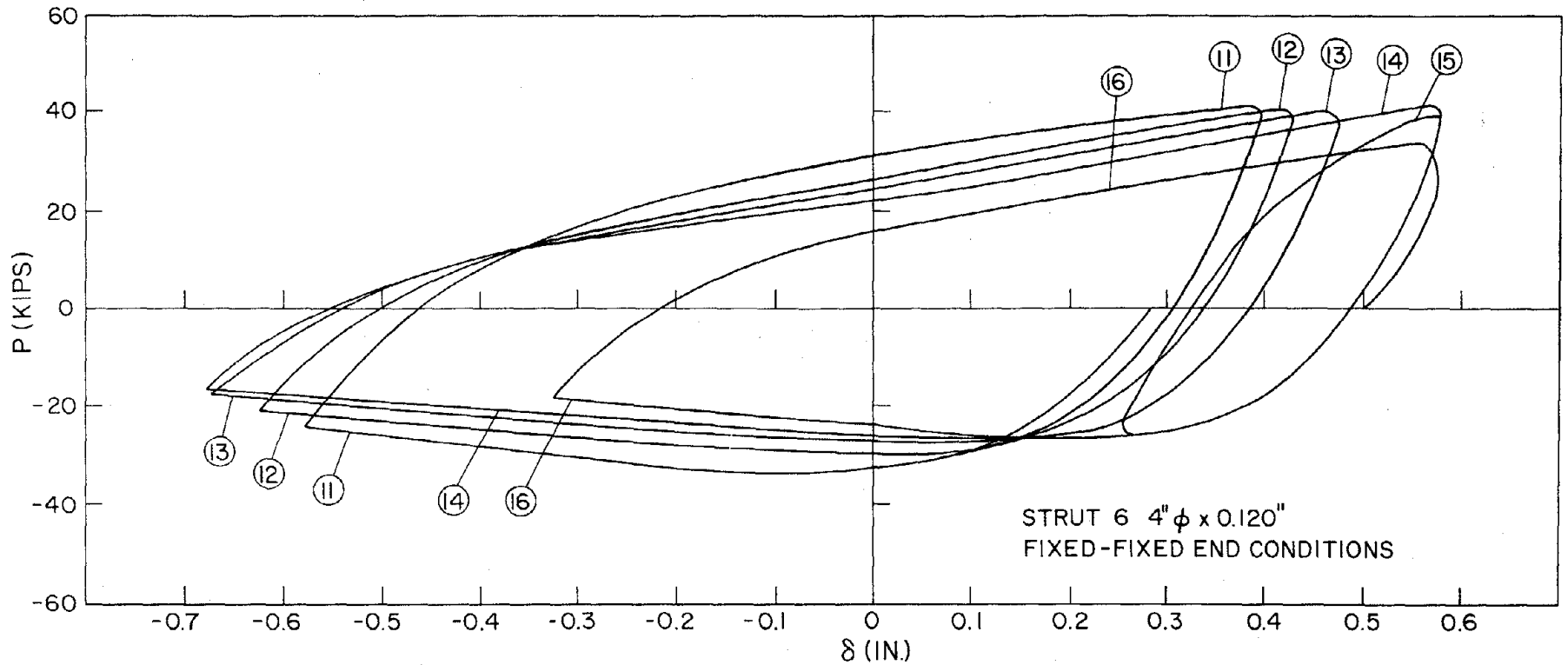
Fig. 3.14   Axial Load vs. Axial Displacement – Strut 6, Cycles 11-16
(1 kip = 4.45 kN; 1 in. = 25.4 mm)
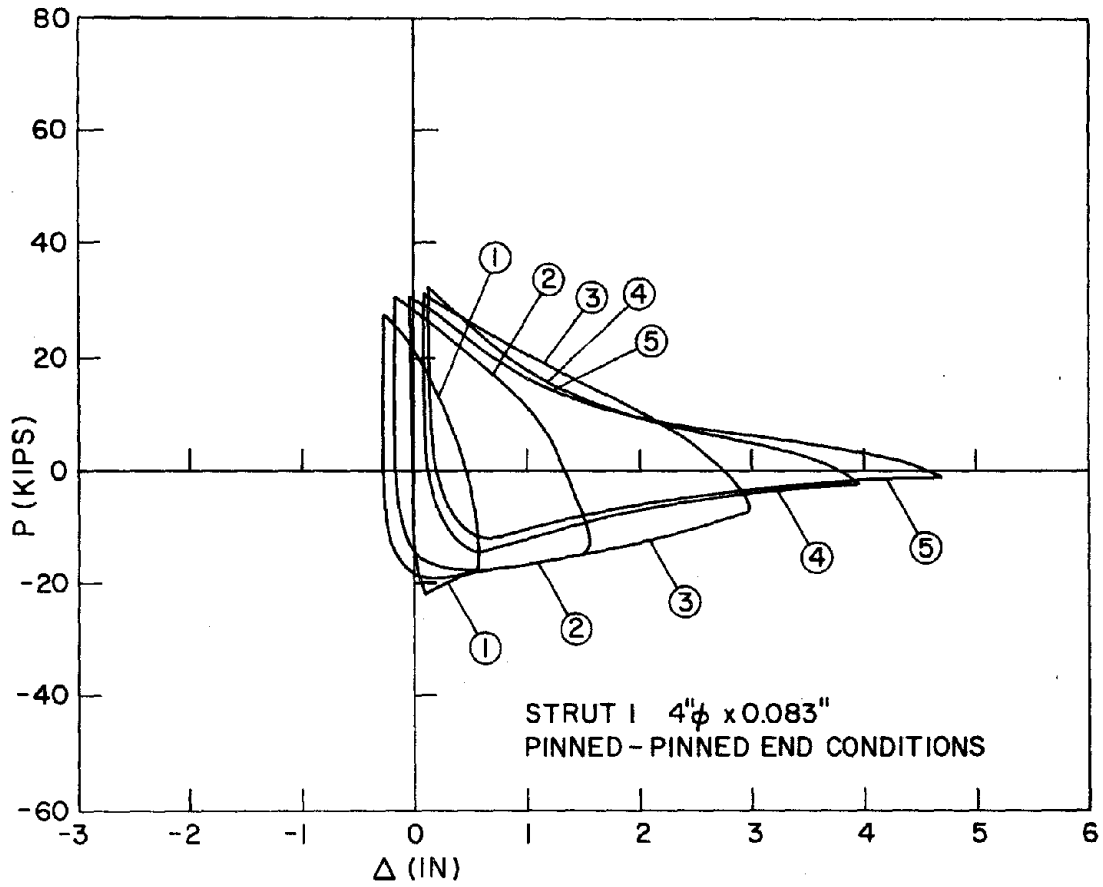
Fig. 3.15 Axial Load vs. Lateral Displacement – Strut 1, Cycles 1-5
(1 kip = 4.45 kN; 1 in. = 25.4 mm)

99
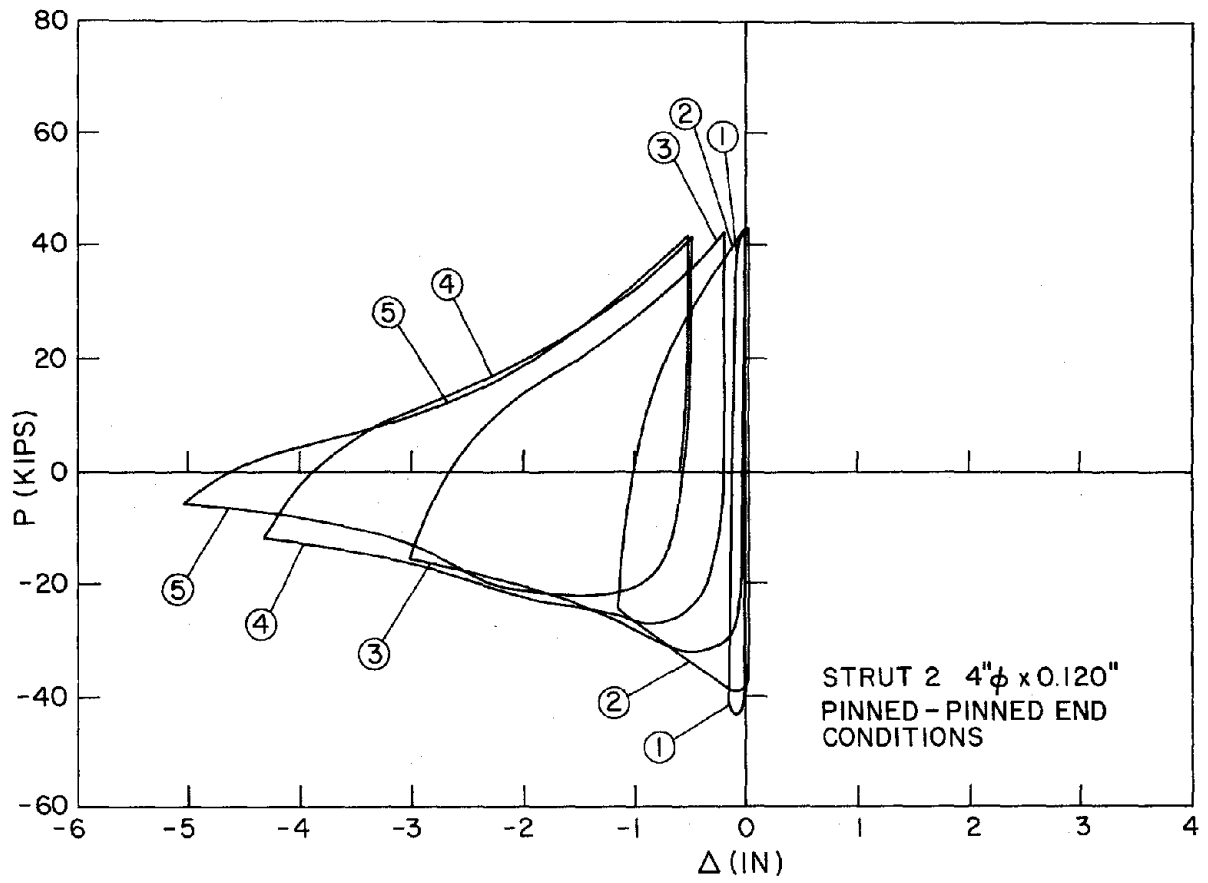
Fig. 3.16   Axial Load vs. Lateral Displacement – Strut 2, Cycles 1–5
(1 kip = 4.45 kN; 1 in. = 25.4 mm)
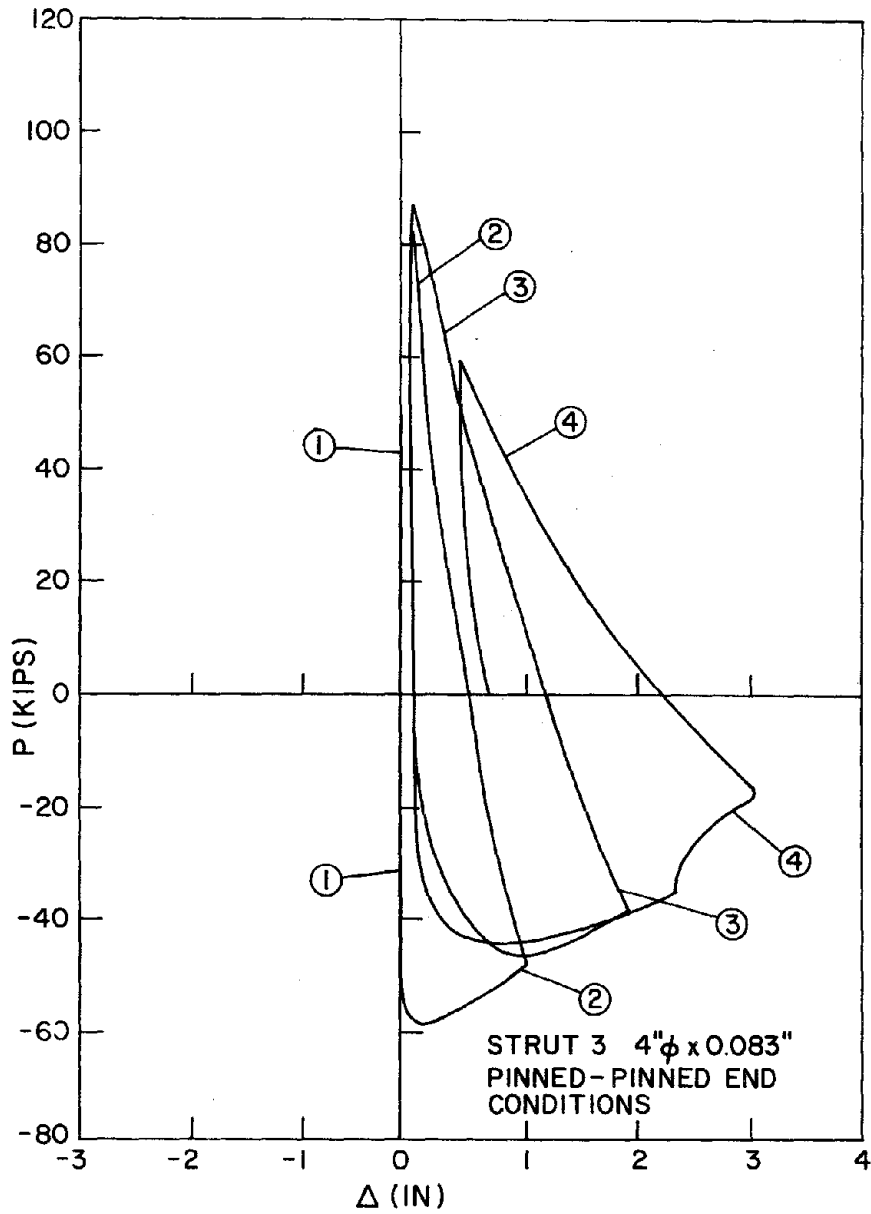
Fig. 3.17 Axial Load vs. Lateral Displacement – Strut 3, Cycles 1-5
(1 kip = 4.45 kN; 1 in. = 25.4 mm)
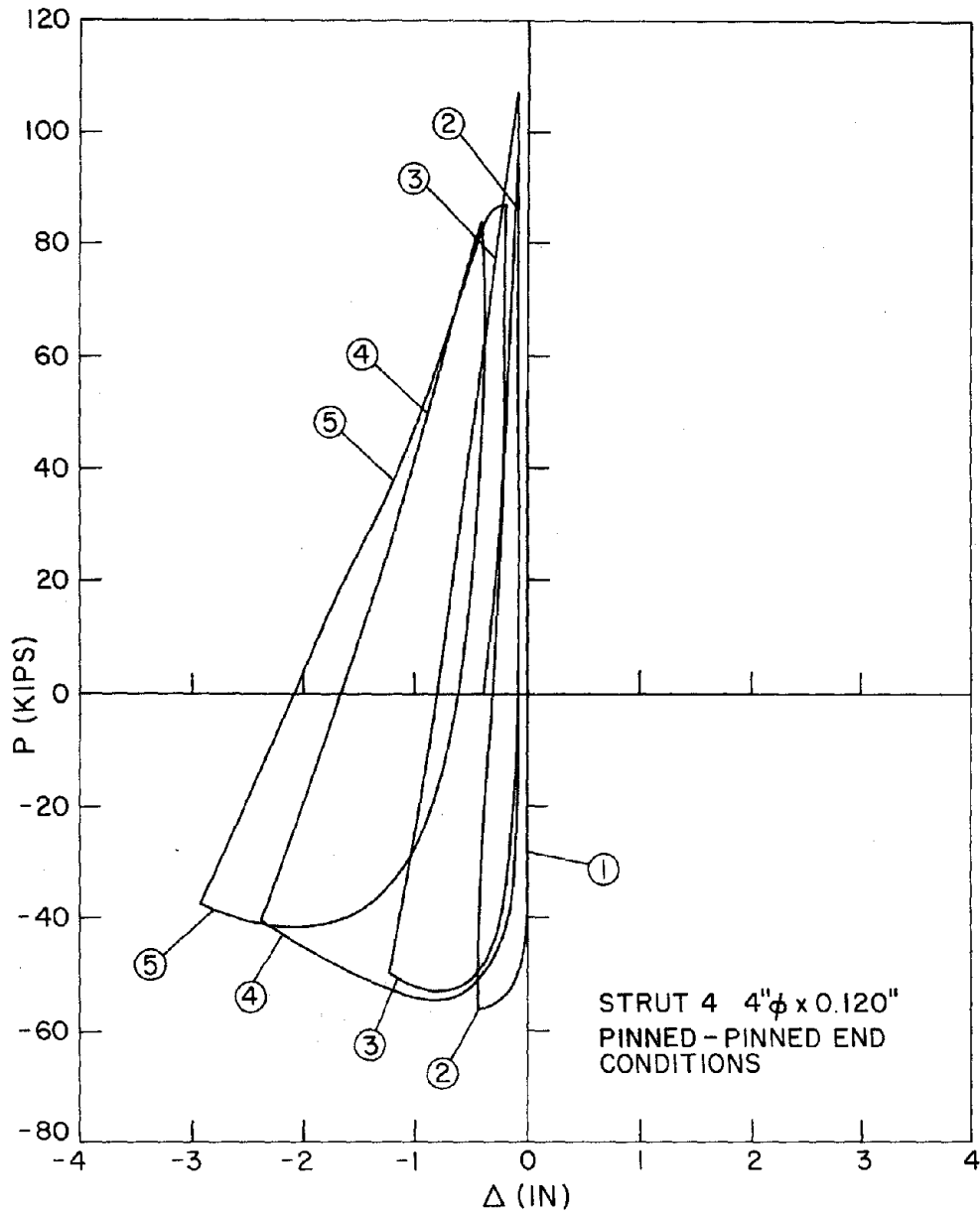
Fig. 3.18 Axial Load vs. Lateral Displacement – Strut 4, Cycles 1-5
(1 kip = 4.45 kN; 1 in. = 25.4 mm)
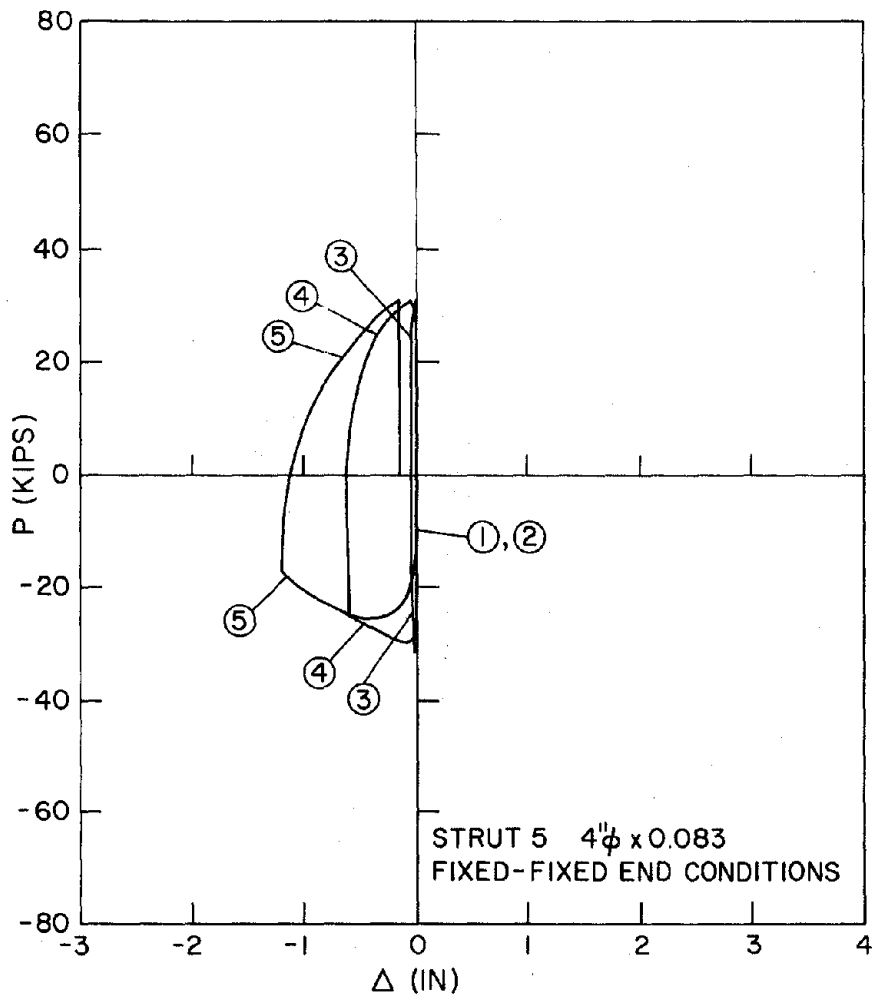
Fig. 3.19 Axial Load vs. Lateral Displacement – Strut 5, Cycles 1-5
(1 kip = 4.45 kN; 1 in. = 25.4 mm)

103
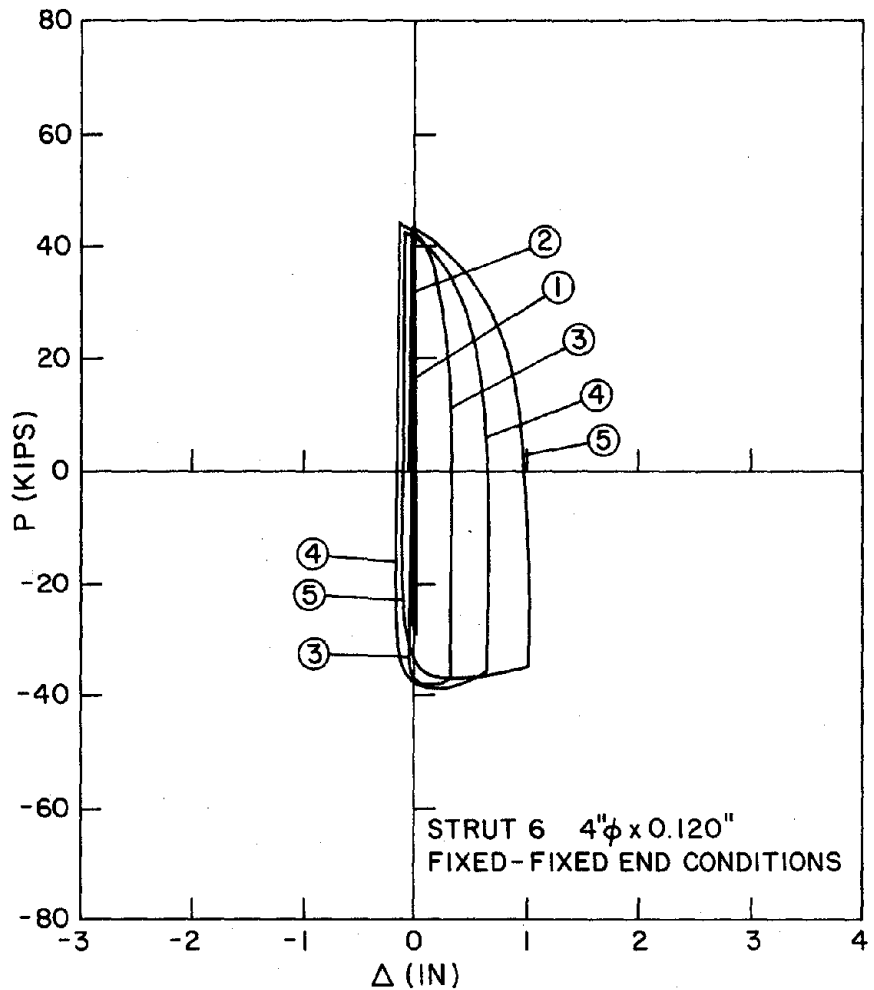
Fig. 3.20 Axial Load vs. Lateral Displacement – Strut 6, Cycles 1-5
(1 kip = 4.45 kN; 1 in. = 25.4 mm)

104
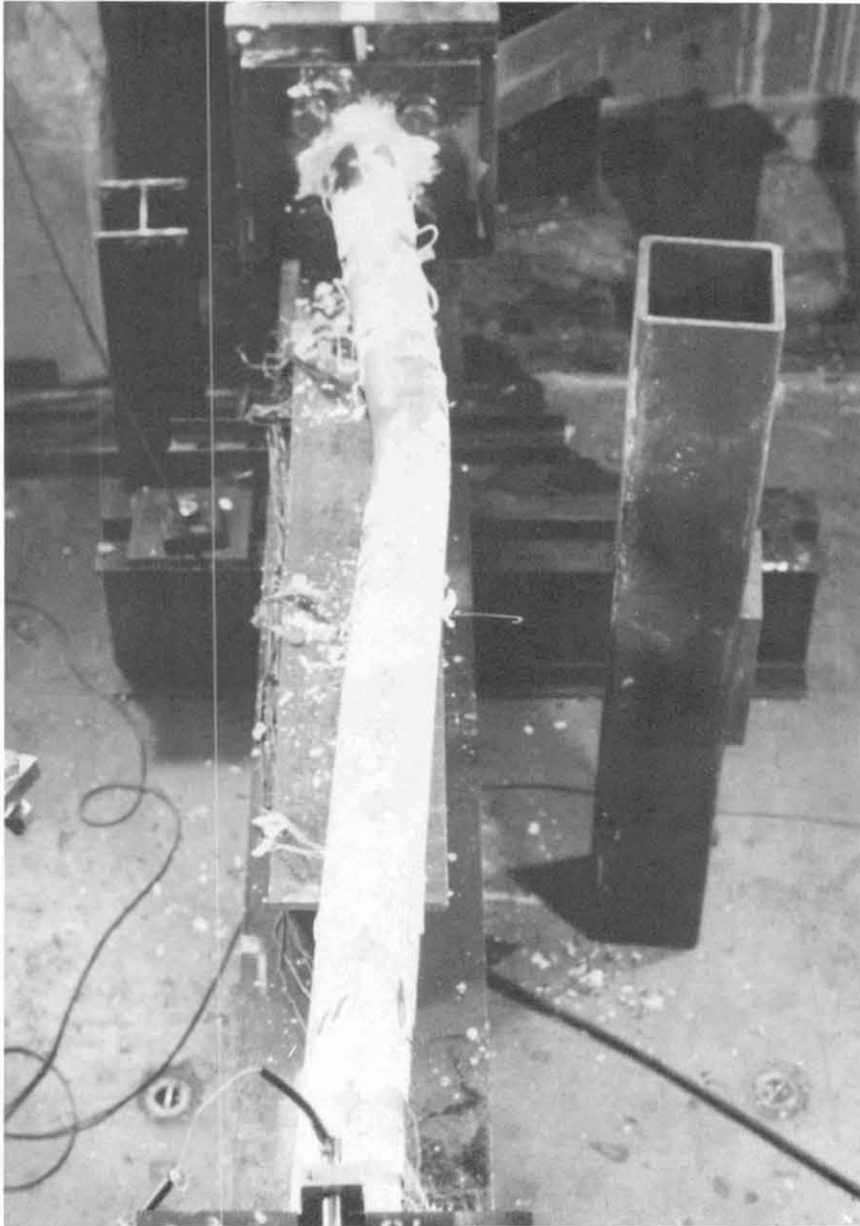
Fig. 3.21 View of Overall Buckled Strut
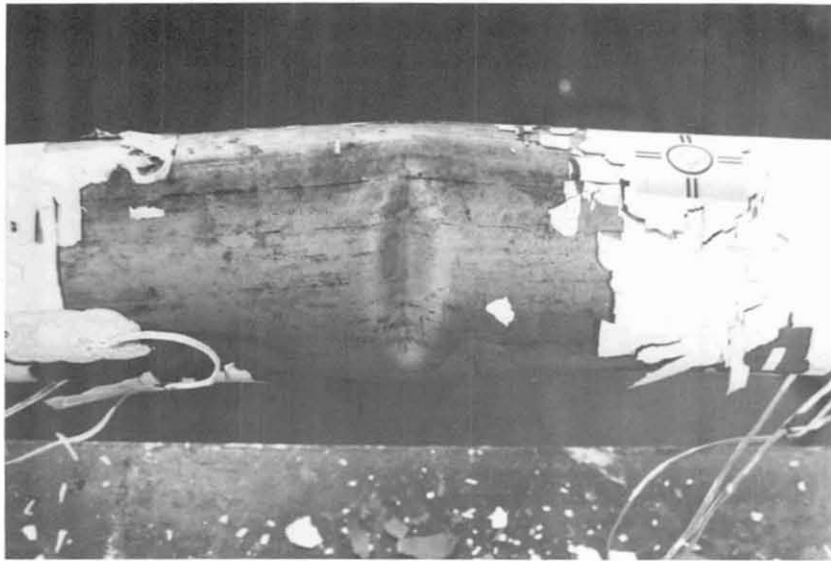
a) Original Local Buckle
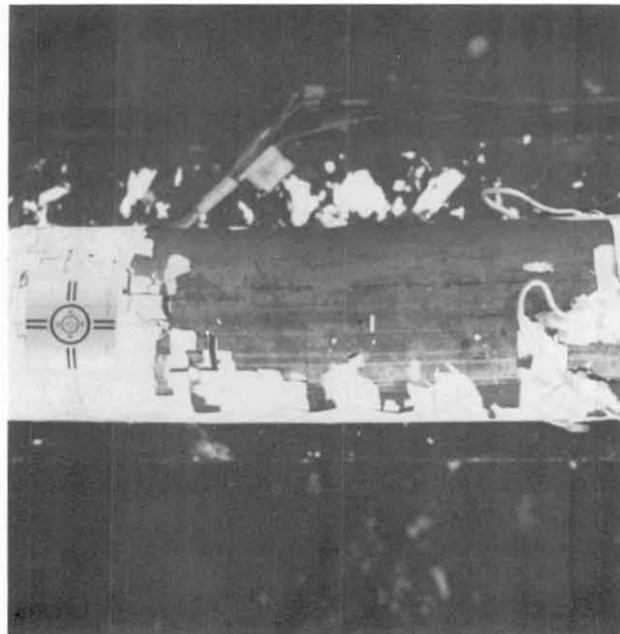
b) Straightening After Tension

Fig. 3.22 Local Buckling at Selected Load Points for
Strut 5 — Center Hinge
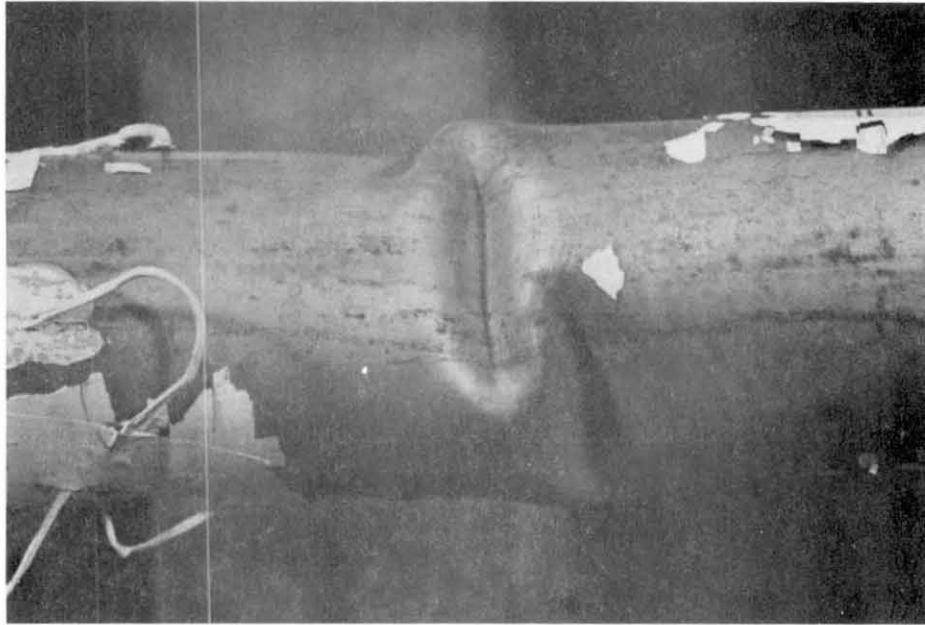
a)   Severe Local Buckle

b)   Tearing in Tension

Fig. 3.23   Local Buckling at Selected Load Points for
Strut 5 - Center Hinge
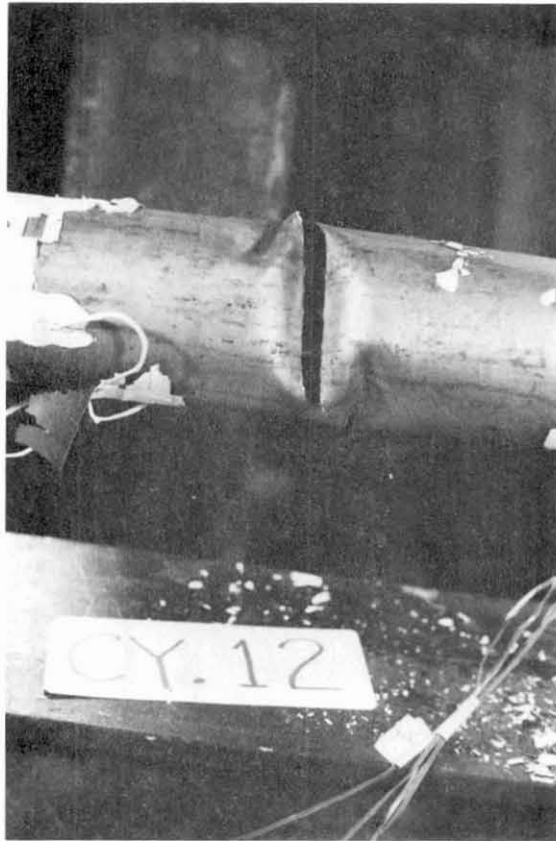
a) Severe Tearing in Tension
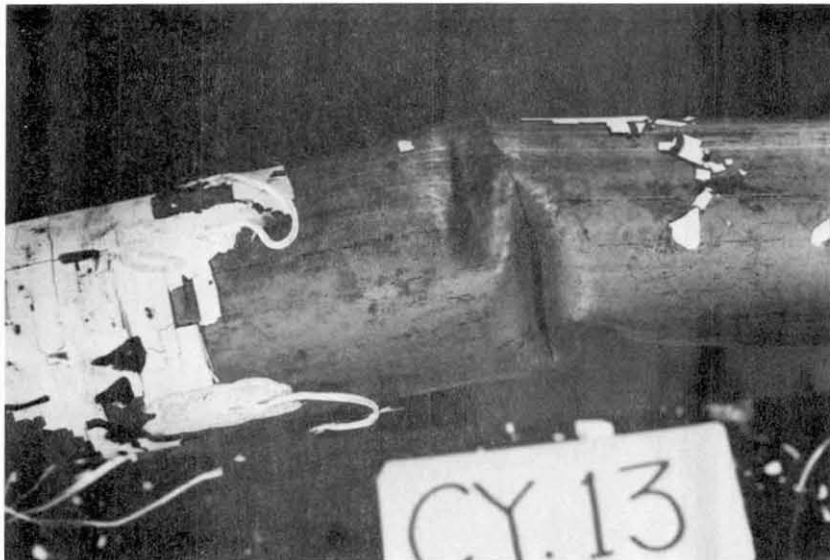
b) Post-Tearing Buckle

Fig. 3.24 Local Buckling at Selected Load Points for
Strut 5 - Center Hinge
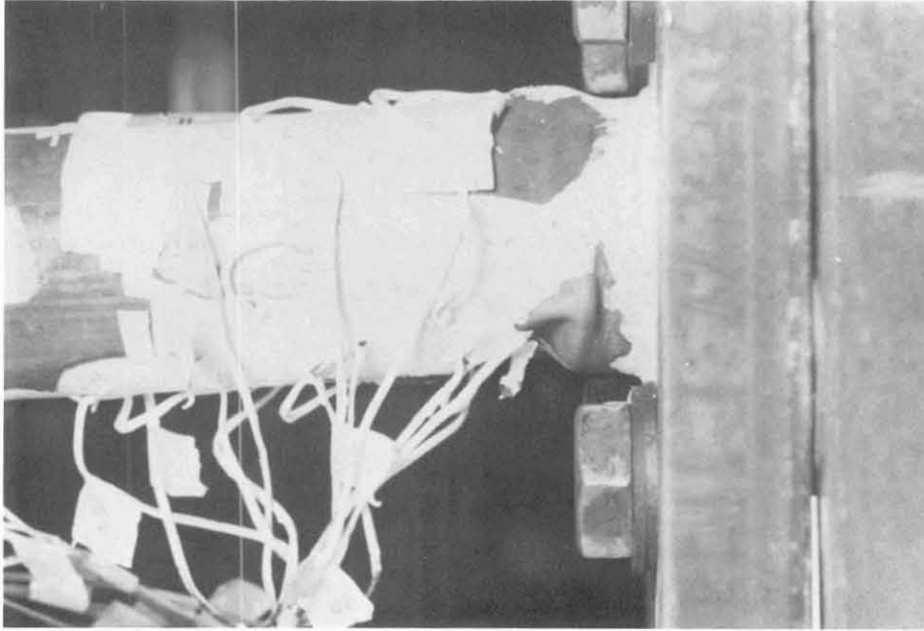
a)   Severe Local Buckle
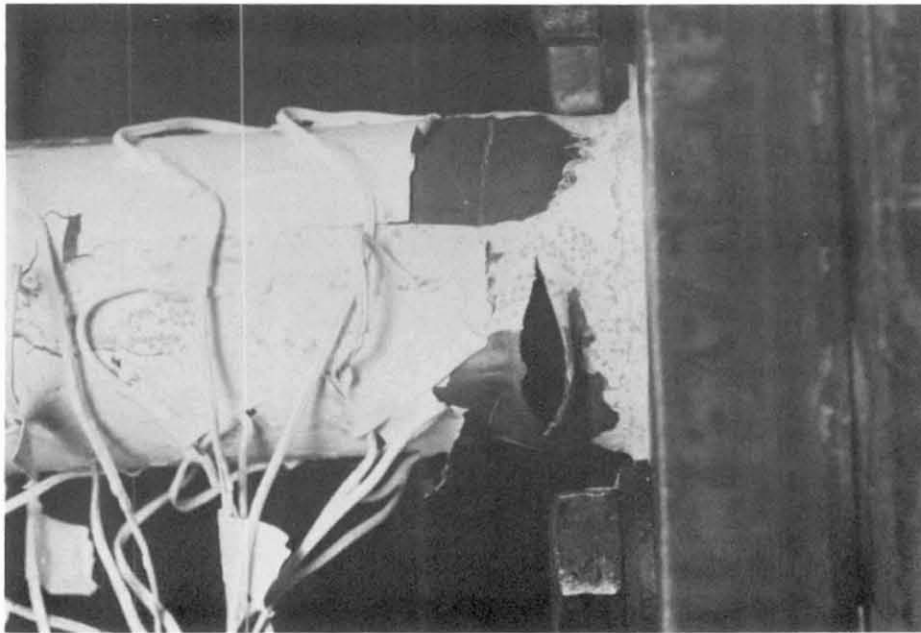
b)   Tensile Tearing

Fig. 3.25   Local Buckling at Foot Hinge - Strut 5
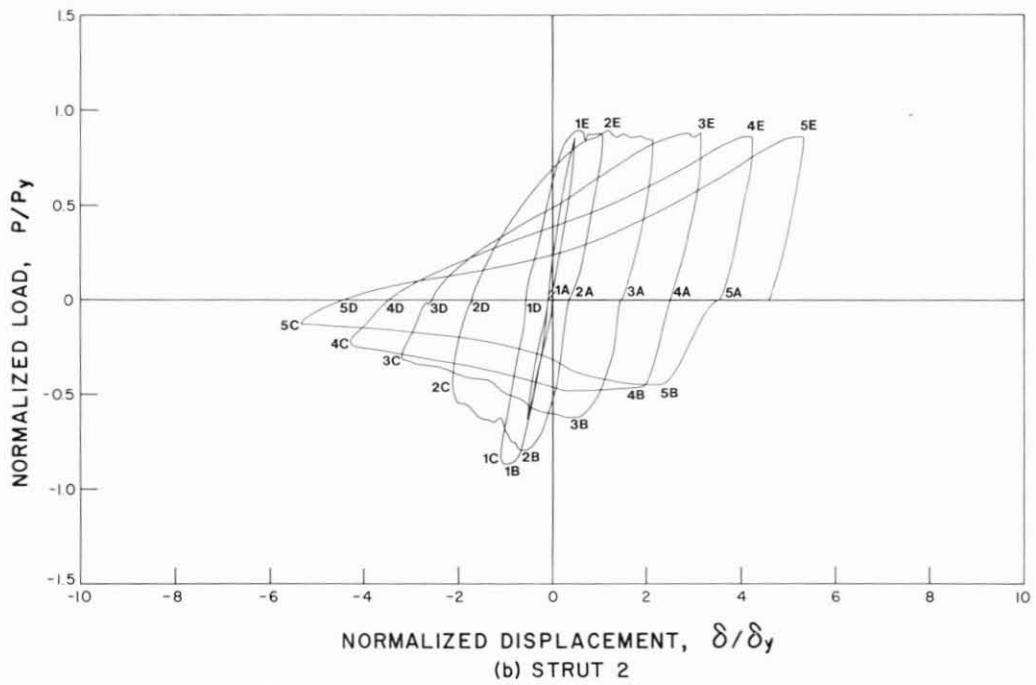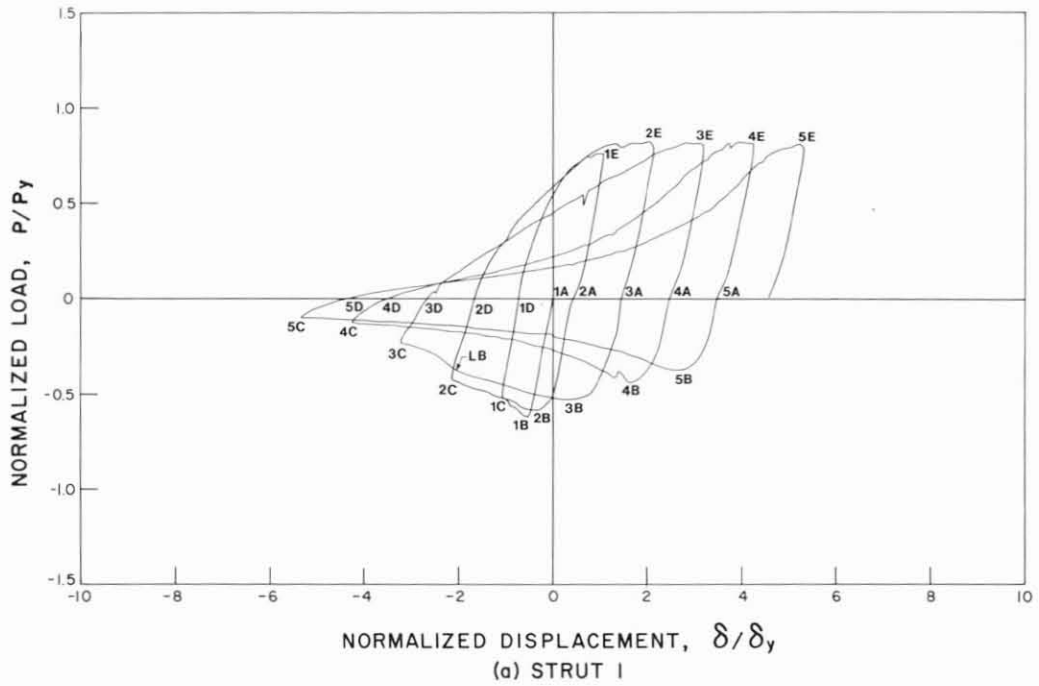
Fig. 3.26 Axial Load vs. Axial Displacement - Normalized

110
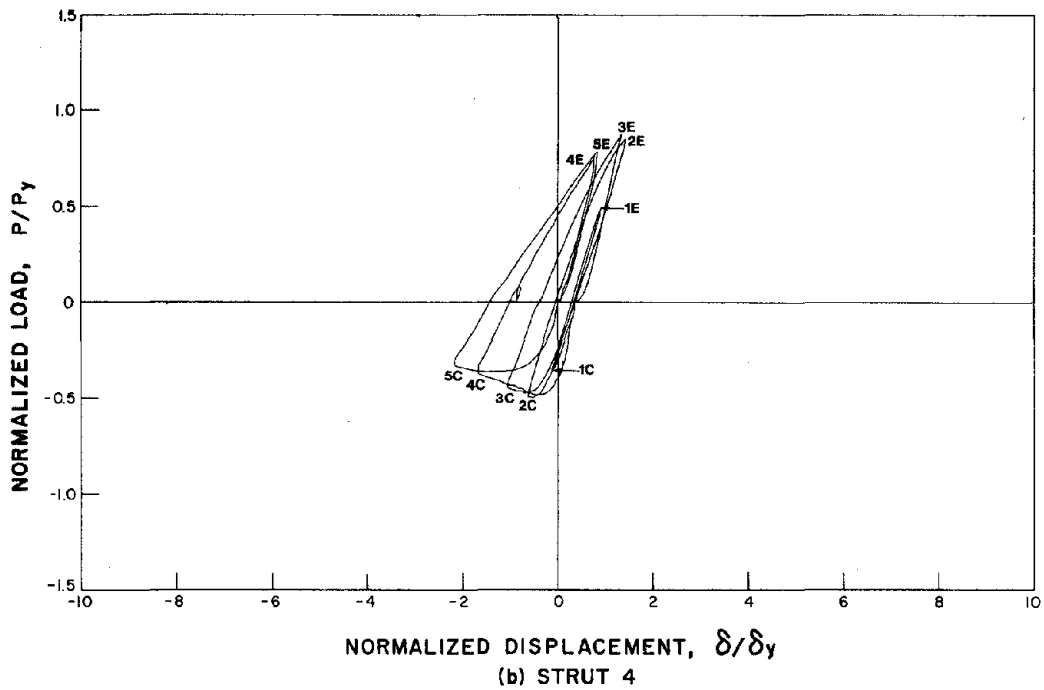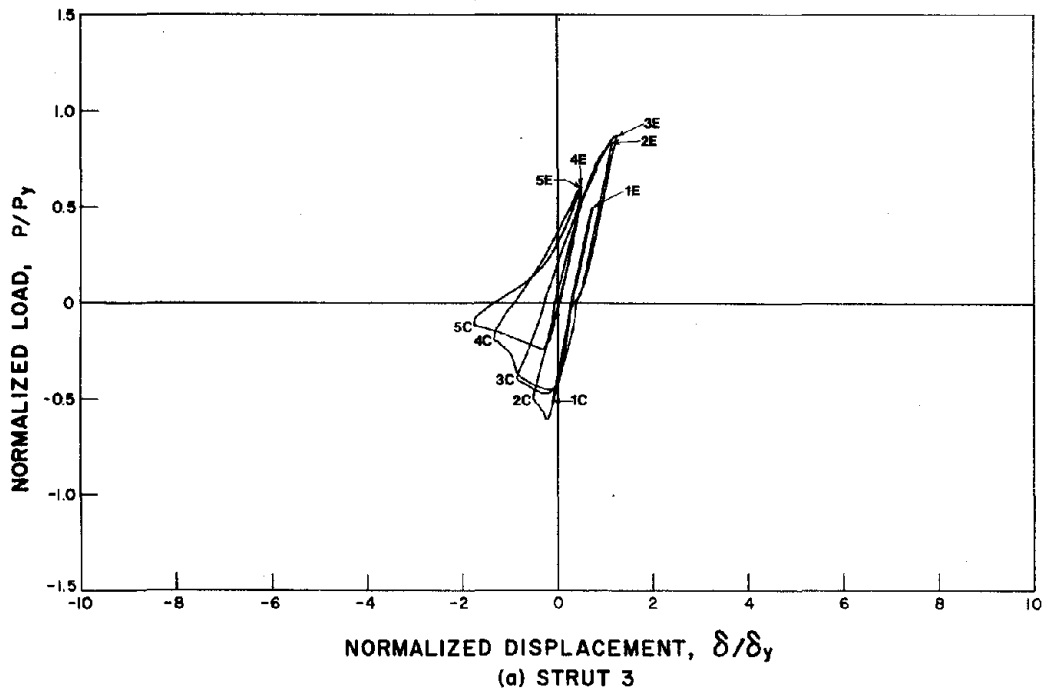
Fig. 3.27   Axial Load vs. Axial Displacement – Normalized

Fig. 3.28   Axial Load vs. Axial Displacement − Normalized

112

Strut 1: pinned, annealed, D/t = 48
Strut 2: pinned, annealed, D/t = 33
Strut 3: pinned, unannealed, D/t = 48
Strut 4: pinned, unannlealed, D/t = 33
Strut 5: fixed, annealed, D/t = 48
Strut 6: fixed, annealed, D/t = 33
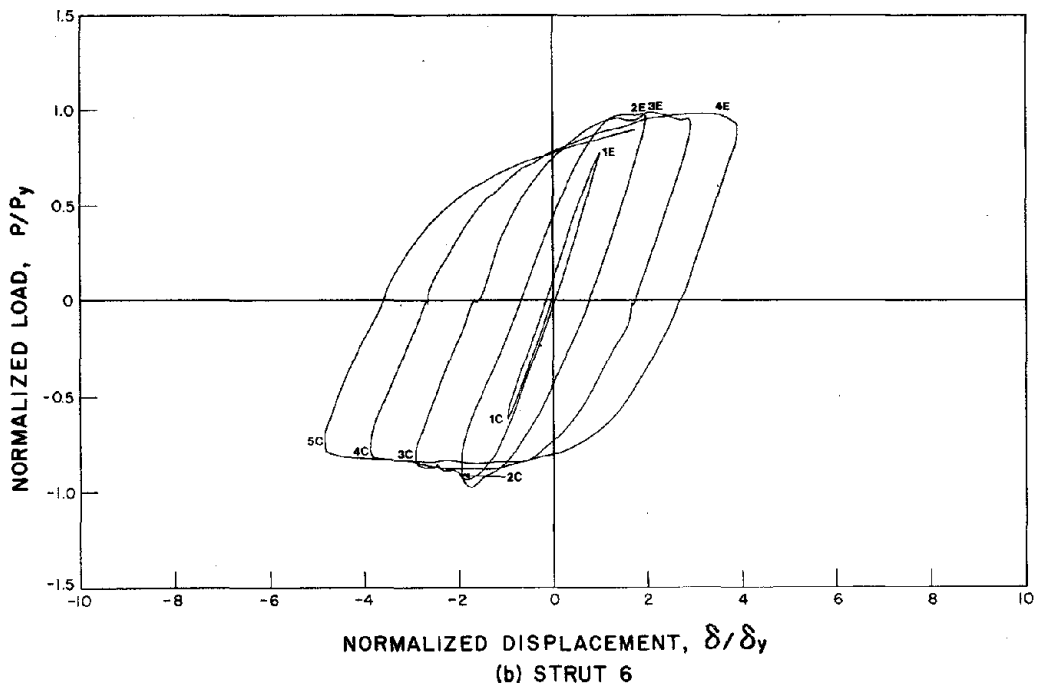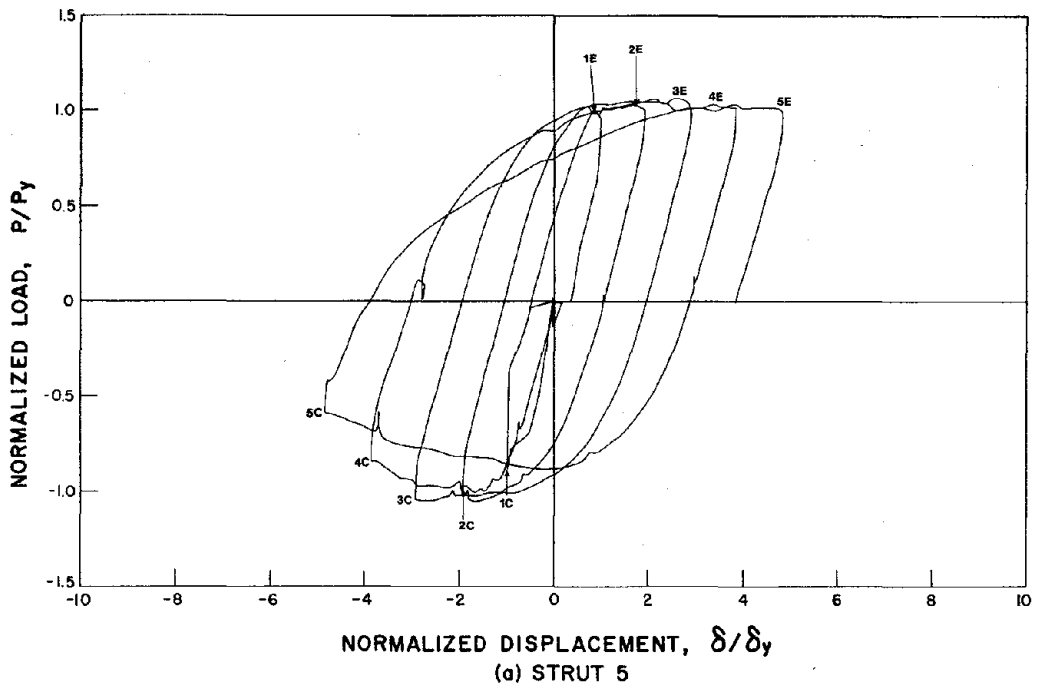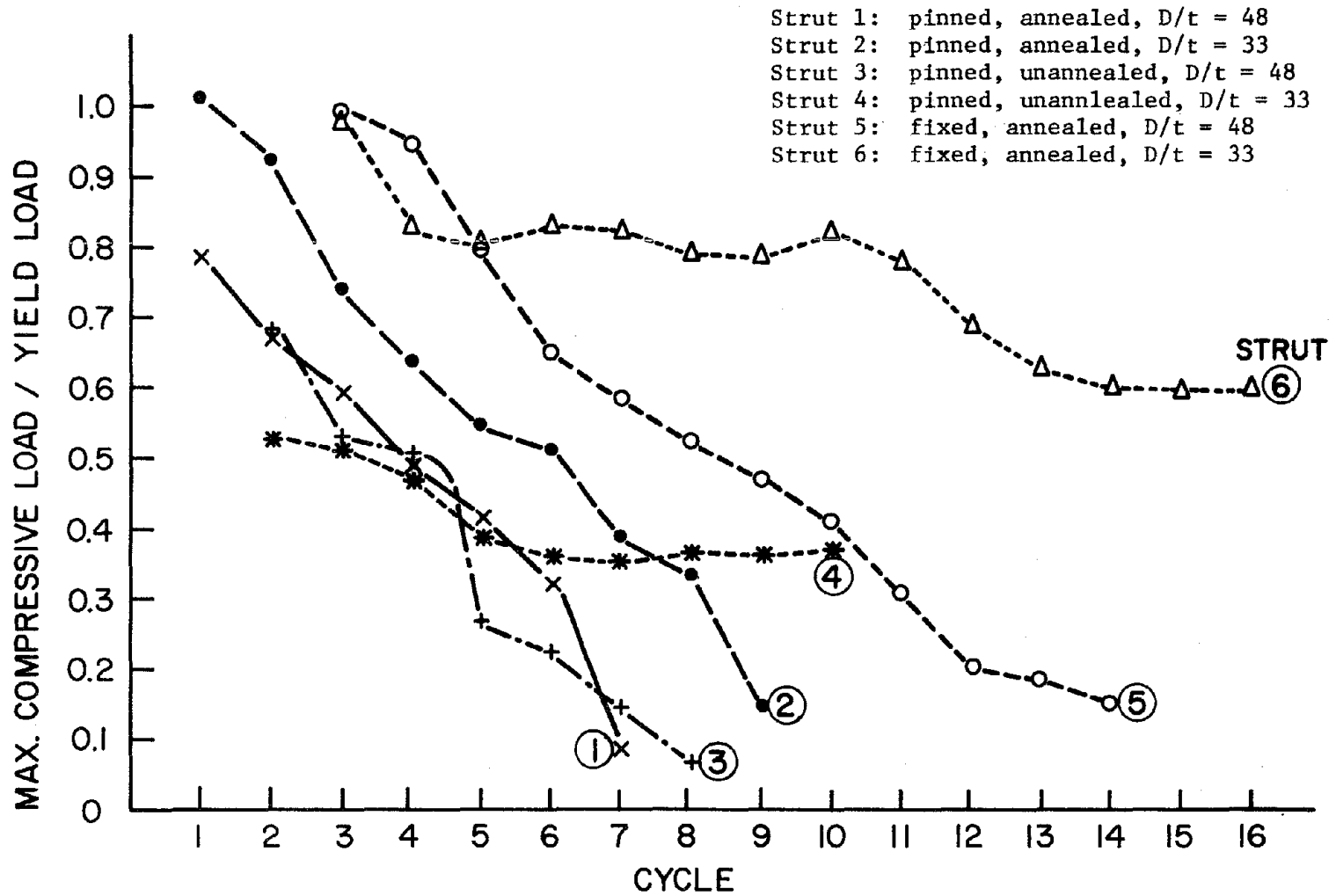
Fig. 3.29 Deterioration of Buckling Loads

(a)

(b)

(c)

(d)
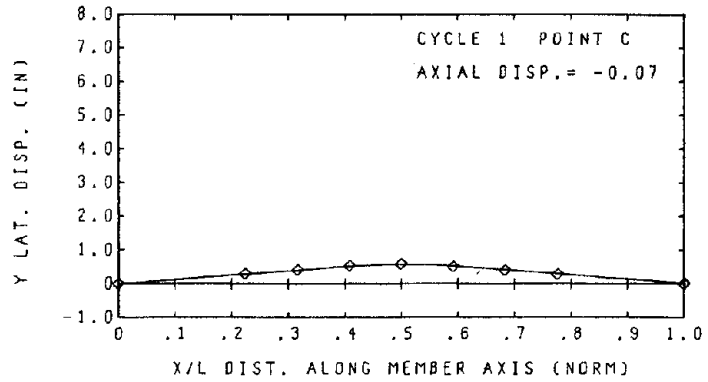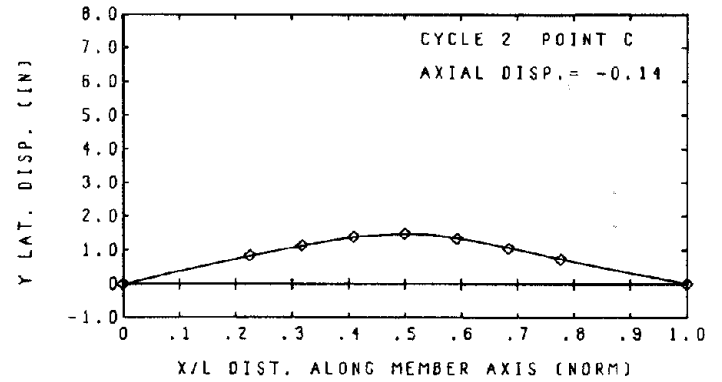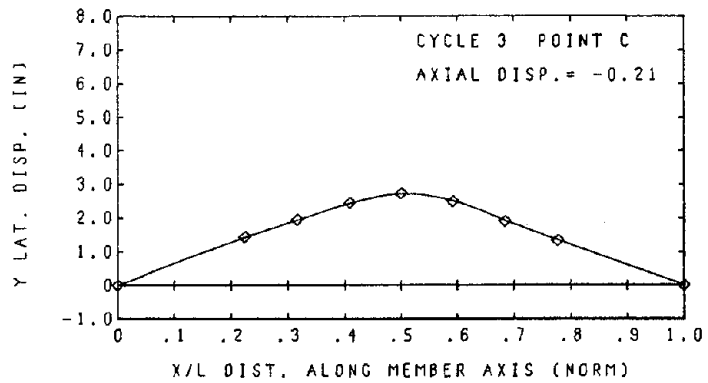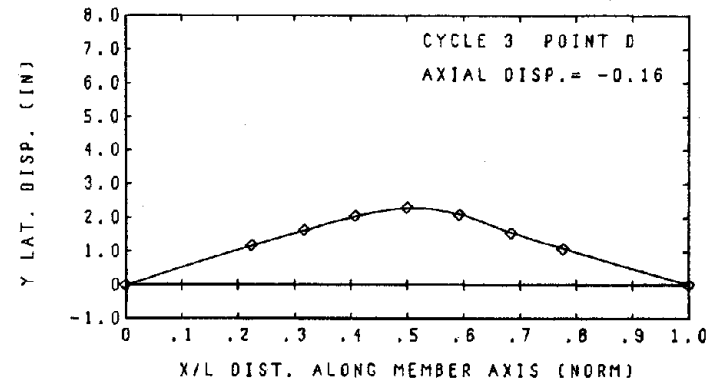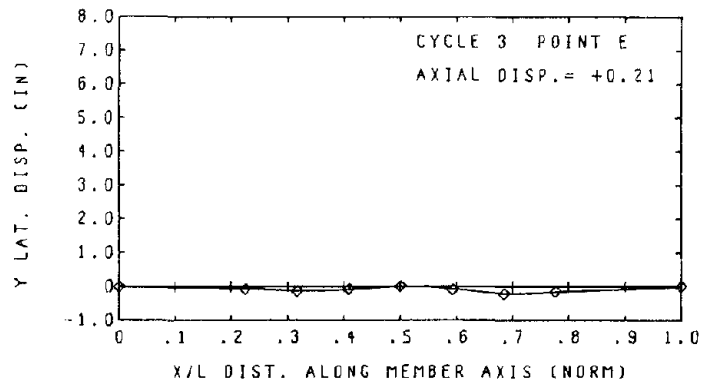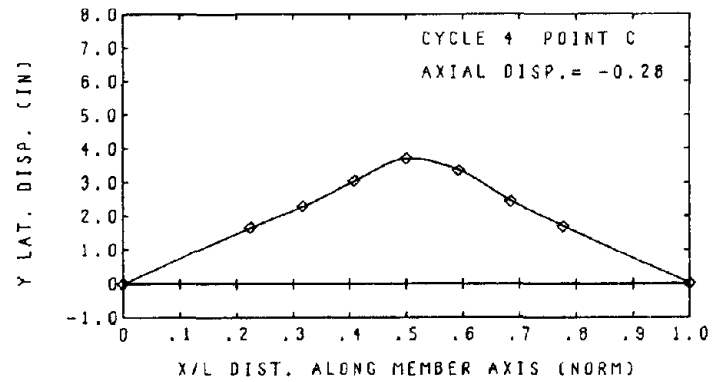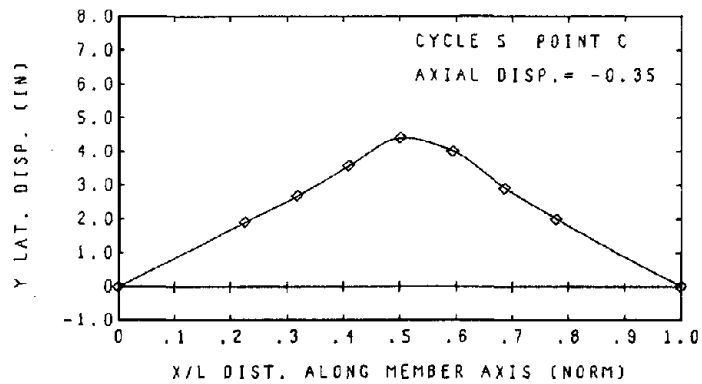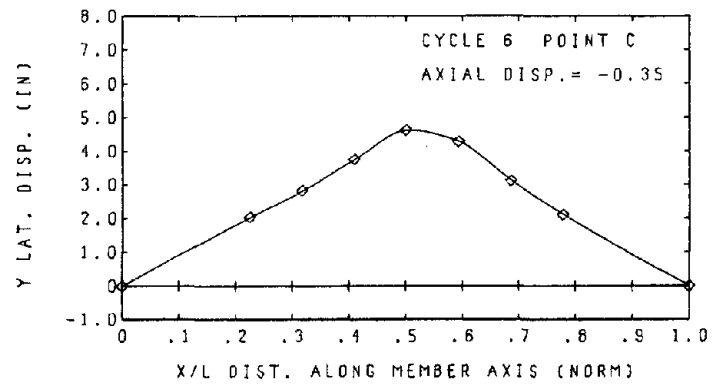
Fig. 3.30   Deflected Shapes - Strut 1 (1 in. = 25.4 mm)
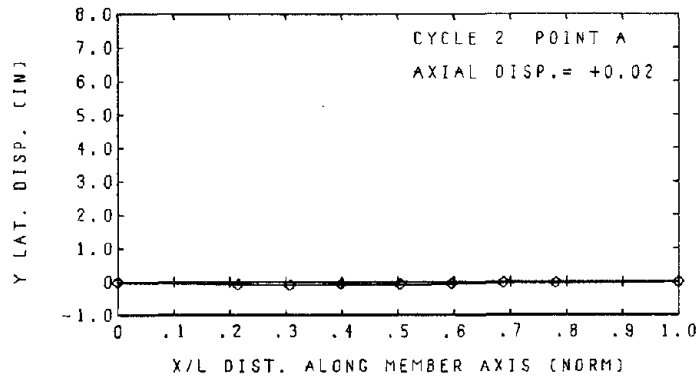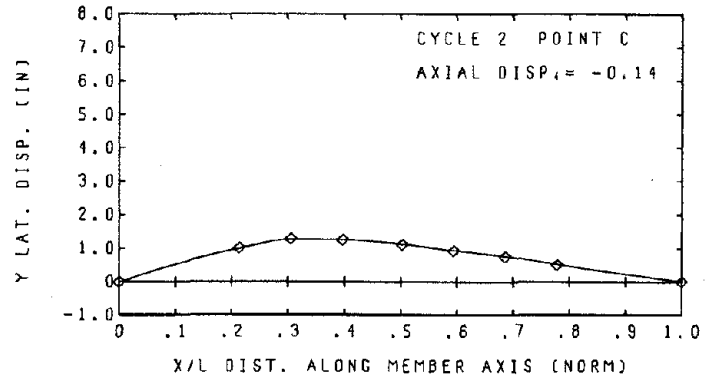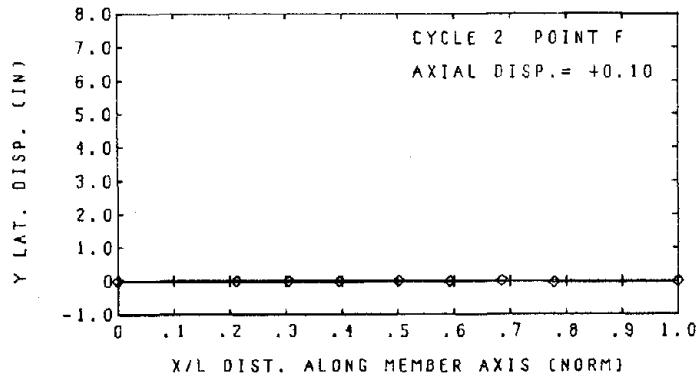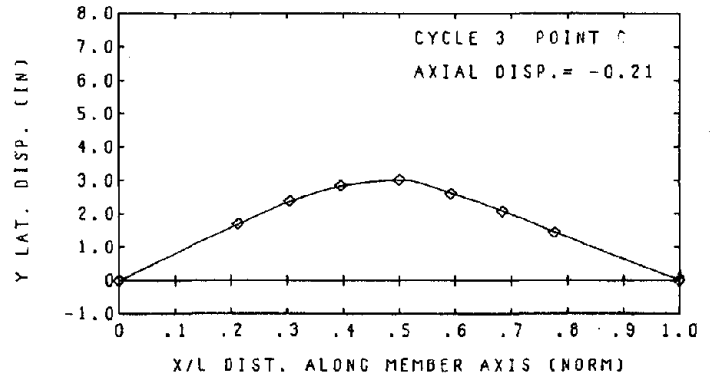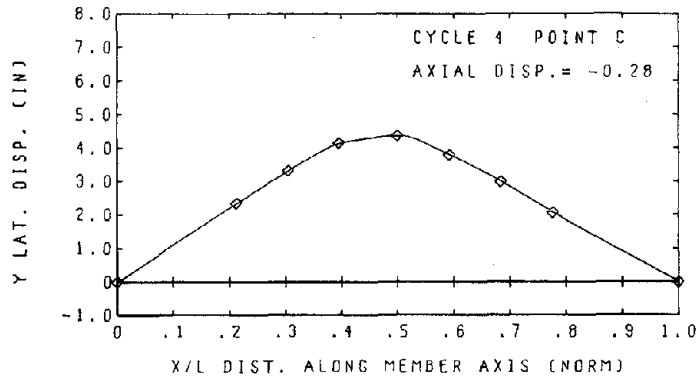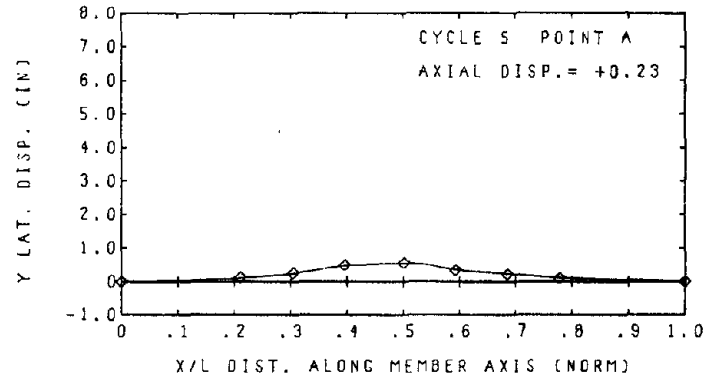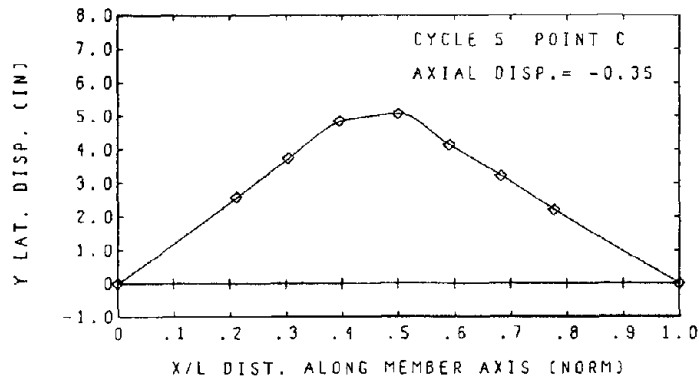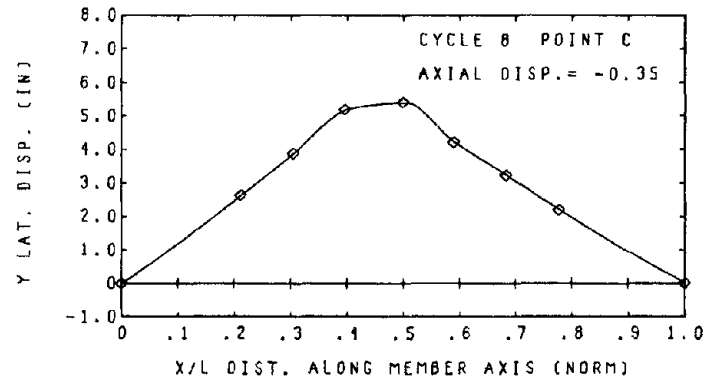
Fig. 3.31 Deflected Shapes – Strut 2 (1 in. = 25.4 mm)
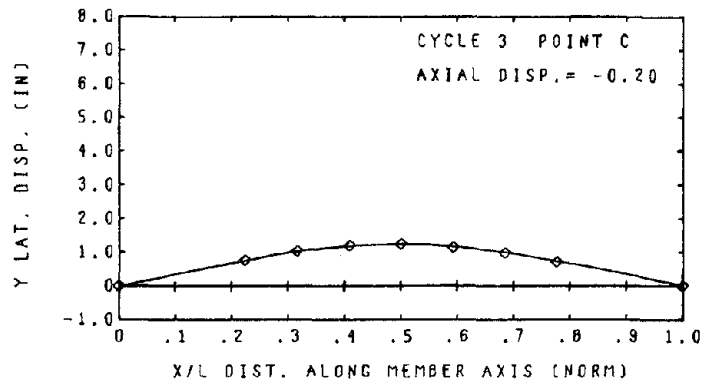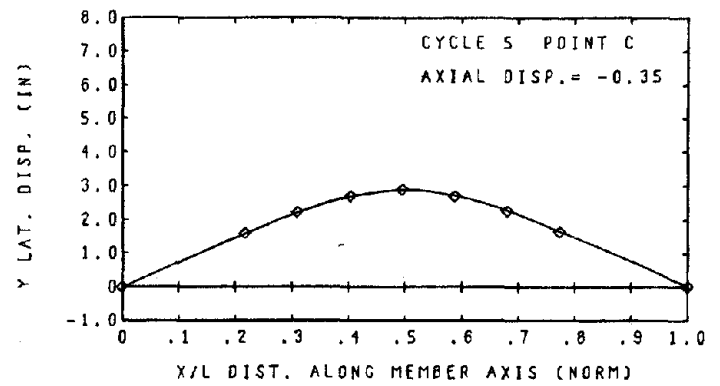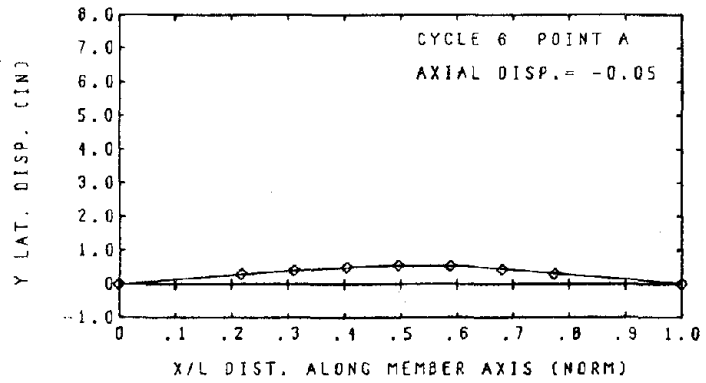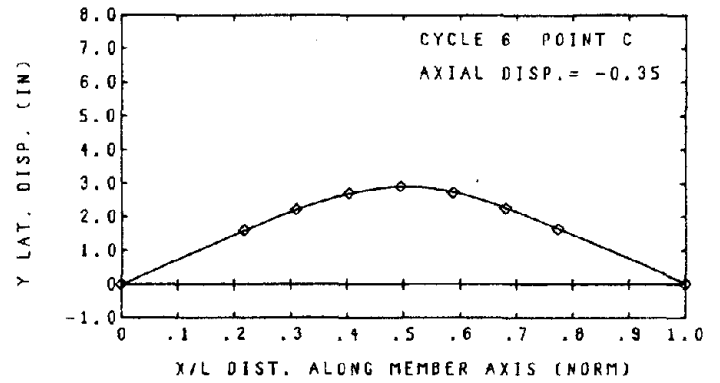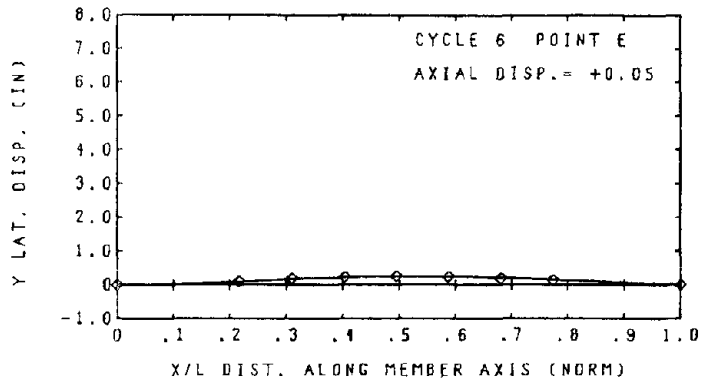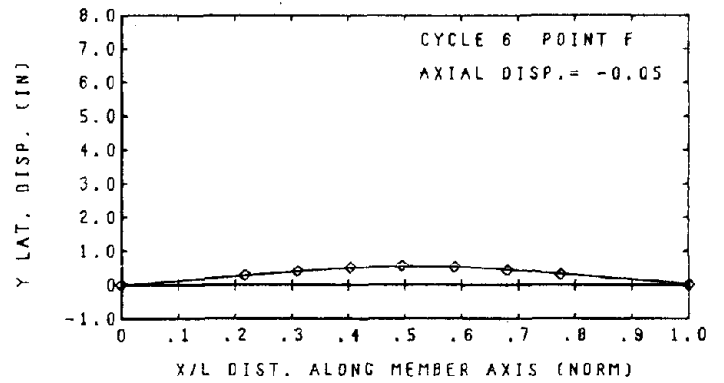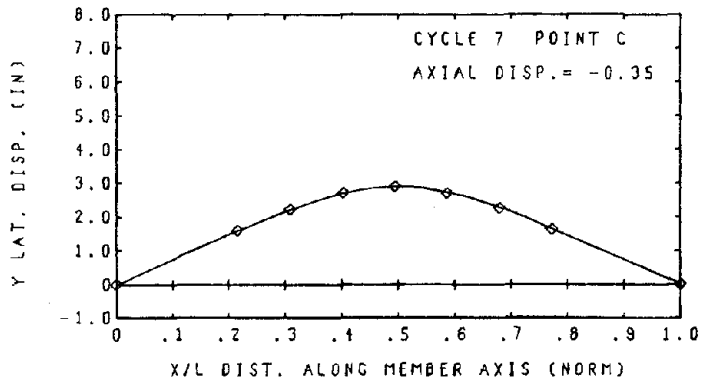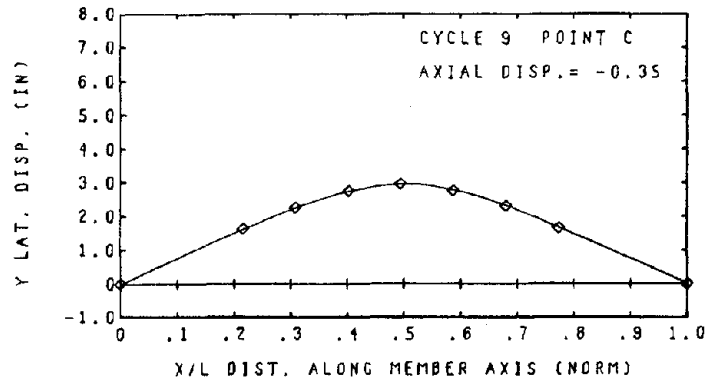
Fig. 3.32 Deflected Shapes – Strut 4 (1 in. = 25.4 mm)

(a) CYCLE 3 POINT C AXIAL DISP.= -0.20

Y LAT. DISP. (IN)
X/L DIST. ALONG MEMBER AXIS (NORM)

(b) CYCLE 5 POINT C AXIAL DISP.= -0.30

Y LAT. DISP. (IN)
X/L DIST. ALONG MEMBER AXIS (NORM)

(c) CYCLE 6 POINT A AXIAL DISP.= +0.01

Y LAT. DISP. (IN)
X/L DIST. ALONG MEMBER AXIS (NORM)

(d) CYCLE 6 POINT C AXIAL DISP.= -0.30

Y LAT. DISP. (IN)
X/L DIST. ALONG MEMBER AXIS (NORM)
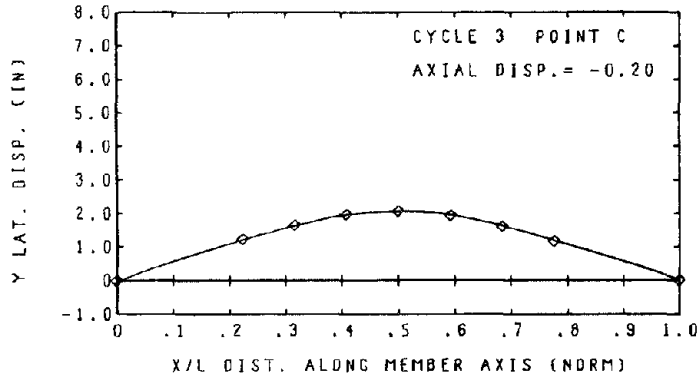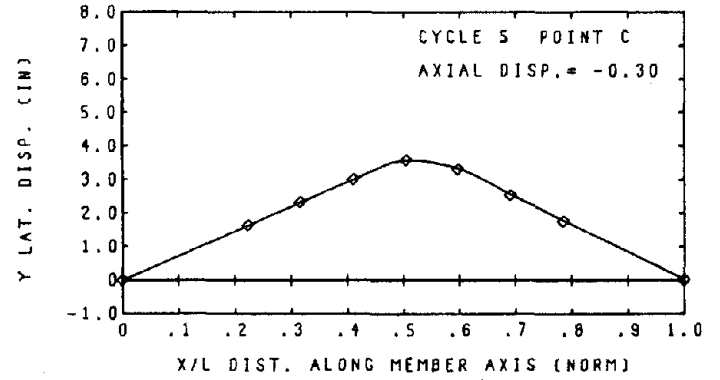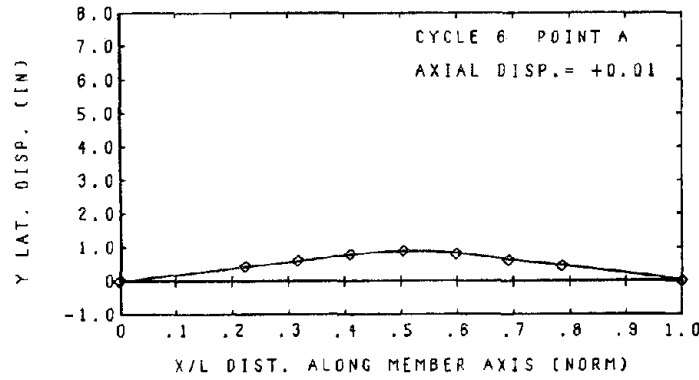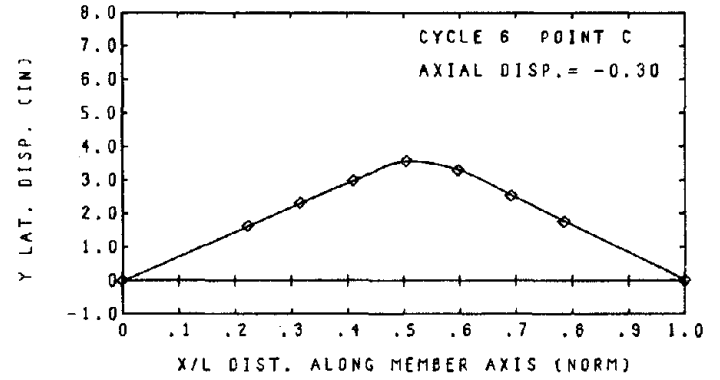
Fig. 3.33 Deflected Shapes – Strut 3 (1 in. = 25.4 mm)
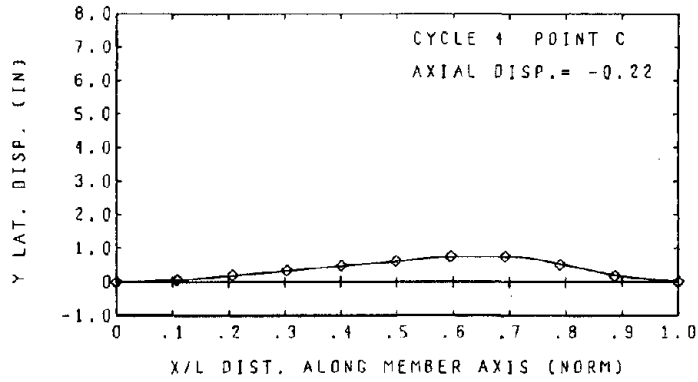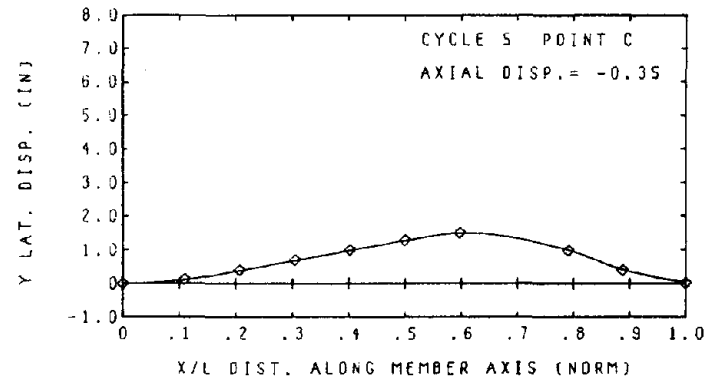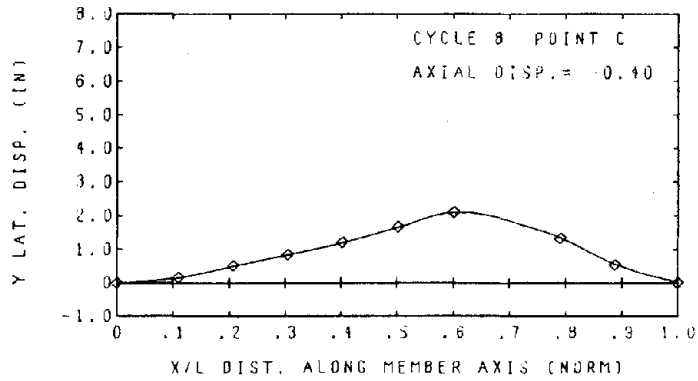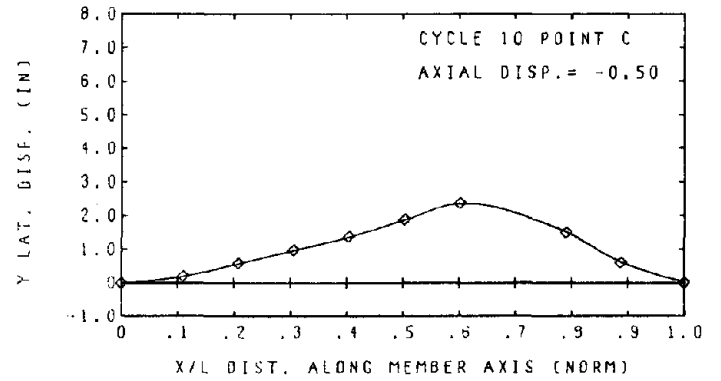
Fig. 3.34   Deflected Shapes – Strut 5 (1 in. = 25.4 mm)
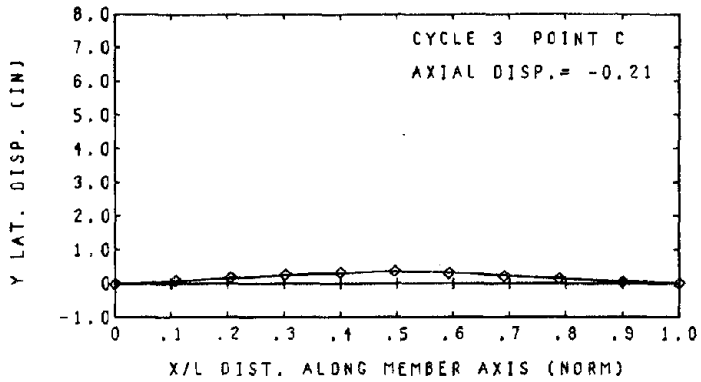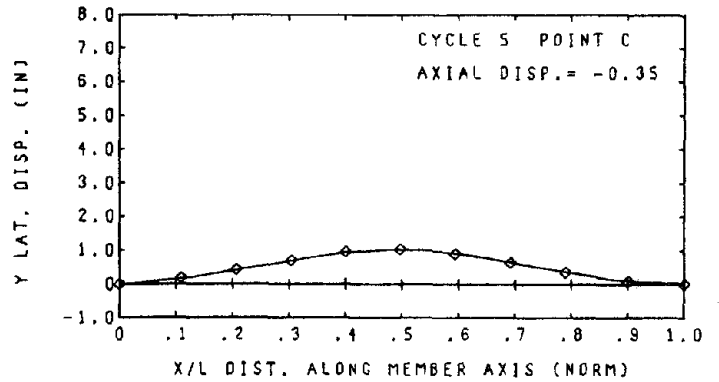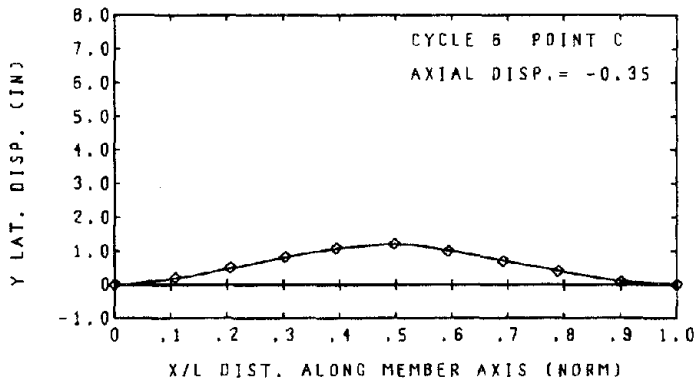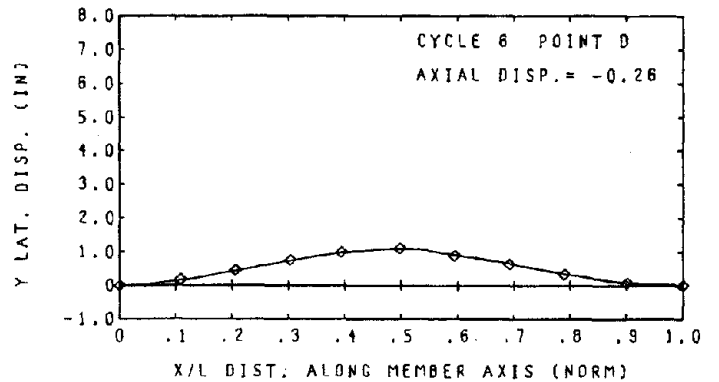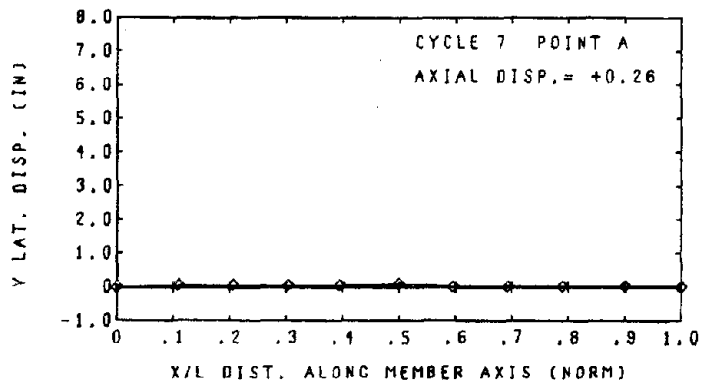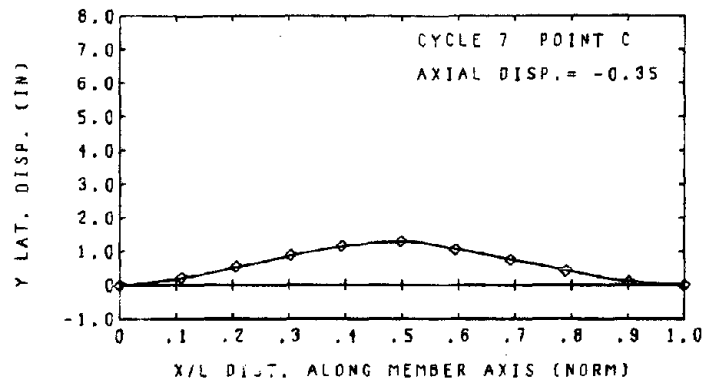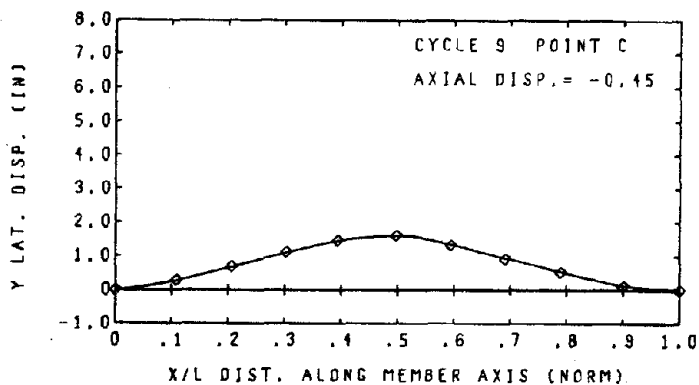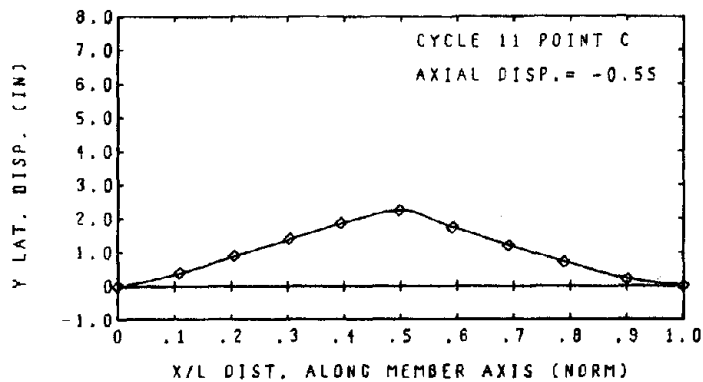
Fig. 3.35 Deflected Shapes - Strut 6 (1 in. = 2.54 mm)
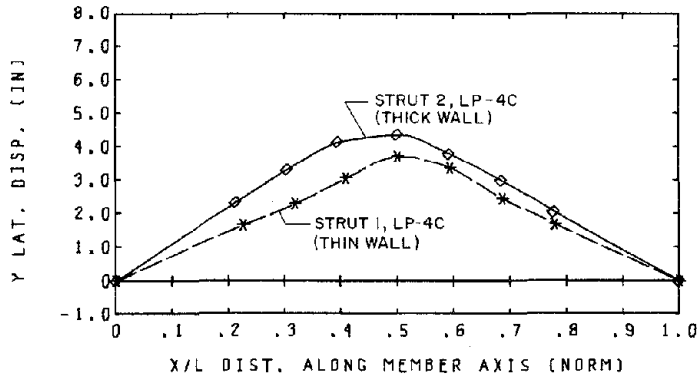
(a) THICK WALL (ST. 2) vs. THIN WALL (ST. 1)
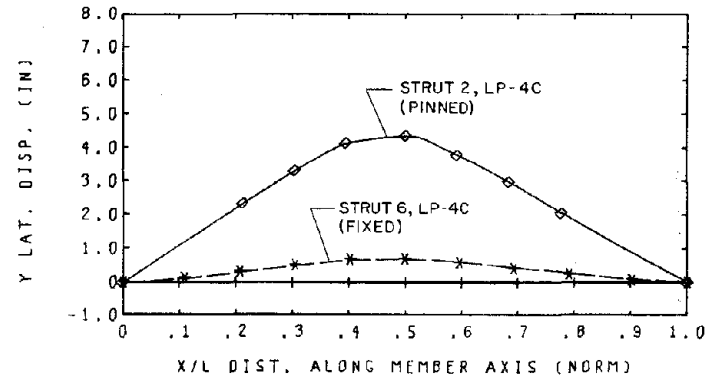
(b) PINNED (ST. 2) vs. FIXED (ST. 6)
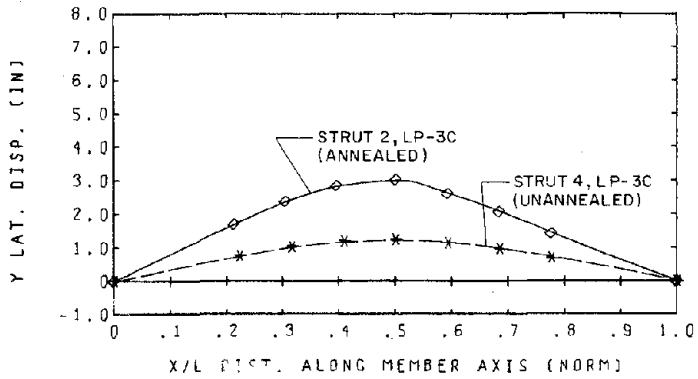
(c) ANNEALED (ST. 2) vs. UNANNEALED (ST. 4)
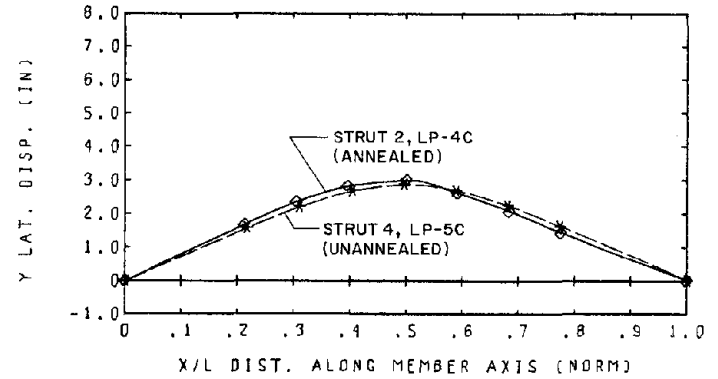
(d) ANNEALED (ST. 2) vs. UNANNEALED (ST. 4)

Fig. 3.36 Deflected Shapes – Comparisons between Struts
(1 in. = 25.4 mm)
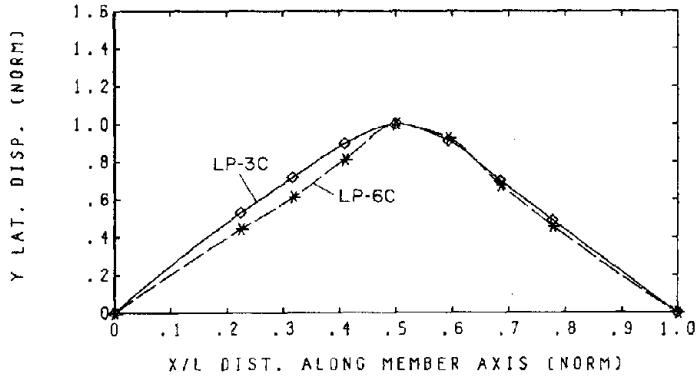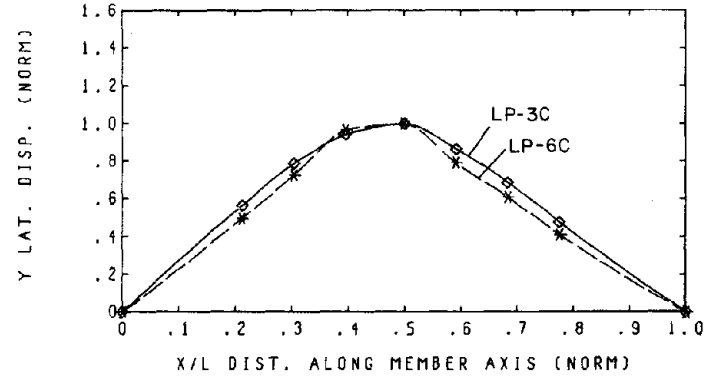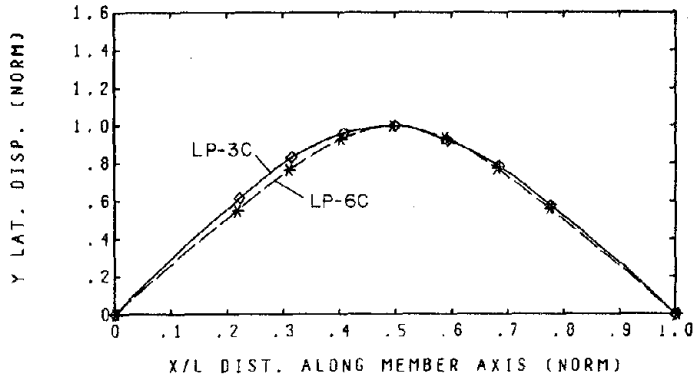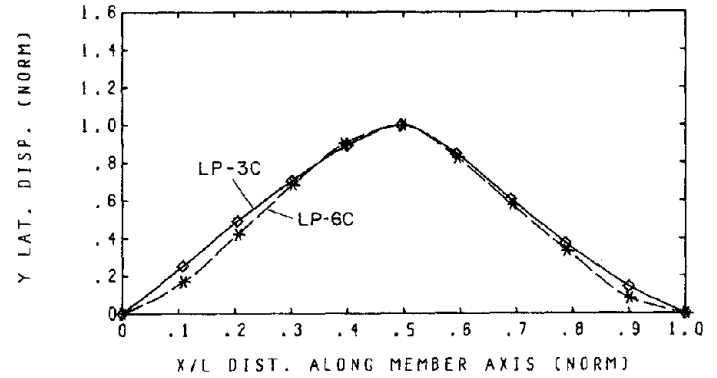
Fig. 3.37 Deflected Shapes - Comparisons between Cycles

Strut 1: pinned, annealed, D/t = 48
Strut 2: pinned, annealed, D/t = 33
Strut 3: pinned, unannealed, D/t = 48
Strut 4: pinned, unannealed, D/t = 33
Strut 5: fixed, annealed, D/t = 48
Strut 6: fixed, annealed, D/t = 33

RIDGID PLASTIC ELEMENT

STRUT

E_i = STRUT ENERGY DISSIPATED IN CYCLE i

$$RP_i = P_y (\delta_{Ei} + 2\delta_{Ci} + \delta_{Ai})$$

DISSIPATION EFFICIENCY = $\dfrac{E_i}{RP_i}$
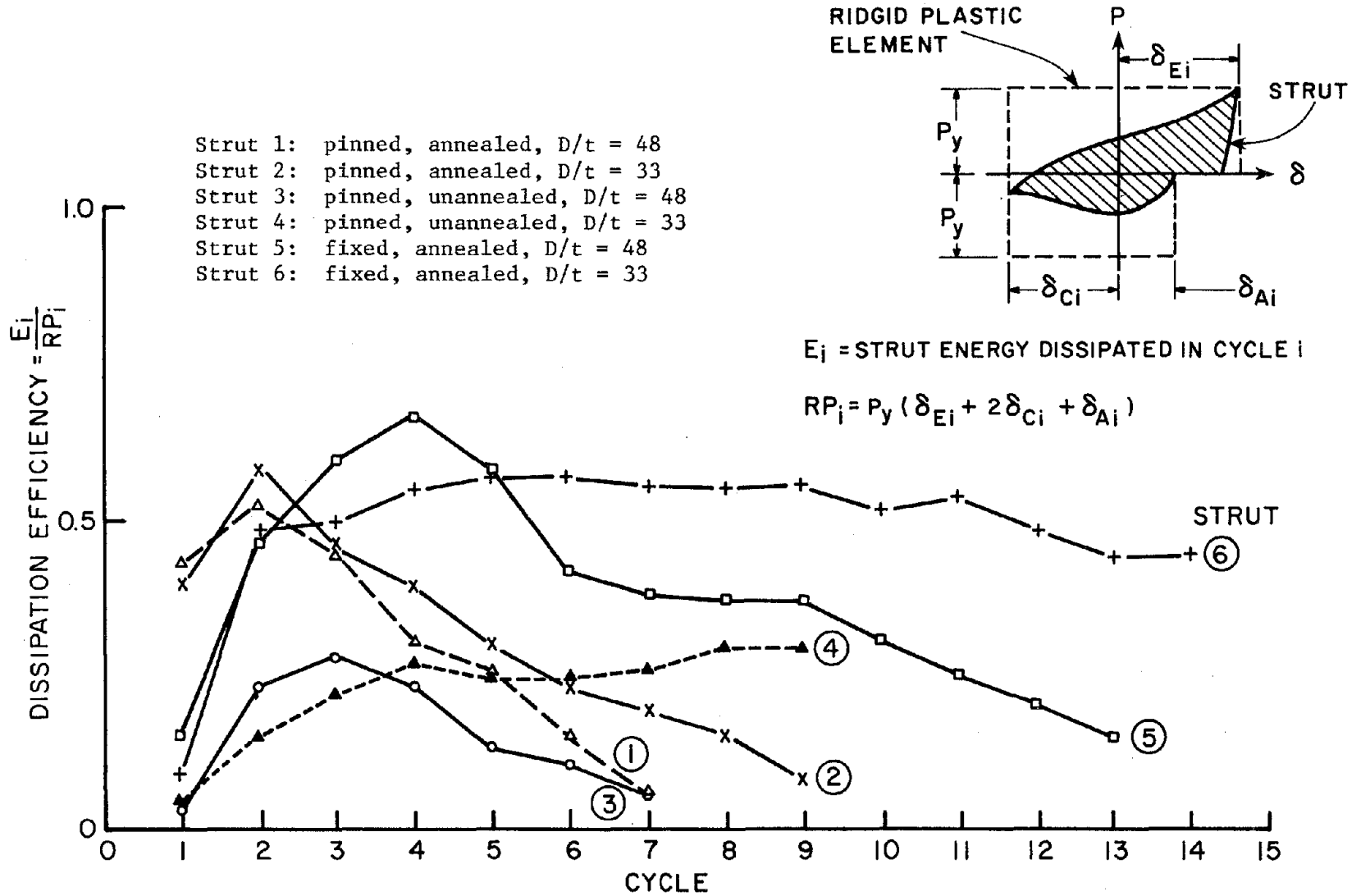
CYCLE

Fig. 3.38 Energy Dissipation Efficiencies per Cycle
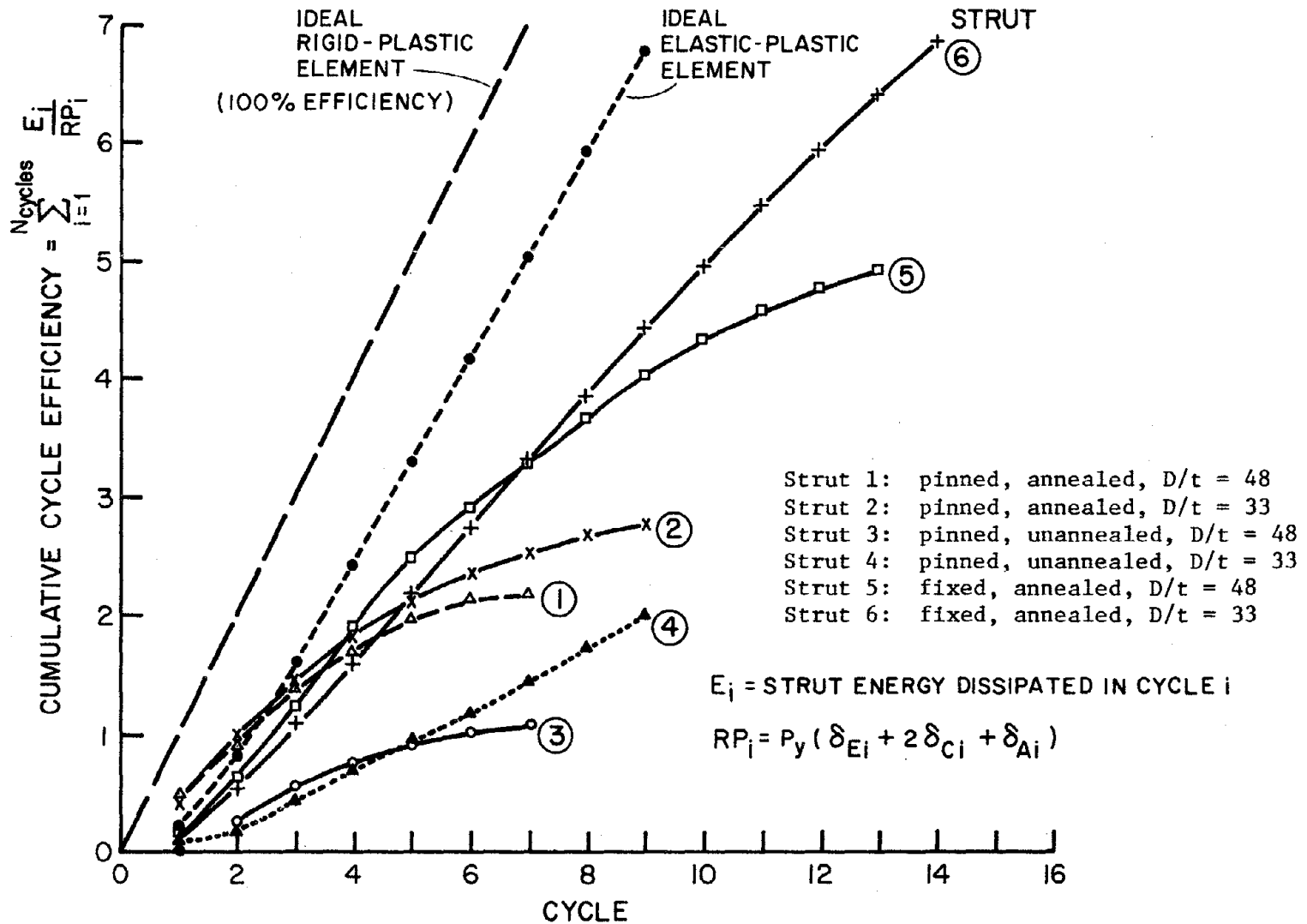
Fig. 3.39 Cumulative Cycle Efficiencies

a) PINNED - END STRUT

In this figure:

CENTER PLASTIC REGION #1 and CENTER PLASTIC REGION #2 are at the center, labeled with PLASTIC HINGE.

$$P = \frac{M_P}{\Delta}$$

$$\frac{P}{M_P} = \frac{1}{\Delta}$$

Labels: $-P$, $-M_P$, Δ, $L/2$

b) FIXED - END STRUT

Labels: PLASTIC HINGE, CENTER PLASTIC REGION#1, CENTER PLASTIC REGION#2, HEAD PLASTIC REGION, FOOT PLASTIC REGION, POINTS OF INFLECTION

$$P = \frac{2M_P}{\Delta}$$

$$\frac{P}{M_P} = \frac{2}{\Delta}$$

Labels: $-P$, $-M_P$, Δ, $L/2$
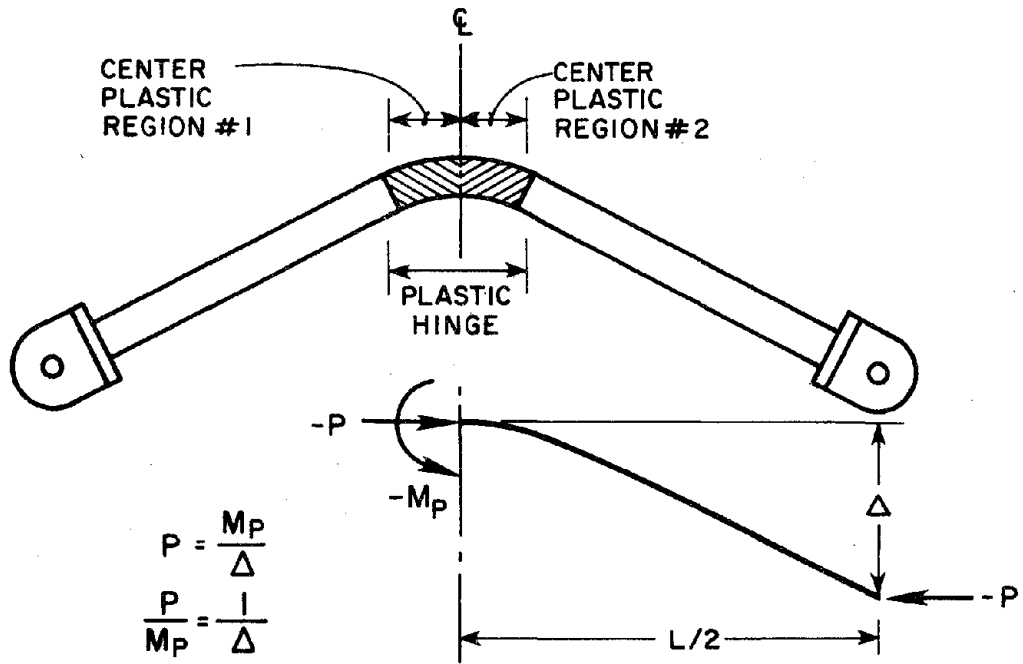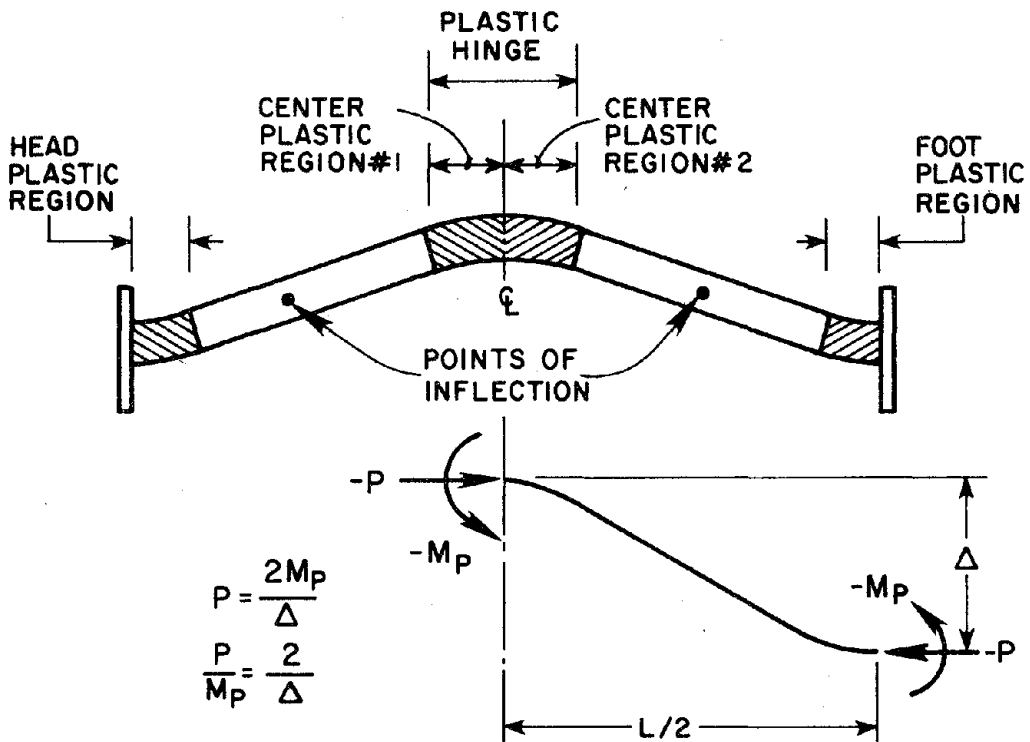
Fig. 4.1 Formation of Plastic Hinges

128
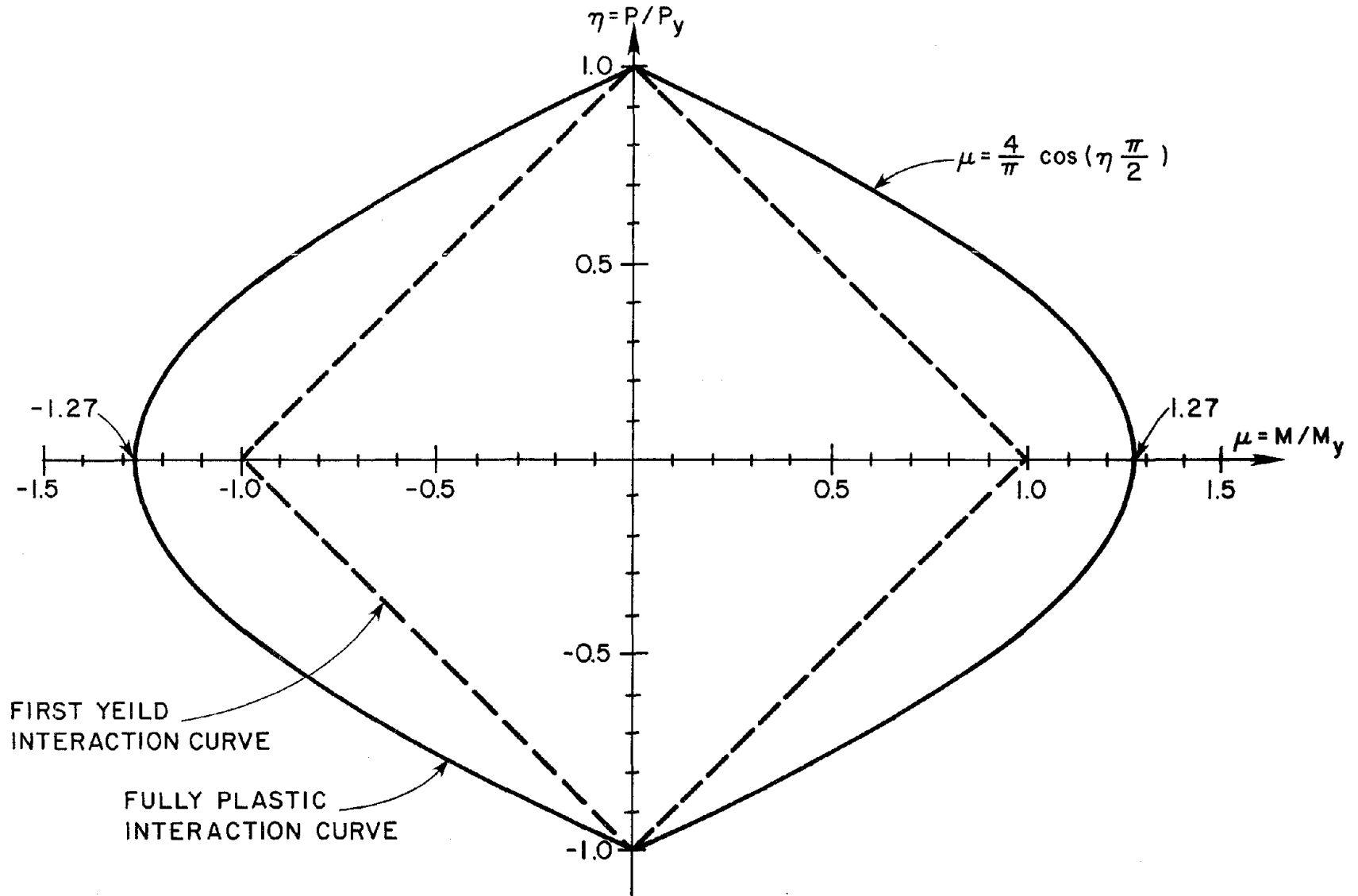
Fig. 4.2   Axial Load–Bending Moment Interaction Curves for
Elastic–Perfectly Plastic Thin Tubular Pipe Section
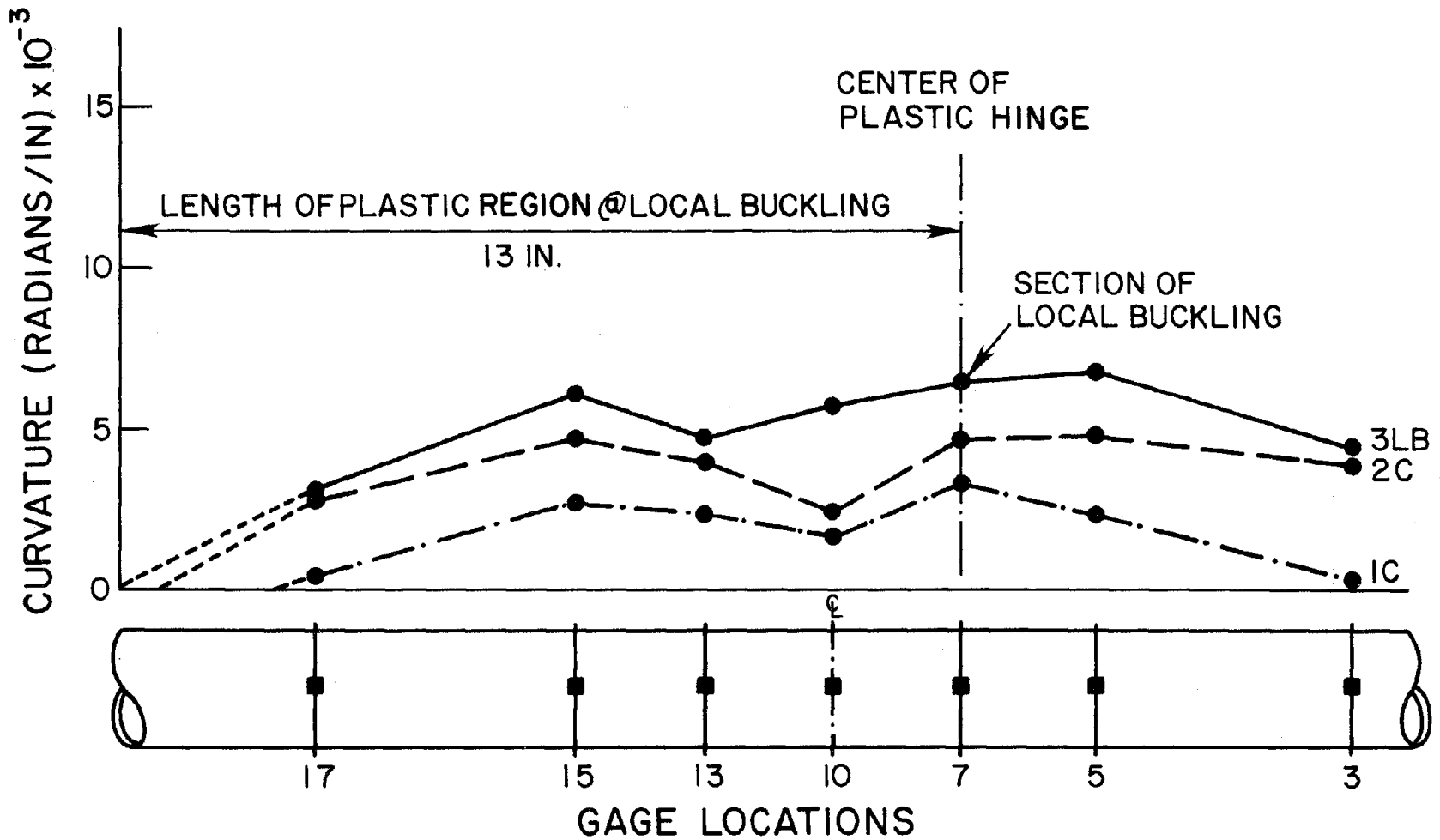
Fig. 4.3   Curvatures within Plastic Hinge – Strut 1 (Load Points C)
(1 in. = 25.4 mm)

130
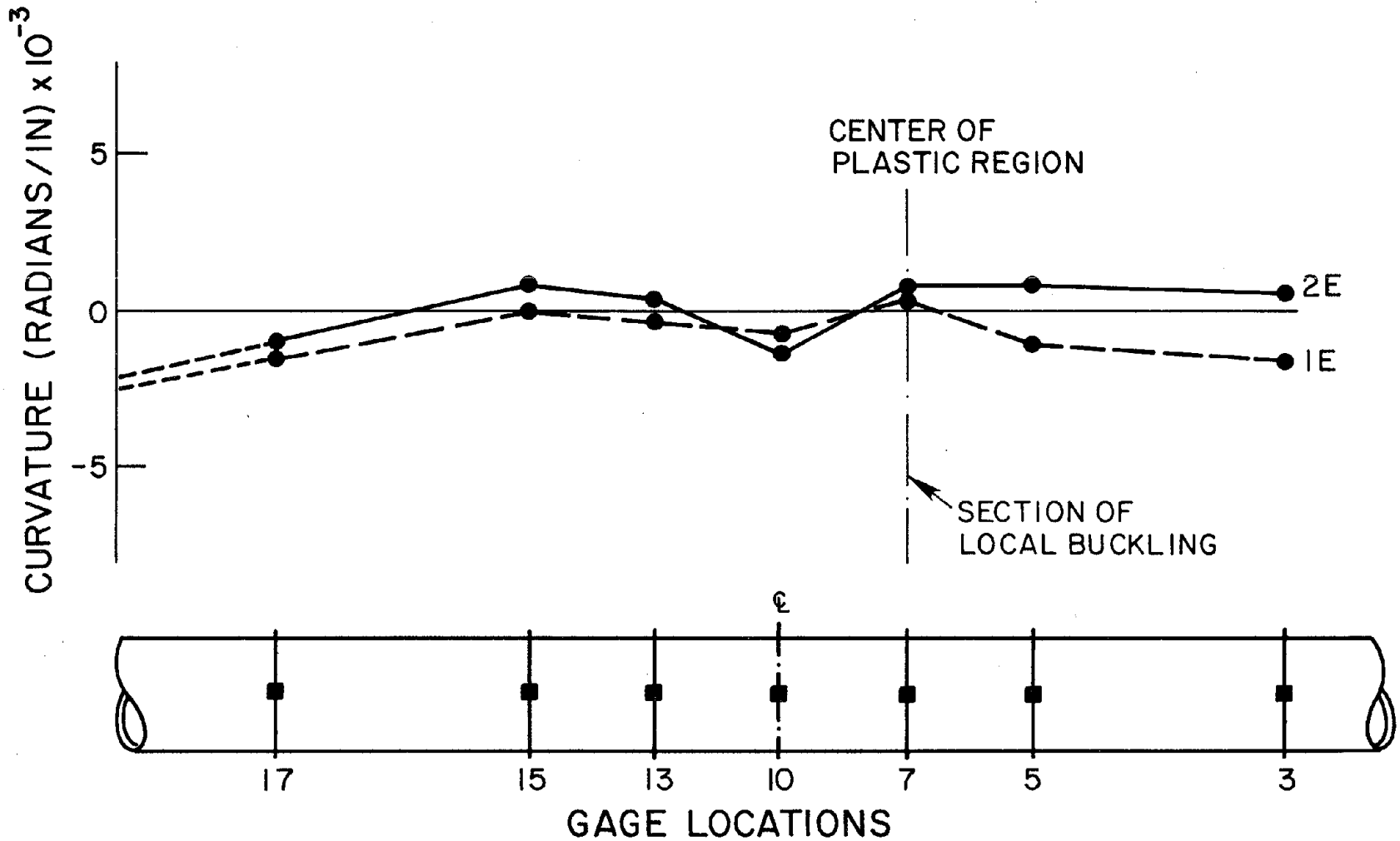
Fig. 4.4 Curvatures within Plastic Hinge – Strut 1 (Load Point E)
(1 in. = 25.4 mm)

131
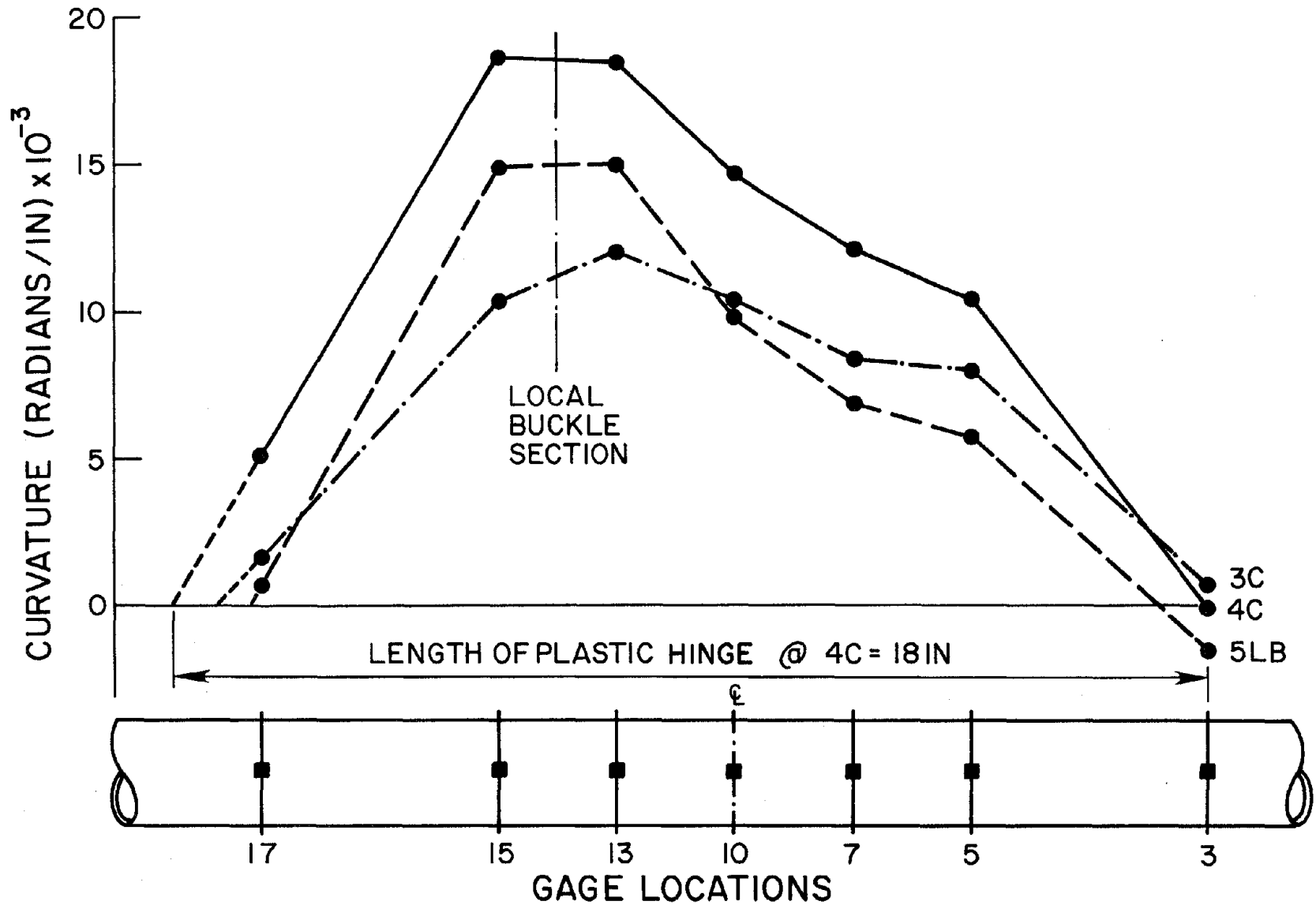
Fig. 4.5   Curvatures within Plastic Hinge – Strut 2 (Load Points C)
(1 in. = 25.4 mm)
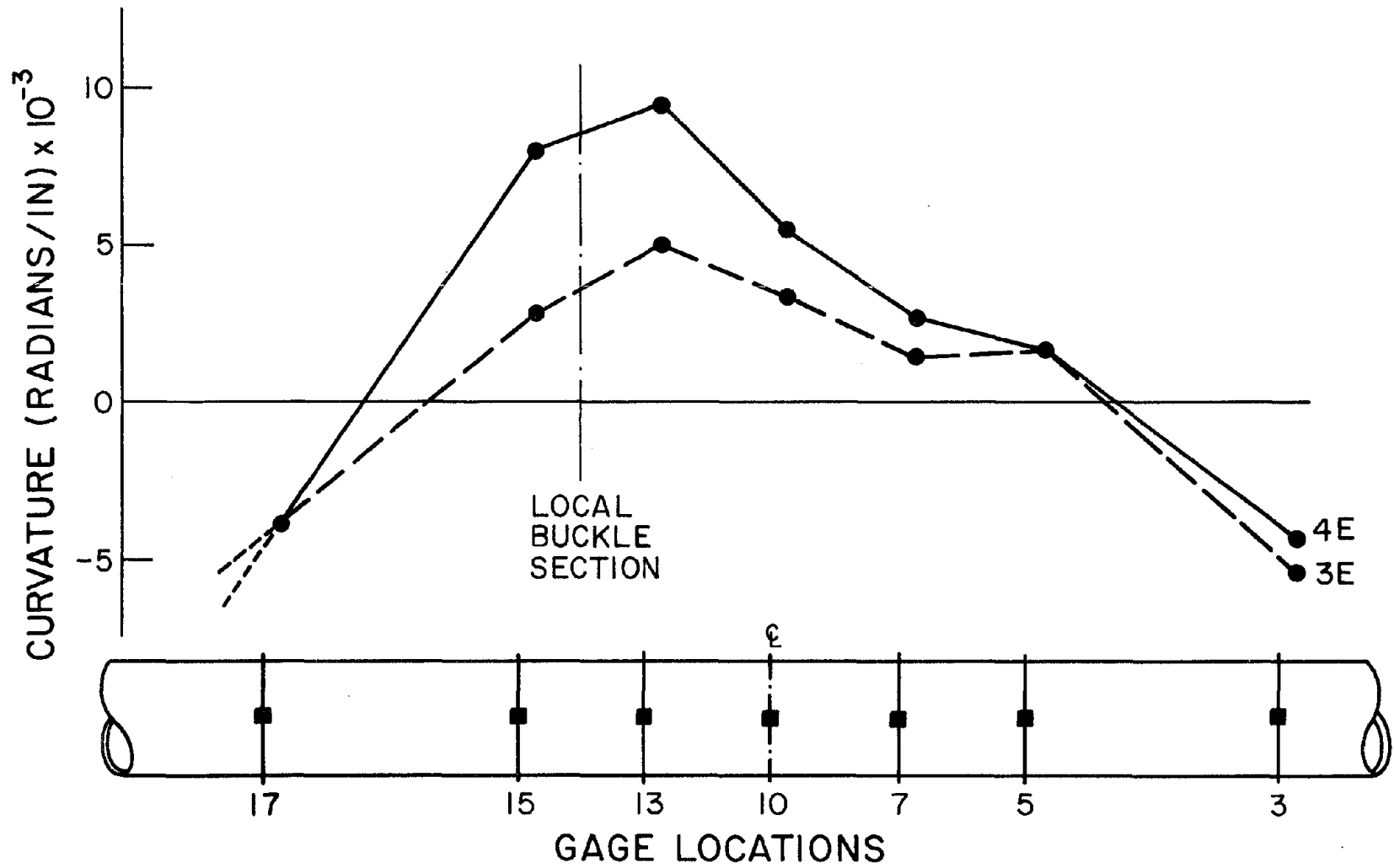
Fig. 4.6 Curvatures within Plastic Hinge – Strut 2 (Load Points E)
(1 in. = 25.4 mm)
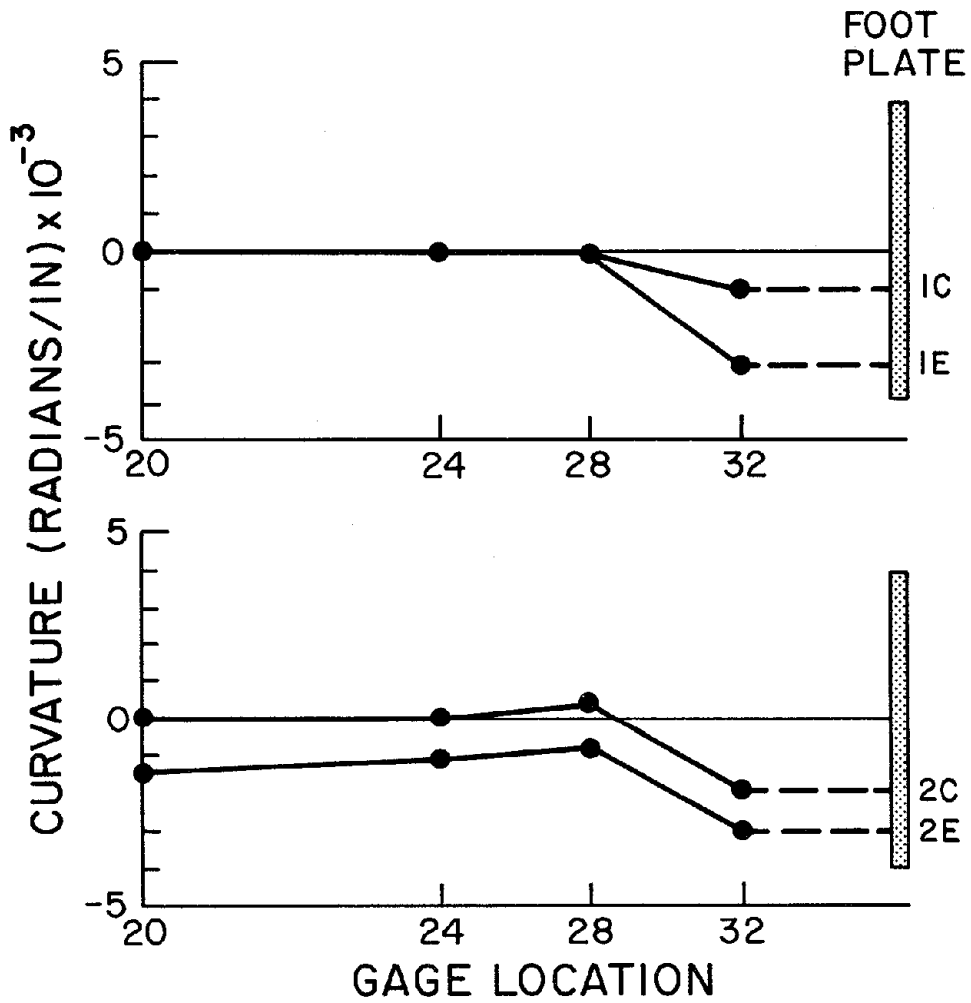
Fig. 4.7 Curvatures within Foot Plastic Region – Strut 5
(1 in. = 25.4 mm)
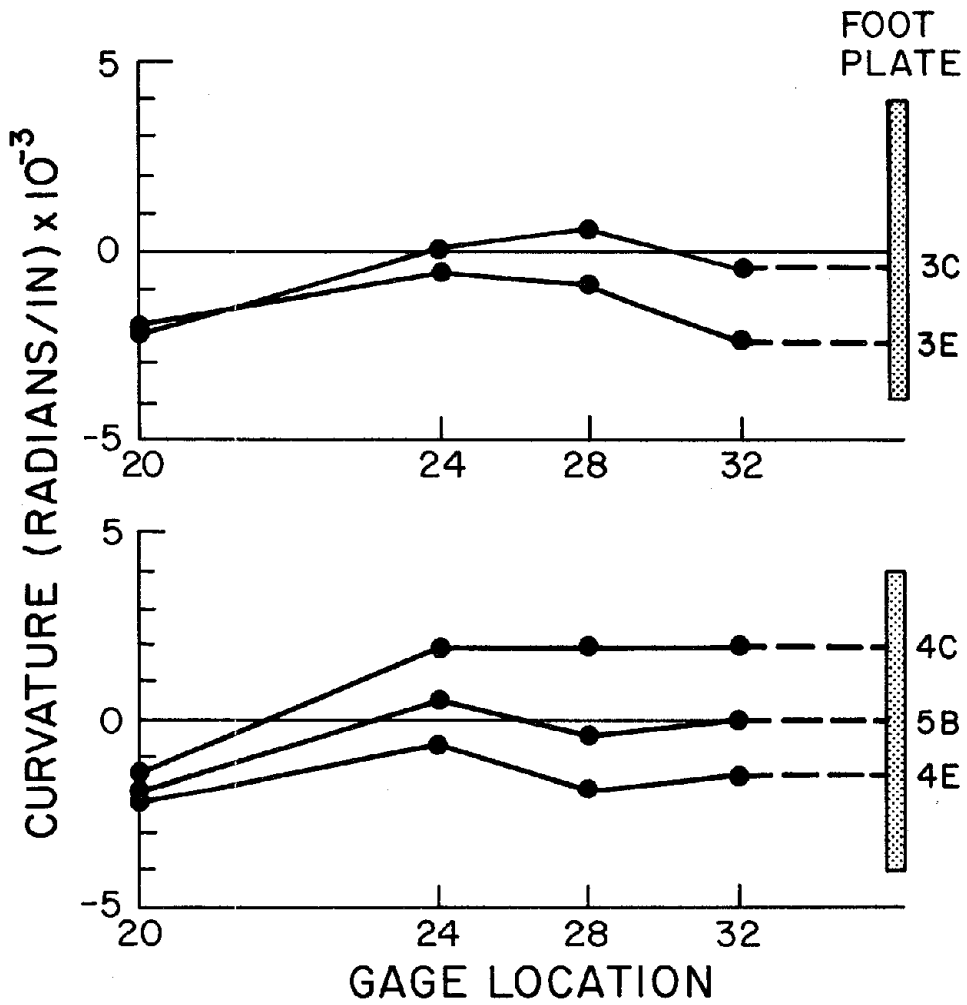
Fig. 4.8 Curvatures within Foot Plastic Region - Strut 5
(1 in. = 25.4 mm)
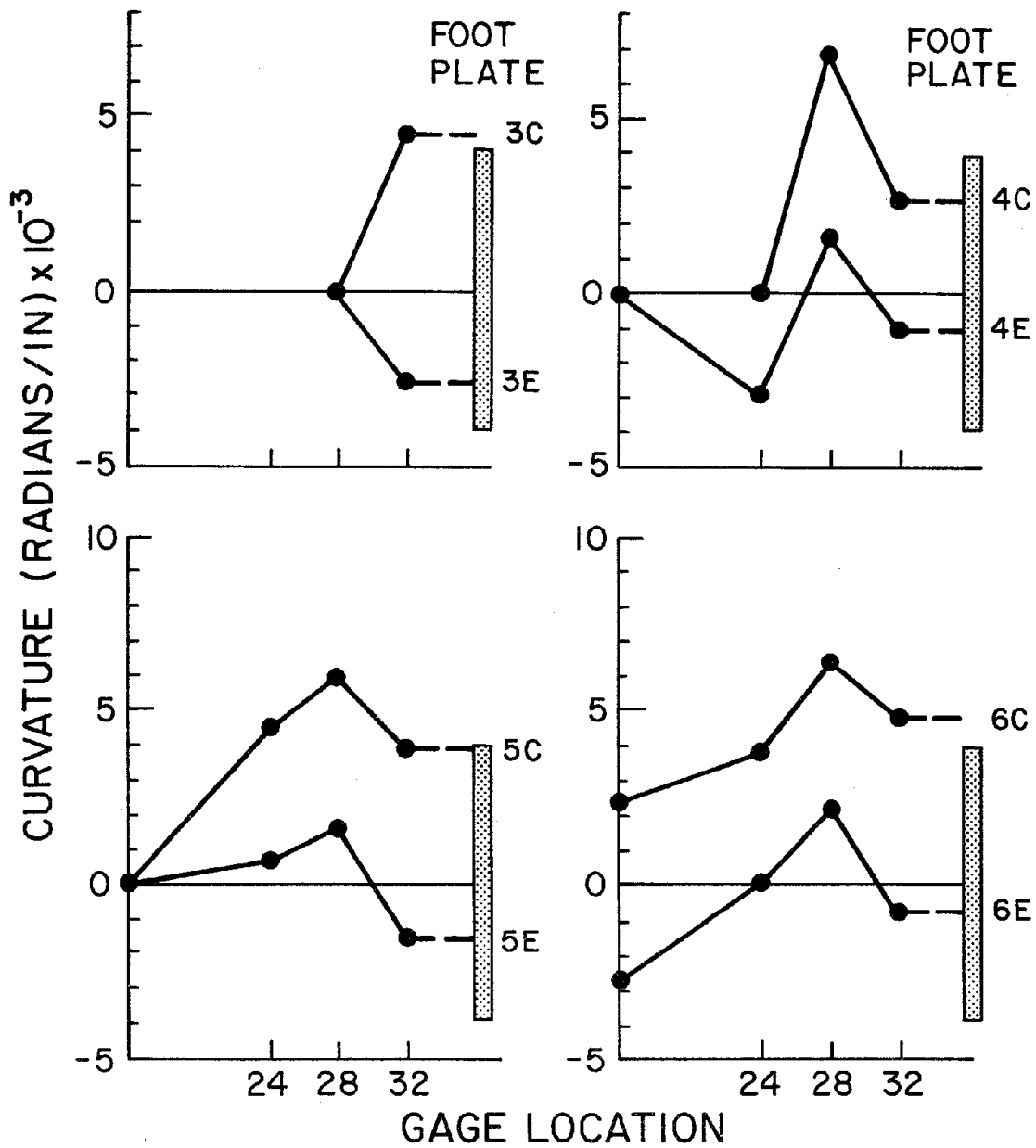
Fig. 4.9   Curvatures within Foot Plastic Region - Strut 6
            (1 in. = 25.4 mm)
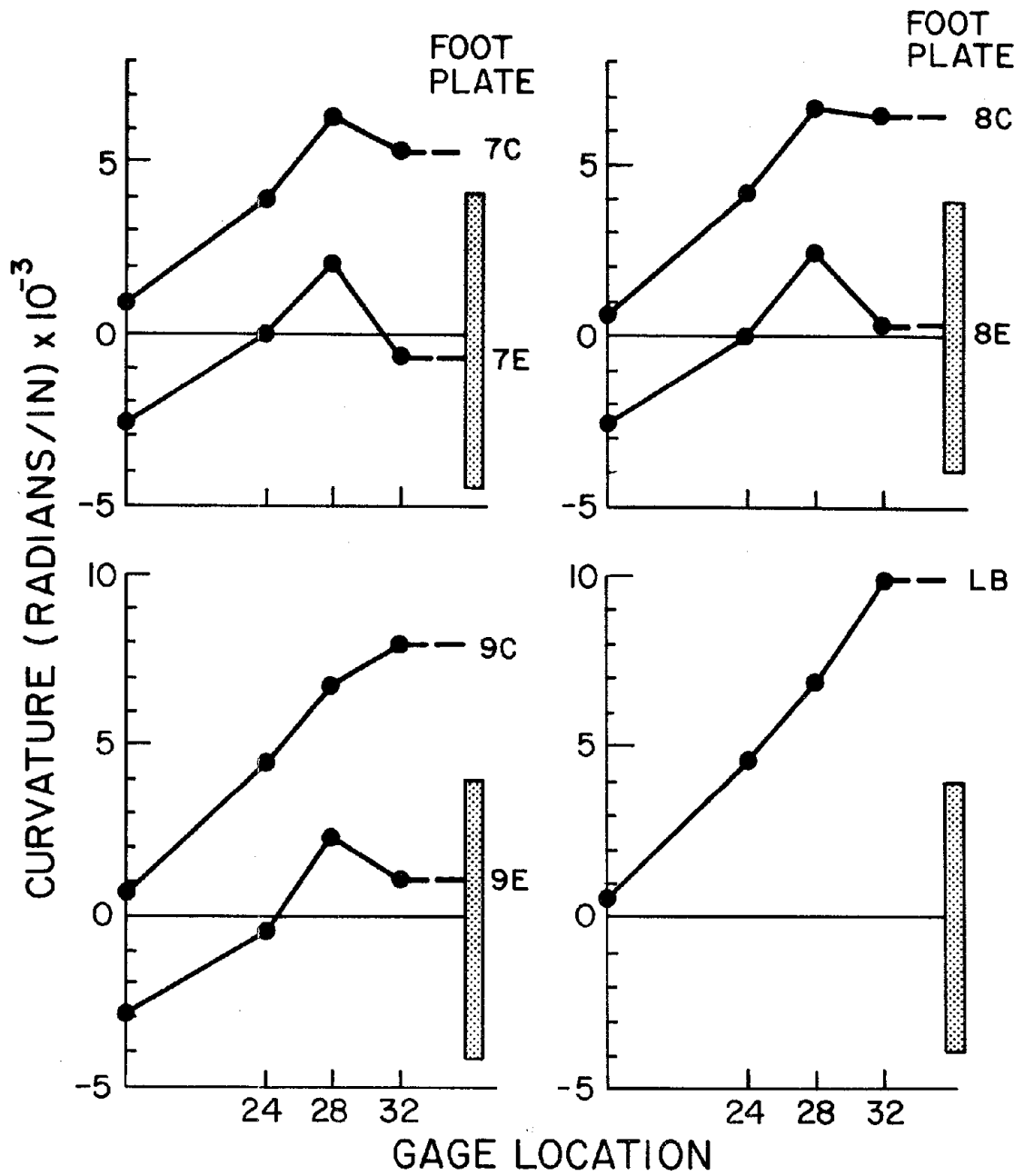
Fig. 4.10 Curvatures within Foot Plastic Region – Strut 6
(1 in. = 25.4 mm)
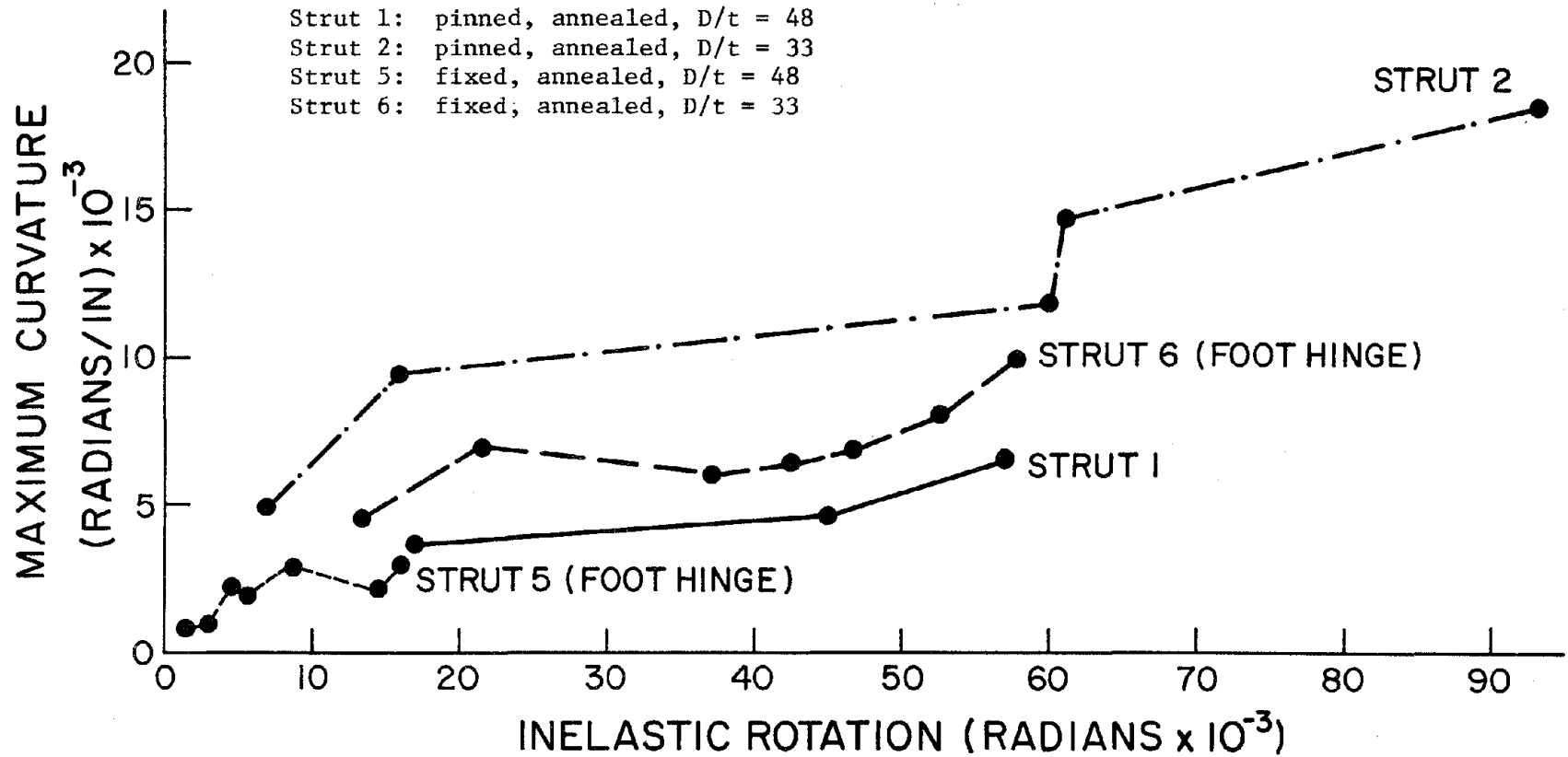
Fig. 4.11 Maximum Curvature vs. Inelastic Rotation
(1 in. = 25.4 mm)
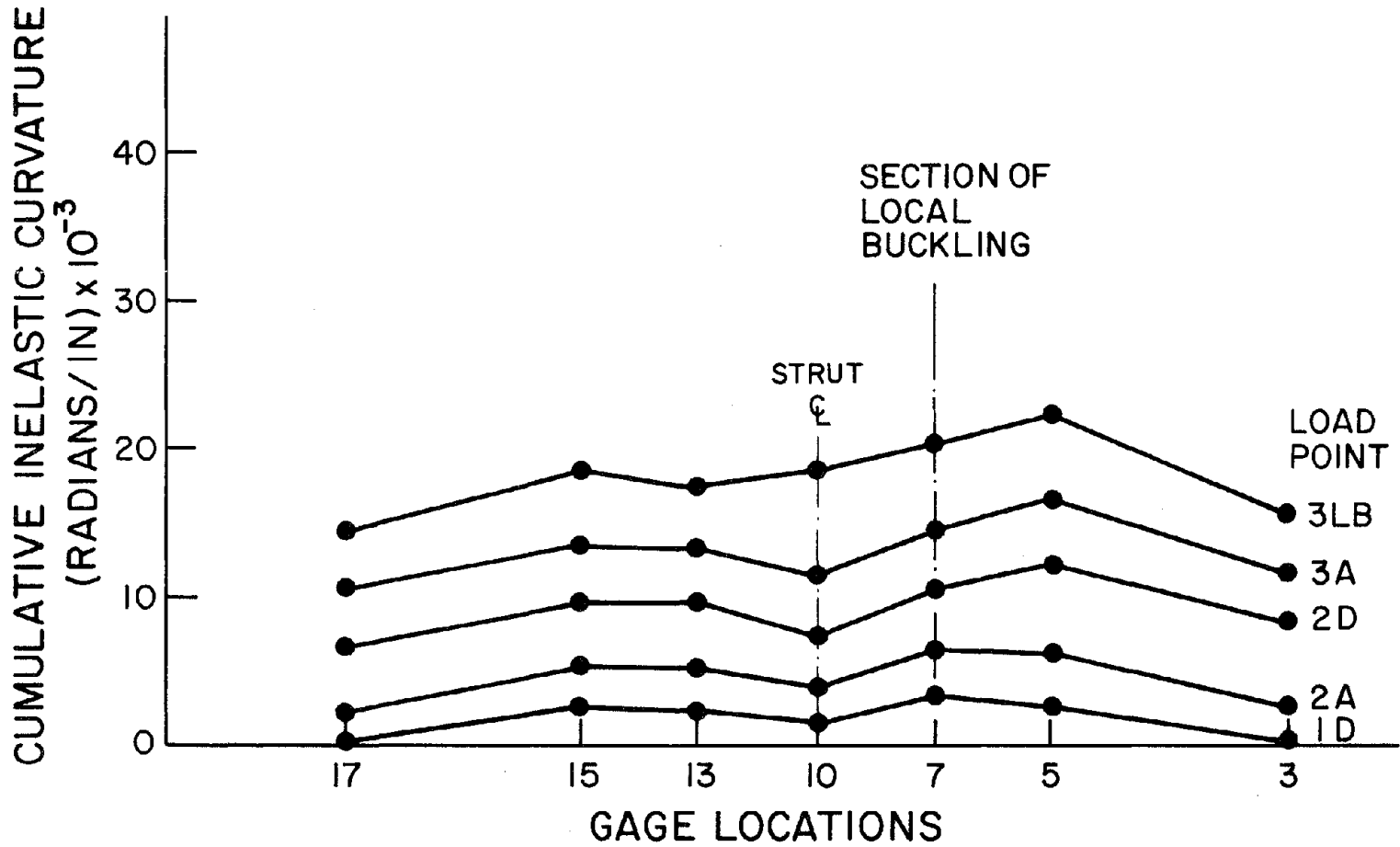
Fig. 4.12 Cumulative Inelastic Curvatures with the Center Plastic Hinge – Strut 1
(1 in. = 25.4 mm)
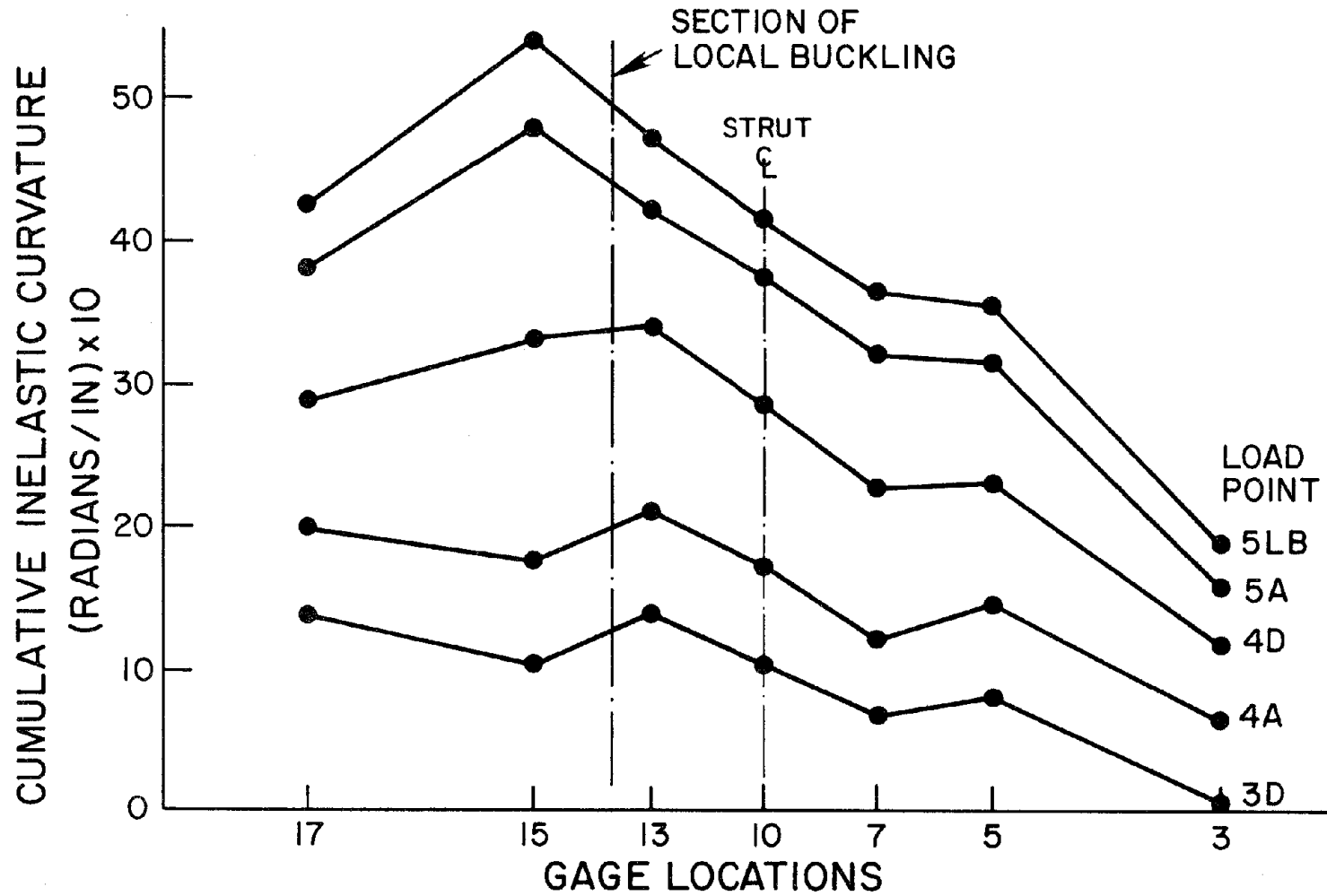
Fig. 4.13   Cumulative Inelastic Curvatures within the Center Plastic Hinge – Strut 2
(1 in. = 25.4 mm)
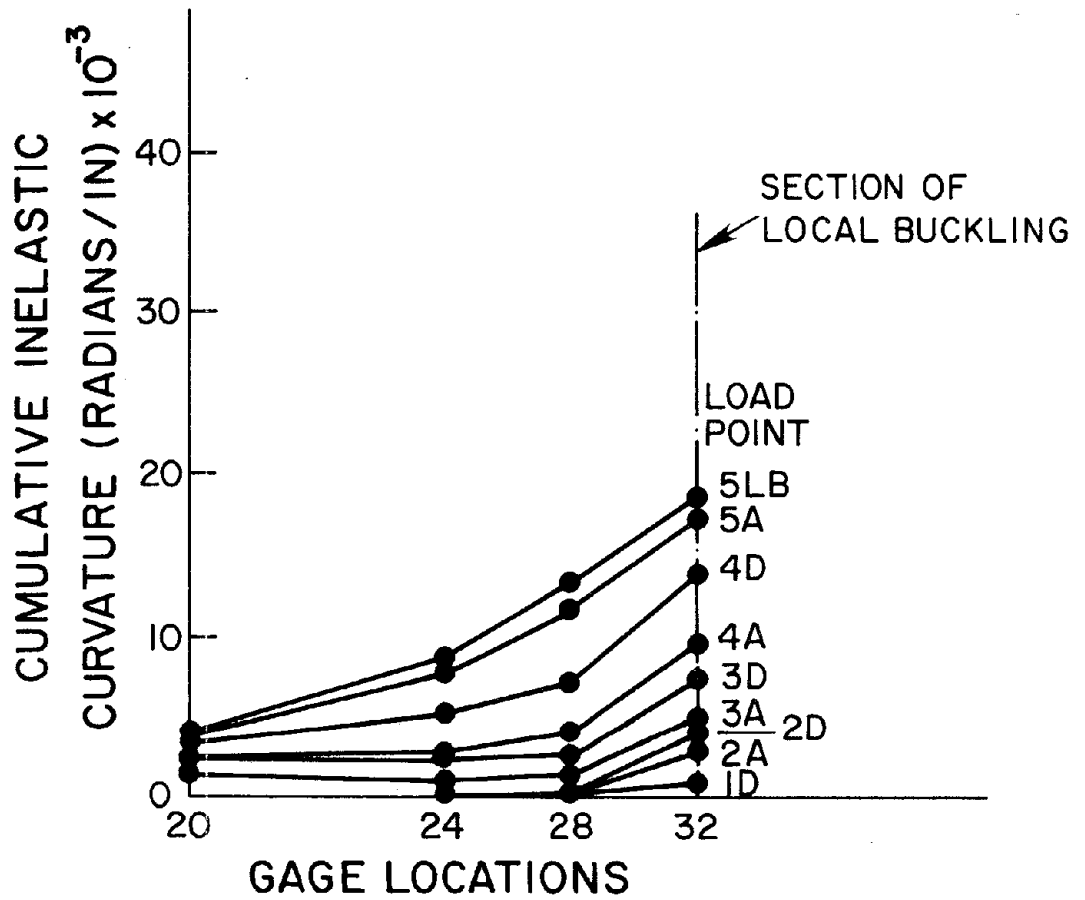
Fig. 4.14 Cumulative Inelastic Curvatures within the Foot Plastic
Region – Strut 5 (1 in. = 25.4 mm)

141
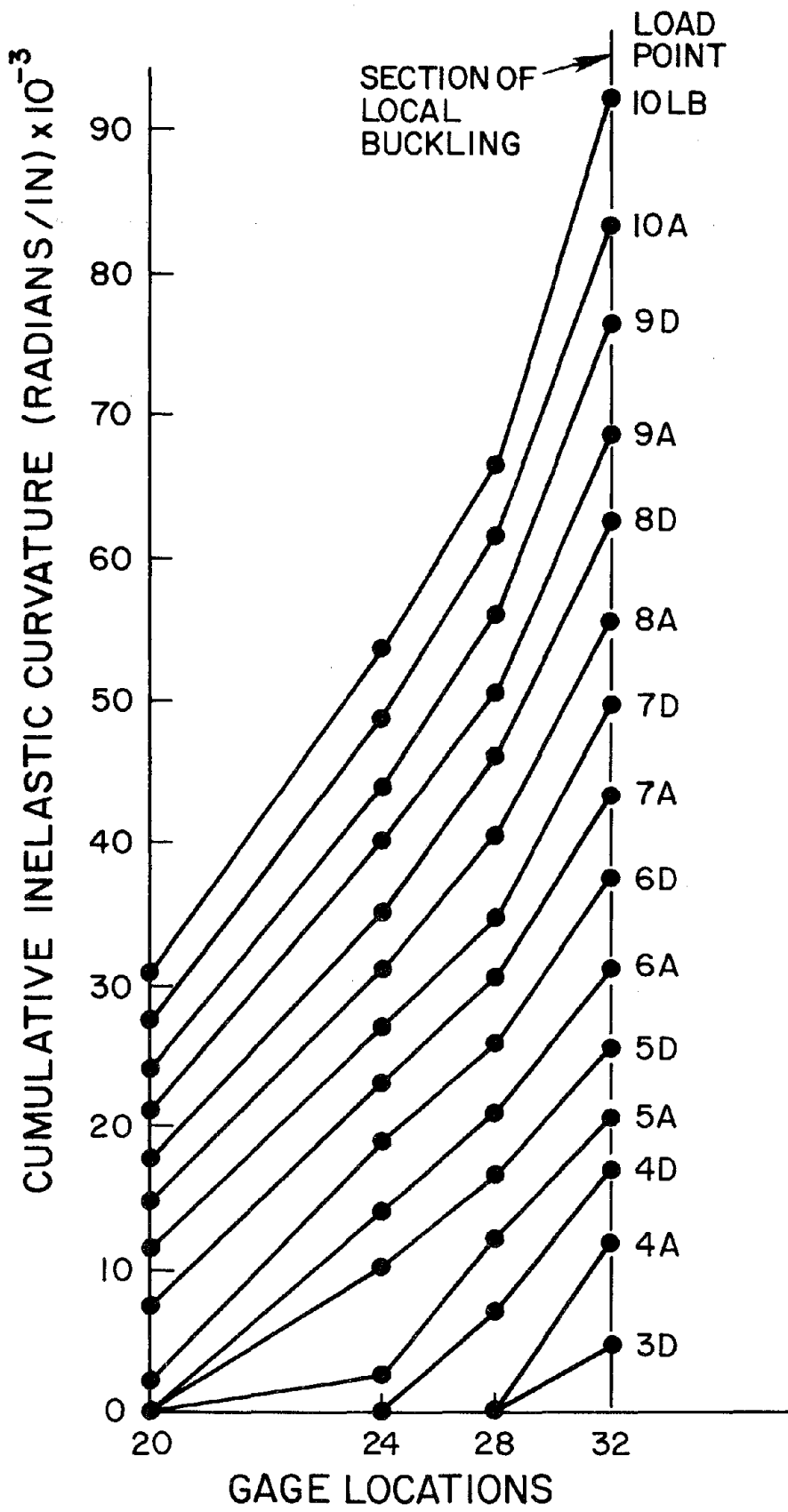
Fig. 4.15   Cumulative Inelastic Curvatures within the Foot Plastic
Region – Strut 6   (1 in. = 25.4 mm)
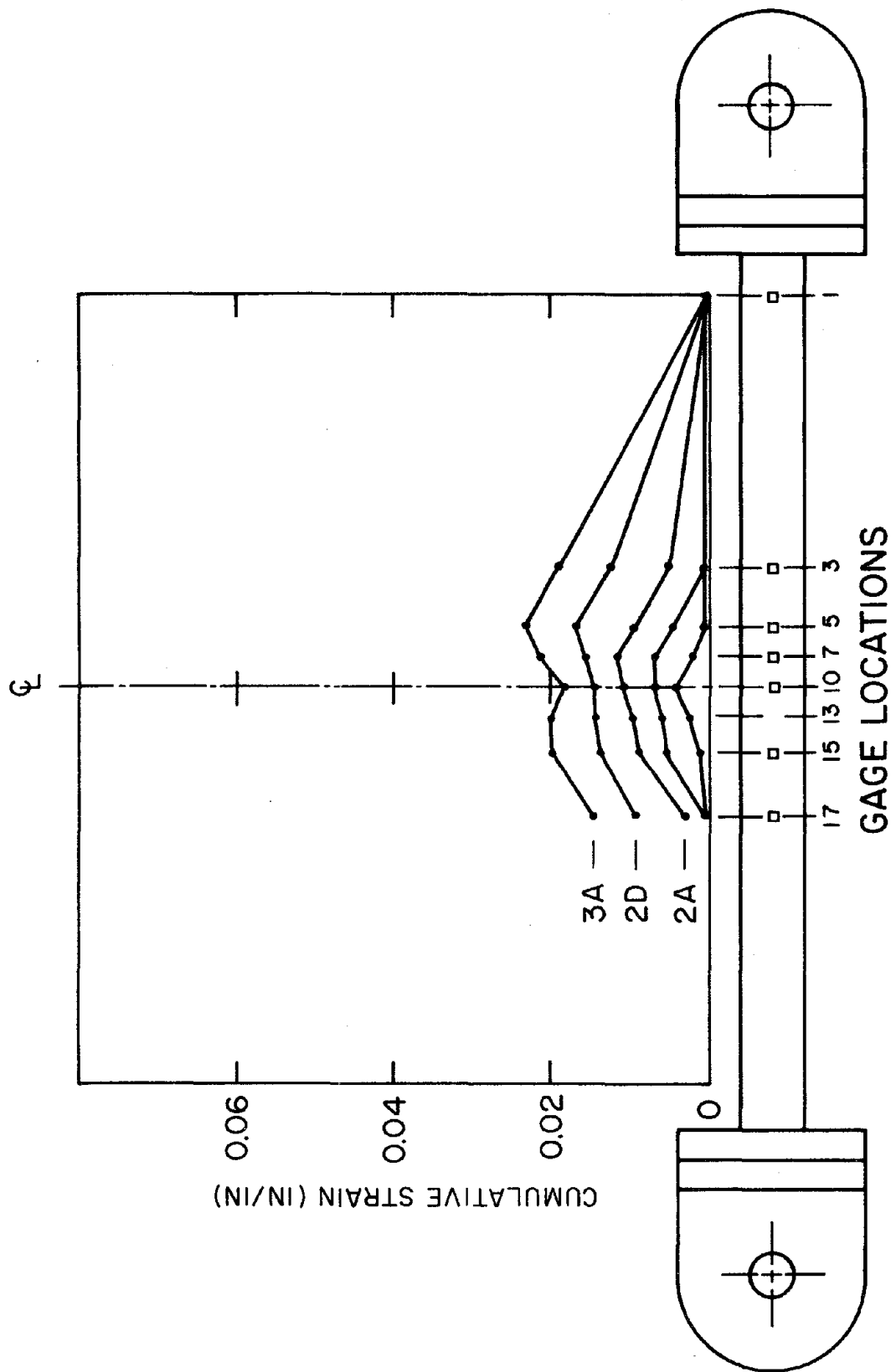
Fig. 4.16 Cumulative Inelastic Axial Strain – Strut 1

143
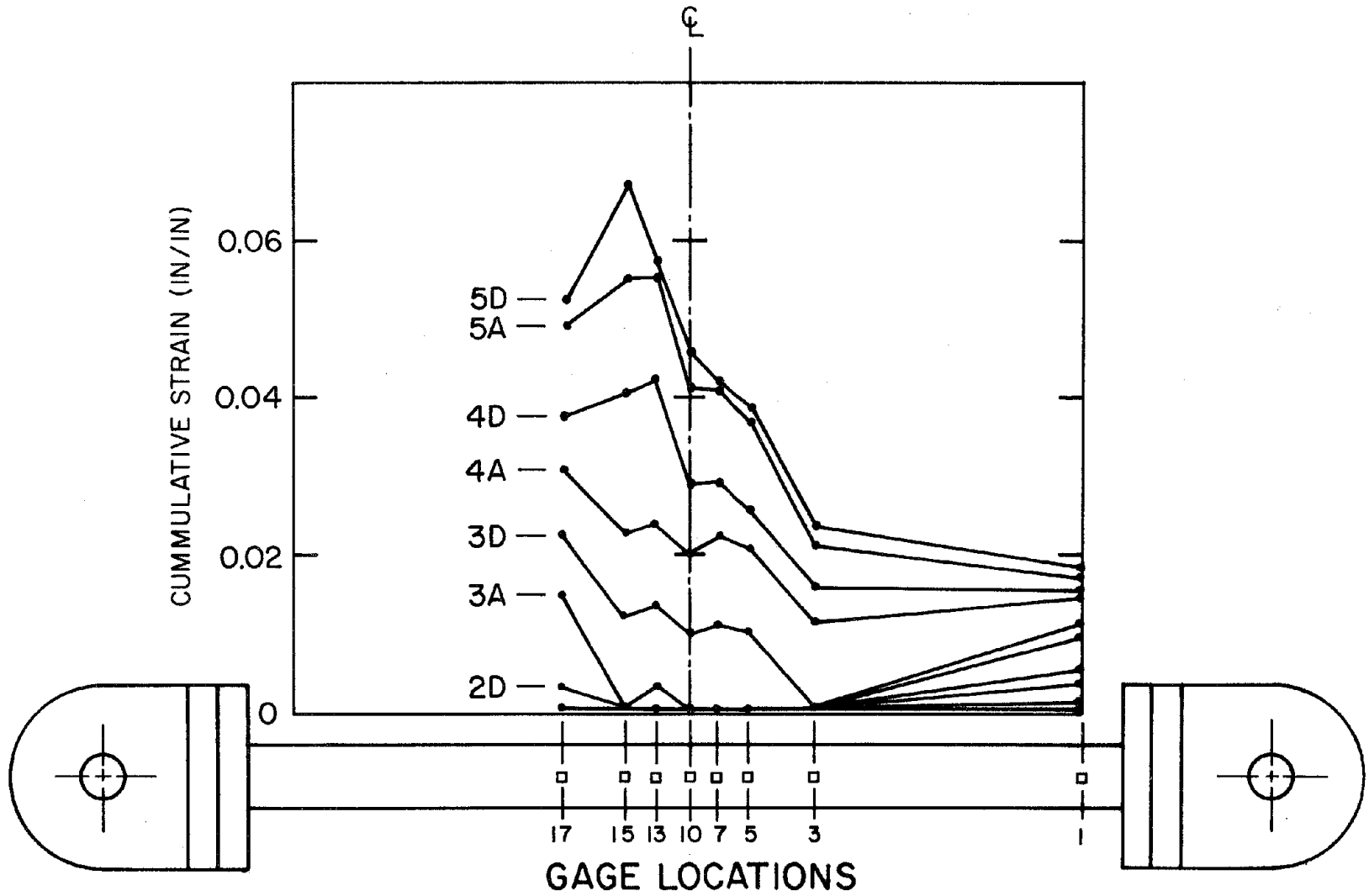
Fig. 4.17   Cumulative Inelastic Axial Strain - Strut 2
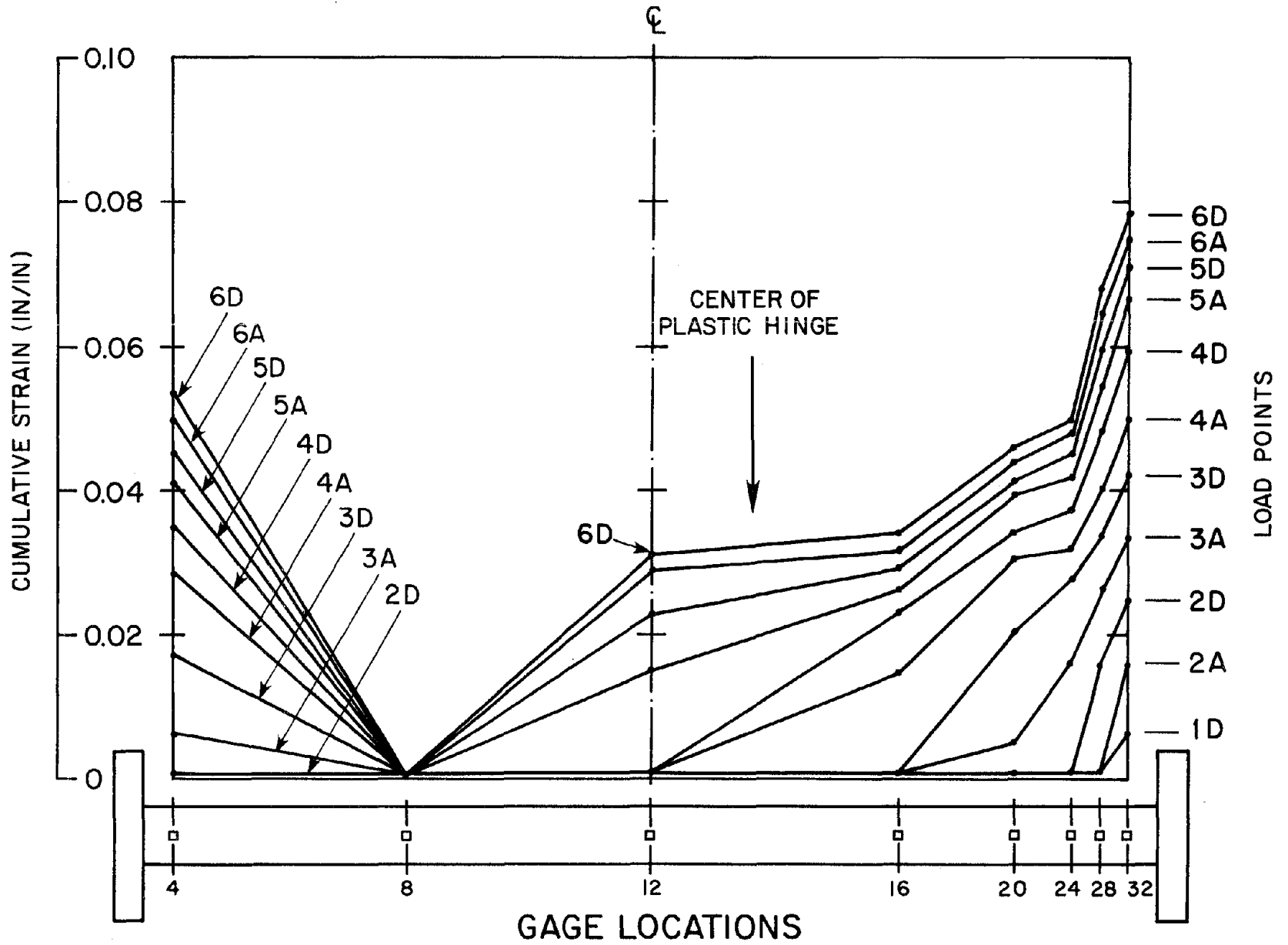
Fig. 4.18   Cumulative Inelastic Axial Strain - Strut 5
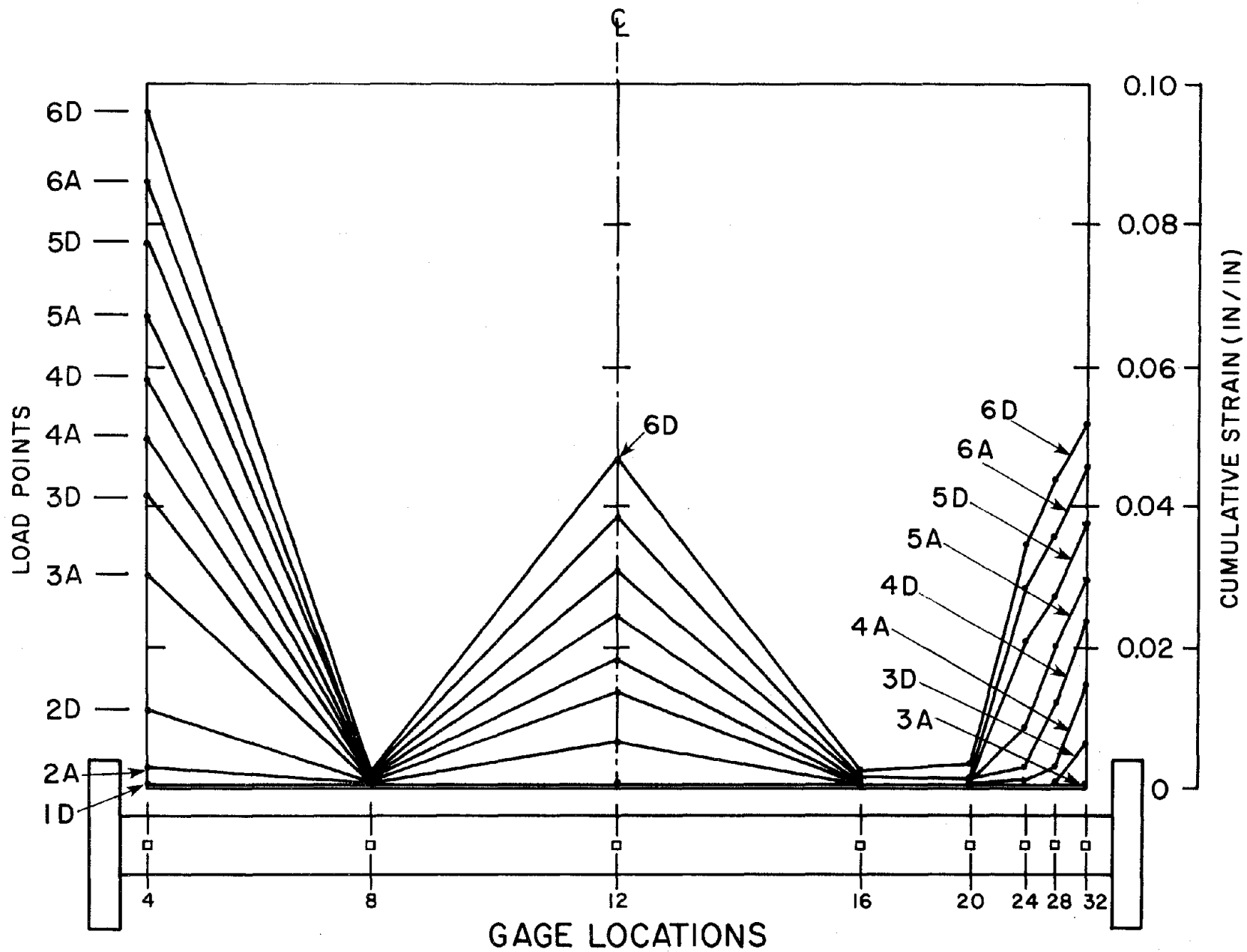
Fig. 4.19   Cumulative Inelastic Axial Strain - Strut 6
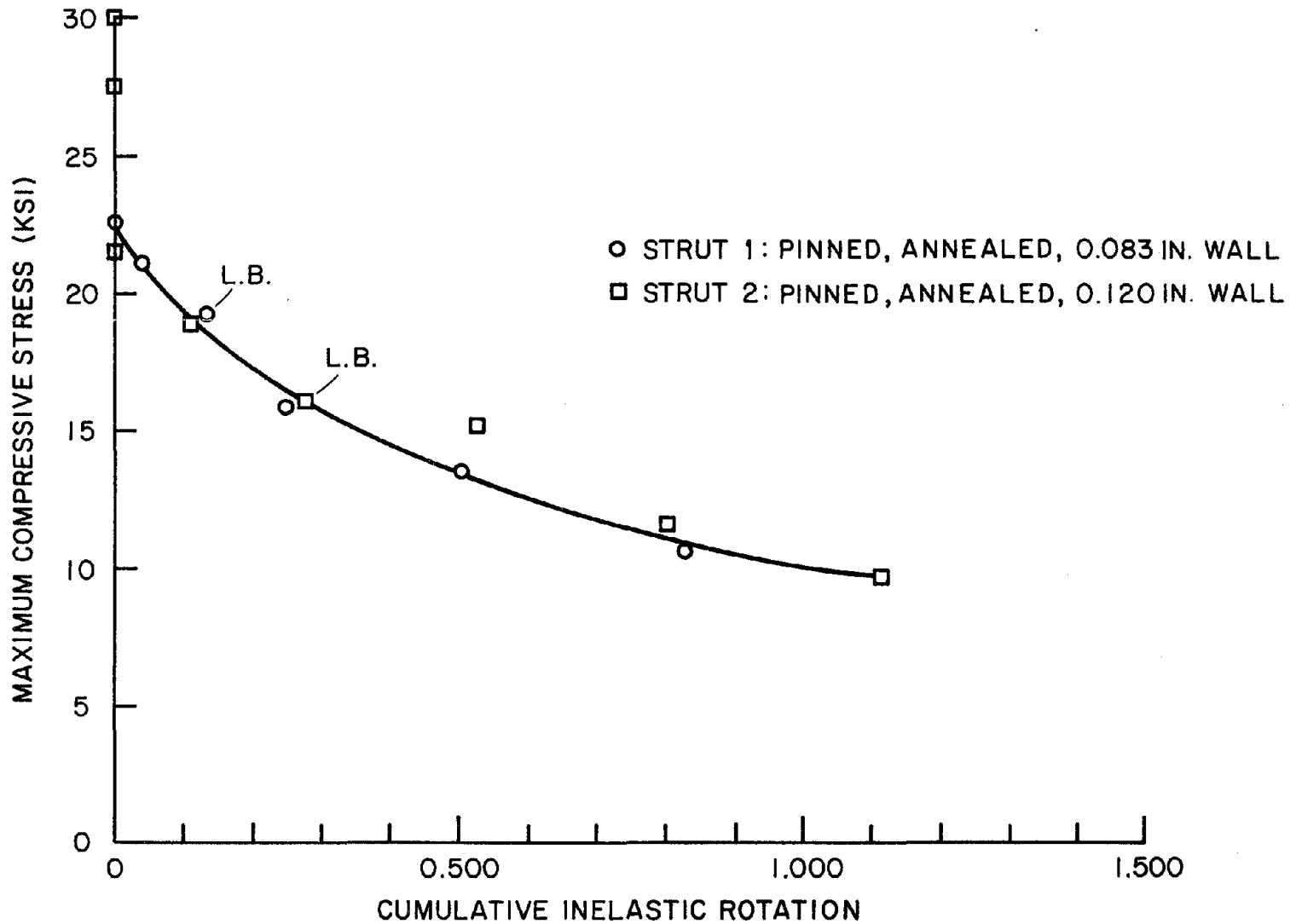
Fig. 4.20   Maximum Compressive Stress vs. Cumulative Inelastic Rotation
(1 ksi = 6.9 MPa)
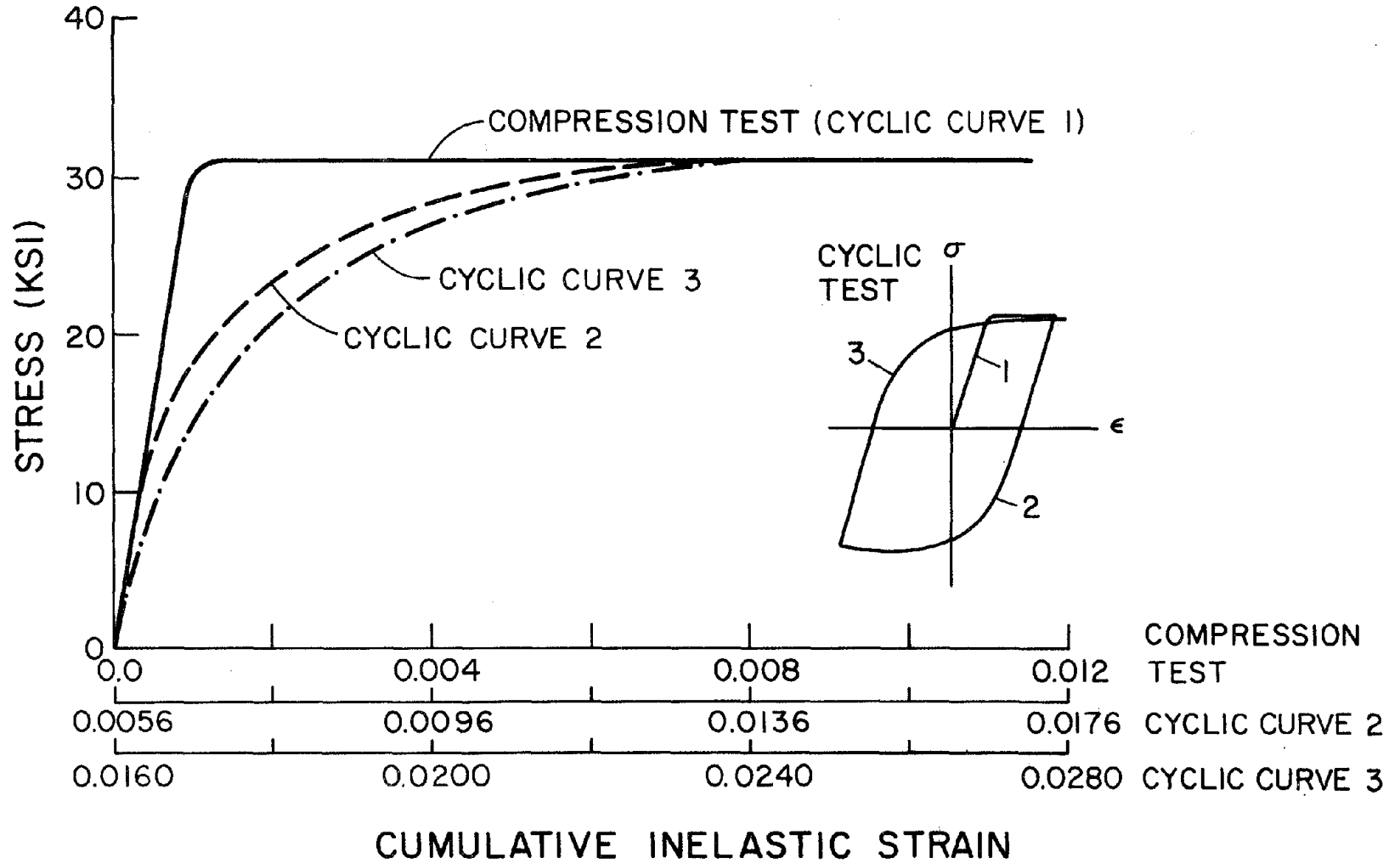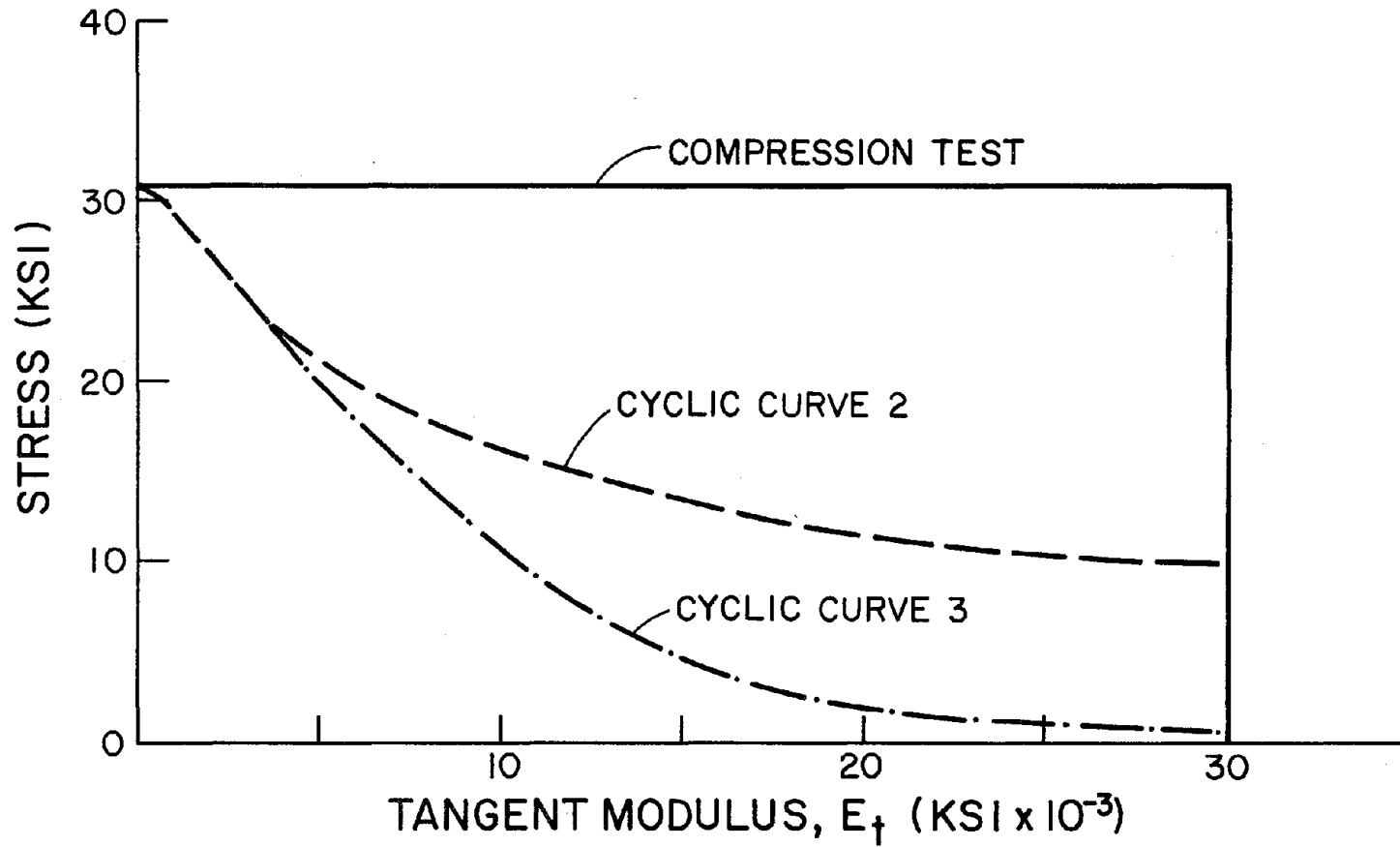
Fig. 5.1   Stress-Strain Curves from Cyclic Test - Annealed Material
(1 ksi = g.9 MPa)

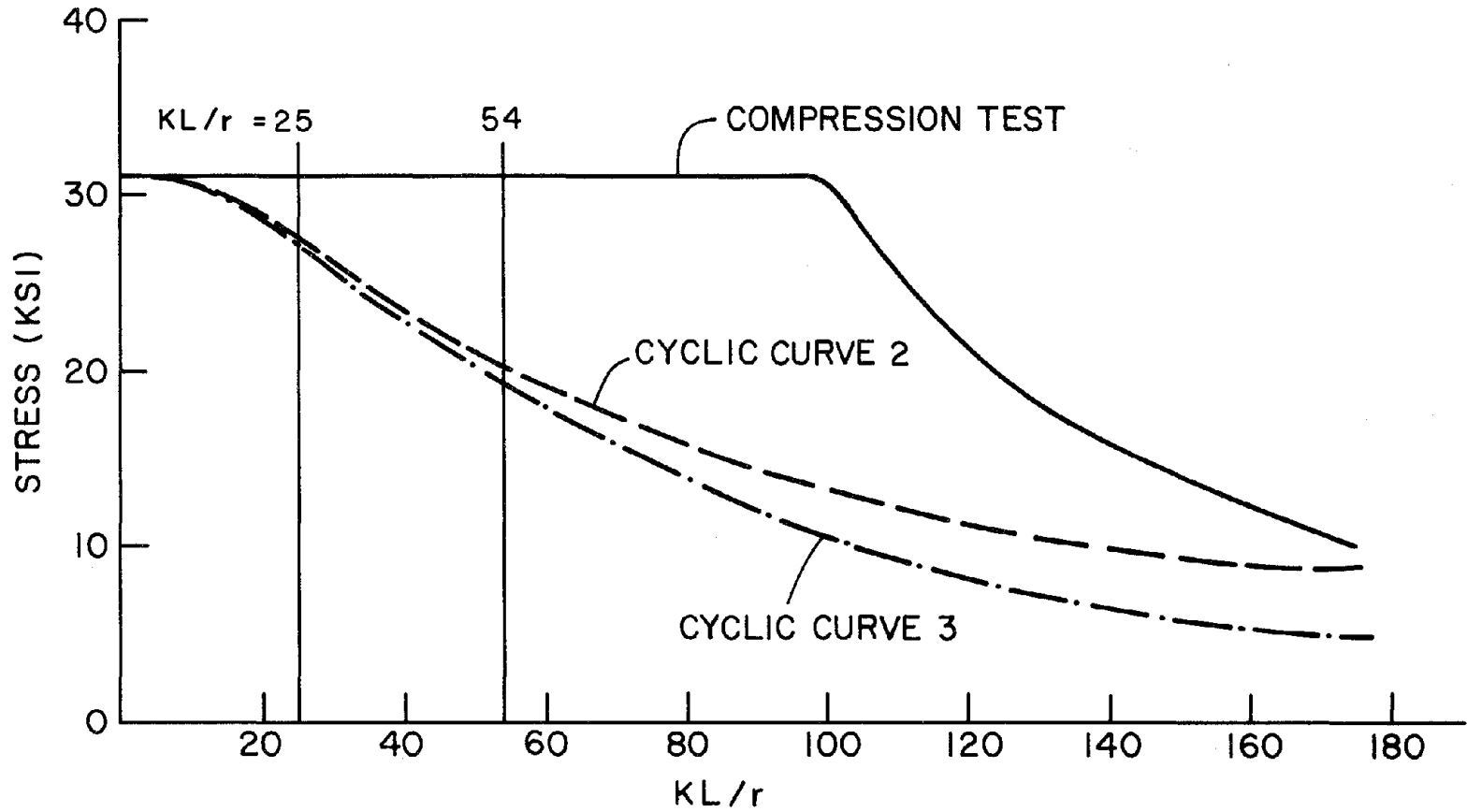Fig. 5.2 Stress-E_t Curves, Annealed Material (1 ksi = 6.9 MPa)

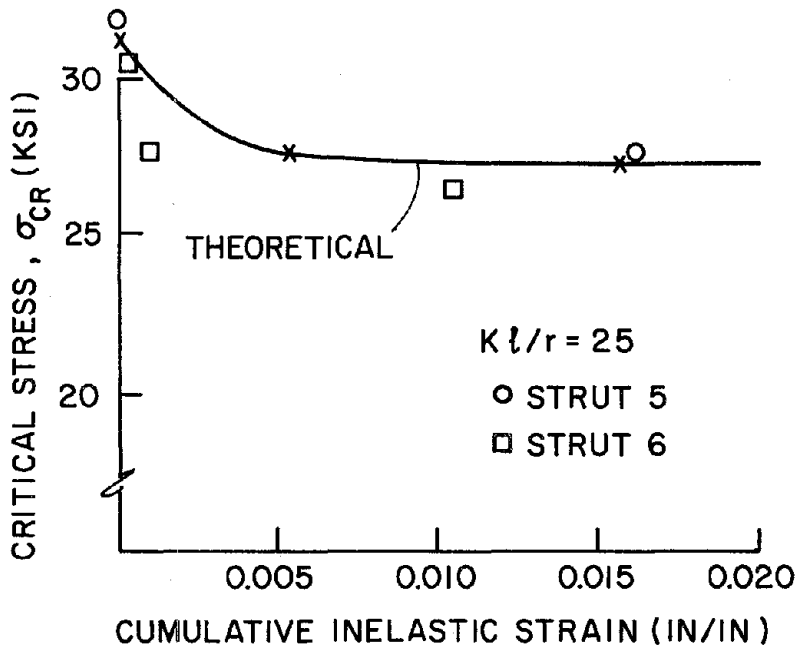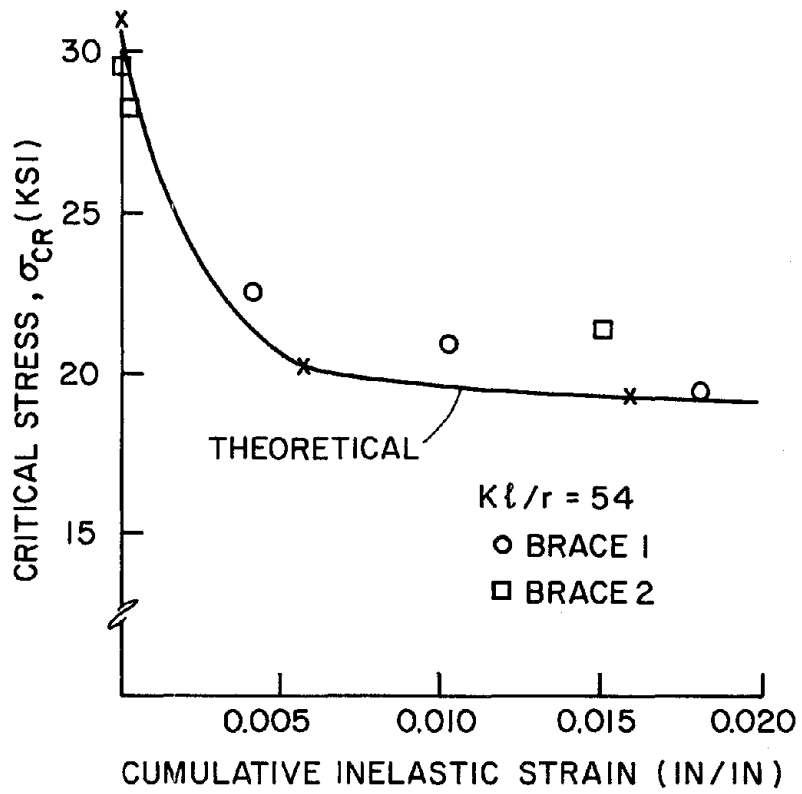Fig. 5.3 Stress-KL/r Curves, Annealed Material (1 ksi = 6.9 MPa)

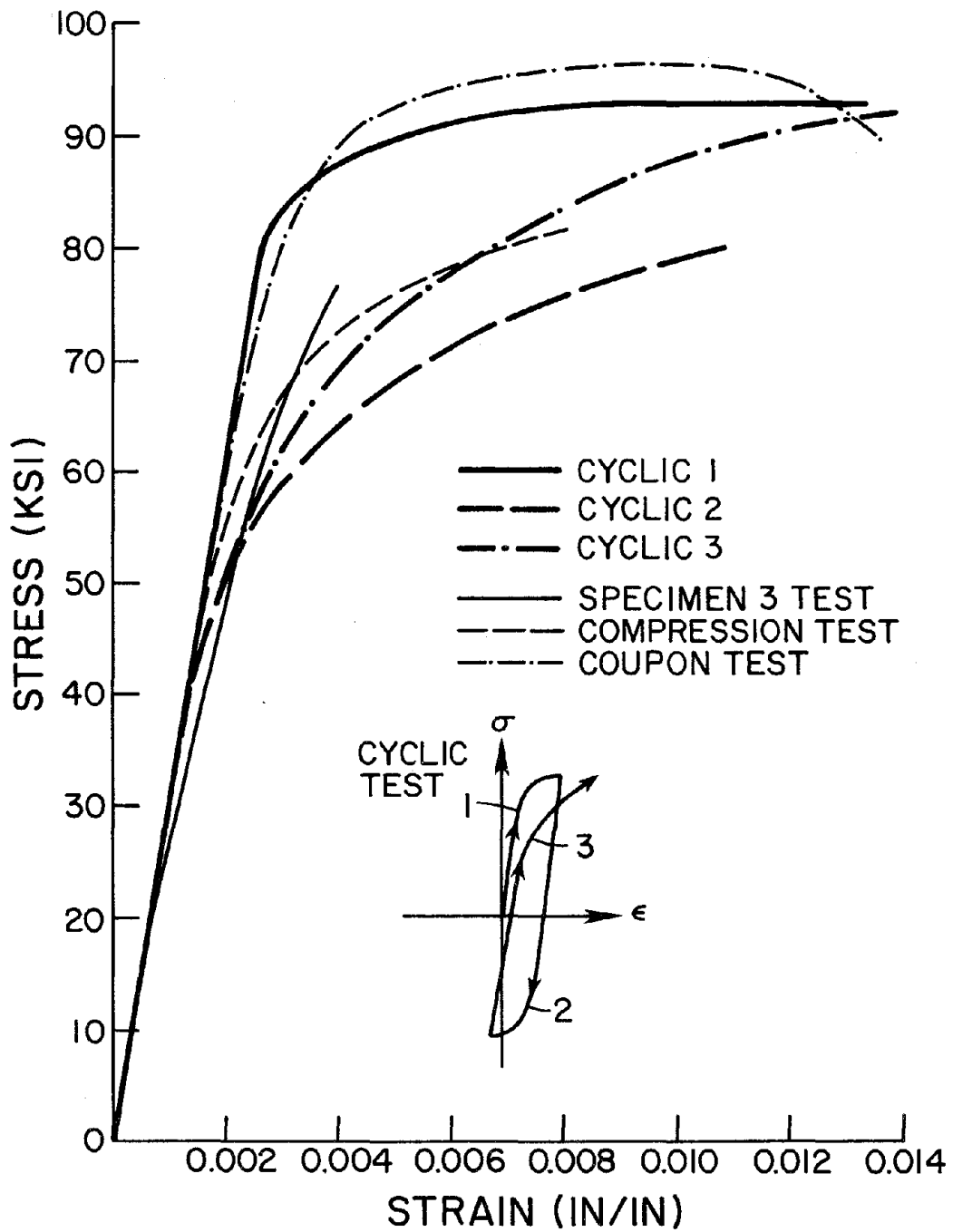Fig. 5.4 σ_{cr} vs. CIS (1 ksi = 6.9 MPa)

Fig. 6.1 Variation in Stress-Strain Curves (D/t=48)
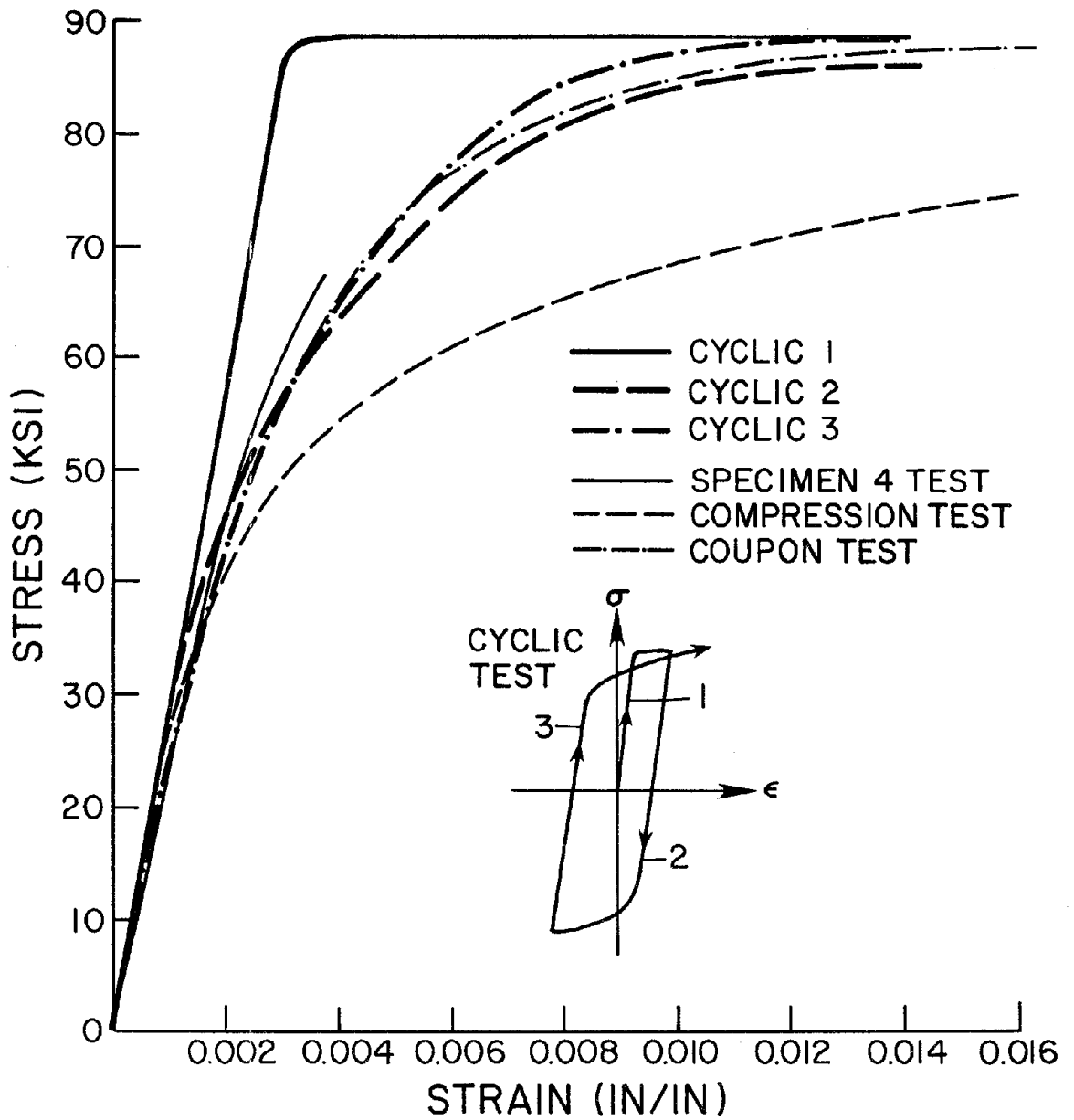Unannealed Material (1 ksi = 6.9 MPa)

Fig. 6.2 Variation in Stress-Strain Curves (D/t=33)
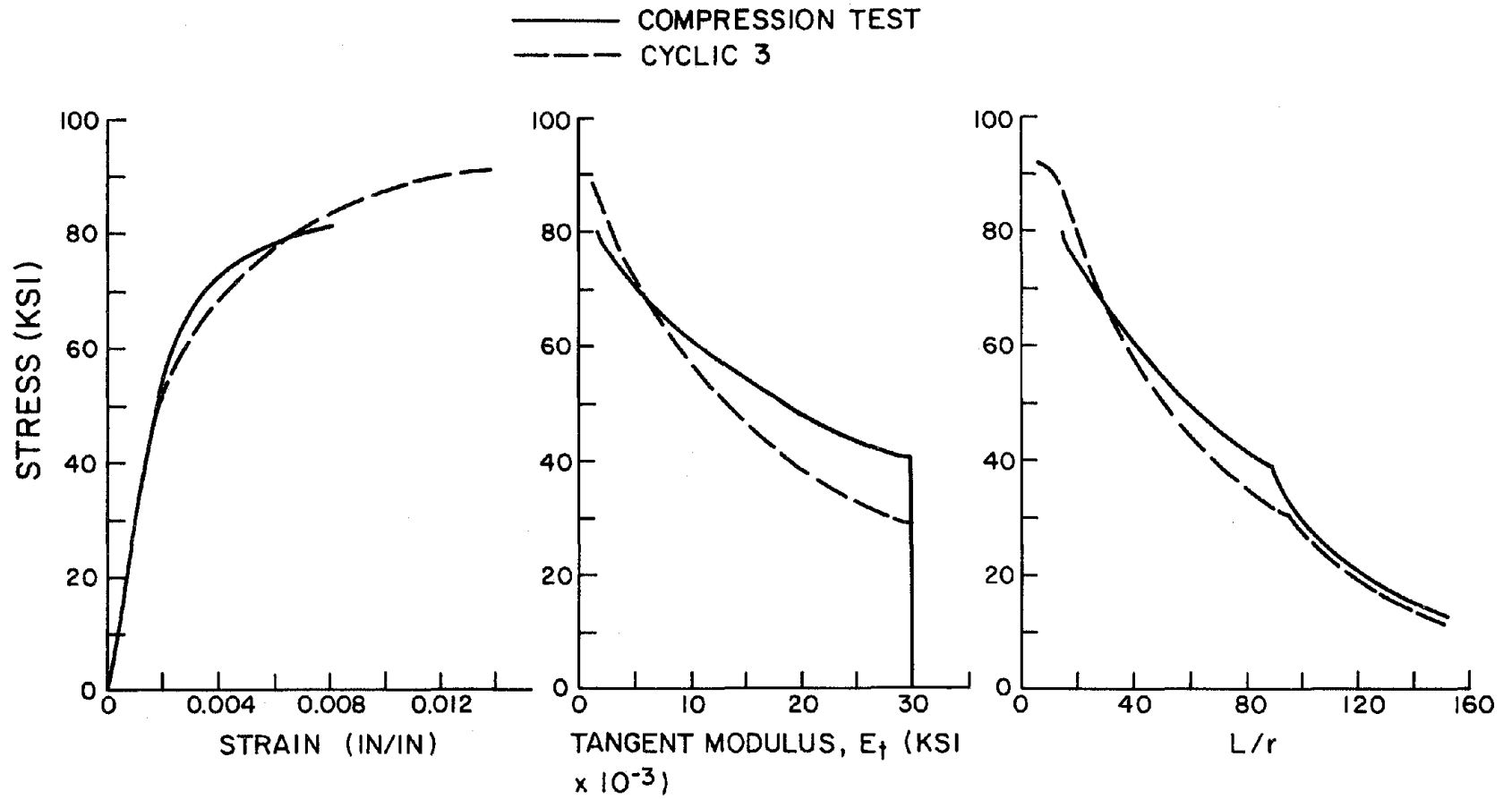Unannealed Material (1 ksi = 6.9 MPa)

Fig. 6.3 Stress vs. Strain, E_t, L/r (0.083" w.t.), Unannealed Material
(1 ksi = 6.9 MPa)

COMPRESSION TEST
CYCLIC 3

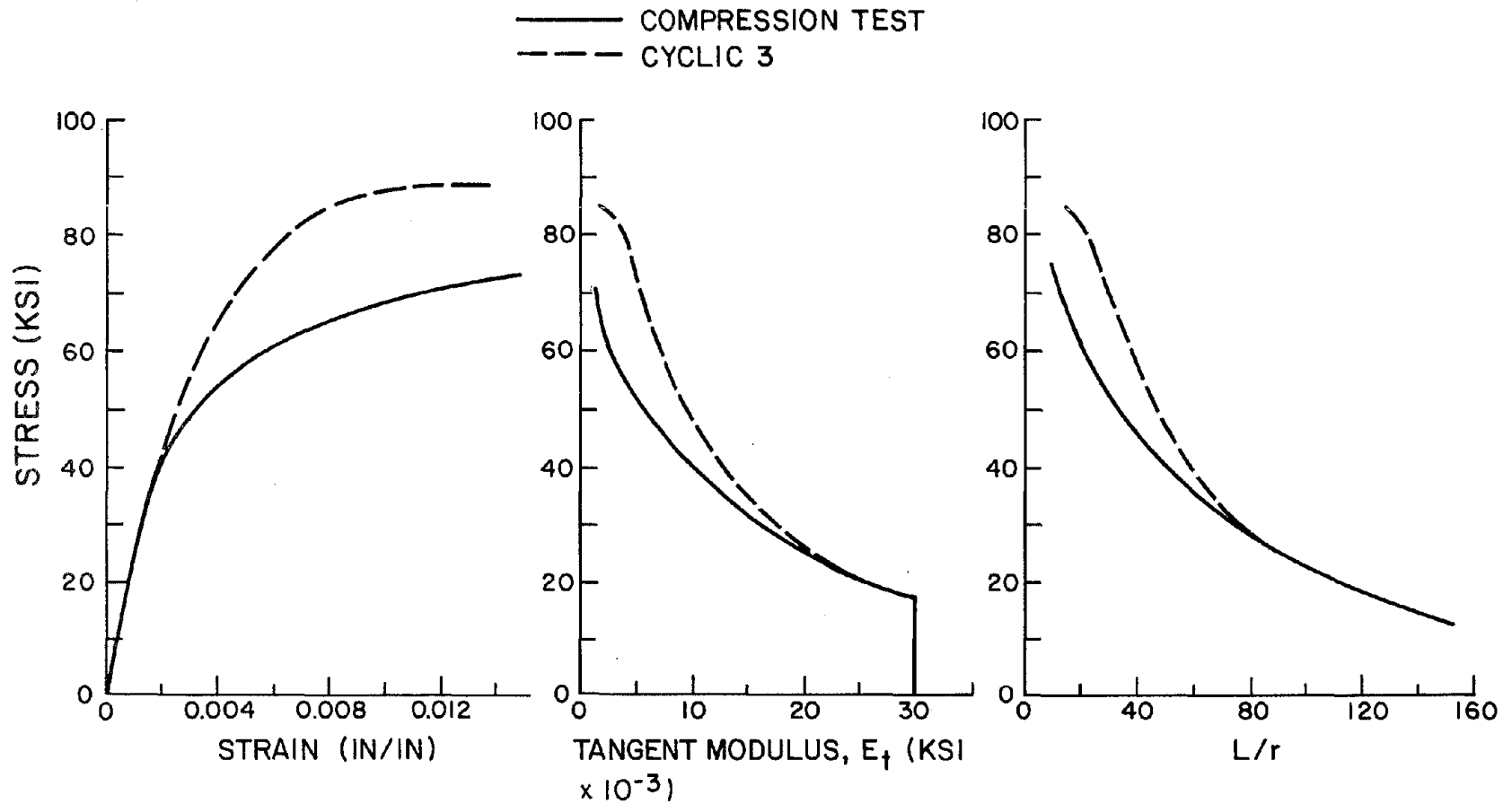Fig. 6.4   Stress vs. Strain, E_t, L/r   (0.120" w.t.), Unannealed Material
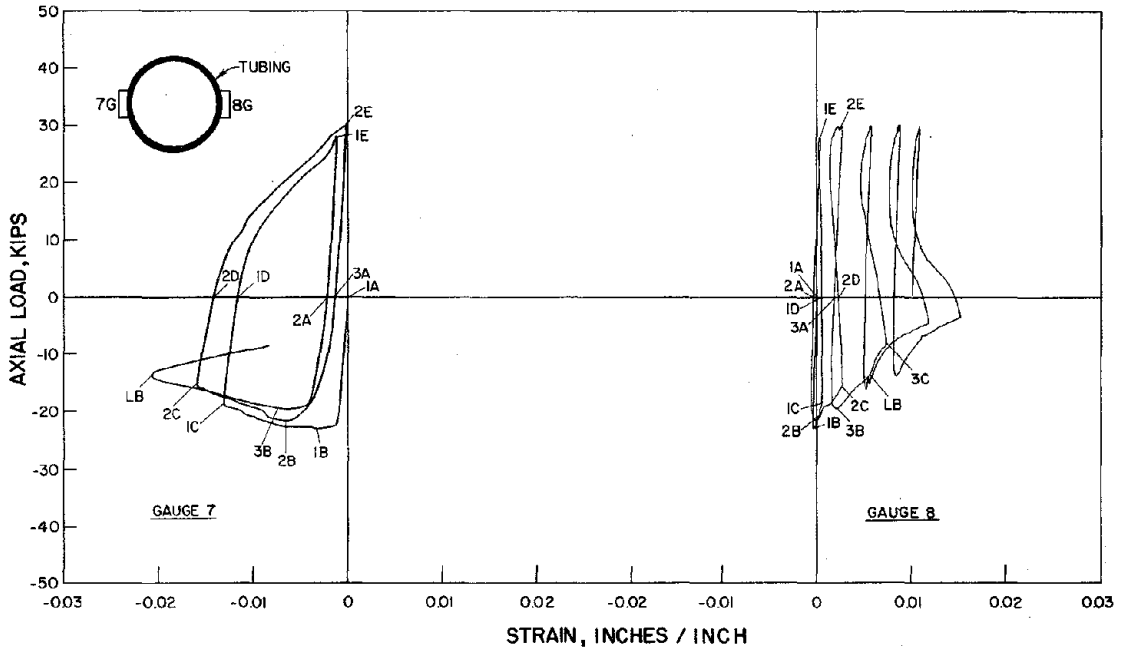(1 ksi = 6.9 MPa)

Fig. A.1 Strut 1 - Axial Load vs. Strain (Gages 7 and 8 - Cycles 1-5)

Fig. A.2 Strut 1 - Axial Load vs. Strain (Gages 9 and 11 - Cycles 1-5)

156

Fig. A.3 Strut 1 - Axial Load vs. Strain (Gages 10 and 12 - Cycles 1-5)

Fig. A.4 Strut 2 - Axial Load vs. Strain (Gages 1 and 2 - Cycles 1-5)

157

Fig. A.5   Strut 2 – Axial Load vs. Strain (Gages 7 and 8 – Cycles 1-5)

Fig. A.6   Strut 2 – Axial Load vs. Strain (Gages 9 and 11 – Cycles 1-5)

158
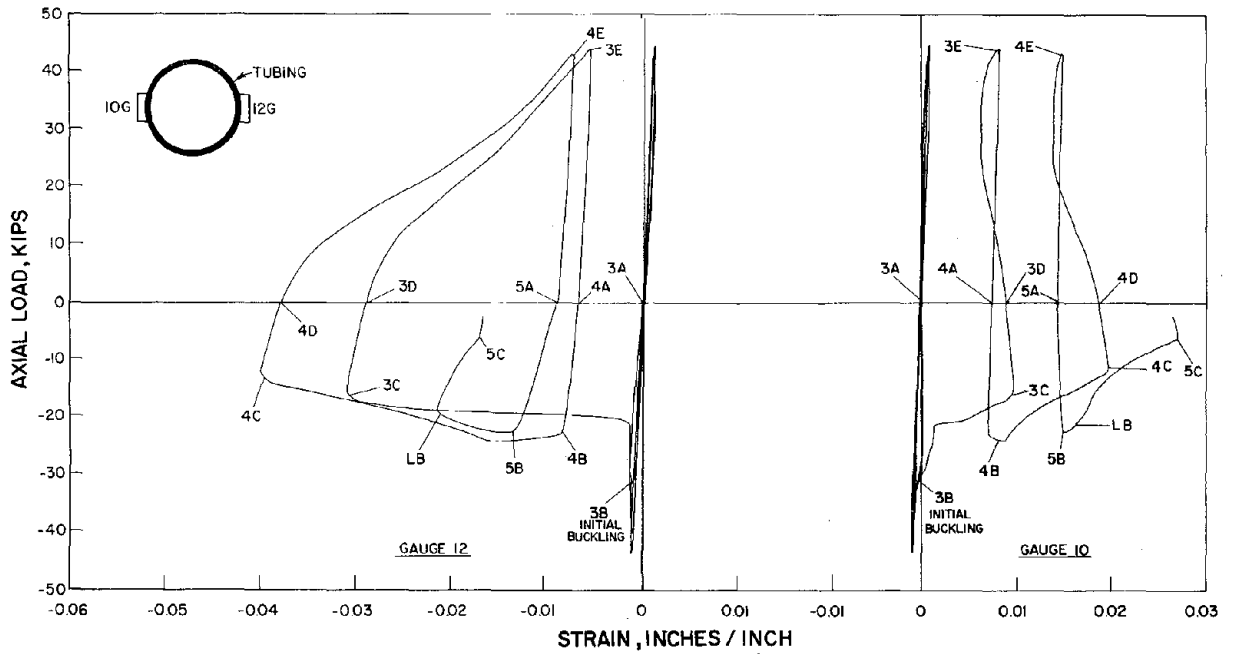
Fig. A.7   Strut 2 - Axial Load vs. Strain (Gages 10 and 12 - Cycles 1-5)
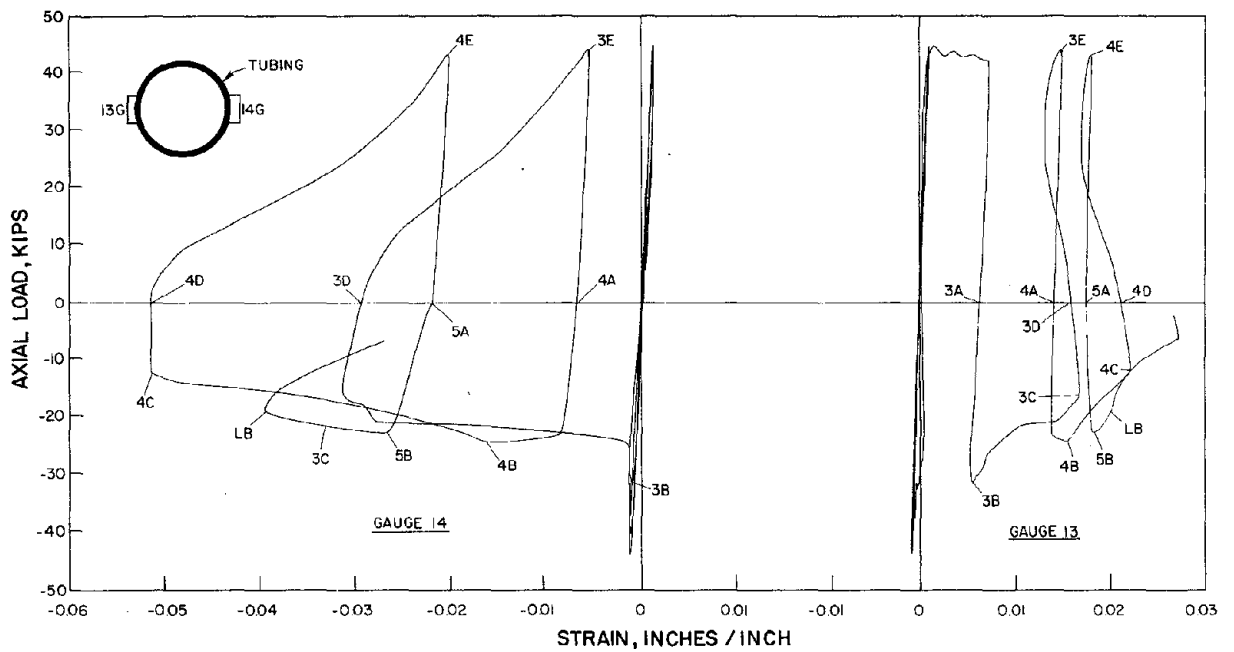
Fig. A.8   Strut 2 - Axial Load vs. Strain (Gages 13 and 14 - Cycles 1-5)
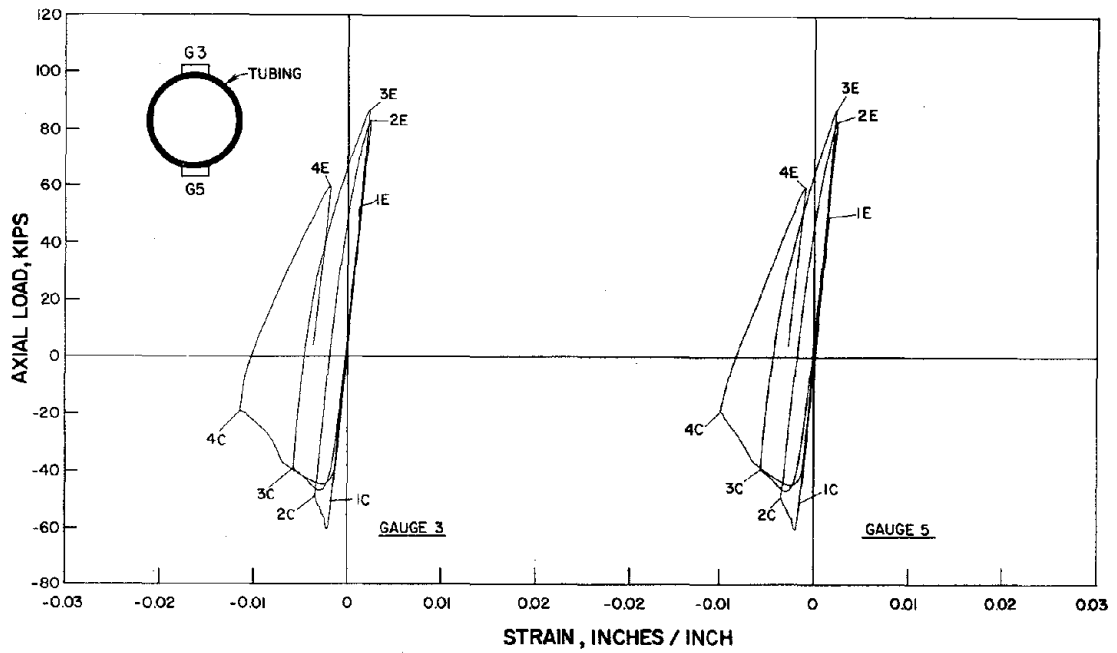
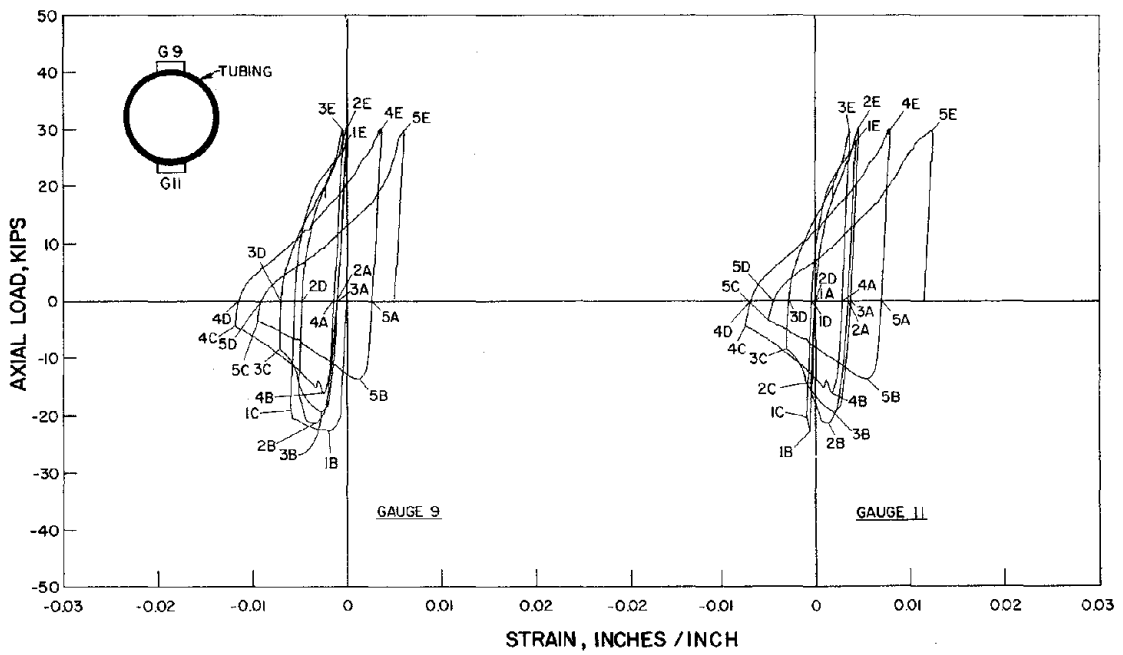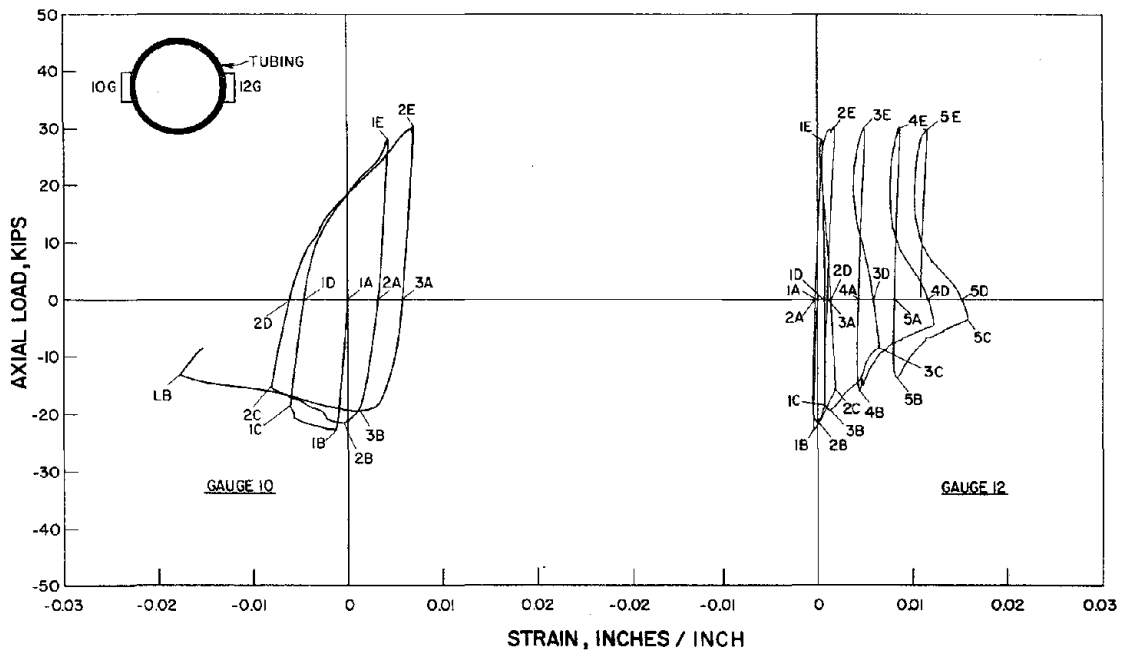Fig. A.9   Strut 3 – Axial Load vs. Strain (Gages 3 and 5 – Cycles 1-5)
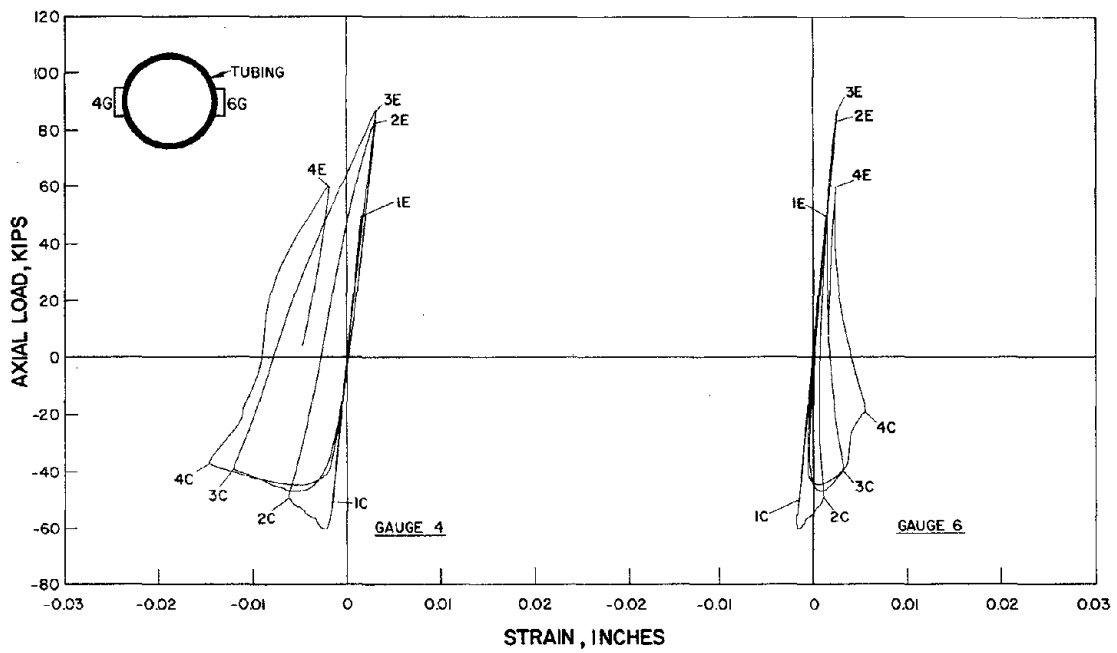
Fig. A.10   Strut 3 – Axial Load vs. Strain (Gages 4 and 6 – Cycles 1-5)
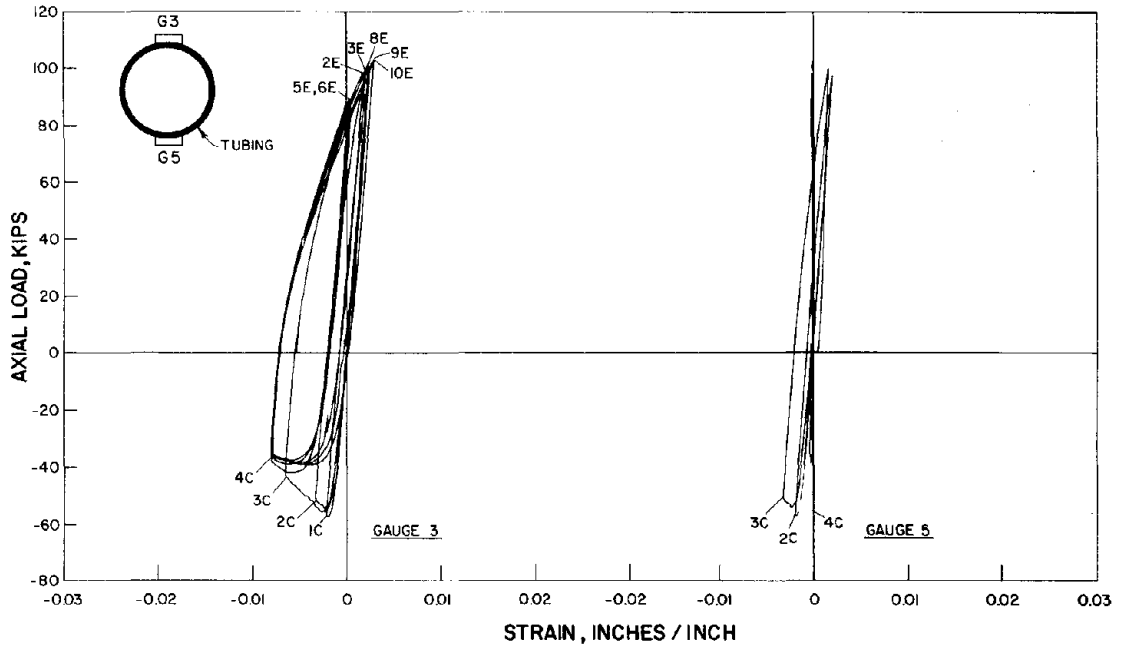
Fig. A.11 Strut 4 - Axial Load vs. Strain (Gages 3 and 5 - Cycles 1-5)
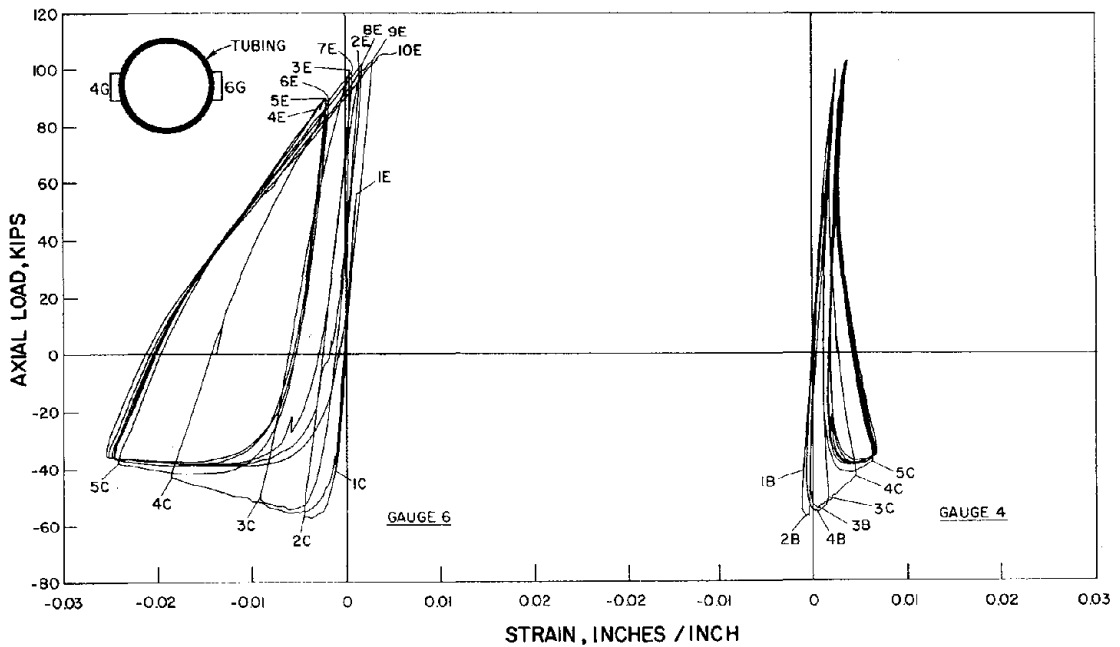
Fig. A.12 Strut 4 - Axial Load vs. Strain (Gages 4 and 6 - Cycles 1-5)

161
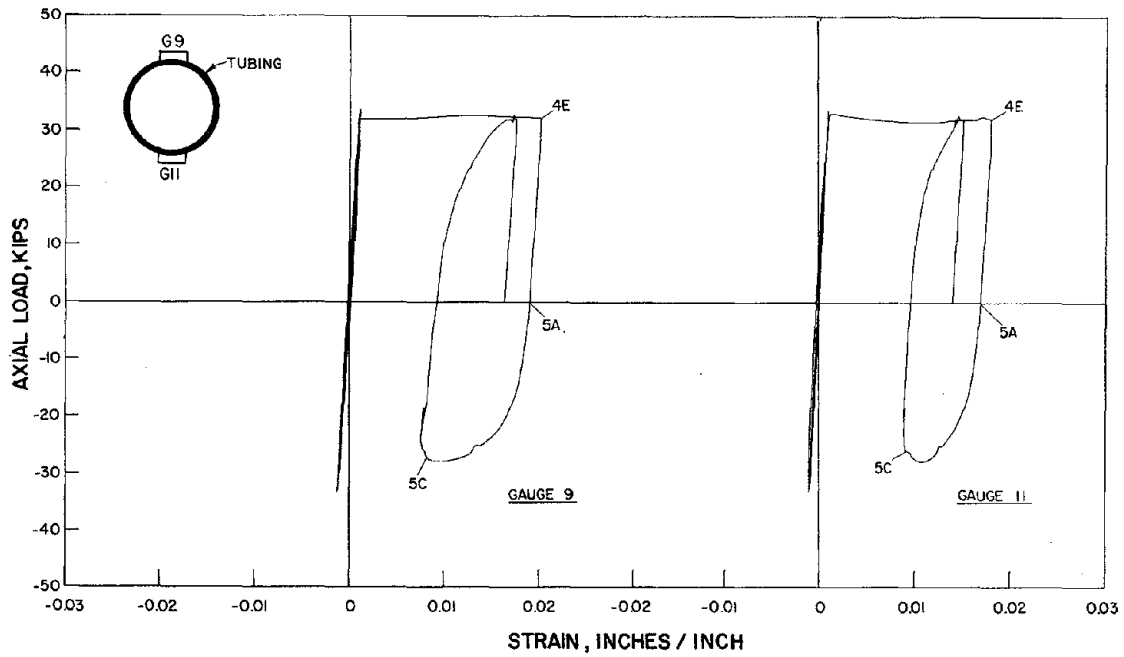
Fig. A.13   Strut 5 – Axial Load vs. Strain (Gages 9 and 11 – Cycles 1-5)
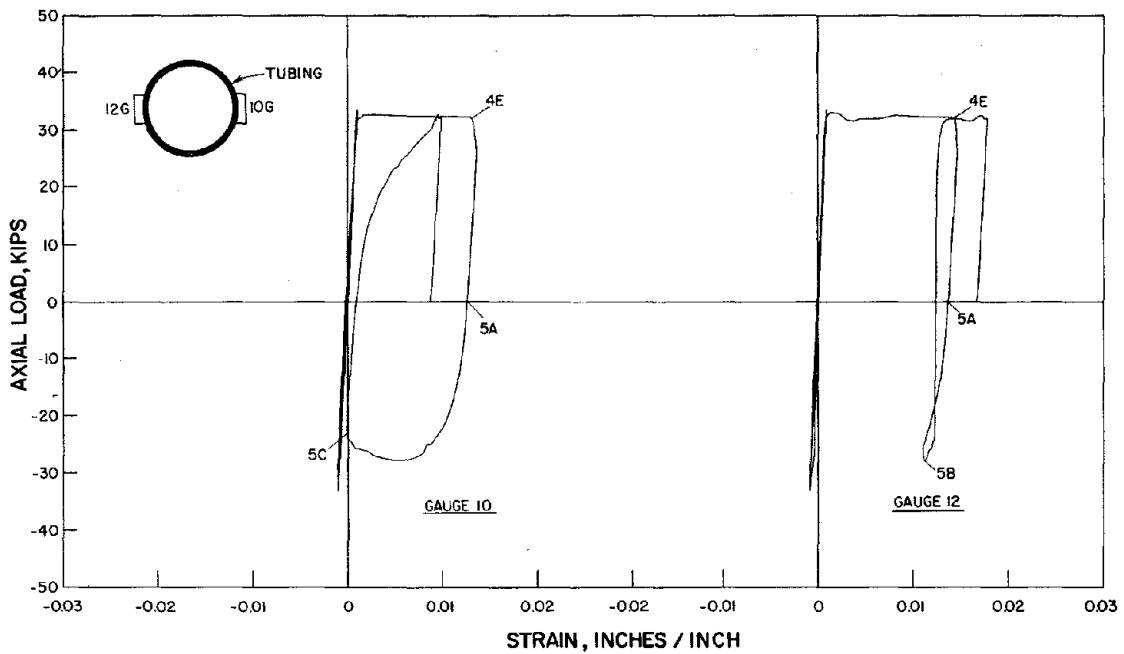
Fig. A.14   Strut 5 – Axial Load vs. Strain (Gages 10 and 12 – Cycles 1-5)

162
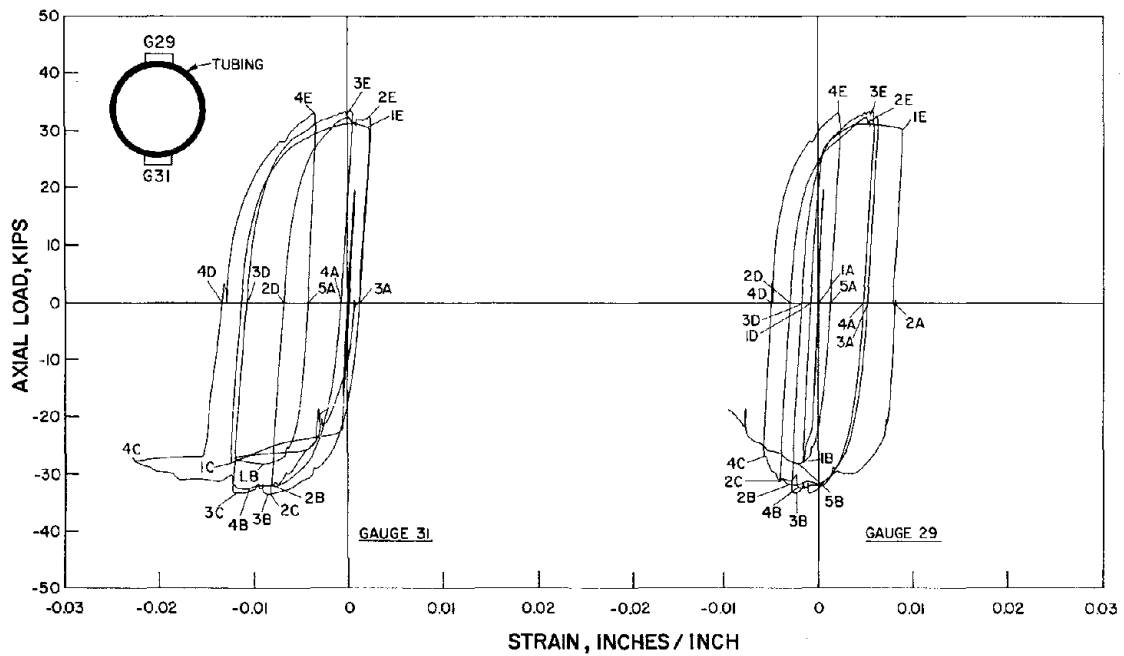
Fig. A.15 Strut 5 – Axial Load vs. Strain (Gages 29 and 31 – Cycles 1–5)
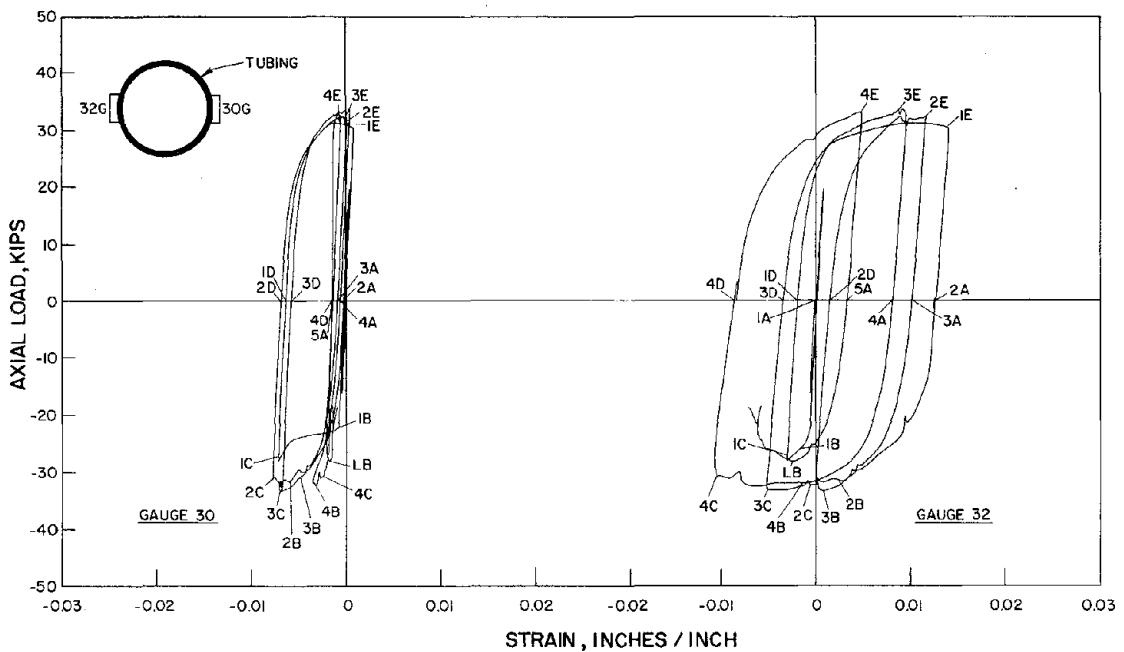
Fig. A.16 Strut 5 – Axial Load vs. Strain (Gages 30 and 32 – Cycles 1–5)
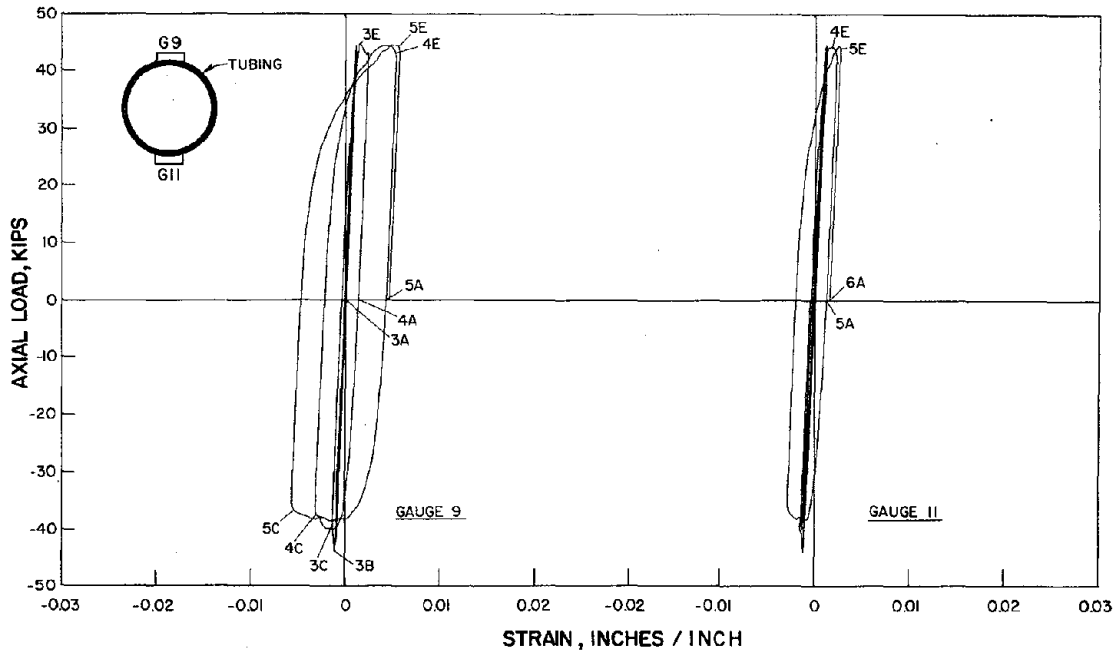
Fig. A.17   Strut 6 – Axial Load vs. Strain (Gages 9 and 11 – Cycles 1-5)
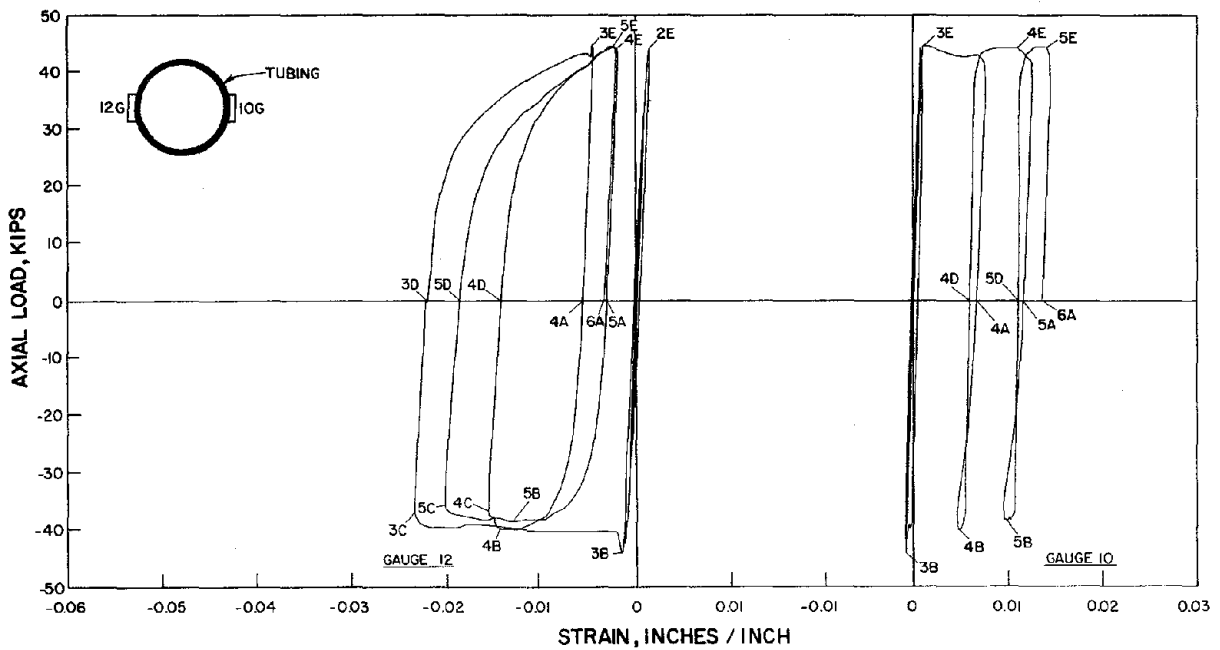
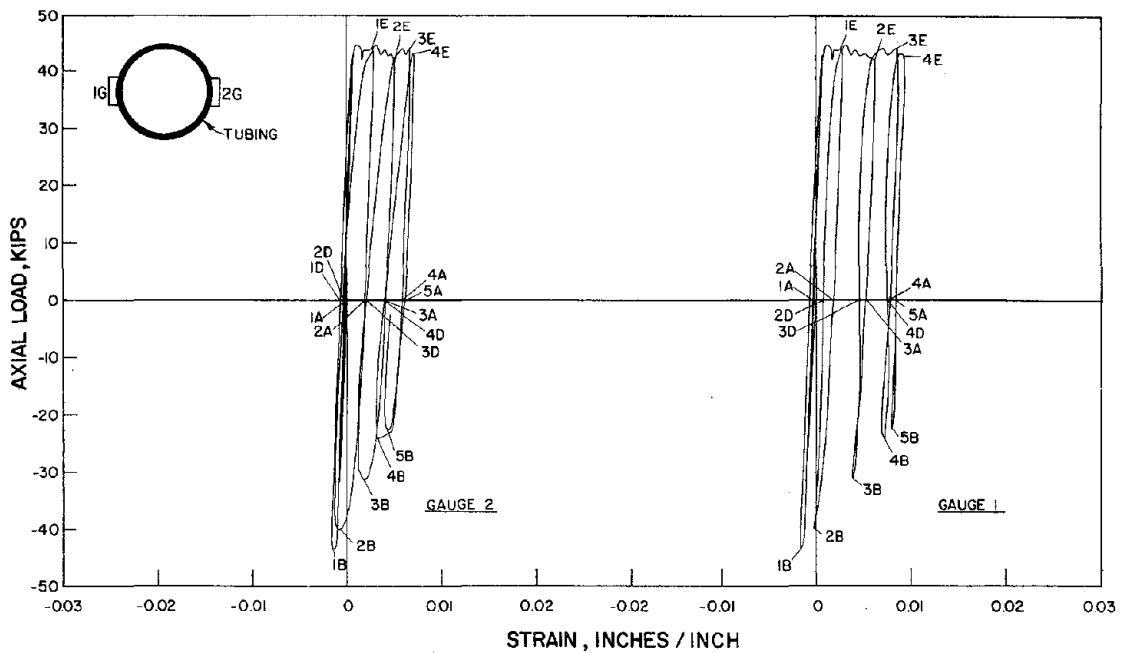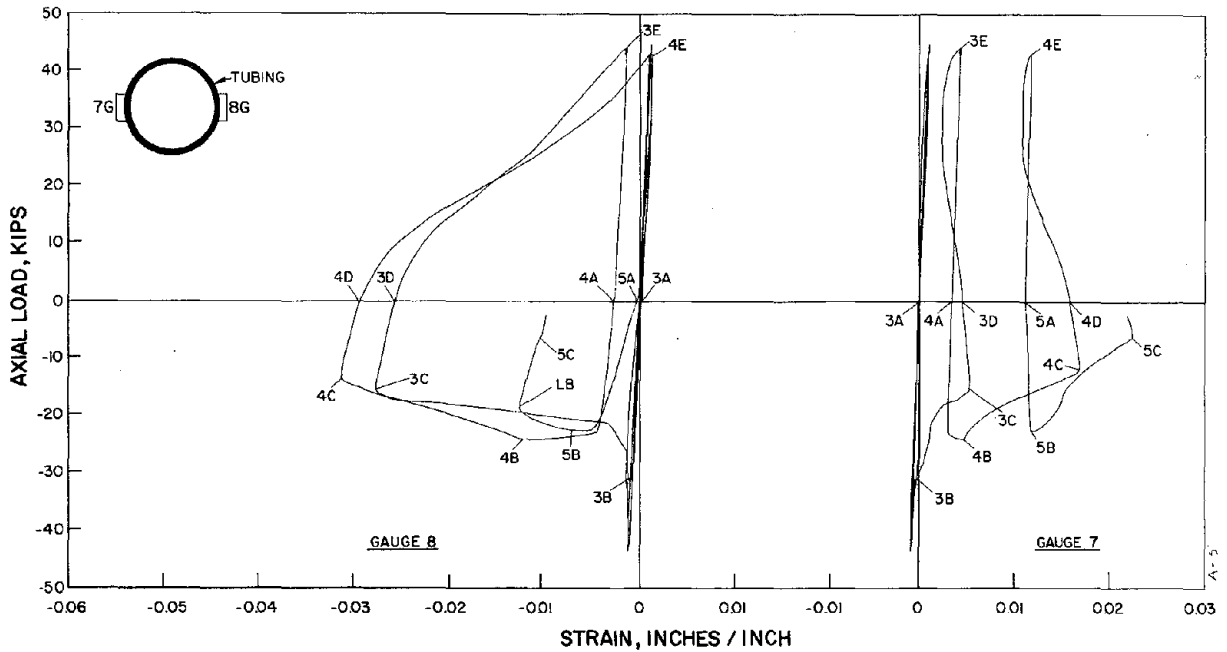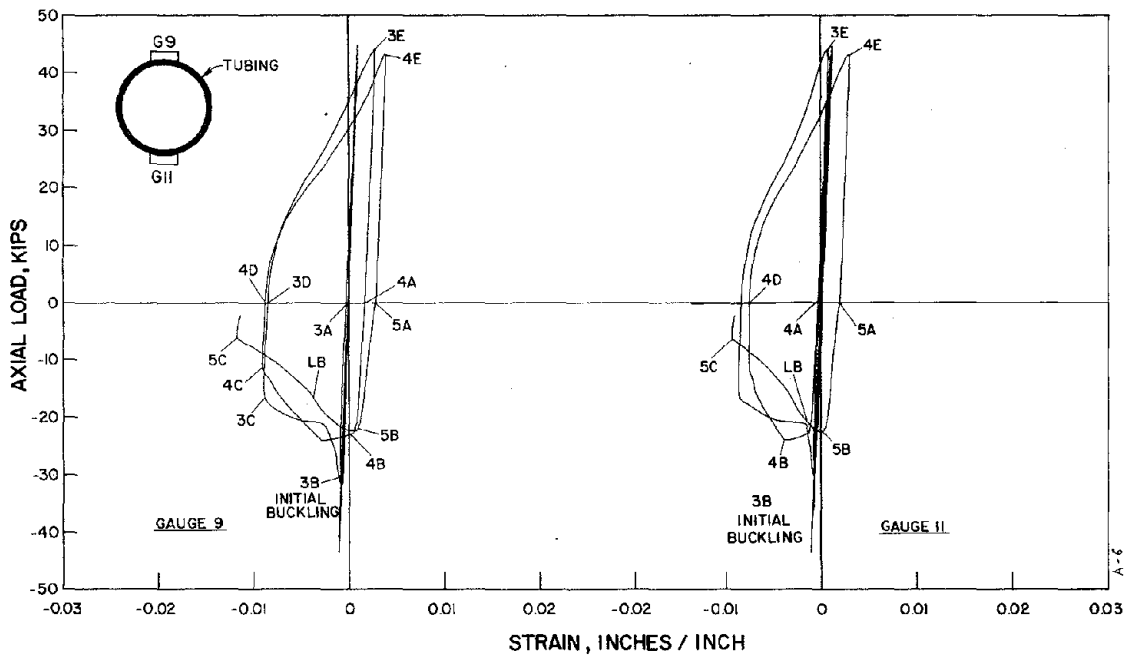Fig. A.18   Strut 6 – Axial Load vs. Strain (Gages 10 and 12 – Cycles 1-5)

164
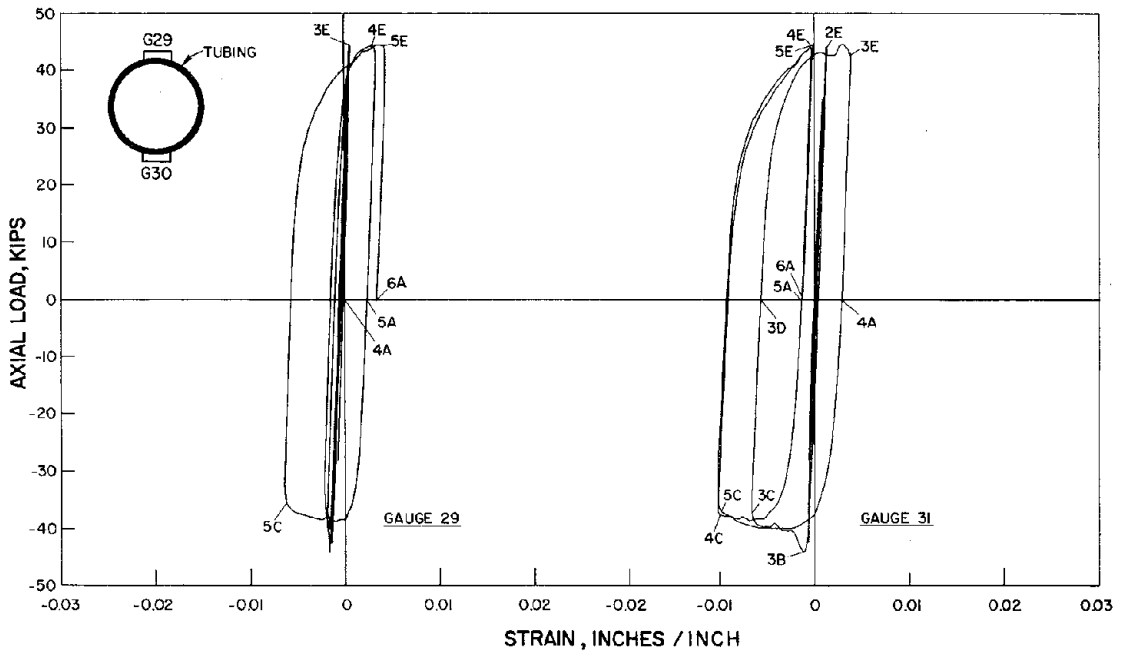
Fig. A.19   Strut 6 – Axial Load vs. Strain (Gages 29 and 31 – Cycles 1-5)
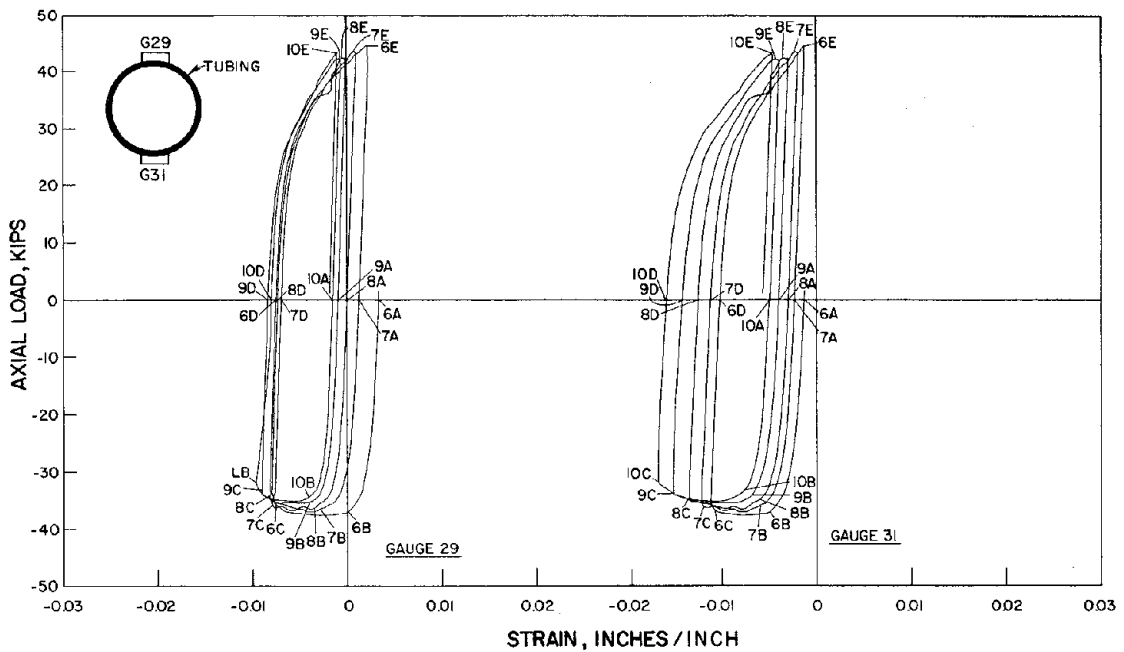
Fig. A.20   Strut 6 – Axial Load vs. Strain (Gages 29 and 31 – Cycles 6-10)

165
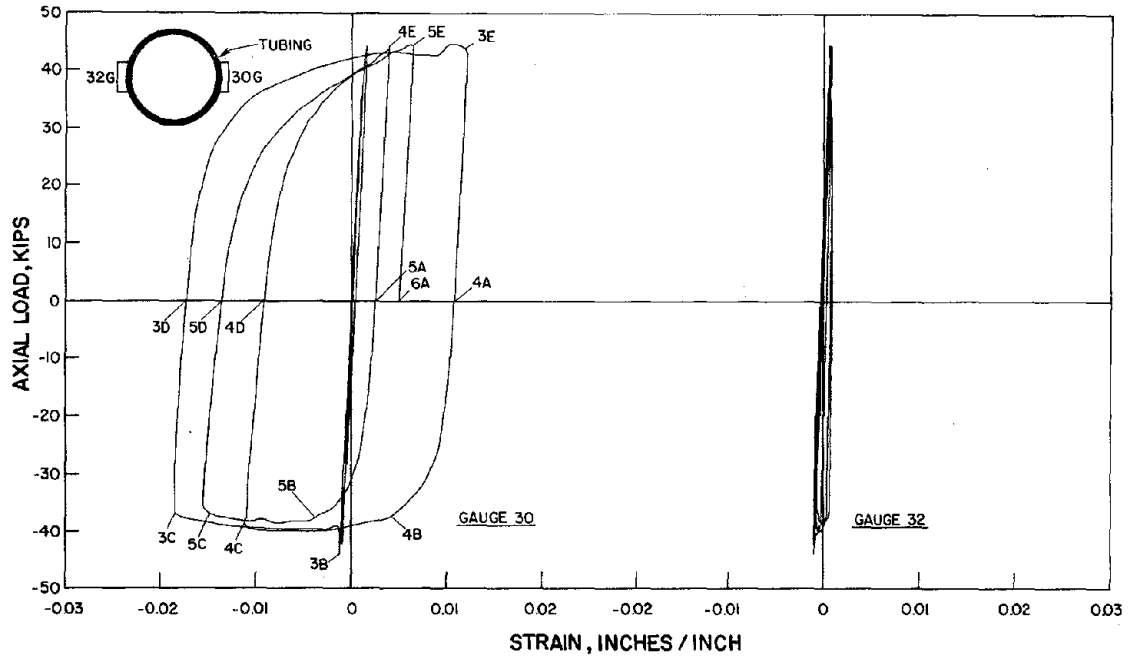
Fig. A.21 Strut 6 – Axial Load vs. Strain (Gages 30 and 32 – Cycles 1-5)
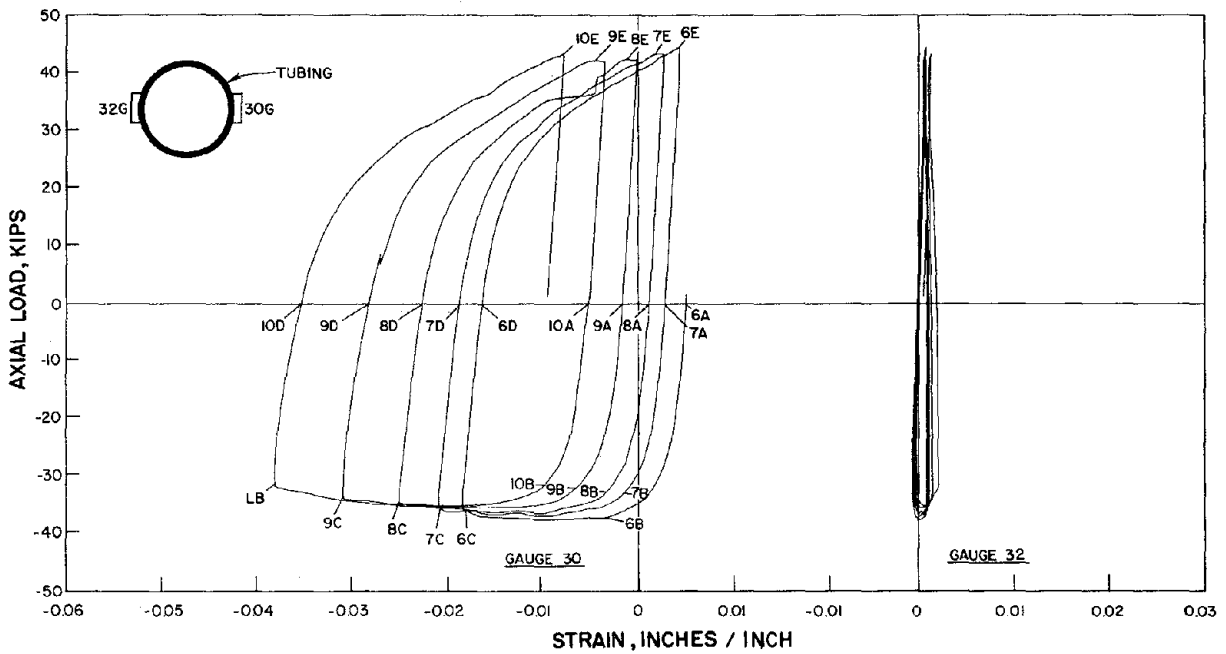
Fig. A.22 Strut 6 – Axial Load vs. Strain (Gages 30 and 32 – Cycles 6-10)

166

Fig. A.23 Strut 1 - Axial Load vs. Section Curvature (Gages 1,2 - Cycles 1-5)

Fig. A.24 Strut 1 - Axial Load vs. Section Curvature (Gages 3,4 - Cycles 1-5)
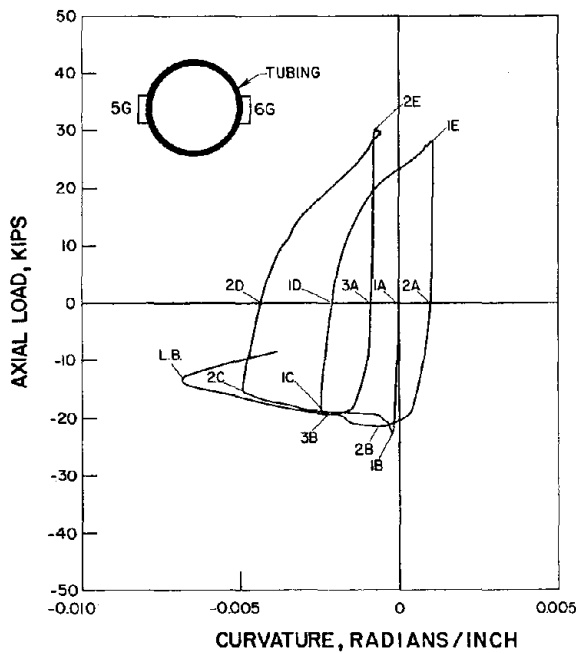
Fig. A.25 Strut 1 - Axial Load vs. Section Curvature (Gages 5,6 - Cycles 1-5)
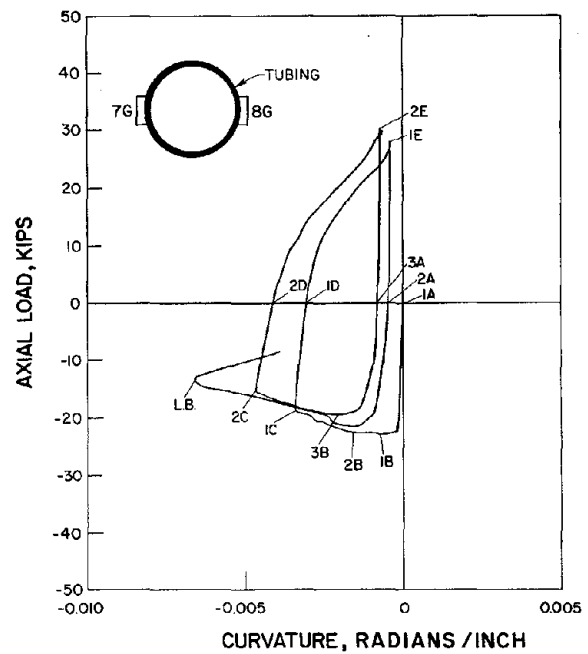
Fig. A.26 Strut 1 - Axial Load vs. Section Curvature (Gages 7,8 - Cycles 1-5)
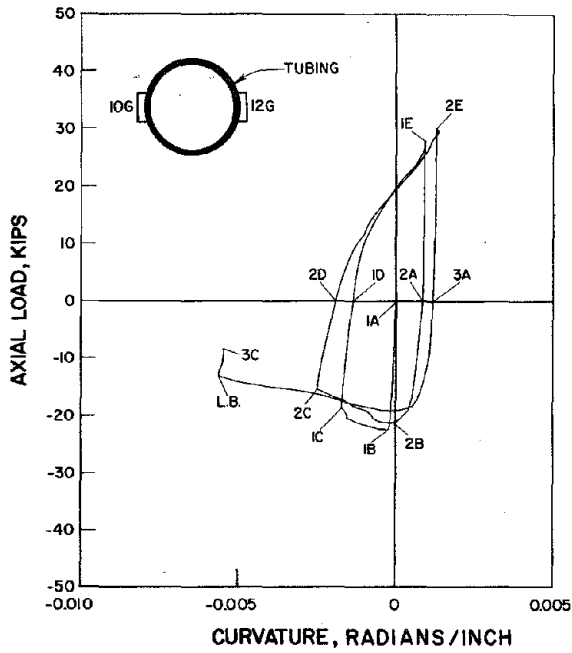
Fig. A.27 Strut 1 - Axial Load vs.
          Section Curvature
          (Gages 10,12 - Cycles 1-5)
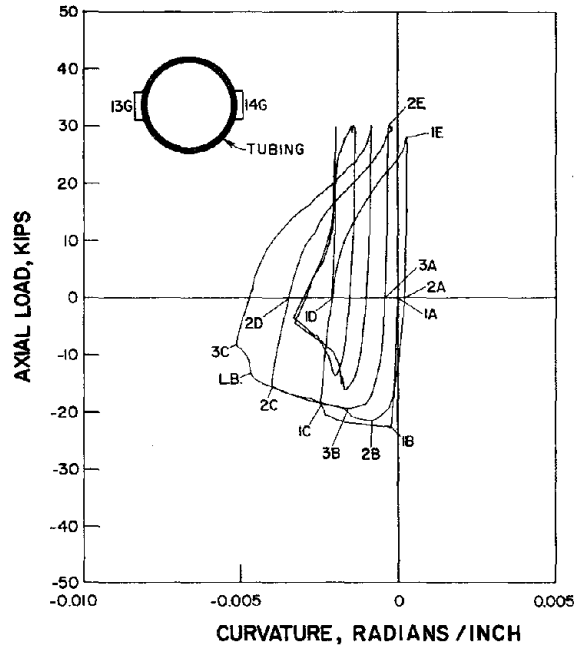
Fig. A.28 Strut 1 - Axial Load vs.
          Section Curvature
          (Gages 7,8 - Cycles 1-5)
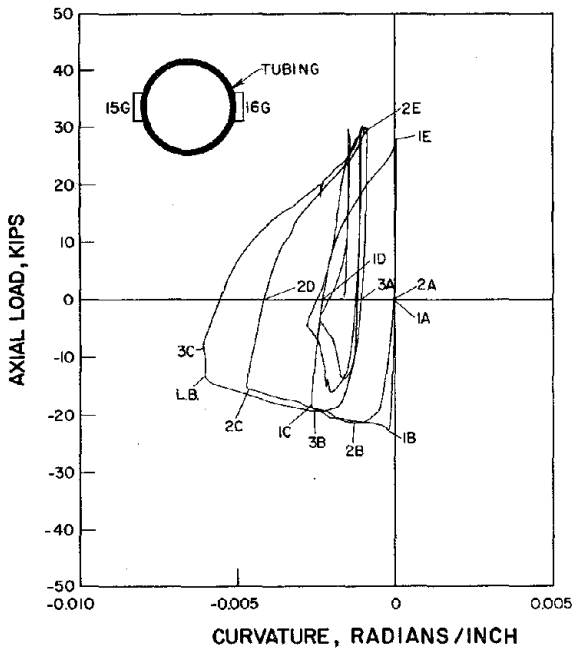
Fig. A.29 Strut 1 - Axial Load vs.
          Section Curvature
          (Gages 15,16 - Cycles 1-5)
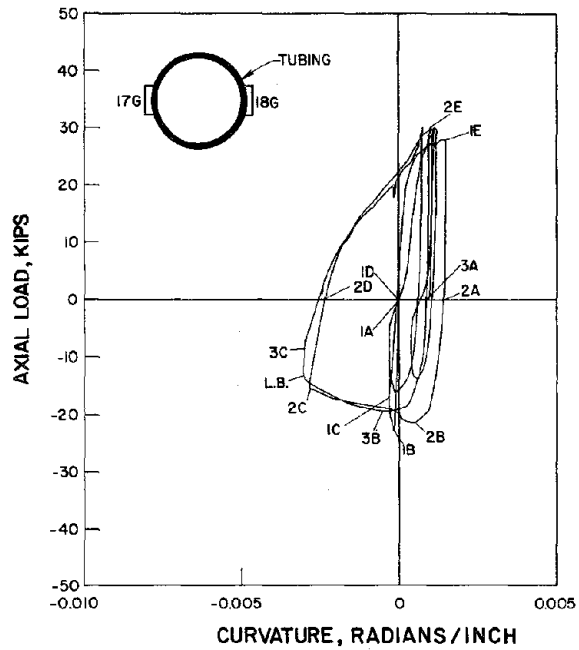
Fig. A.30 Strut 1 - Axial Load vs.
          Section Curvature
          (Gages 17,18 - Cycles 1-5)

168
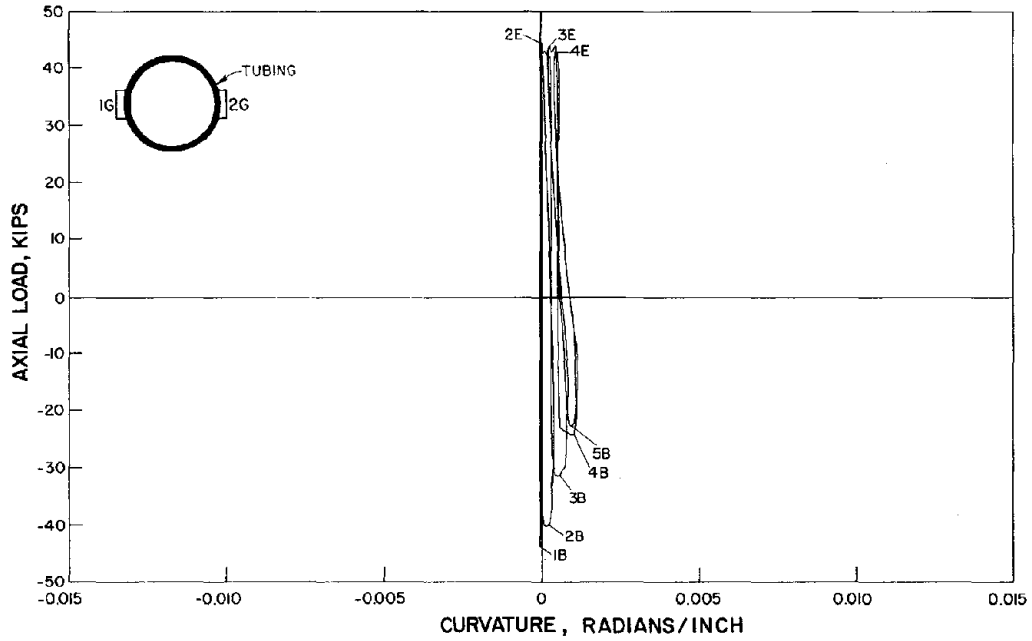
Fig. A.31 Strut 2 - Axial Load vs. Section Curvature
(Gages 1,2 - Cycles 1-5)
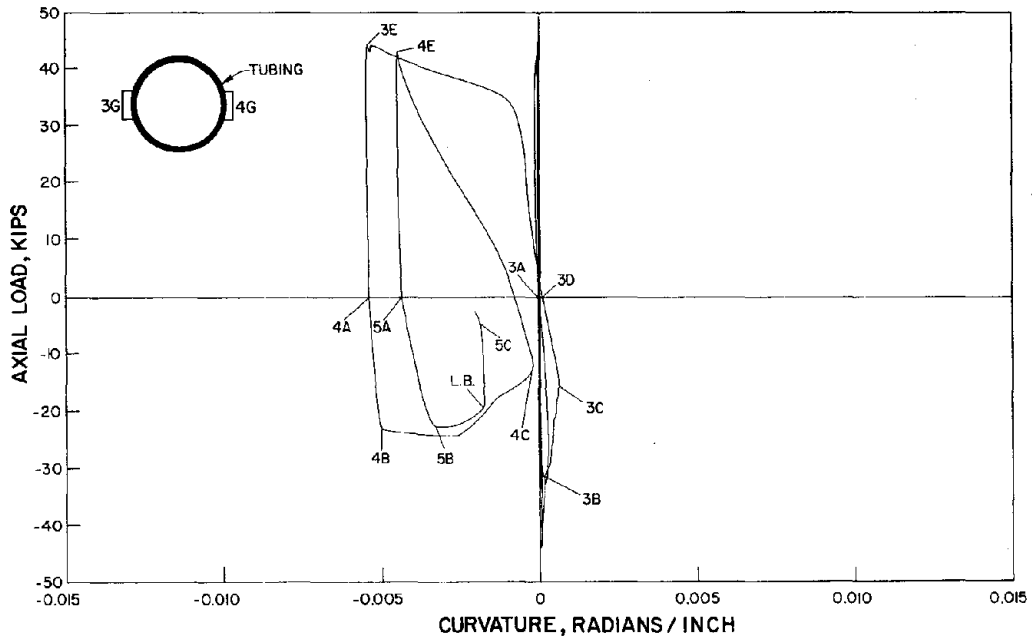
Fig. A.32 Strut 2 - Axial Load vs. Section Curvature
(Gages 3,4 - Cycles 1-5)

169
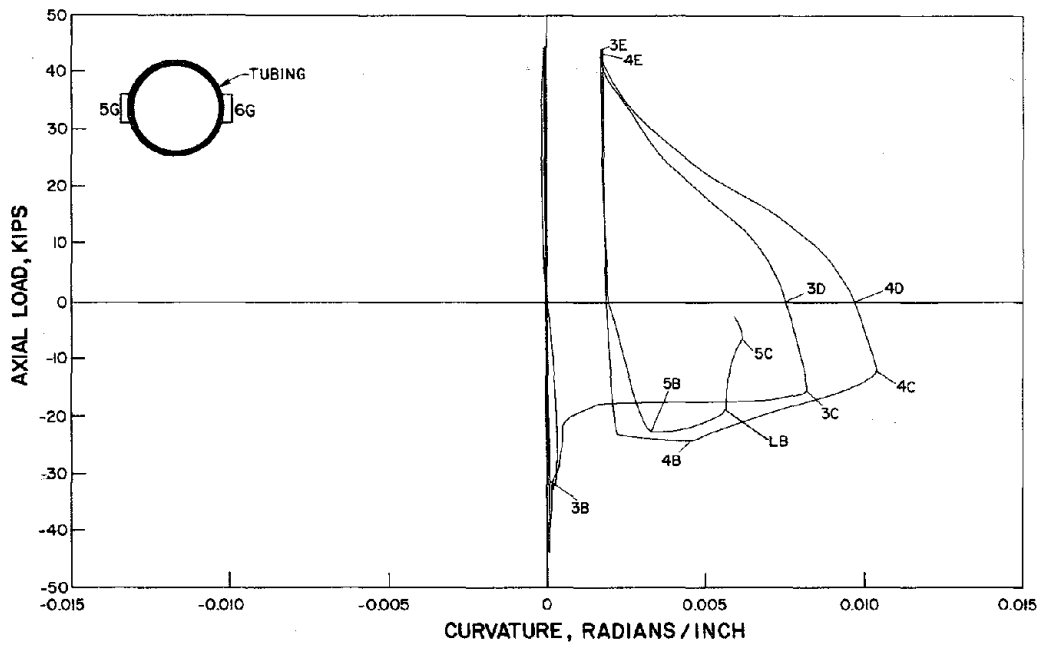
Fig. A.33   Strut 2 – Axial Load vs. Section Curvature
(Gages 5,6 – Cycles 1-5)
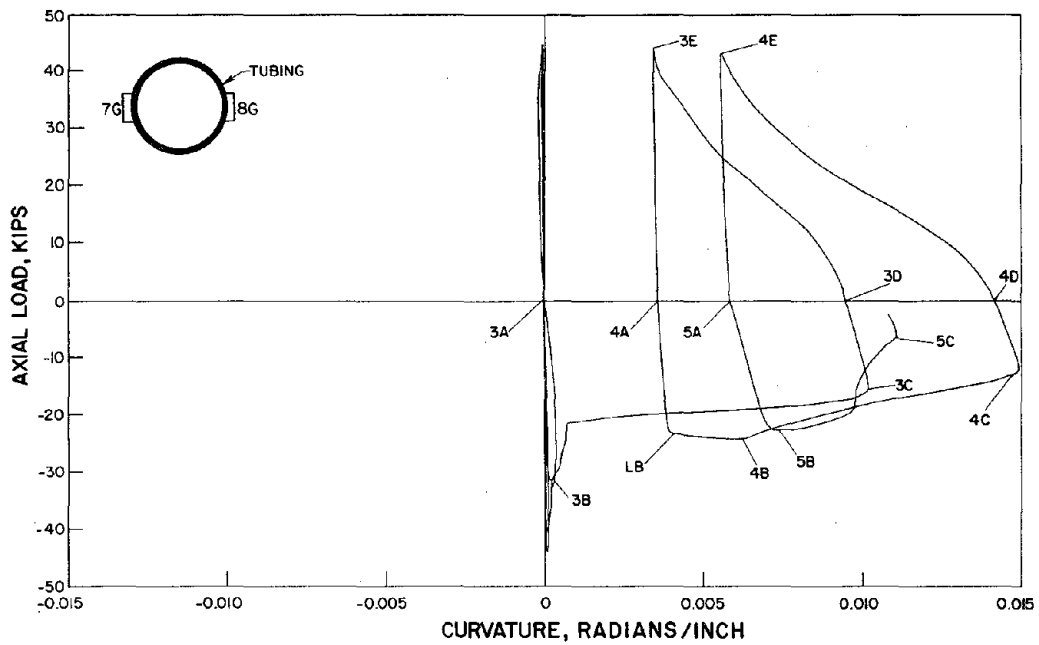
Fig. A.34   Strut 2 – Axial Load vs. Section Curvature
(Gages 7,8 – Cycles 1-5)
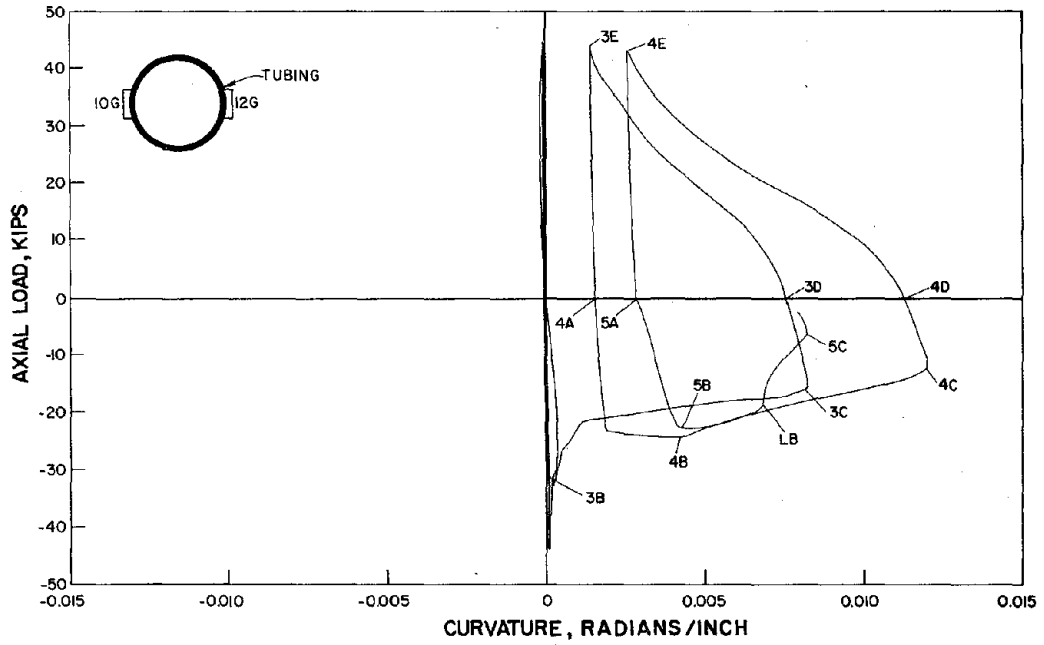
Fig. A.35 Strut 2 – Axial Load vs. Section Curvature
(Gages 10,12 – Cycles 1-5)
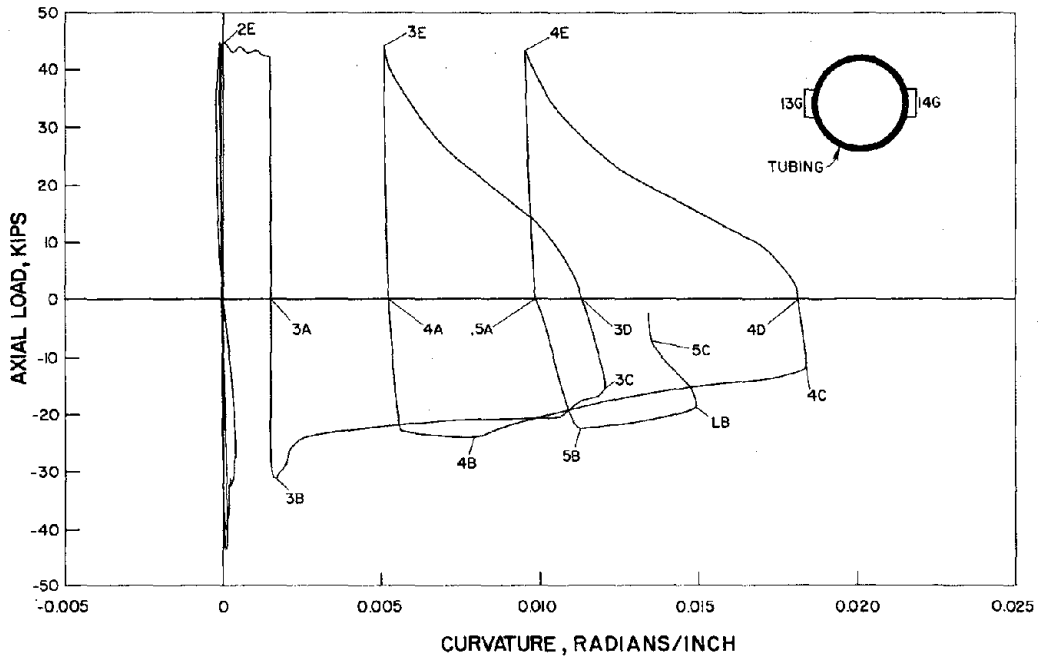
Fig. A.36 Strut 2 – Axial Load vs. Section Curvature
(Gages 13,14 – Cycles 1-5)

171
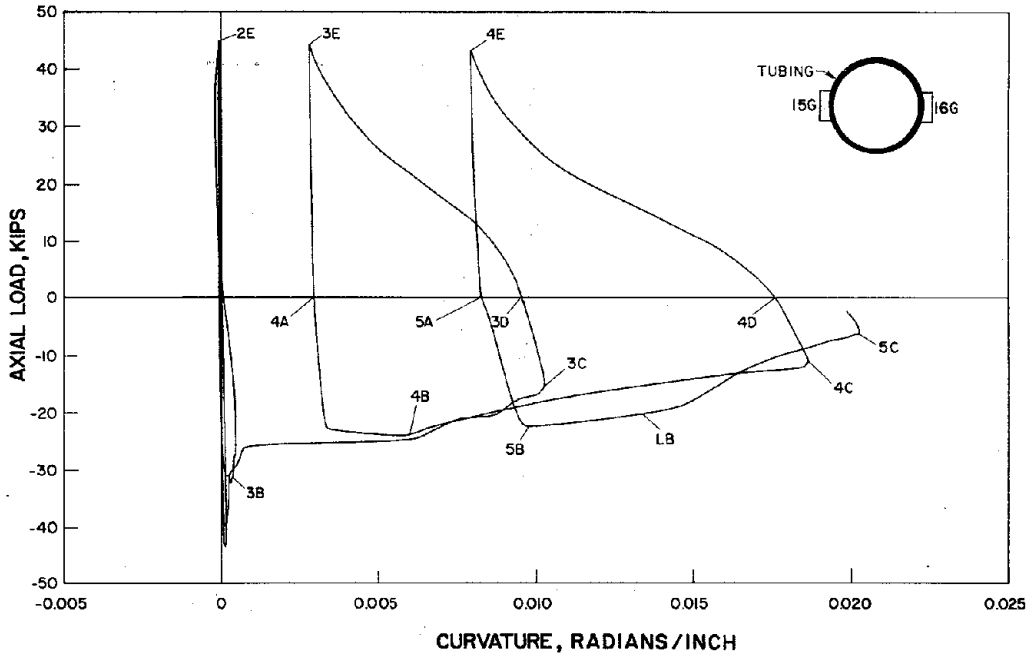
Fig. A.37   Strut 2 - Axial Load vs. Section Curvature
(Gages 15,16 - Cycles 1-5)
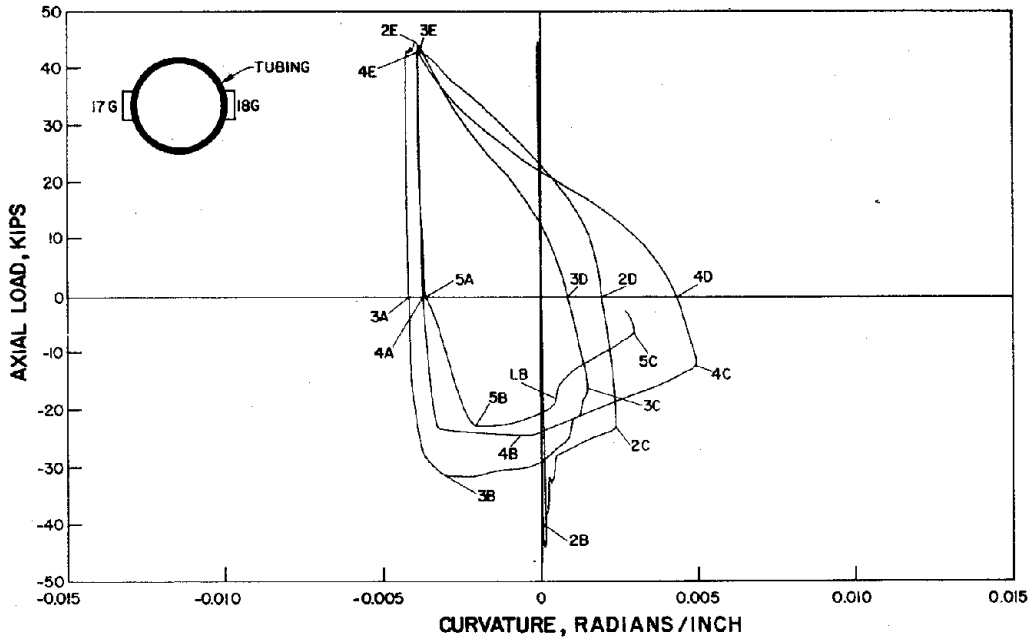
Fig. A.38   Strut 2 - Axial Load vs. Section Curvature
(Gages 17,18 - Cycles 1-5)
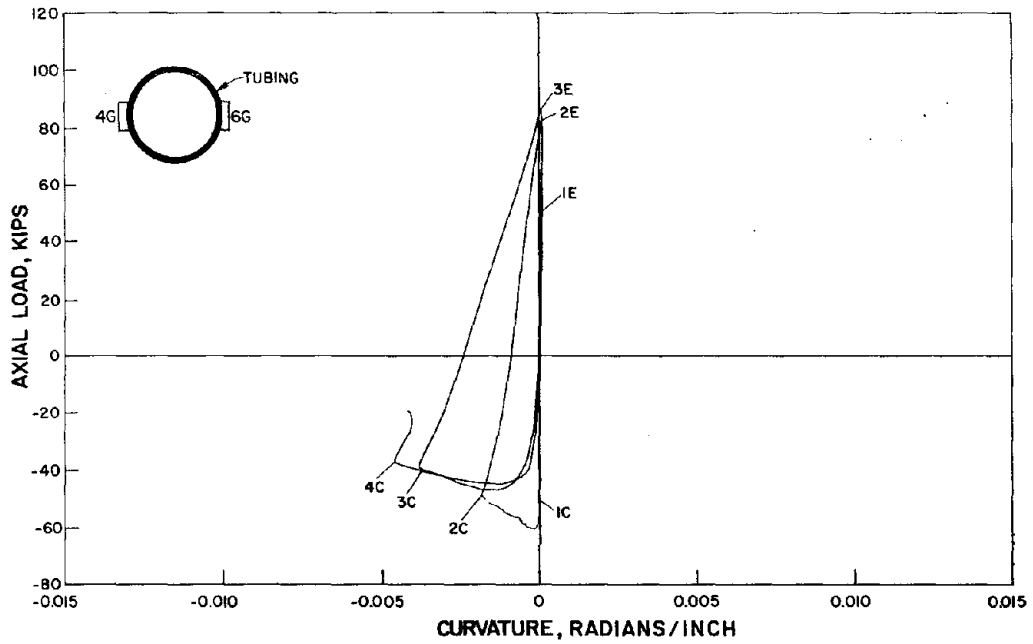
Fig. A.39   Strut 3 — Axial Load vs. Section Curvature
(Gages 4,6 — Cycles 1-5)
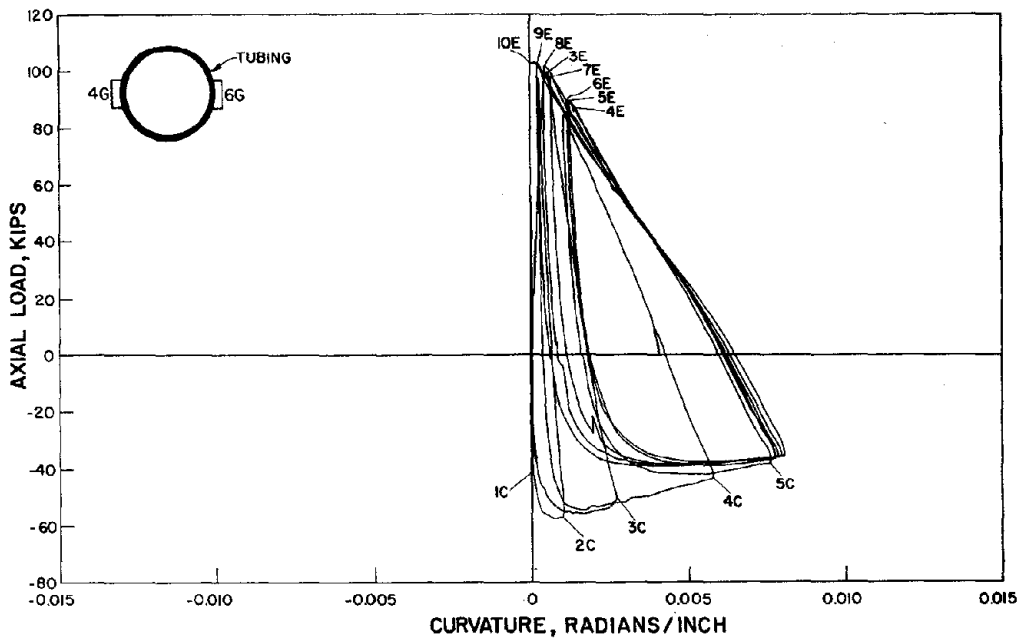
Fig. A.40   Strut 4 — Axial Load vs. Section Curvature
(Gages 4,6 — Cycles 1-5)

173
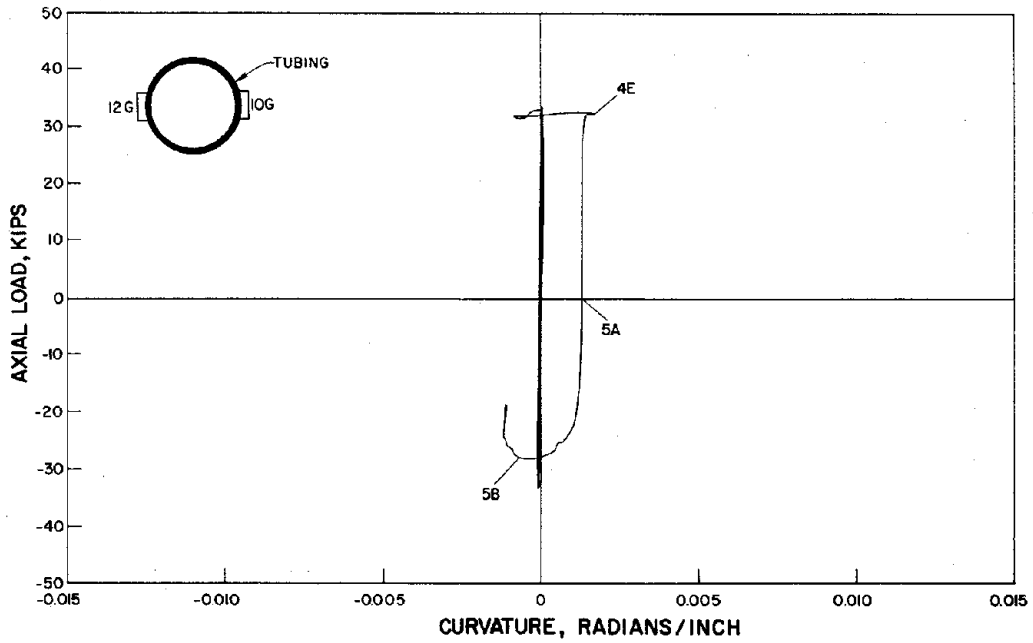
Fig. A.41 Strut 5 – Axial Load vs. Section Curvature
(Gages 10,12 – Cycles 1-5)
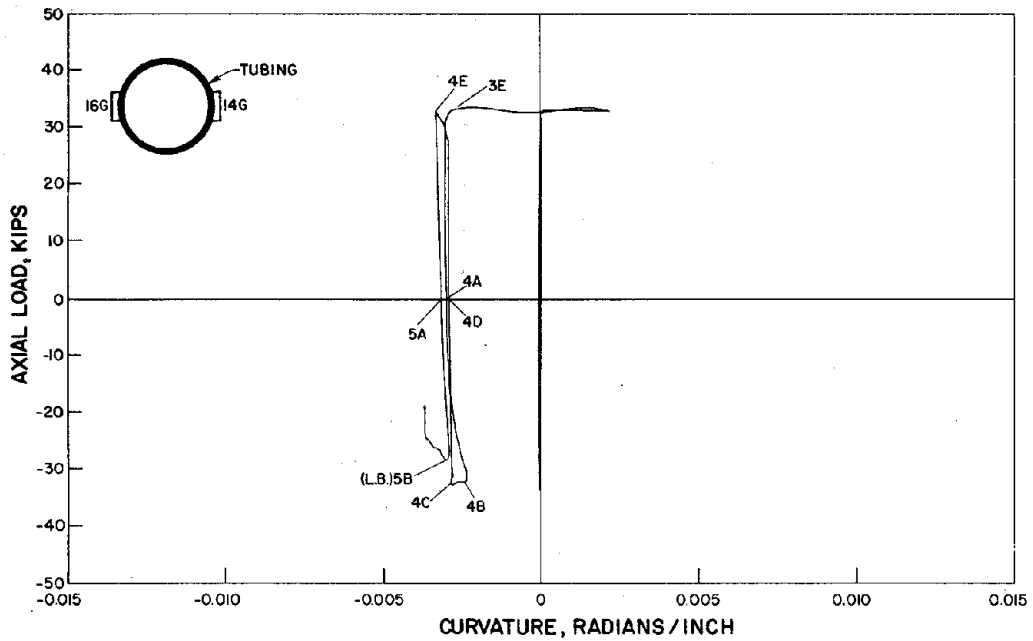
Fig. A.42 Strut 5 – Axial Load vs. Section Curvature
(Gages 14,16 – Cycles 1-5)
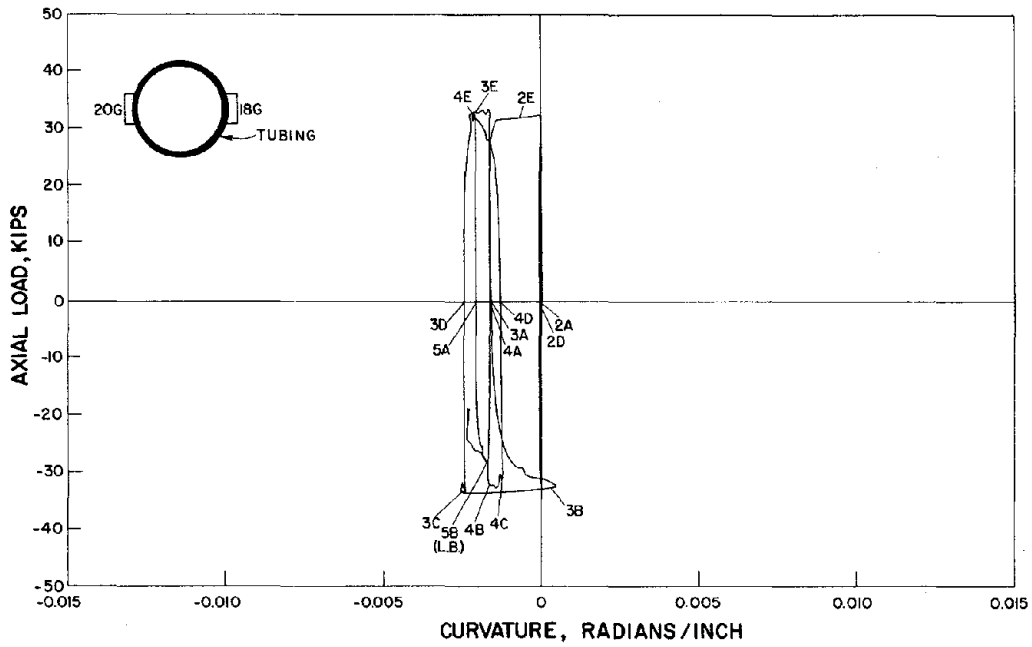
Fig. A.43   Strut 5 – Axial Load vs. Section Curvature
(Gages 18,20 – Cycles 1-5)
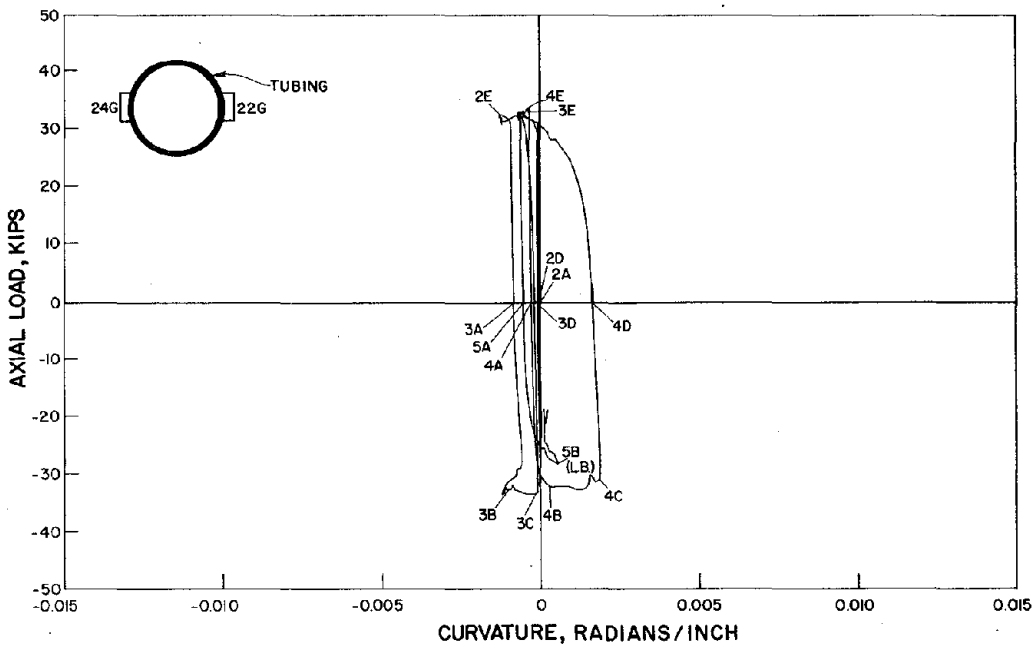
Fig. A.44   Strut 5 – Axial Load vs. Section Curvature
(Gages 22,24 – Cycles 1-5)
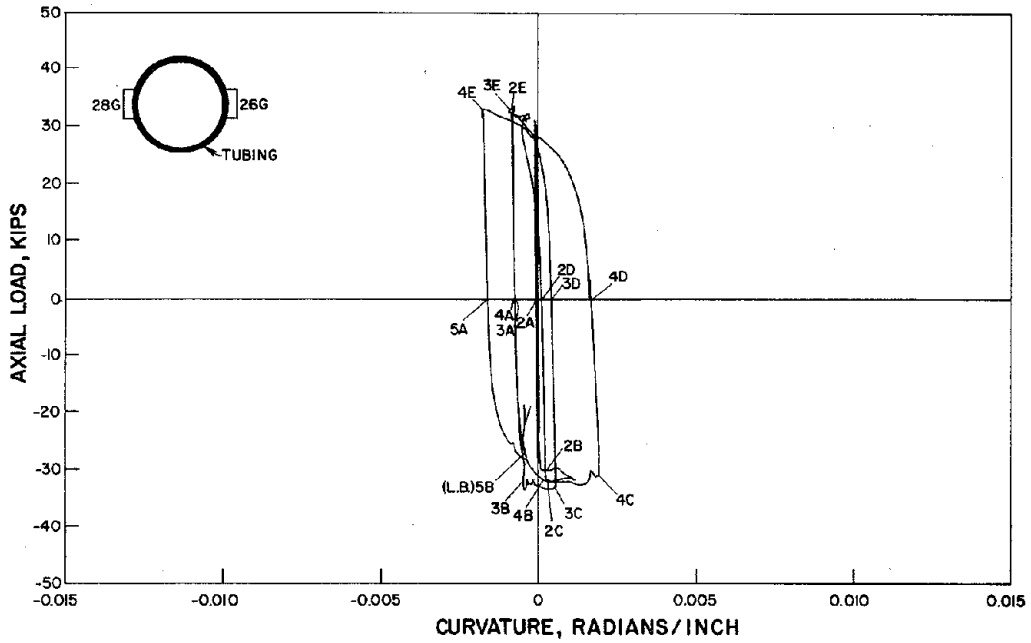
Fig. A.45 Strut 5 – Axial Load vs. Section Curvature
(Gages 26,28 – Cycles 1-5)
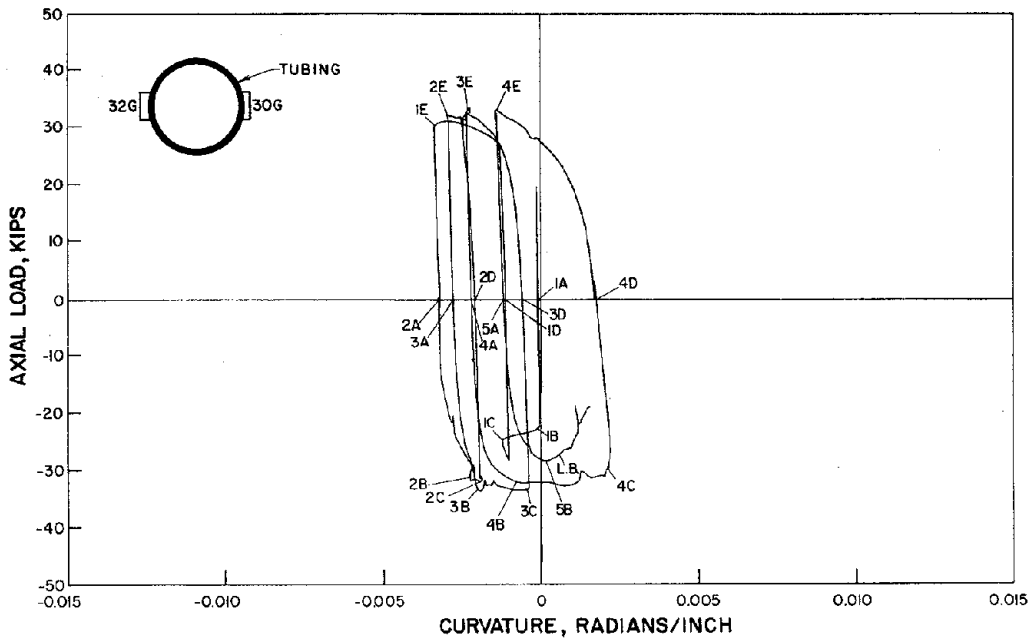
Fig. A.46 Strut 5 – Axial Load vs. Section Curvature
(Gages 30,32 – Cycles 1-5)

176
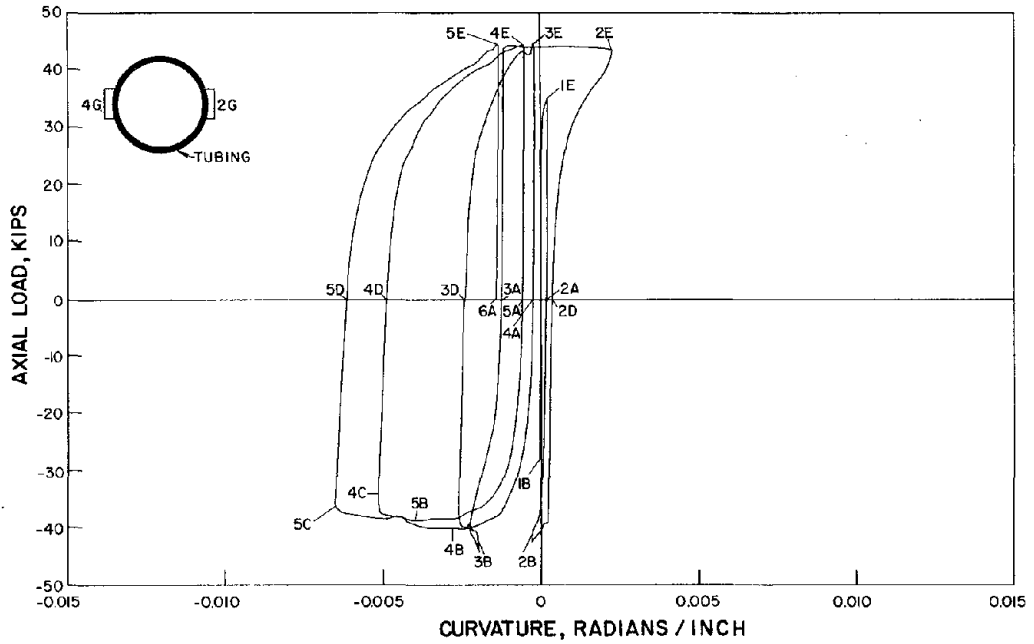
Fig. A.47 Strut 6 - Axial Load vs. Section Curvature
(Gages 2,4 - Cycles 1-5)
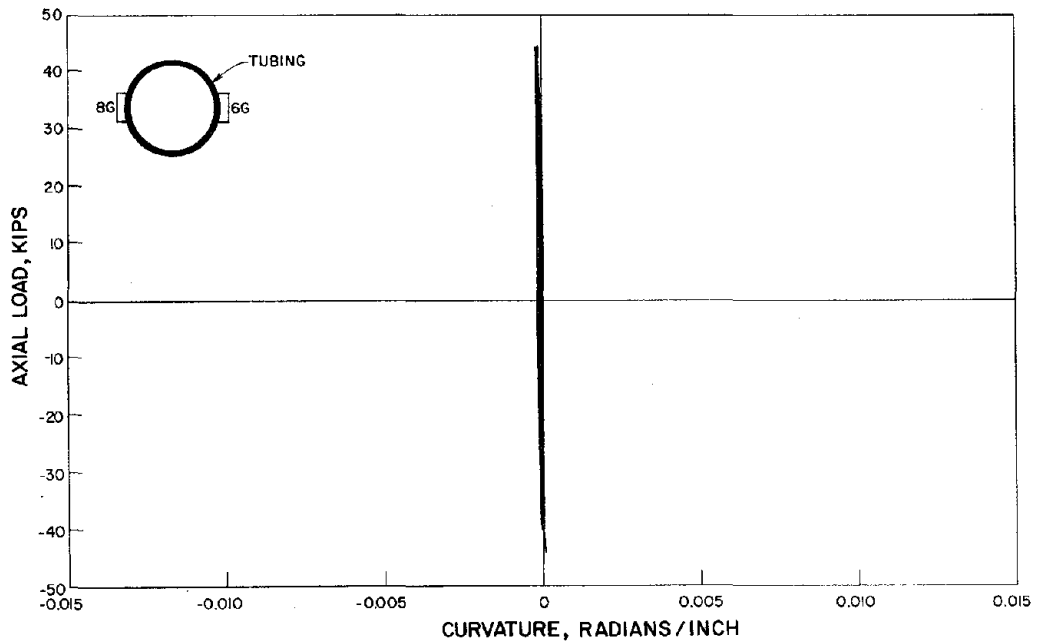
Fig. A.48 Strut 6 - Axial Load vs. Section Curvature
(Gages 6,8 - Cycles 1-5)

177
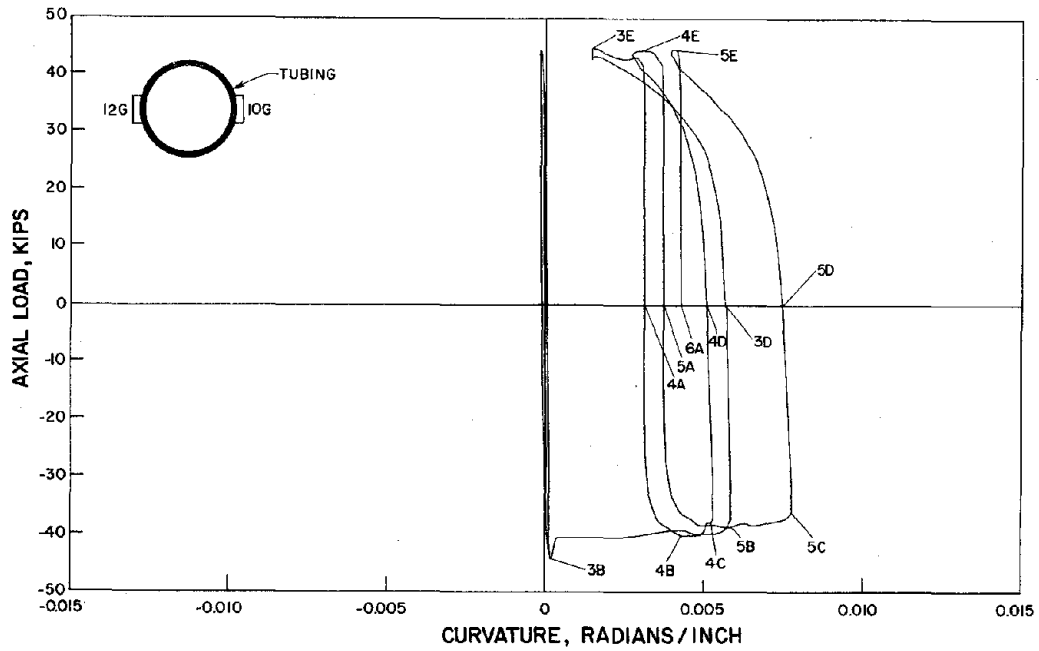
Fig. A.49 Strut 6 – Axial Load vs. Section Curvature
(Gages 10,12 – Cycles 1-5)
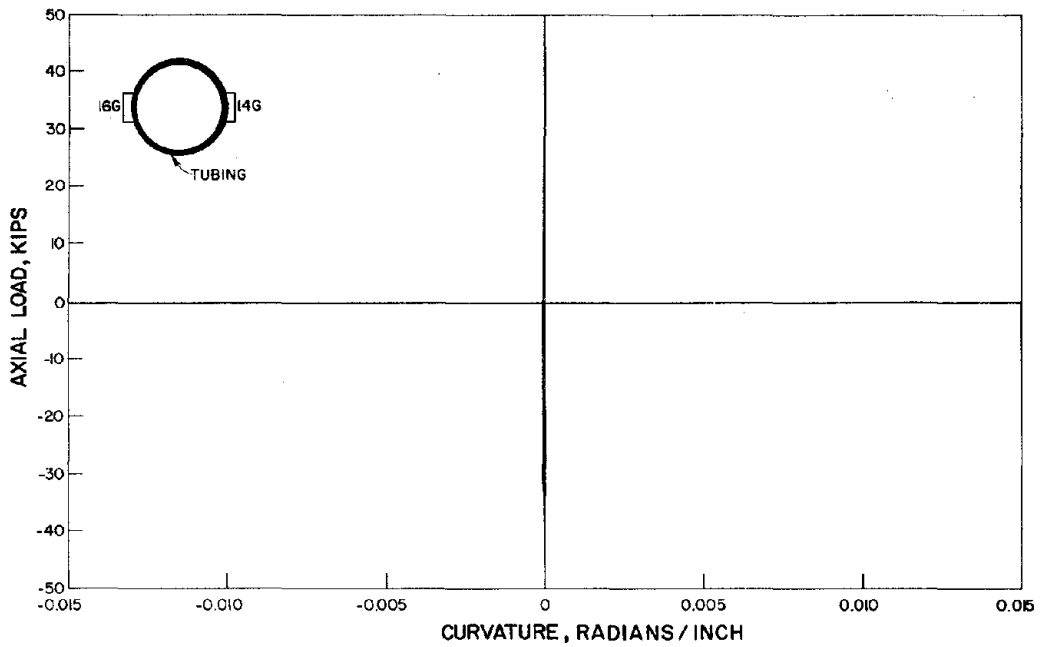
Fig. A.50 Strut 6 – Axial Load vs. Section Curvature
(Gages 14,16 – Cycles 1-5)

178
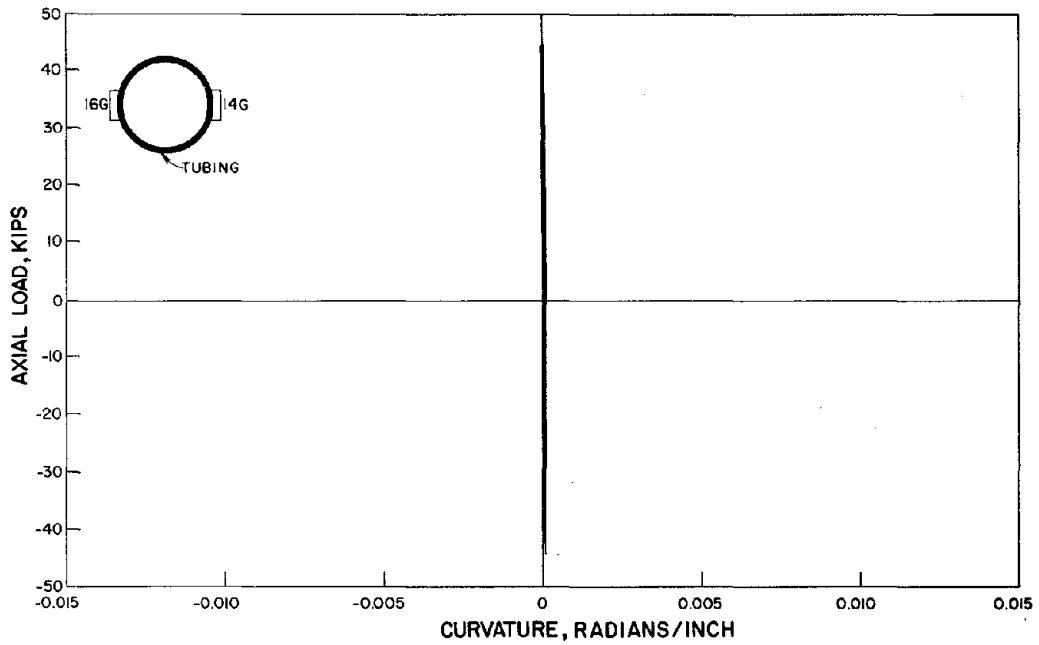
Fig. A.51   Strut 6 – Axial Load vs. Section Curvature
(Gages 14,16 – Cycles 6-10)
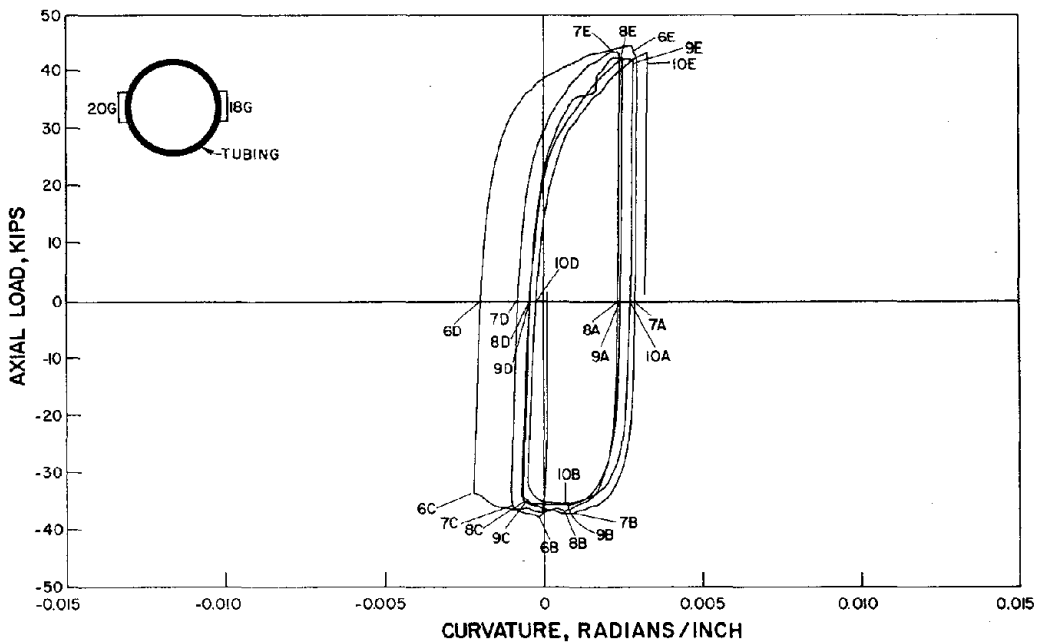
Fig. A.52   Strut 6 – Axial Load vs. Section Curvature
(Gages 16,18 – Cycles 6-10)

179
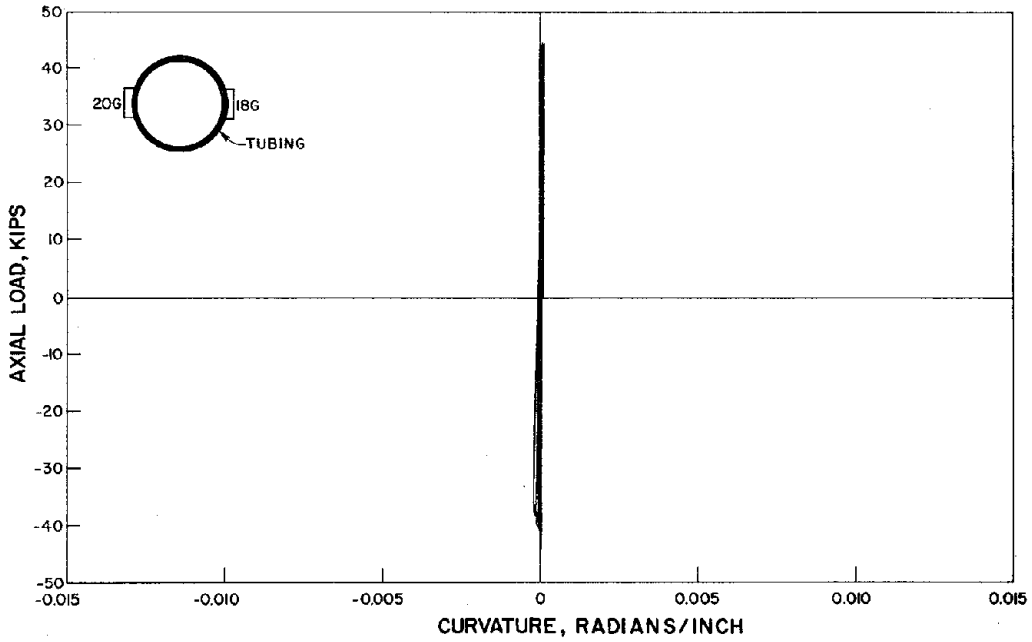
Fig. A.53   Strut 6 - Axial Load vs. Section Curvature
(Gages 18,20 - Cycles 1-5)
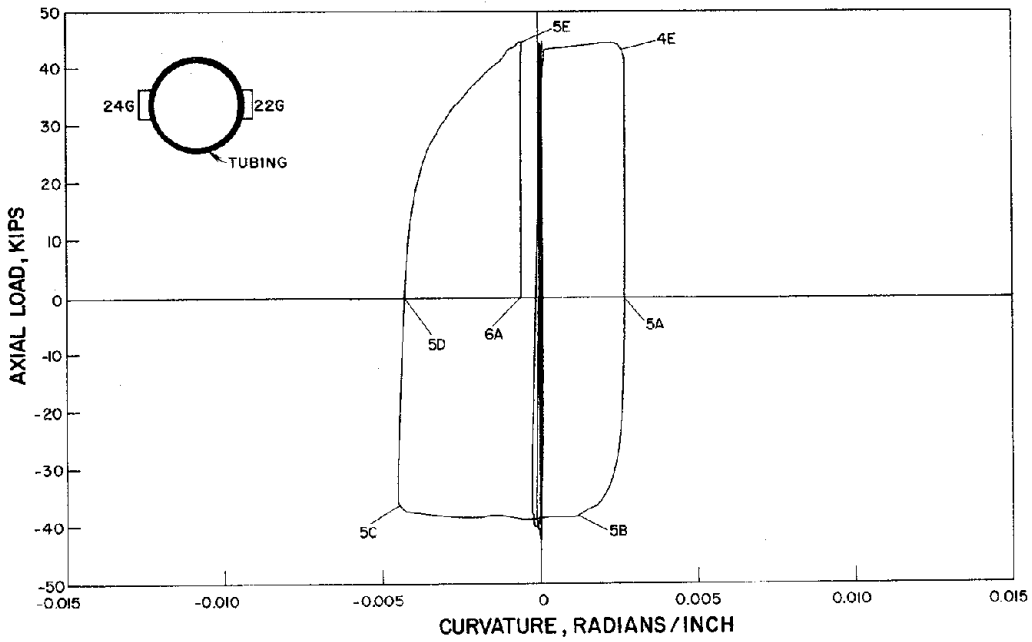
Fig. A.54   Strut 6 - Axial Load vs. Section Curvature
(Gages 22,24 - Cycles 1-5)

180
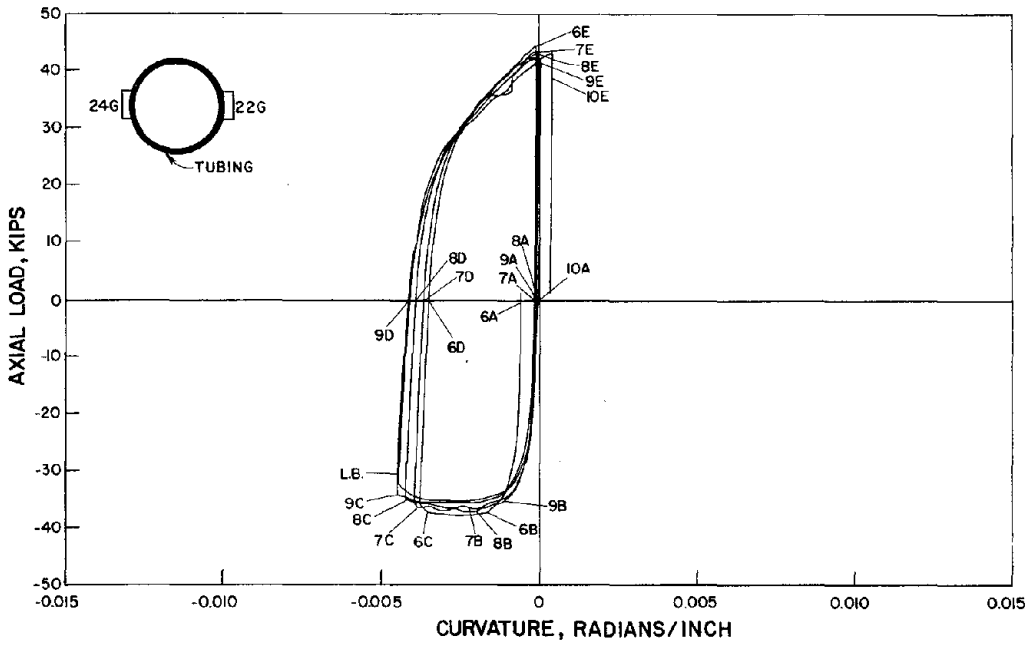
Fig. A.55   Strut 6 – Axial Load vs. Section Curvature
(Gages 22,24 – Cycles 6–10)
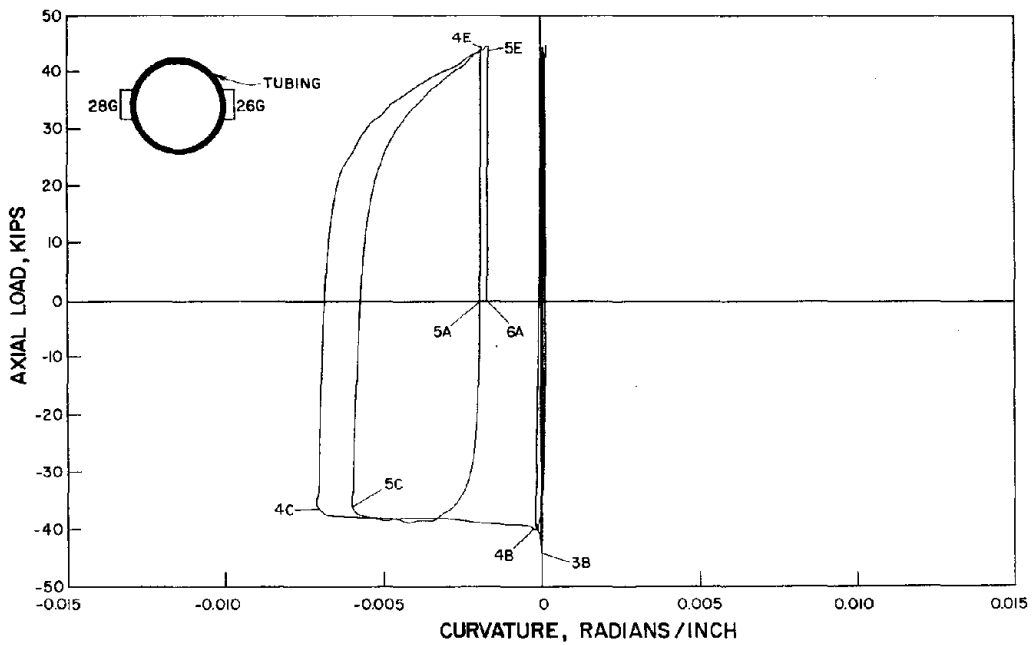
Fig. A.56   Strut 6 – Axial Load vs. Section Curvature
(Gages 26,28 – Cycles 1–5)

Fig. A.57   Strut 6 – Axial Load vs. Section Curvature
(Gages 26,28 – Cycles 6–10)
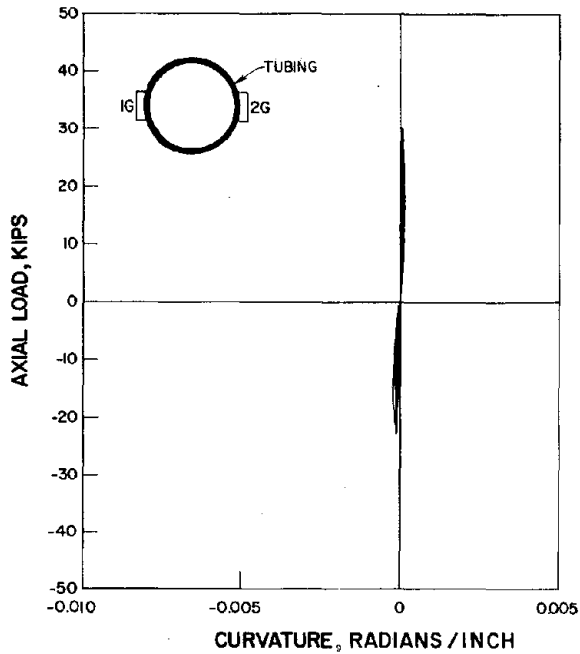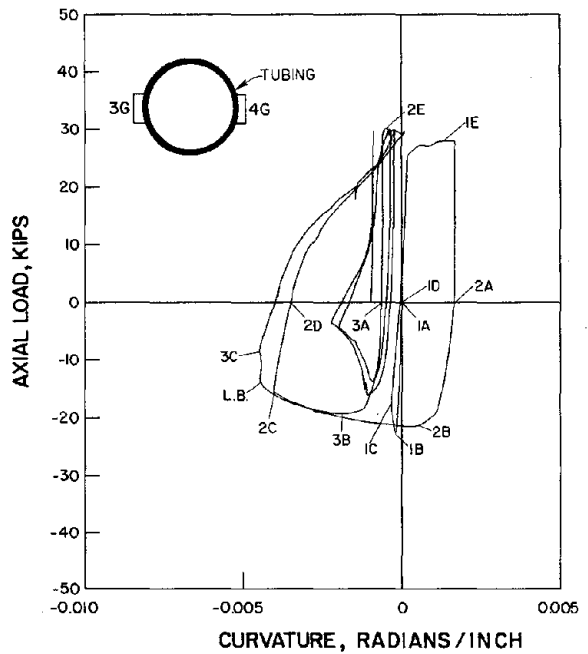

Fig. A.58   Strut 6 – Axial Load vs. Section Curvature
(Gages 30,30 – Cycles 1–5)

182
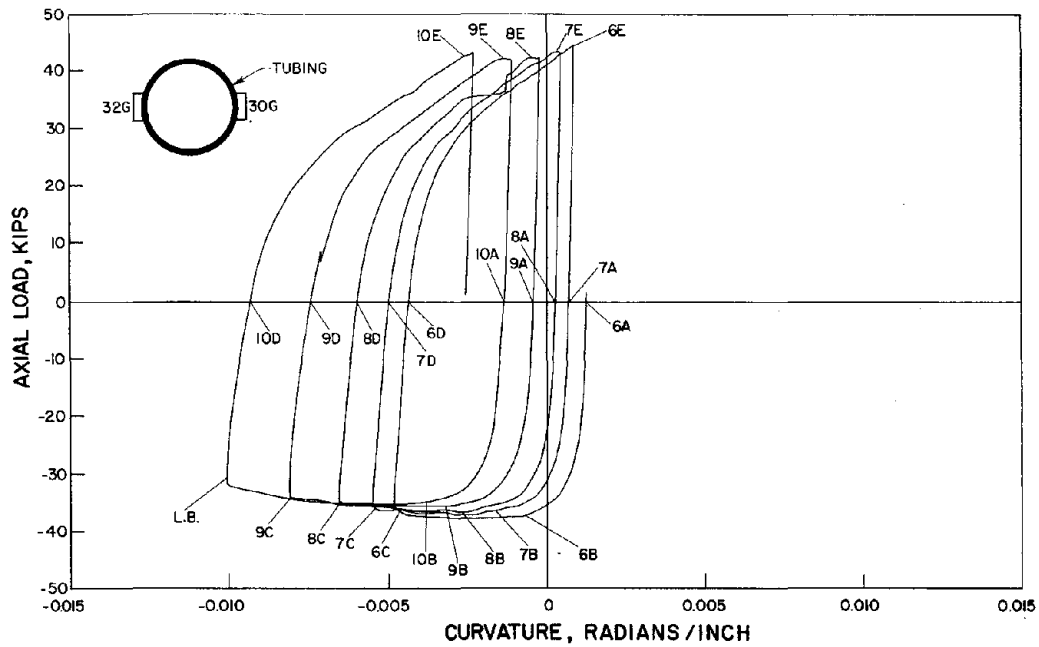
Fig. A.59   Strut 6 – Axial Load vs. Section Curvature
(Gages 30,32 – Cycles 6-10)

EARTHQUAKE ENGINEERING RESEARCH CENTER REPORTS

NOTE: Numbers in parenthesis are Accession Numbers assigned by the National Technical Information Service; these are followed by a price code. Copies of the reports may be ordered from the National Technical Information Service, 5285 Port Royal Road, Springfield, Virginia, 22161. Accession Numbers should be quoted on orders for reports (PB --- ---) and remittance must accompany each order. Reports without this information were not available at time of printing. Upon request, EERC will mail inquirers this information when it becomes available.

EERC 67-1   "Feasibility Study Large-Scale Earthquake Simulator Facility," by J. Penzien, J.G. Bouwkamp, R.W. Clough and D. Rea – 1967 (PB 187 905)A07

EERC 68-1   Unassigned

EERC 68-2   "Inelastic Behavior of Beam-to-Column Subassemblages Under Repeated Loading," by V.V. Bertero - 1968 (PB 184 888)A05

EERC 68-3   "A Graphical Method for Solving the Wave Reflection-Refraction Problem," by H.D. McNiven and Y. Mengi - 1968 (PB 187 943)A03

EERC 68-4   "Dynamic Properties of McKinley School Buildings," by D. Rea, J.G. Bouwkamp and R.W. Clough - 1968 (PB 187 902)A07

EERC 68-5   "Characteristics of Rock Motions During Earthquakes," by H.B. Seed, I.M. Idriss and F.W. Kiefer - 1968 (PB 188 338)A03

EERC 69-1   "Earthquake Engineering Research at Berkeley," - 1969 (PB 187 906)A11

EERC 69-2   "Nonlinear Seismic Response of Earth Structures," by M. Dibaj and J. Penzien - 1969 (PB 187 904)A08

EERC 69-3   "Probabilistic Study of the Behavior of Structures During Earthquakes," by R. Ruiz and J. Penzien - 1969 (PB 187 886)A06

EERC 69-4   "Numerical Solution of Boundary Value Problems in Structural Mechanics by Reduction to an Initial Value Formulation," by N. Distefano and J. Schujman - 1969 (PB 187 942)A02

EERC 69-5   "Dynamic Programming and the Solution of the Biharmonic Equation," by N. Distefano - 1969 (PB 187 941)A03

EERC 69-6   "Stochastic Analysis of Offshore Tower Structures," by A.K. Malhotra and J. Penzien - 1969 (PB 187 903)A09

EERC 69-7   "Rock Motion Accelerograms for High Magnitude Earthquakes," by H.B. Seed and I.M. Idriss - 1969 (PB 187 940)A02

EERC 69-8   "Structural Dynamics Testing Facilities at the University of California, Berkeley," by R.M. Stephen, J.G. Bouwkamp, R.W. Clough and J. Penzien - 1969 (PB 189 111)A04

EERC 69-9   "Seismic Response of Soil Deposits Underlain by Sloping Rock Boundaries," by H. Dezfulian and H.B. Seed 1969 (PB 189 114)A03

EERC 69-10   "Dynamic Stress Analysis of Axisymmetric Structures Under Arbitrary Loading," by S. Ghosh and E.L. Wilson 1969 (PB 189 026)A10

EERC 69-11   "Seismic Behavior of Multistory Frames Designed by Different Philosophies," by J.C. Anderson and V. V. Bertero – 1969 (PB 190 662)A10

EERC 69-12   "Stiffness Degradation of Reinforcing Concrete Members Subjected to Cyclic Flexural Moments," by V.V. Bertero, B. Bresler and H. Ming Liao - 1969 (PB 202 942)A07

EERC 69-13   "Response of Non-Uniform Soil Deposits to Travelling Seismic Waves," by H. Dezfulian and H.B. Seed - 1969 (PB 191 023)A03

EERC 69-14   "Damping Capacity of a Model Steel Structure," by D. Rea, R.W. Clough and J.G. Bouwkamp - 1969 (PB 190 663)A06

EERC 69-15   "Influence of Local Soil Conditions on Building Damage Potential during Earthquakes," by H.B. Seed and I.M. Idriss – 1969 (PB 191 036)A03

EERC 69-16   "The Behavior of Sands Under Seismic Loading Conditions," by M.L. Silver and H.B. Seed - 1969 (AD 714 982)A07

EERC 70-1   "Earthquake Response of Gravity Dams," by A.K. Chopra - 1970 (AD 709 640)A03

EERC 70-2   "Relationships between Soil Conditions and Building Damage in the Caracas Earthquake of July 29, 1967," by H.B. Seed, I.M. Idriss and H. Dezfulian - 1970 (PB 195 762)A05

EERC 70-3   "Cyclic Loading of Full Size Steel Connections," by E.P. Popov and R.M. Stephen - 1970 (PB 213 545)A04

EERC 70-4   "Seismic Analysis of the Charaima Building, Caraballeda, Venezuela," by Subcommittee of the SEAONC Research Committee: V.V. Bertero, P.F. Fratessa, S.A. Mahin, J.H. Sexton, A.C. Scordelis, E.L. Wilson, L.A. Wyllie, H.B. Seed and J. Penzien, Chairman - 1970 (PB 201 455)A06

Preceding page blank

186

EERC 70-5   "A Computer Program for Earthquake Analysis of Dams," by A.K. Chopra and P. Chakrabarti - 1970 (AD 723 994)A05

EERC 70-6   "The Propagation of Love Waves Across Non-Horizontally Layered Structures," by J. Lysmer and L.A. Drake
1970 (PB 197 896)A03

EERC 70-7   "Influence of Base Rock Characteristics on Ground Response," by J. Lysmer, H.B. Seed and P.B. Schnabel
1970 (PB 197 897)A03

EERC 70-8   "Applicability of Laboratory Test Procedures for Measuring Soil Liquefaction Characteristics under Cyclic
Loading," by H.B. Seed and W.H. Peacock - 1970 (PB 198 016)A03

EERC 70-9   "A Simplified Procedure for Evaluating Soil Liquefaction Potential," by H.B. Seed and I.M. Idriss - 1970
(PB 198 009)A03

EERC 70-10   "Soil Moduli and Damping Factors for Dynamic Response Analysis," by H.B. Seed and I.M. Idriss - 1970
(PB 197 869)A03

EERC 71-1   "Koyna Earthquake of December 11, 1967 and the Performance of Koyna Dam," by A.K. Chopra and P. Chakrabarti
1971 (AD 731 496)A06

EERC 71-2   "Preliminary In-Situ Measurements of Anelastic Absorption in Soils Using a Prototype Earthquake Simulator,"
by R.D. Borcherdt and P.W. Rodgers - 1971 (PB 201 454)A03

EERC 71-3   "Static and Dynamic Analysis of Inelastic Frame Structures," by F.L. Porter and G.H. Powell - 1971
(PB 210 135)A06

EERC 71-4   "Research Needs in Limit Design of Reinforced Concrete Structures," by V.V. Bertero - 1971 (PB 202 943)A04

EERC 71-5   "Dynamic Behavior of a High-Rise Diagonally Braced Steel Building," by D. Rea, A.A. Shah and J.G. Bouwkamp
1971 (PB 203 584)A06

EERC 71-6   "Dynamic Stress Analysis of Porous Elastic Solids Saturated with Compressible Fluids," by J. Ghaboussi and
E. L. Wilson - 1971 (PB 211 396)A06

EERC 71-7   "Inelastic Behavior of Steel Beam-to-Column Subassemblages," by H. Krawinkler, V.V. Bertero and E.P. Popov
1971 (PB 211 335)A14

EERC 71-8   "Modification of Seismograph Records for Effects of Local Soil Conditions," by P. Schnabel, H.B. Seed and
J. Lysmer - 1971 (PB 214 450)A03

EERC 72-1   "Static and Earthquake Analysis of Three Dimensional Frame and Shear Wall Buildings," by E.L. Wilson and
H.H. Dovey - 1972 (PB 212 904)A05

EERC 72-2   "Accelerations in Rock for Earthquakes in the Western United States," by P.B. Schnabel and H.B. Seed - 1972
(PB 213 100)A03

EERC 72-3   "Elastic-Plastic Earthquake Response of Soil-Building Systems," by T. Minami - 1972 (PB 214 868)A08

EERC 72-4   "Stochastic Inelastic Response of Offshore Towers to Strong Motion Earthquakes," by M.K. Kaul - 1972
(PB 215 713)A05

EERC 72-5   "Cyclic Behavior of Three Reinforced Concrete Flexural Members with High Shear," by E.P. Popov, V.V. Bertero
and H. Krawinkler - 1972 (PB 214 555)A05

EERC 72-6   "Earthquake Response of Gravity Dams Including Reservoir Interaction Effects," by P. Chakrabarti and
A.K. Chopra - 1972 (AD 762 330)A08

EERC 72-7   "Dynamic Properties of Pine Flat Dam," by D. Rea, C.Y. Liaw and A.K. Chopra - 1972 (AD 763 928)A05

EERC 72-8   "Three Dimensional Analysis of Building Systems," by E.L. Wilson and H.H. Dovey - 1972 (PB 222 438)A06

EERC 72-9   "Rate of Loading Effects on Uncracked and Repaired Reinforced Concrete Members," by S. Mahin, V.V. Bertero,
D. Rea and M. Atalay - 1972 (PB 224 520)A08

EERC 72-10   "Computer Program for Static and Dynamic Analysis of Linear Structural Systems," by E.L. Wilson, K.-J. Bathe,
J.E. Peterson and H.H.Dovey - 1972 (PB 220 437)A04

EERC 72-11   "Literature Survey - Seismic Effects on Highway Bridges," by T. Iwasaki, J. Penzien and R.W. Clough - 1972
(PB 215 613)A19

EERC 72-12   "SHAKE-A Computer Program for Earthquake Response Analysis of Horizontally Layered Sites," by P.B. Schnabel
and J. Lysmer - 1972 (PB 220 207)A06

EERC 73-1   "Optimal Seismic Design of Multistory Frames," by V.V. Bertero and H. Kamil - 1973

EERC 73-2   "Analysis of the Slides in the San Fernando Dams During the Earthquake of February 9, 1971," by H.B. Seed,
K.L. Lee, I.M. Idriss and F. Makdisi - 1973 (PB 223 402)A14

EERC 73-3   "Computer Aided Ultimate Load Design of Unbraced Multistory Steel Frames," by M.B. El-Hafez and G.H. Powell 1973 (PB 248 315)A09

EERC 73-4   "Experimental Investigation into the Seismic Behavior of Critical Regions of Reinforced Concrete Components as Influenced by Moment and Shear," by M. Celebi and J. Penzien - 1973 (PB 215 884)A09

EERC 73-5   "Hysteretic Behavior of Epoxy-Repaired Reinforced Concrete Beams," by M. Celebi and J. Penzien - 1973 (PB 239 568)A03

EERC 73-6   "General Purpose Computer Program for Inelastic Dynamic Response of Plane Structures," by A. Kanaan and G.H. Powell - 1973 (PB 221 260)A08

EERC 73-7   "A Computer Program for Earthquake Analysis of Gravity Dams Including Reservoir Interaction," by P. Chakrabarti and A.K. Chopra - 1973 (AD 766 271)A04

EERC 73-8   "Behavior of Reinforced Concrete Deep Beam-Column Subassemblages Under Cyclic Loads," by O. Küstü and J.G. Bouwkamp - 1973 (PB 246 117)A12

EERC 73-9   "Earthquake Analysis of Structure-Foundation Systems," by A.K. Vaish and A.K. Chopra - 1973 (AD 766 272)A07

EERC 73-10   "Deconvolution of Seismic Response for Linear Systems," by R.B. Reimer - 1973 (PB 227 179)A08

EERC 73-11   "SAP IV: A Structural Analysis Program for Static and Dynamic Response of Linear Systems," by K.-J. Bathe, E.L. Wilson and F.E. Peterson - 1973 (PB 221 967)A09

EERC 73-12   "Analytical Investigations of the Seismic Response of Long, Multiple Span Highway Bridges," by W.S. Tseng and J. Penzien - 1973 (PB 227 816)A10

EERC 73-13   "Earthquake Analysis of Multi-Story Buildings Including Foundation Interaction," by A.K. Chopra and J.A. Gutierrez - 1973 (PB 222 970)A03

EERC 73-14   "ADAP: A Computer Program for Static and Dynamic Analysis of Arch Dams," by R.W. Clough, J.M. Raphael and S. Mojtahedi - 1973 (PB 223 763)A09

EERC 73-15   "Cyclic Plastic Analysis of Structural Steel Joints," by R.B. Pinkney and R.W. Clough - 1973 (PB 226 843)A08

EERC 73-16   "QUAD-4: A Computer Program for Evaluating the Seismic Response of Soil Structures by Variable Damping Finite Element Procedures," by I.M. Idriss, J. Lysmer, R. Hwang and H.B. Seed - 1973 (PB 229 424)A05

EERC 73-17   "Dynamic Behavior of a Multi-Story Pyramid Shaped Building," by R.M. Stephen, J.P. Hollings and J.G. Bouwkamp - 1973 (PB 240 718)A06

EERC 73-18   "Effect of Different Types of Reinforcing on Seismic Behavior of Short Concrete Columns," by V.V. Bertero, J. Hollings, O. Küstü, R.M. Stephen and J.G. Bouwkamp - 1973

EERC 73-19   "Olive View Medical Center Materials Studies, Phase I," by B. Bresler and V.V. Bertero - 1973 (PB 235 986)A06

EERC 73-20   "Linear and Nonlinear Seismic Analysis Computer Programs for Long Multiple-Span Highway Bridges," by W.S. Tseng and J. Penzien - 1973

EERC 73-21   "Constitutive Models for Cyclic Plastic Deformation of Engineering Materials," by J.M. Kelly and P.P. Gillis 1973 (PB 226 024)A03

EERC 73-22   "DRAIN - 2D User's Guide," by G.H. Powell - 1973 (PB 227 016)A05

EERC 73-23   "Earthquake Engineering at Berkeley - 1973," (PB 226 033)A11

EERC 73-24   Unassigned

EERC 73-25   "Earthquake Response of Axisymmetric Tower Structures Surrounded by Water," by C.Y. Liaw and A.K. Chopra 1973 (AD 773 052)A09

EERC 73-26   "Investigation of the Failures of the Olive View Stairtowers During the San Fernando Earthquake and Their Implications on Seismic Design," by V.V. Bertero and R.G. Collins - 1973 (PB 235 106)A13

EERC 73-27   "Further Studies on Seismic Behavior of Steel Beam-Column Subassemblages," by V.V. Bertero, H. Krawinkler and E.P. Popov - 1973 (PB 234 172)A06

EERC 74-1   "Seismic Risk Analysis," by C.S. Oliveira - 1974 (PB 235 920)A06

EERC 74-2   "Settlement and Liquefaction of Sands Under Multi-Directional Shaking," by R. Pyke, C.K. Chan and H.B. Seed 1974

EERC 74-3   "Optimum Design of Earthquake Resistant Shear Buildings," by D. Ray, K.S. Pister and A.K. Chopra - 1974 (PB 231 172)A06

EERC 74-4   "LUSH - A Computer Program for Complex Response Analysis of Soil-Structure Systems," by J. Lysmer, T. Udaka, H.B. Seed and R. Hwang - 1974 (PB 236 796)A05

EERC 74-5   "Sensitivity Analysis for Hysteretic Dynamic Systems: Applications to Earthquake Engineering," by D. Ray
1974 (PB 233 213)A06

EERC 74-6   "Soil Structure Interaction Analyses for Evaluating Seismic Response," by H.B. Seed, J. Lysmer and R. Hwang
1974 (PB 236 519)A04

EERC 74-7   Unassigned

EERC 74-8   "Shaking Table Tests of a Steel Frame - A Progress Report," by R.W. Clough and D. Tang - 1974 (PB 240 869)A03

EERC 74-9   "Hysteretic Behavior of Reinforced Concrete Flexural Members with Special Web Reinforcement," by
V.V. Bertero, E.P. Popov and T.Y. Wang - 1974 (PB 236 797)A07

EERC 74-10   "Applications of Reliability-Based, Global Cost Optimization to Design of Earthquake Resistant Structures,"
by E. Vitiello and K.S. Pister - 1974 (PB 237 231)A06

EERC 74-11   "Liquefaction of Gravelly Soils Under Cyclic Loading Conditions," by R.T. Wong, H.B. Seed and C.K. Chan
1974 (PB 242 042)A03

EERC 74-12   "Site-Dependent Spectra for Earthquake-Resistant Design," by H.B. Seed, C. Ugas and J. Lysmer - 1974
(PB 240 953)A03

EERC 74-13   "Earthquake Simulator Study of a Reinforced Concrete Frame," by P. Hidalgo and R.W. Clough - 1974
(PB 241 944)A13

EERC 74-14   "Nonlinear Earthquake Response of Concrete Gravity Dams," by N. Pal - 1974 (AD/A 006 583)A06

EERC 74-15   "Modeling and Identification in Nonlinear Structural Dynamics - I. One Degree of Freedom Models," by
N. Distefano and A. Rath - 1974 (PB 241 548)A06

EERC 75-1   "Determination of Seismic Design Criteria for the Dumbarton Bridge Replacement Structure, Vol. I: Description,
Theory and Analytical Modeling of Bridge and Parameters," by F. Baron and S.-H. Pang - 1975 (PB 259 407)A15

EERC 75-2   "Determination of Seismic Design Criteria for the Dumbarton Bridge Replacement Structure, Vol. II: Numerical
Studies and Establishment of Seismic Design Criteria," by F. Baron and S.-H. Pang - 1975 (PB 259 408)A11
(For set of EERC 75-1 and 75-2 (PB 259 406))

EERC 75-3   "Seismic Risk Analysis for a Site and a Metropolitan Area," by C.S. Oliveira - 1975 (PB 248 134)A09

EERC 75-4   "Analytical Investigations of Seismic Response of Short, Single or Multiple-Span Highway Bridges," by
M.-C. Chen and J. Penzien - 1975 (PB 241 454)A09

EERC 75-5   "An Evaluation of Some Methods for Predicting Seismic Behavior of Reinforced Concrete Buildings," by S.A.
Mahin and V.V. Bertero - 1975 (PB 246 306)A16

EERC 75-6   "Earthquake Simulator Study of a Steel Frame Structure, Vol. I: Experimental Results," by R.W. Clough and
D.T. Tang - 1975 (PB 243 981)A13

EERC 75-7   "Dynamic Properties of San Bernardino Intake Tower," by D. Rea, C.-Y. Liaw and A.K. Chopra - 1975 (AD/A008 406)
A05

EERC 75-8   "Seismic Studies of the Articulation for the Dumbarton Bridge Replacement Structure, Vol. I: Description,
Theory and Analytical Modeling of Bridge Components," by F. Baron and R.E. Hamati - 1975 (PB 251 539)A07

EERC 75-9   "Seismic Studies of the Articulation for the Dumbarton Bridge Replacement Structure, Vol. 2: Numerical
Studies of Steel and Concrete Girder Alternates," by F. Baron and R.E. Hamati - 1975 (PB 251 540)A10

EERC 75-10   "Static and Dynamic Analysis of Nonlinear Structures," by D.P. Mondkar and G.H. Powell - 1975 (PB 242 434)A08

EERC 75-11   "Hysteretic Behavior of Steel Columns," by E.P. Popov, V.V. Bertero and S. Chandramouli - 1975 (PB 252 365)A11

EERC 75-12   "Earthquake Engineering Research Center Library Printed Catalog," - 1975 (PB 243 711)A26

EERC 75-13   "Three Dimensional Analysis of Building Systems (Extended Version)," by E.L. Wilson, J.P. Hollings and
H.H. Dovey - 1975 (PB 243 989)A07

EERC 75-14   "Determination of Soil Liquefaction Characteristics by Large-Scale Laboratory Tests," by P. De Alba,
C.K. Chan and H.B. Seed - 1975 (NUREG 0027)A08

EERC 75-15   "A Literature Survey - Compressive, Tensile, Bond and Shear Strength of Masonry," by R.L. Mayes and R.W.
Clough - 1975 (PB 246 292)A10

EERC 75-16   "Hysteretic Behavior of Ductile Moment Resisting Reinforced Concrete Frame Components," by V.V. Bertero and
E.P. Popov - 1975 (PB 246 388)A05

EERC 75-17   "Relationships Between Maximum Acceleration, Maximum Velocity, Distance from Source, Local Site Conditions
for Moderately Strong Earthquakes," by H.B. Seed, R. Murarka, J. Lysmer and I.M. Idriss - 1975 (PB 248 172)A03

EERC 75-18   "The Effects of Method of Sample Preparation on the Cyclic Stress-Strain Behavior of Sands," by J. Mulilis,
C.K. Chan and H.B. Seed - 1975 (Summarized in EERC 75-28)

EERC 75-19 "The Seismic Behavior of Critical Regions of Reinforced Concrete Components as Influenced by Moment, Shear and Axial Force," by M.B. Atalay and J. Penzien - 1975 (PB 258 842)A11

EERC 75-20 "Dynamic Properties of an Eleven Story Masonry Building," by R.M. Stephen, J.P. Hollings, J.G. Bouwkamp and D. Jurukovski - 1975 (PB 246 945)A04

EERC 75-21 "State-of-the-Art in Seismic Strength of Masonry - An Evaluation and Review," by R.L. Mayes and R.W. Clough 1975 (PB 249 040)A07

EERC 75-22 "Frequency Dependent Stiffness Matrices for Viscoelastic Half-Plane Foundations," by A.K. Chopra, P. Chakrabarti and G. Dasgupta - 1975 (PB 248 121)A07

EERC 75-23 "Hysteretic Behavior of Reinforced Concrete Framed Walls," by T.Y. Wong, V.V. Bertero and E.P. Popov - 1975

EERC 75-24 "Testing Facility for Subassemblages of Frame-Wall Structural Systems," by V.V. Bertero, E.P. Popov and T. Endo - 1975

EERC 75-25 "Influence of Seismic History on the Liquefaction Characteristics of Sands," by H.B. Seed, K. Mori and C.K. Chan - 1975 (Summarized in EERC 75-28)

EERC 75-26 "The Generation and Dissipation of Pore Water Pressures during Soil Liquefaction," by H.B. Seed, P.P. Martin and J. Lysmer - 1975 (PB 252 648)A03

EERC 75-27 "Identification of Research Needs for Improving Aseismic Design of Building Structures," by V.V. Bertero 1975 (PB 248 136)A05

EERC 75-28 "Evaluation of Soil Liquefaction Potential during Earthquakes," by H.B. Seed, I. Arango and C.K. Chan - 1975 (NUREG 0026)A13

EERC 75-29 "Representation of Irregular Stress Time Histories by Equivalent Uniform Stress Series in Liquefaction Analyses," by H.B. Seed, I.M. Idriss, F. Makdisi and N. Banerjee - 1975 (PB 252 635)A03

EERC 75-30 "FLUSH - A Computer Program for Approximate 3-D Analysis of Soil-Structure Interaction Problems," by J. Lysmer, T. Udaka, C.-F. Tsai and H.B. Seed - 1975 (PB 259 332)A07

EERC 75-31 "ALUSH - A Computer Program for Seismic Response Analysis of Axisymmetric Soil-Structure Systems," by E. Berger, J. Lysmer and H.B. Seed - 1975

EERC 75-32 "TRIP and TRAVEL - Computer Programs for Soil-Structure Interaction Analysis with Horizontally Travelling Waves," by T. Udaka, J. Lysmer and H.B. Seed - 1975

EERC 75-33 "Predicting the Performance of Structures in Regions of High Seismicity," by J. Penzien - 1975 (PB 248 130)A03

EERC 75-34 "Efficient Finite Element Analysis of Seismic Structure - Soil - Direction," by J. Lysmer, H.B. Seed, T. Udaka, R.N. Hwang and C.-F. Tsai - 1975 (PB 253 570)A03

EERC 75-35 "The Dynamic Behavior of a First Story Girder of a Three-Story Steel Frame Subjected to Earthquake Loading," by R.W. Clough and L.-Y. Li - 1975 (PB 248 841)A05

EERC 75-36 "Earthquake Simulator Study of a Steel Frame Structure, Volume II - Analytical Results," by D.T. Tang - 1975 (PB 252 926)A10

EERC 75-37 "ANSR-I General Purpose Computer Program for Analysis of Non-Linear Structural Response," by D.P. Mondkar and G.H. Powell - 1975 (PB 252 386)A08

EERC 75-38 "Nonlinear Response Spectra for Probabilistic Seismic Design and Damage Assessment of Reinforced Concrete Structures," by M. Murakami and J. Penzien - 1975 (PB 259 530)A05

EERC 75-39 "Study of a Method of Feasible Directions for Optimal Elastic Design of Frame Structures Subjected to Earthquake Loading," by N.D. Walker and K.S. Pister - 1975 (PB 257 781)A06

EERC 75-40 "An Alternative Representation of the Elastic-Viscoelastic Analogy," by G. Dasgupta and J.L. Sackman - 1975 (PB 252 173)A03

EERC 75-41 "Effect of Multi-Directional Shaking on Liquefaction of Sands," by H.B. Seed, R. Pyke and G.R. Martin - 1975 (PB 258 781)A03

EERC 76-1 "Strength and Ductility Evaluation of Existing Low-Rise Reinforced Concrete Buildings - Screening Method," by T. Okada and B. Bresler - 1976 (PB 257 906)A11

EERC 76-2 "Experimental and Analytical Studies on the Hysteretic Behavior of Reinforced Concrete Rectangular and T-Beams," by S.-Y.M. Ma, E.P. Popov and V.V. Bertero - 1976 (PB 260 843)A12

EERC 76-3 "Dynamic Behavior of a Multistory Triangular-Shaped Building," by J. Petrovski, R.M. Stephen, E. Gartenbaum and J.G. Bouwkamp - 1976 (PB 273 279)A07

EERC 76-4 "Earthquake Induced Deformations of Earth Dams," by N. Serff, H.B. Seed, F.I. Makdisi & C.-Y. Chang - 1976 (PB 292 065)A08

EERC 76-5   "Analysis and Design of Tube-Type Tall Building Structures," by H. de Clercq and G.H. Powell - 1976 (PB 252 220) A10

EERC 76-6   "Time and Frequency Domain Analysis of Three-Dimensional Ground Motions, San Fernando Earthquake," by T. Kubo and J. Penzien (PB 260 556)A11

EERC 76-7   "Expected Performance of Uniform Building Code Design Masonry Structures," by R.L. Mayes, Y. Omote, S.W. Chen and R.W. Clough - 1976 (PB 270 098)A05

EERC 76-8   "Cyclic Shear Tests of Masonry Piers, Volume 1 - Test Results," by R.L. Mayes, Y. Omote, R.W. Clough - 1976 (PB 264 424)A06

EERC 76-9   "A Substructure Method for Earthquake Analysis of Structure - Soil Interaction," by J.A. Gutierrez and A.K. Chopra - 1976 (PB 257 783)A08

EERC 76-10   "Stabilization of Potentially Liquefiable Sand Deposits using Gravel Drain Systems," by H.B. Seed and J.R. Booker - 1976 (PB 258 820)A04

EERC 76-11   "Influence of Design and Analysis Assumptions on Computed Inelastic Response of Moderately Tall Frames," by G.H. Powell and D.G. Row - 1976 (PB 271 409)A06

EERC 76-12   "Sensitivity Analysis for Hysteretic Dynamic Systems: Theory and Applications," by D. Ray, K.S. Pister and E. Polak - 1976 (PB 262 859)A04

EERC 76-13   "Coupled Lateral Torsional Response of Buildings to Ground Shaking," by C.L. Kan and A.K. Chopra - 1976 (PB 257 907)A09

EERC 76-14   "Seismic Analyses of the Banco de America," by V.V. Bertero, S.A. Mahin and J.A. Hollings - 1976

EERC 76-15   "Reinforced Concrete Frame 2: Seismic Testing and Analytical Correlation," by R.W. Clough and J. Gidwani - 1976 (PB 261 323)A08

EERC 76-16   "Cyclic Shear Tests of Masonry Piers, Volume 2 - Analysis of Test Results," by R.L. Mayes, Y. Omote and R.W. Clough - 1976

EERC 76-17   "Structural Steel Bracing Systems: Behavior Under Cyclic Loading," by E.P. Popov, K. Takanashi and C.W. Roeder - 1976 (PB 260 715)A05

EERC 76-18   "Experimental Model Studies on Seismic Response of High Curved Overcrossings," by D. Williams and W.G. Godden - 1976 (PB 269 548)A08

EERC 76-19   "Effects of Non-Uniform Seismic Disturbances on the Dumbarton Bridge Replacement Structure," by F. Baron and R.E. Hamati - 1976 (PB 282 981)A16

EERC 76-20   "Investigation of the Inelastic Characteristics of a Single Story Steel Structure Using System Identification and Shaking Table Experiments," by V.C. Matzen and H.D. McNiven - 1976 (PB 258 453)A07

EERC 76-21   "Capacity of Columns with Splice Imperfections," by E.P. Popov, R.M. Stephen and R. Philbrick - 1976 (PB 260 378)A04

EERC 76-22   "Response of the Olive View Hospital Main Building during the San Fernando Earthquake," by S. A. Mahin, V.V. Bertero, A.K. Chopra and R. Collins - 1976 (PB 271 425)A14

EERC 76-23   "A Study on the Major Factors Influencing the Strength of Masonry Prisms," by N.M. Mostaghel, R.L. Mayes, R. W. Clough and S.W. Chen - 1976 (Not published)

EERC 76-24   "GADFLEA - A Computer Program for the Analysis of Pore Pressure Generation and Dissipation during Cyclic or Earthquake Loading," by J.R. Booker, M.S. Rahman and H.B. Seed - 1976 (PB 263 947)A04

EERC 76-25   "Seismic Safety Evaluation of a R/C School Building," by B. Bresler and J. Axley - 1976

EERC 76-26   "Correlative Investigations on Theoretical and Experimental Dynamic Behavior of a Model Bridge Structure," by K. Kawashima and J. Penzien - 1976 (PB 263 388)A11

EERC 76-27   "Earthquake Response of Coupled Shear Wall Buildings," by T. Srichatrapimuk - 1976 (PB 265 157)A07

EERC 76-28   "Tensile Capacity of Partial Penetration Welds," by E.P. Popov and R.M. Stephen - 1976 (PB 262 899)A03

EERC 76-29   "Analysis and Design of Numerical Integration Methods in Structural Dynamics," by H.M. Hilber - 1976 (PB 264 410)A06

EERC 76-30   "Contribution of a Floor System to the Dynamic Characteristics of Reinforced Concrete Buildings," by L.E. Malik and V.V. Bertero - 1976 (PB 272 247)A13

EERC 76-31   "The Effects of Seismic Disturbances on the Golden Gate Bridge," by F. Baron, M. Arikan and R.E. Hamati - 1976 (PB 272 279)A09

EERC 76-32   "Infilled Frames in Earthquake Resistant Construction," by R.E. Klingner and V.V. Bertero - 1976 (PB 265 892)A13

UCB/EERC-77/01   "PLUSH - A Computer Program for Probabilistic Finite Element Analysis of Seismic Soil-Structure Interaction," by M.P. Romo Organista, J. Lysmer and H.B. Seed - 1977

UCB/EERC-77/02   "Soil-Structure Interaction Effects at the Humboldt Bay Power Plant in the Ferndale Earthquake of June 7, 1975," by J.E. Valera, H.B. Seed, C.F. Tsai and J. Lysmer - 1977 (PB 265 795)A04

UCB/EERC-77/03   "Influence of Sample Disturbance on Sand Response to Cyclic Loading," by K. Mori, H.B. Seed and C.K. Chan - 1977 (PB 267 352)A04

UCB/EERC-77/04   "Seismological Studies of Strong Motion Records," by J. Shoja-Taheri - 1977 (PB 269 655)A10

UCB/EERC-77/05   "Testing Facility for Coupled-Shear Walls," by L. Li-Hyung, V.V. Bertero and E.P. Popov - 1977

UCB/EERC-77/06   "Developing Methodologies for Evaluating the Earthquake Safety of Existing Buildings," by No. 1 - B. Bresler; No. 2 - B. Bresler, T. Okada and D. Zisling; No. 3 - T. Okada and B. Bresler; No. 4 - V.V. Bertero and B. Bresler - 1977 (PB 267 354)A08

UCB/EERC-77/07   "A Literature Survey - Transverse Strength of Masonry Walls," by Y. Omote, R.L. Mayes, S.W. Chen and R.W. Clough - 1977 (PB 277 933)A07

UCB/EERC-77/08   "DRAIN-TABS: A Computer Program for Inelastic Earthquake Response of Three Dimensional Buildings," by R. Guendelman-Israel and G.H. Powell - 1977 (PB 270 693)A07

UCB/EERC-77/09   "SUBWALL: A Special Purpose Finite Element Computer Program for Practical Elastic Analysis and Design of Structural Walls with Substructure Option," by D.Q. Le, H. Peterson and E.P. Popov - 1977 (PB 270 567)A05

UCB/EERC-77/10   "Experimental Evaluation of Seismic Design Methods for Broad Cylindrical Tanks," by D.P. Clough (PB 272 280)A13

UCB/EERC-77/11   "Earthquake Engineering Research at Berkeley - 1976," - 1977 (PB 273 507)A09

UCB/EERC-77/12   "Automated Design of Earthquake Resistant Multistory Steel Building Frames," by N.D. Walker, Jr. - 1977 (PB 276 526)A09

UCB/EERC-77/13   "Concrete Confined by Rectangular Hoops Subjected to Axial Loads," by J. Vallenas, V.V. Bertero and E.P. Popov - 1977 (PB 275 165)A06

UCB/EERC-77/14   "Seismic Strain Induced in the Ground During Earthquakes," by Y. Sugimura - 1977 (PB 284 201)A04

UCB/EERC-77/15   "Bond Deterioration under Generalized Loading," by V.V. Bertero, E.P. Popov and S. Viwathanatepa - 1977

UCB/EERC-77/16   "Computer Aided Optimum Design of Ductile Reinforced Concrete Moment Resisting Frames," by S.W. Zagajeski and V.V. Bertero - 1977 (PB 280 137)A07

UCB/EERC-77/17   "Earthquake Simulation Testing of a Stepping Frame with Energy-Absorbing Devices," by J.M. Kelly and D.F. Tsztoo - 1977 (PB 273 506)A04

UCB/EERC-77/18   "Inelastic Behavior of Eccentrically Braced Steel Frames under Cyclic Loadings," by C.W. Roeder and E.P. Popov - 1977 (PB 275 526)A15

UCB/EERC-77/19   "A Simplified Procedure for Estimating Earthquake-Induced Deformations in Dams and Embankments," by F.I. Makdisi and H.B. Seed - 1977 (PB 276 820)A04

UCB/EERC-77/20   "The Performance of Earth Dams during Earthquakes," by H.B. Seed, F.I. Makdisi and P. de Alba - 1977 (PB 276 821)A04

UCB/EERC-77/21   "Dynamic Plastic Analysis Using Stress Resultant Finite Element Formulation," by P. Lukkunapvasit and J.M. Kelly - 1977 (PB 275 453)A04

UCB/EERC-77/22   "Preliminary Experimental Study of Seismic Uplift of a Steel Frame," by R.W. Clough and A.A. Huckelbridge 1977 (PB 278 769)A08

UCB/EERC-77/23   "Earthquake Simulator Tests of a Nine-Story Steel Frame with Columns Allowed to Uplift," by A.A. Huckelbridge - 1977 (PB 277 944)A09

UCB/EERC-77/24   "Nonlinear Soil-Structure Interaction of Skew Highway Bridges," by M.-C. Chen and J. Penzien - 1977 (PB 276 176)A07

UCB/EERC-77/25   "Seismic Analysis of an Offshore Structure Supported on Pile Foundations," by D.D.-N. Liou and J. Penzien 1977 (PB 283 180)A06

UCB/EERC-77/26   "Dynamic Stiffness Matrices for Homogeneous Viscoelastic Half-Planes," by G. Dasgupta and A.K. Chopra - 1977 (PB 279 654)A06

UCB/EERC-77/27   "A Practical Soft Story Earthquake Isolation System," by J.M. Kelly, J.M. Eidinger and C.J. Derham - 1977 (PB 276 814)A07

UCB/EERC-77/28   "Seismic Safety of Existing Buildings and Incentives for Hazard Mitigation in San Francisco: An Exploratory Study," by A.J. Meltsner - 1977 (PB 281 970)A05

UCB/EERC-77/29   "Dynamic Analysis of Electrohydraulic Shaking Tables," by D. Rea, S. Abedi-Hayati and Y. Takahashi 1977 (PB 282 569)A04

UCB/EERC-77/30   "An Approach for Improving Seismic - Resistant Behavior of Reinforced Concrete Interior Joints," by B. Galunic, V.V. Bertero and E.P. Popov - 1977 (PB 290 870)A06

UCB/EERC-78/01   "The Development of Energy-Absorbing Devices for Aseismic Base Isolation Systems," by J.M. Kelly and D.F. Tsztoo - 1978 (PB 284 978)A04

UCB/EERC-78/02   "Effect of Tensile Prestrain on the Cyclic Response of Structural Steel Connections, by J.G. Bouwkamp and A. Mukhopadhyay - 1978

UCB/EERC-78/03   "Experimental Results of an Earthquake Isolation System using Natural Rubber Bearings," by J.M. Eidinger and J.M. Kelly - 1978 (PB 281 686)A04

UCB/EERC-78/04   "Seismic Behavior of Tall Liquid Storage Tanks," by A. Niwa - 1978 (PB 284 017)A14

UCB/EERC-78/05   "Hysteretic Behavior of Reinforced Concrete Columns Subjected to High Axial and Cyclic Shear Forces," by S.W. Zagajeski, V.V. Bertero and J.G. Bouwkamp - 1978 (PB 283 858)A13

UCB/EERC-78/06   "Inelastic Beam-Column Elements for the ANSR-I Program," by A. Riahi, D.G. Row and G.H. Powell - 1978

UCB/EERC-78/07   "Studies of Structural Response to Earthquake Ground Motion," by O.A. Lopez and A.K. Chopra - 1978 (PB 282 790)A05

UCB/EERC-78/08   "A Laboratory Study of the Fluid-Structure Interaction of Submerged Tanks and Caissons in Earthquakes," by R.C. Byrd - 1978 (PB 284 957)A08

UCB/EERC-78/09   "Model for Evaluating Damageability of Structures," by I. Sakamoto and B. Bresler - 1978

UCB/EERC-78/10   "Seismic Performance of Nonstructural and Secondary Structural Elements," by I. Sakamoto - 1978

UCB/EERC-78/11   "Mathematical Modelling of Hysteresis Loops for Reinforced Concrete Columns," by S. Nakata, T. Sproul and J. Penzien - 1978

UCB/EERC-78/12   "Damageability in Existing Buildings," by T. Blejwas and B. Bresler - 1978

UCB/EERC-78/13   "Dynamic Behavior of a Pedestal Base Multistory Building," by R.M. Stephen, E.L. Wilson, J.G. Bouwkamp and M. Button - 1978 (PB 286 650)A08

UCB/EERC-78/14   "Seismic Response of Bridges - Case Studies," by R.A. Imbsen, V. Nutt and J. Penzien - 1978 (PB 286 503)A10

UCB/EERC-78/15   "A Substructure Technique for Nonlinear Static and Dynamic Analysis," by D.G. Row and G.H. Powell - 1978 (PB 288 077)A10

UCB/EERC-78/16   "Seismic Risk Studies for San Francisco and for the Greater San Francisco Bay Area," by C.S. Oliveira - 1978

UCB/EERC-78/17   "Strength of Timber Roof Connections Subjected to Cyclic Loads," by P. Gülkan, R.L. Mayes and R.W. Clough - 1978

UCB/EERC-78/18   "Response of K-Braced Steel Frame Models to Lateral Loads," by J.G. Bouwkamp, R.M. Stephen and E.P. Popov - 1978

UCB/EERC-78/19   "Rational Design Methods for Light Equipment in Structures Subjected to Ground Motion," by J.L. Sackman and J.M. Kelly - 1978 (PB 292 357)A04

UCB/EERC-78/20   "Testing of a Wind Restraint for Aseismic Base Isolation," by J.M. Kelly and D.E. Chitty - 1978 (PB 292 833)A03

UCB/EERC-78/21   "APOLLO - A Computer Program for the Analysis of Pore Pressure Generation and Dissipation in Horizontal Sand Layers During Cyclic or Earthquake Loading," by P.P. Martin and H.B. Seed - 1978 (PB 292 835)A04

UCB/EERC-78/22   "Optimal Design of an Earthquake Isolation System," by M.A. Bhatti, K.S. Pister and E. Polak - 1978 (PB 294 735)A06

UCB/EERC-78/23   "MASH - A Computer Program for the Non-Linear Analysis of Vertically Propagating Shear Waves in Horizontally Layered Deposits," by P.P. Martin and H.B. Seed - 1978 (PB 293 101)A05

UCB/EERC-78/24   "Investigation of the Elastic Characteristics of a Three Story Steel Frame Using System Identification," by I. Kaya and H.D. McNiven - 1978

UCB/EERC-78/25   "Investigation of the Nonlinear Characteristics of a Three-Story Steel Frame Using System Identification," by I. Kaya and H.D. McNiven - 1978

UCB/EERC-78/26   "Studies of Strong Ground Motion in Taiwan," by Y.M. Hsiung, B.A. Bolt and J. Penzien - 1978

UCB/EERC-78/27   "Cyclic Loading Tests of Masonry Single Piers: Volume 1 - Height to Width Ratio of 2," by P.A. Hidalgo, R.L. Mayes, H.D. McNiven and R.W. Clough - 1978

UCB/EERC-78/28   "Cyclic Loading Tests of Masonry Single Piers: Volume 2 - Height to Width Ratio of 1," by S.-W.J. Chen, P.A. Hidalgo, R.L. Mayes, R.W. Clough and H.D. McNiven - 1978

UCB/EERC-78/29   "Analytical Procedures in Soil Dynamics," by J. Lysmer - 1978

UCB/EERC-79/01   "Hysteretic Behavior of Lightweight Reinforced Concrete Beam-Column Subassemblages," by B. Forzani, E.P. Popov, and V.V. Bertero - 1979

UCB/EERC-79/02   "The Development of a Mathematical Model to Predict the Flexural Response of Reinforced Concrete Beams to Cyclic Loads, Using System Identification," by J.F. Stanton and H.D. McNiven - 1979

UCB/EERC-79/03   "Linear and Nonlinear Earthquake Response of Simple Torsionally Coupled Systems," by C.L. Kan and A.K. Chopra - 1979

UCB/EERC-79/04   "A Mathematical Model of Masonry for Predicting Its Linear Seismic Response Characteristics," by Y. Mengi and H.D. McNiven - 1979

UCB/EERC-79/05   "Mechanical Behavior of Lightweight Concrete Confined by Different Types of Lateral Reinforcement," by M.A. Manrique, V.V. Bertero and E.P. Popov - 1979

UCB/EERC-79/06   "Static Tilt Tests of a Tall Cylindrical Liquid Storage Tank," by R.W. Clough and A. Niwa - 1979

UCB/EERC-79/07   "The Design of Steel Energy Absorbing Restrainers and Their Incorporation Into Nuclear Power Plants for Enhanced Safety: Volume 1 - Summary Report," by P.N. Spencer, V.F. Zackay, and E.R. Parker - 1979

UCB/EERC-79/08   "The Design of Steel Energy Absorbing Restrainers and Their Incorporation Into Nuclear Power Plants for Enhanced Safety: Volume 2 - The Development of Analyses for Reactor System Piping," "Simple Systems" by M.C. Lee, J. Penzien, A.K. Chopra, and K. Suzuki "Complex Systems" by G.H. Powell, E.L. Wilson,R.W. Clough and D.G. Row - 1979

UCB/EERC-79/09   "The Design of Steel Energy Absorbing Restrainers and Their Incorporation Into Nuclear Power Plants for Enhanced Safety: Volume 3 - Evaluation of Commerical Steels," by W.S. Owen, R.M.N. Pelloux, R.O. Ritchie, M. Faral, T. Ohhashi, J. Toplosky, S.J. Hartman, V.F. Zackay, and E.R. Parker - 1979

UCB/EERC-79/10   "The Design of Steel Energy Absorbing Restrainers and Their Incorporation Into Nuclear Power Plants for Enhanced Safety: Volume 4 - A Review of Energy-Absorbing Devices," by J.M. Kelly and M.S. Skinner - 1979

UCB/EERC-79/11   "Conservatism In Summation Rules for Closely Spaced Modes," by J.M. Kelly and J.L. Sackman - 1979

UCB/EERC-79/12   "Cyclic Loading Tests of Masonry Single Piers Volume 3 - Height to Width Ratio of 0.5," by P.A. Hidalgo, R.L. Mayes, H.D. McNiven and R.W. Clough - 1979

UCB/EERC-79/13   "Cyclic Behavior of Dense Coarse-Grained Materials in Relation to the Seismic Stability of Dams," by N.G. Banerjee, H.B. Seed and C.K. Chan - 1979

UCB/EERC-79/14   "Seismic Behavior of Reinforced Concrete Interior Beam-Column Subassemblages," by S. Viwathanatepa, E.P. Popov and V.V. Bertero - 1979

UCB/EERC-79/15   "Optimal Design of Localized Nonlinear Systems with Dual Performance Criteria Under Earthquake Excitations," by M.A. Bhatti - 1979

UCB/EERC-79/16   "OPTDYN - A General Purpose Optimization Program for Problems with or without Dynamic Constraints," by M.A. Bhatti, E. Polak and K.S. Pister - 1979

UCB/EERC-79/17   "ANSR-II, Analysis of Nonlinear Structural Response, Users Manual," by D.P. Mondkar and G.H. Powell - 1979

UCB/EERC-79/18   "Soil Structure Interaction in Different Seismic Environments," A. Gomez-Masso, J. Lysmer, J.-C. Chen and H.B. Seed - 1979

UCB/EERC-79/19   "ARMA Models for Earthquake Ground Motions," by M.K. Chang, J.W. Kwiatkowski, R.F. Nau, R.M. Oliver and K.S. Pister - 1979

UCB/EERC-79/20   "Hysteretic Behavior of Reinforced Concrete Structural Walls," by J.M. Vallenas, V.V. Bertero and E.P. Popov - 1979

UCB/EERC-79/21   "Studies on High-Frequency Vibrations of Buildings I: The Column Effects," by J. Lubliner - 1979

UCB/EERC-79/22   "Effects of Generalized Loadings on Bond Reinforcing Bars Embedded in Confined Concrete Blocks," by S. Viwathanatepa, E.P. Popov and V.V. Bertero - 1979

UCB/EERC-79/23   "Shaking Table Study of Single-Story Masonry Houses, Volume 1: Test Structures 1 and 2," by P. Gülkan, R.L. Mayes and R.W. Clough - 1979

UCB/EERC-79/24   "Shaking Table Study of Single-Story Masonry Houses, Volume 2: Test Structures 3 and 4," by P. Gülkan, R.L. Mayes and R.W. Clough - 1979

UCB/EERC-79/25   "Shaking Table Study of Single-Story Masonry Houses, Volume 3: Summary, Conclusions and Recommendations," by R.W. Clough, R.L. Mayes and P. Gülkan - 1979

UCB/EERC-79/26   "Recommendations for a U.S.-Japan Cooperative Research Program Utilizing Large-Scale Testing Facilities," by U.S.-Japan Planning Group - 1979

UCB/EERC-79/27   "Earthquake-Induced Liquefaction Near Lake Amatitlan, Guatemala," by H.B. Seed, I. Arango, C.K. Chan, A. Gomez-Masso and R. Grant de Ascoli - 1979

UCB/EERC-79/28   "Infill Panels: Their Influence on Seismic Response of Buildings," by J.W. Axley and V.V. Bertero - 1979

UCB/EERC-79/29   "3D Truss Bar Element (Type 1) for the ANSR-II Program," by D.P. Mondkar and G.H. Powell - 1979

UCB/EERC-79/30   "2D Beam-Column Element (Type 5 - Parallel Element Theory) for the ANSR-II Program," by D.G. Row, G.H. Powell and D.P. Mondkar

UCB/EERC-79/31   "3D Beam-Column Element (Type 2 - Parallel Element Theory) for the ANSR-II Program," by A. Riahi, G.H. Powell and D.P. Mondkar - 1979

UCB/EERC-79/32   "On Response of Structures to Stationary Excitation," by A. Der Kiureghian - 1979

UCB/EERC-79/33   "Undisturbed Sampling and Cyclic Load Testing of Sands," by S. Singh, H.B. Seed and C.K. Chan - 1979

UCB/EERC-79/34   "Interaction Effects of Simultaneous Torsional and Compressional Cyclic Loading of Sand," by P.M. Griffin and W.N. Houston - 1979

UCB/EERC-80/01   "Earthquake Response of Concrete Gravity Dams Including Hydrodynamic and Foundation Interaction Effects," by A.K. Chopra, P. Chakrabarti and S. Gupta - 1980

UCB/EERC-80/02   "Rocking Response of Rigid Blocks to Earthquakes," by C.S. Yim, A.K. Chopra and J. Penzien - 1980

UCB/EERC-80/03   "Optimum Inelastic Design of Seismic-Resistant Reinforced Concrete Frame Structures," by S.W. Zagajeski and V.V. Bertero - 1980

UCB/EERC-80/04   "Effects of Amount and Arrangement of Wall-Panel Reinforcement on Hysteretic Behavior of Reinforced Concrete Walls," by R. Iliya and V.V. Bertero - 1980

UCB/EERC-80/05   "Shaking Table Research on Concrete Dam Models," by R.W. Clough and A. Niwa - 1980

UCB/EERC-80/06   "Piping With Energy Absorbing Restrainers: Parameter Study on Small Systems," by G.H. Powell, C. Oughourlian and J. Simons - 1980

UCB/EERC-80/07   "Inelastic Torsional Response of Structures Subjected
                  to Earthquake Ground Motions," by Y. Yamazaki - 1980

UCB/EERC-80/08   "Study of X-Braced Steel Frame Structures Under
                  Earthquake Simulation," by Y. Ghanaat - 1980

UCB/EERC-80/09   "Hybrid Modelling of Soil-Structure Interaction," by
                  S. Gupta, T.W. Lin, J. Penzien and C.S. Yeh - 1980

UCB/EERC-80/10   "General Applicability of a Nonlinear Model of a One
                  Story Steel Frame," by B.I. Sveinsson and H. McNiven - 1980

UCB/EERC-80/11   "A Green-Function Method for Wave Interaction with a
                  Submerged Body," by W. Kioka - 1980

UCB/EERC-80/12   "Hydrodynamic Pressure and Added Mass for Axisymmetric
                  Bodies," by F. Nilrat - 1980

UCB/EERC-80/13   "Treatment of Non-Linear Drag Forces Acting on Offshore
                  Platforms," by B.V. Dao and J. Penzien - 1980

UCB/EERC-80/14   "2D Plane/Axisymmetric Solid Element (Type 3 - Elastic
                  or Elastic-Perfectly Plastic) for the ANSR-II Program,"
                  by D.P. Mondkar and G.H. Powell - 1980

UCB/EERC-80/15   "A Response Spectrum Method for Random Vibrations," by
                  A. Der Kiureghian - 1980

UCB/EERC-80/16   "Cyclic Inelastic Buckling of Tubular Steel Braces," by
                  V.A. Zayas, E.P. Popov and S.A. Mahin - June 1980